New Larger Aeroplanes — Infringement of the Obstacle Free Zone: Operational Measures and Aeronautical Study

Cir 301
AN/174

New Larger Aeroplanes — Infringement of the Obstacle Free Zone: Operational Measures and Aeronautical Study

Approved by the Secretary General
and published under his authority

December 2005

International Civil Aviation Organization

FOREWORD

PURPOSE

The purpose of this document is to provide operational information to Contracting States wishing to introduce new larger aeroplane (NLA) operations on existing aerodromes having precision approach runways category I, II or III. The information is based on the results of an aeronautical study conducted by the United States Federal Aviation Administration (FAA) investigating the probability of collision during a balked landing for code letter F aeroplane operations at code letter E aerodromes. The aeronautical study primarily investigated the dimensions of the obstacle limitation balked landing surfaces and the obstacle free zone (OFZ) described in Table A-1 in Appendix A.

The FAA Balked Landing Study Programme focused on the risk analysis and probability of collision using balked-landing-type scenarios for NLAs, i.e. code letter F aeroplane operations. Studies were performed for both autopilot-coupled and flight director operations. The autopilot study used both flight simulator testing and computer simulations and generated the following outcomes:

a) Iso-probability contours used to assess the impact of obstacles based on their distance from the runway centre line at any specific point along the length of the runway;

b) Data projecting excursions (lateral displacement from centre line) for NLAs based on a wide range of flight profiles;

c) Airport elevation considerations; and

d) Additional elements that were identified as operationally pertinent to the risk analysis of existing aerodromes.

For flight director flown approaches, a mature, validated pilot model was not available for the computational process used for the autopilot study. Therefore, the risk of penetrating the Code E OFZ was evaluated using a statistical methodology known as Extreme Value Analysis (EVA). The process is explained in Chapter 7, Extreme Value Analysis (EVA) of Flight Simulator Data, in Part II of this circular.

The study focused on the investigation of code letter F aeroplane operations at existing aerodromes. The code letter "F" is found in Table A-2 in Appendix A and is a designation reference for aerodromes serving the operation of aeroplanes with wingspans of 65 m up to but not including 80 m. In addition, Annex 14 — *Aerodromes,* Volume I — *Aerodrome Design and Operations* contains Standards and Recommended Practices (SARPs) for runways, taxiways and taxiway minimum separation distances related to code letter F aeroplane operations. It also prescribes the physical characteristics and obstacle limitation surfaces to be provided for at aerodromes with aerodrome reference code letter F as shown in Table A-1.

This circular provides operational information that addresses runway to taxiway minimum separation distances and obstacle limitation surfaces referenced in Table A-1 in Appendix A of this circular. This is in accordance with Recommendation 3.9.7 and Note 1 in Annex 14, Volume I (Fourth Edition), which states that "… it may be permissible to operate with lower separation distances at an existing aerodrome if an aeronautical study indicates that such lower separation distances would not adversely affect the safety or significantly affect the regularity of operations of aeroplanes".

Recommendation 3.9.7 also references Doc 9157 — *Aerodrome Design Manual*, Part 2 (Fourth Edition, 2005) for obtaining information on the factors that may be considered in an aeronautical study and as such was used in conducting the FAA study and in outlining its objective and scope. Paragraph 1.2.29 of the manual states "The prime objective of an aeronautical study is to assess the adequacy of the protection provided by the existing layout for the operation of the critical aircraft ...". Paragraph 1.2.32 states "An aeronautical study will consist essentially of a risk analysis based on pertinent criteria to assess: a) probability of collision; b) probability of run-off; and c) risk of engine ingestion".

It is expected that the outcome of this study will assist Contracting States in conducting similar aeronautical studies. It should be noted that risks and responsibility rest with the Contracting State in accordance with the Chicago Convention.

OUTLINE

This circular is divided into two parts. Part I should be consulted for an executive summary of the study. It contains three chapters. Chapter 1 provides an introduction and describes the purpose and objectives of the study. Chapter 2 provides the study overview. Chapter 3 contains guidance material on how the study findings might be implemented in an operational environment. It also provides guidance material for taxiing aircraft and air traffic services (ATS) in light of the findings from the simulations.

The technical details concerning the study are found in Part II, which is divided into seven chapters. Chapter 1 provides background information on the history and description of ICAO obstacle limitation surfaces.

Chapter 2 provides examples of actual balked-landing-type events as recorded in ICAO and FAA database records. The database records and the FAA Aviation Safety Statistical Handbook were useful sources of information employed in the design of balked landing scenarios for the NASA Ames simulator trials. A description of the findings from the trials conducted on a 747-400 simulator provided by the Crew Vehicle Systems Research Facility located at the NASA Ames Research Center in the United States, and for those on the A340-300 simulators at Airbus in Toulouse, France, and the Zentrum für Flugsimulation Berlin GmbH (ZFB) located at the Technical University of Berlin, Germany, is found in Chapter 3. Volunteer airline crews who were current and certified to fly the relevant type performed these trials at NASA and ZFB. Airline crews and Airbus training personnel with airline experience were used in the Toulouse simulator. The knowledge gained from the simulator trials was used to specify inputs for the Monte Carlo[1] computer simulation of the auto-coupled balked landing scenarios and for direct input to the EVA of flight director guided operations.

Chapters 4 to 6 discuss the Monte Carlo computer simulation study. Chapter 4 is a statistical analysis of pilot response time data observed in the NASA Ames simulator facility. The analysis provides the basis for statistical distributions used in the Monte Carlo simulation describing the delays in pilot response while executing the go-around procedure during a balked landing.

Chapter 5 describes the details on the wind model information that was used in the simulations. It is based on data collected from 40 airports where new larger aeroplanes are expected to land and take-off.

---

1. The Monte Carlo method, also called Monte Carlo analysis, is a means of statistical evaluation of mathematical functions using random examples.

Chapter 6 provides study details on the findings from the computer simulations based on the use of the autopilot in the approach, and on the A340 autoland simulator validation process. The iso-probability contours generated from this study can serve as useful information for assessment of the balked landing obstacle limitation surfaces for autopilot operations.

Chapter 7 describes the extreme value analysis used for conducting a statistical study of the flight tracks produced from airline crews conducting balked landings in flight simulator facilities at NASA Ames and at Airbus and ZFB. The selected EVA method uses a non-parametric extrapolation technique for estimating the probability of an aircraft infringing on the obstacle limitation surfaces. A subsequent circular will discuss the use of a simulated model of a pilot flying an approach receiving guidance from a flight director in the modeling effort with application to the collision risk model.

The appendices provide background material relating to the aeronautical study. Appendix A provides reference data, including aeroplane dimension data, a comparison of ICAO and FAA aerodrome reference codes and design standards, and tables and figures on the obstacle limitation surfaces. Appendix B contains the FAA and the Joint Aviation Authorities (JAA) wind model for approach and landing simulation. Appendix C is a description of the ASAT tool. Appendix D is a description of the 747-400 Integrated Aircraft Configuration. Appendices E and F include information bulletins provided by the NASA Ames and ZFB simulator test facilities.

———————————

TABLE OF CONTENTS

Page

— — — — — — — —

List of tables

Part II

— — — — — — — —

List of figures

Part I

Chapter 4

Appendix to Chapter 6

Chapter 7

Appendices

Appendix A

Appendix B

_____

ACRONYMS AND ABBREVIATIONS

747/NLA   NLA with autopilot and flight director characteristics and performance as good as or better than the 747-400

A340/NLA   NLA with autopilot and flight director characteristics and performance as good as or better than the A340-300

ADIZ   Air defence identification zone

AGL   Above ground level

AIP   Aeronautical information publication

ANC   Air Navigation Commission

ANOVA   Analysis of variance

ASAT   Airspace Simulation and Analysis Tools

ATC   Air Traffic Control

ATS   Air Traffic Services

CG   Centre of Gravity

CC   Controller Call

CRM   Collision Risk Model

DH   Decision height

EOS   Experimental Observers Station

EVA   Extreme Value Analysis

FAA   Federal Aviation Administration

FAR   Federal Aviation Regulation

F/D   Flight director

FTE   Flight technical error

GA   Go-around

GEV   Generalized Extreme Value (distribution)

IFR   Instrument Flight Rules

ILS   Instrument landing system

IMC   Instrument meteorological conditions

ISWO   International surface weather observations

JAA   Joint Aviation Authority

LNAV   Lateral navigation

MAC   Mean aerodynamic chord

MDA	Minimum descent altitude
MDH	Minimum descent height
MLS	Microwave landing system
MOU	Memorandum of understanding
NASA	National Aeronautics and Space Administration
NLA	New larger aeroplane
NLR	Nationaal Lucht– en Ruimtevaartlaboratorium (National Aerospace Laboratory)
NORAD	North American Aerospace Defense
OAG	Official Airline Guide
OCP	Obstacle Clearance Panel
OFZ	Obstacle free zone
PANS-OPS	Procedures for Air Navigation Services — Aircraft Operations
PD	Pilot deviation
PDF	Probability density function
RESA	Runway end safety area
RI	Runway incursion
RI/EO	Runway incursion with one engine out
RMS	Root mean square
RVR	Runway visual range
SARPs	Standards and Recommended Practices
TERPS	Terminal instrument procedures
TLA	Throttle lever angle
TLS	Target level of safety
TO/GA	Take-off or go-around
VL	Visual Loss
VNAV	Vertical navigation
VPD	Vehicle/pedestrian deviation

ABBREVIATIONS

cmd	command
ft	foot
in	inch
intl.	international
km	kilometre
kt	knot
lb	pound
m	metre
mi	statute mile

mph	miles per hour
NM	nautical mile
rwy	runway
s	second
tfc	traffic

AIRPORT ABBREVIATIONS

DEN   Denver International, Denver (Colorado), United States

GRU   Guarulhos International, Sao Paulo, Brazil

JFK   John F. Kennedy International, New York City (New York), United States

LAX   Los Angeles International Airport, Los Angeles (California), United States

MMX   Licenciado Benito Juarez International, Mexico City, Mexico

_____

DEFINITION OF TERMS

Aerodrome. A defined area on land or water (including any buildings, installations and equipment) intended to be used either wholly or in part for the arrival, departure and surface movement of aircraft.

Aerodrome elevation. The elevation of the highest point of the landing area.

ASAT. The Airspace Simulation and Analysis Tools system is a computer simulation facility developed by the Flight Procedure Standards Branch of the United States Federal Aviation Administration (FAA). The system incorporates high-fidelity models with empirical data to perform a wide range of aviation-related simulations. It has been used extensively by the FAA to develop new standards and criteria and perform risk analyses for aviation studies.

Automatic Landing System. The airborne equipment which provides automatic control of the aeroplane during the approach and landing.

Balked landing. A landing manoeuvre which is unexpectedly discontinued.

Instrument runway. One of the following types of runways intended for the operation of aircraft using instrument approach procedures:

a) *Non-precision approach runway.* An instrument runway served by visual aids and a non-visual aid providing at least directional guidance adequate for a straight-in approach.

b) *Precision approach runway, category I.* An instrument runway served by ILS and/or MLS and visual aids intended for operations with a decision height not lower than 60 m (200 ft) and either a visibility not less than 800 m or a runway visual range not less than 550 m.

c) *Precision approach runway, category II.* An instrument runway served by ILS and/or MLS and visual aids intended for operations with a decision height lower than 60 m (200 ft) but not lower than 30 m (100 ft) and a runway visual range not less than 350 m.

d) *Precision approach runway, category III.* An instrument runway served by ILS and/or MLS to and along the surface of the runway; and:

A — intended for operations with a decision height lower than 30 m (100 ft), or no decision height and a runway visual range not less than 200 m.

B — intended for operations with a decision height lower than 15 m (50 ft), or no decision height and a runway visual range less than 200 m but not less than 50 m.

C — intended for operations with no decision height and no runway visual range limitations.

Note 1.— See Annex 10, Volume I, Part I, for related ILS and/or MLS specifications

Note 2.— Visual aids need not necessarily be matched to the scale of non-visual aids provided. The criterion for the selection of visual aids is the conditions in which operations are intended to be conducted.

Obstacle. All fixed (whether temporary or permanent) and mobile objects, or parts thereof, that are located on an area intended for the surface movement of aircraft or that extend above a defined surface intended to protect aircraft in flight.

Obstacle free zone (OFZ). The airspace above the inner approach surface, inner transitional surfaces, and balked landing surface and that portion of the strip bounded by these surfaces, which is not penetrated by any fixed obstacle other than a low-mass and frangibly mounted one required for air navigation purposes.

Pilot deviation (PD). The actions of a pilot that result in the violation of a Federal Aviation Regulation (FAR) or a North American Aerospace Defense (NORAD) Command Air Defense Identification Zone (ADIZ) tolerance.

Primary runways. Runways used in preference to others whenever conditions permit.

Runway. A defined rectangular area on a land aerodrome prepared for the landing and take-off of aircraft.

Runway end safety area (RESA). An area symmetrical about the extended runway centre line and adjacent to the end of the strip primarily intended to reduce the risk of damage to an aeroplane undershooting or overrunning the runway.

Runway incursion (RI). Any occurrence at an aerodrome involving the incorrect presence of an aircraft, vehicle or person on the protected area of a surface designated for the landing and take-off of aircraft.

Runway strip. A defined area including the runway and stopway, if provided, intended:

a) to reduce the risk of damage to aircraft running off a runway; and

b) to protect aircraft flying over it during take-off or landing operations.

Runway visual range (RVR). The range over which the pilot of an aircraft on the centre line of a runway can see the runway surface markings or the lights delineating the runway or identifying its centre line.

Taxiway. A defined path on a land aerodrome established for the taxiing of aircraft and intended to provide a link between one part of the aerodrome and another, including:

a) *Aircraft stand taxilane.* A portion of an apron designated as a taxiway and intended to provide access to aircraft stands only.

b) *Apron taxiway.* A portion of a taxiway system located on an apron and intended to provide a through taxi route across the apron.

c) *Rapid exit taxiway.* A taxiway connected to a runway at an acute angle and designed to allow landing aeroplanes to turn off at higher speeds than are achieved on other exit taxiways thereby minimizing runway occupancy times.

Threshold. The beginning of that portion of the runway usable for landing.

Touchdown zone. The portion of the runway, beyond the threshold, where it is intended landing aeroplanes first contact the runway.

Track. The projection on the earth's surface of the path of an aircraft, the direction of which path at any point is usually expressed in degrees from North (true, magnetic or grid).

Vehicle or pedestrian deviation (VPD). Any entry into or movement on the airport movement area by a vehicle or pedestrian that has not been authorized by air traffic control (includes aircraft operated by non-pilots).

———————————

PART I

STUDY OVERVIEW AND
IMPLEMENTATION GUIDANCE

Chapter 1
INTRODUCTION TO THE STUDY

1.1 GENERAL

1.1.1   This circular provides operational information to Contracting States wishing to introduce new larger aeroplane (NLA) operations on existing aerodromes not meeting the requirements of Annex 14[1] — *Aerodromes,* Volume I — *Aerodrome Design and Operations* for code letter F aeroplane operations. It focuses on NLAs meeting, as a minimum, the following requirements:

- guidance by either a coupled (digital) autopilot or a (digital) flight director (F/D); and

- use of ground track holding in the missed approach.

1.1.2   This guidance is based on an aeronautical study conducted by the United States Federal Aviation Administration (FAA) in coordination with the ICAO Obstacle Clearance Panel (OCP), and with participation by the United States National Aeronautics and Space Administration (NASA), Direction Générale de l'Aviation Civile (DGAC–France), the Nationaal Lucht– en Ruimtevaartlaboratorium (NLR, the Netherlands), the United Kingdom's QinetiQ research laboratory, EUROCONTROL, Inspectoraat Verkeer en Waterstaat (IVW), Airbus SAS and The Boeing Company.

1.1.3   Annex 14, Volume I, contains Standards with regard to the obstacle free zone (OFZ), designed to protect for a balked (i.e. aborted) landing resulting in the execution of a missed approach (go-around (GA) manoeuvre) even when below the specified decision height. The OFZ dimension for code letter F is the result of OCP work (OCP/11 meeting, 1997). These Standards could be limiting for various code letter E aerodromes unable to implement code letter F requirements. Therefore, this circular investigates operational mitigations to assist these aerodromes in accommodating an NLA. It should be understood that the results of this study should be considered only for aerodromes having precision runways category I, II or III.

1.1.4   For purposes of discussion within the circular, "track-hold guidance" refers to guidance by means of an avionics system that provides steering commands to maintain an established track (from the projection of the velocity vector on the earth's surface), beginning from go-around commencement through the climb phase of the go-around manoeuvre. It should be noted that in some avionics systems the "track-hold guidance" function involves the on-board storage of the ground track flown during the approach, and use of this track information in the go-around. The function is used in both autopilot and flight director.

1.2 STUDY OBJECTIVE

The study objective was to determine whether credit could be given to an NLA meeting the operational criteria described above in reducing the dimensions of the OFZ. The methodology employed was conducting a risk analysis to determine the probability of infringement of the OFZ.

---

1. All references to Annex 14 are to Volume I (Fourth Edition).

1.3   DEVELOPMENT OF STUDY SCENARIOS

1.3.1   In order to develop the study scenarios, accident/incident data were reviewed from sources within ICAO and the FAA to identify key factors that occur during a balked landing (see Part II, Chapter 2). These factors were included and controlled in experiments on simulators to understand their impact on the reaction of pilots and the flight track of the aircraft during a balked landing (see Part II, Chapters 3 and 4). In addition, a meteorological study was performed for the airports likely to accommodate NLAs. This resulted in the use of an appropriate wind model (see Part II, Chapter 5).

1.3.2   Once key factors were identified in terms of their statistical significance, computers were used to simulate various types of balked landing events. Results from the simulation studies provided adequate data to statistically assess the dimensions of the OFZ (see Part II, Chapter 6).

1.3.3   The simulation study is based on a model of a Boeing 747-400 aircraft that was adapted to represent the flight behaviour of a generic NLA on approach and on the missed approach. Since it was assumed that the roll authority of an NLA would be either as good as or better than that of the Boeing 747-400 as configured for the study, the result would be conservative and all-encompassing. Validation of simulation assumptions and findings was also made with the use of A340-300 full flight simulators.

1.3.4   The study investigated the use of the autopilot as well as manual flight with a flight director for guidance. The pilot model under development for a computer simulation of the F/D case was not available so alternative analysis techniques were developed based on the application of Extreme Value Statistical Analysis to the flight simulator data. Two independent European research organizations, NLR and QinetiQ, were contracted to develop pilot models with the aid of aircraft manufacturers. Once completed, the pilot models will be used to perform a flight director simulation equivalent to the autopilot study. When completed, that study will be published in a separate circular with consideration given to enhancement of the Collision Risk Model (CRM).

———————————

Chapter 2
BALKED LANDING STUDY OVERVIEW

2.1   INTRODUCTION

2.1.1   The FAA has been investigating NLA balked landings (go-arounds below decision height) for eight years (1997-2005), specifically focusing on the risk analysis of the probability of infringing on the OFZ. The study initially examined the performance of modern digital autopilot-equipped aircraft and subsequently addressed the performance in flight director (F/D) mode of aircraft equipped with a track hold guidance function.

2.1.2   The outcome of the study provides guidance on the operation of code letter F aeroplanes at existing aerodromes designed to accommodate Code E operations. The collision risk for NLA autopilot operations was initially assessed. This was done by establishing iso-probability contours of aircraft extremity position using the FAA Airspace Simulation and Analysis Tools (ASAT)[1]. Over 200 000 computer simulations were conducted based on a wide range of flight profiles, variation in airport altitude and other pertinent operational elements.

2.1.3   A Monte Carlo technique involving modelling of the autopilot performance and data from the NASA Ames 747-400 simulator trials was used, and data were adjusted for NLA dimensions. Subsequently, data were collected on an Airbus A340-300 simulator to determine the applicability of the ASAT results to the Airbus NLA.

2.1.4   For the flight director case, a model of piloted flight director performance was not available for ASAT computer simulation and an alternative process was necessary. It consisted of statistical study using Extreme Value Analysis (EVA) techniques of A340-300 flight simulator data from Toulouse and Berlin and B747-400 data from NASA to determine the risk of infringing the Code E OFZ boundary.

2.2   STUDY OUTLINE

2.2.1   The outline for an aeronautical study prescribed in Doc 9157 — *Aerodrome Design Manual, Part 2*, 1.2.32, was followed, taking into account the probability of collision. The purpose was to assess the impact of the balked landing on the definition of the OFZ for aircraft with a wingspan up to 80 m using collision risk methodology.

2.2.2   In accordance with the ICAO CRM, the value of 1×10^{-7} defined the target level of safety (TLS) and was, therefore, the criterion used to define the acceptable risk of collision between an aircraft on the approach and another aircraft, vehicle or object on the ground.

2.2.3   For the autopilot case, iso-probability contours of 10^{-7} were constructed from ASAT simulation flight track data using the NASA Ames full flight simulator data and a complete integrated aircraft

---

1.   A description of ASAT is provided at Appendix C.

configuration simulation (IAC) model of the Boeing 747-400. The contours serve as a basis for evaluating the OFZ definition. The iso-probability contours were constructed at various locations along the flight path of a balked landing beginning at some range point before runway threshold (e.g. 4 200 m) and continuing along the length of the runway after threshold (e.g. 200 m past threshold), similar to the CRM technique.

2.2.4   For the flight director studies, the scenario list included the most difficult ceiling and visibility conditions, critically low balked landing heights and primarily high crosswinds. These conditions were chosen so that the collision risk could be directly assessed using EVA, taking into account the scenario probability.

2.3   AUTOLAND STUDY

2.3.1   Simulator session on the
NASA Ames Boeing 747-400 flight simulator

2.3.1.1   Airline pilots were monitored as they performed balked landing procedures under controlled experimental conditions. For these tests, the balked landings were initiated either by simulated air traffic control (ATC) command issued when the aircraft reached a specified altitude; or by runway incursion (RI) by another aircraft; or by vehicle/pedestrian deviation (VPD); or by active arriving and departing traffic on the runway. Both autopilot and flight director approaches were studied.

2.3.1.2   All landing scenarios used a strong crosswind component. By testing airline pilots under extreme operational conditions, the study results for balked landings within the tested environment could hopefully be generalized. Pilot response time data were used as input to the Monte Carlo[2] simulations.

2.3.1.3   Examination of the NASA Ames simulator data suggested that the Monte Carlo computer simulation should focus on autopilot-controlled balked landings. Compared to manual control with the flight director, the autopilot-controlled balked landings exhibited smaller lateral deviation.

2.3.1.4   The Monte Carlo ASAT computer simulations conducted the balked landings at two airport elevations, namely, at sea level 4 m (13 ft) and at 1 980 m (6 534 ft) to correspond to the simulator study. All approaches in the Monte Carlo simulation were conducted in autoland mode utilizing the pilot response time distributions as determined from examination of NASA Ames Boeing 747-400 flight simulator data. (See Part II, Chapters 3 and 4, for further details.)

2.3.1.5   The ASAT computations were used to produce flight track data at various perpendicular planes or tiles located at intervals along the flight path, similar to the method used in the ILS CRM. A specific composite wind and ILS performance model was used.

2.3.1.6   The iso-probability contour at the runway threshold is shown in Figure 2-1. Details are in Part II, Chapters 5 and 6. The ends of the lower curve indicate the maximum distance from runway centre line for a probability of 1×10^{-7}, which would be found on an aircraft wing tip.

---

2. The Monte Carlo method, also called Monte Carlo analysis, is a means of statistical evaluation of mathematical functions using random samples.
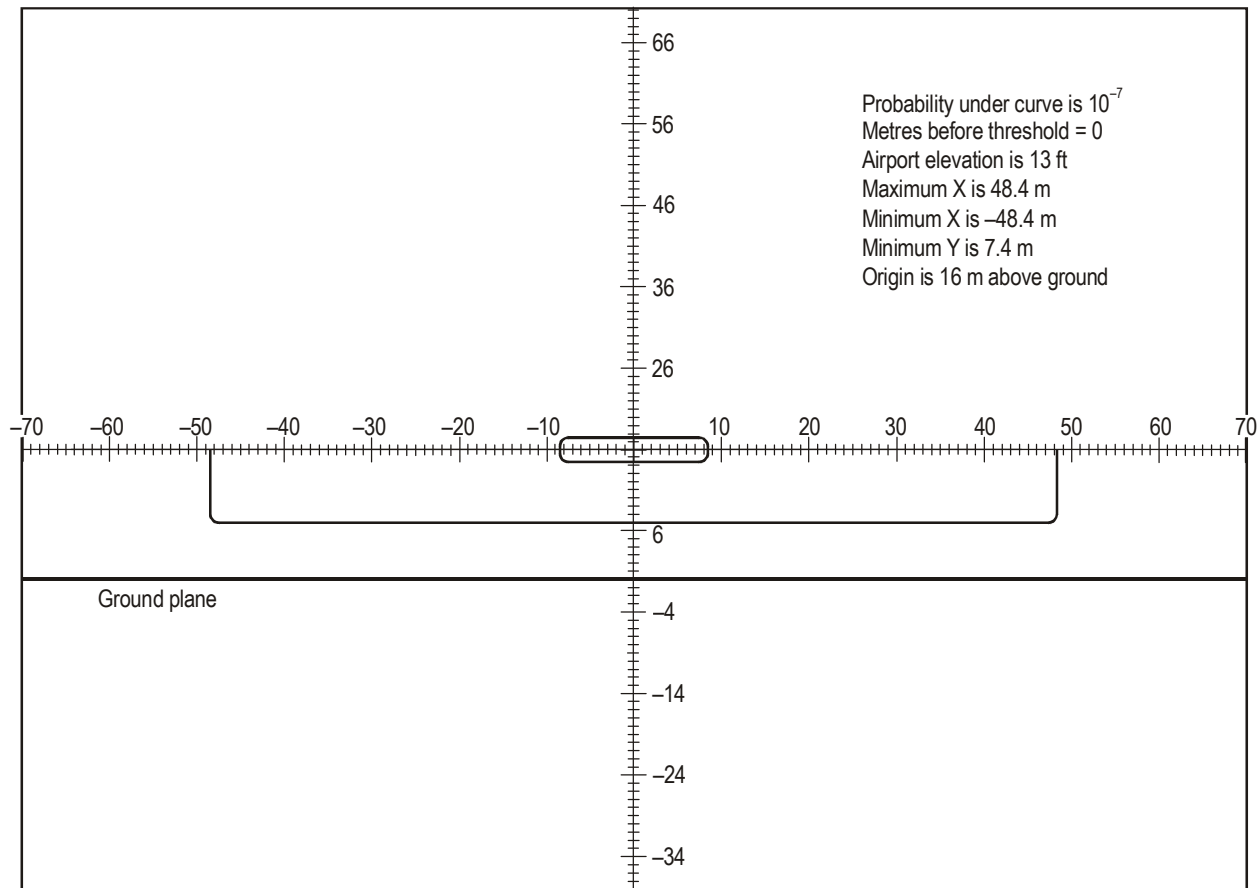
Figure 2-1.   The iso-probability contour at runway threshold

2.3.2   Simulator autoland trials on Airbus A340-300 flight simulators

2.3.2.1   Data were collected from autopilot balked landings on A340-330 full flight simulators at the Airbus training centre at Toulouse in April 2004 and at the Technical University of Berlin in August/September 2004. The purpose was to collect sufficient data to assess the conformance of the Airbus autopilot balked landing performance with the results from the NASA Ames B747-400 autopilot data. This demonstrated that modern flight control systems, even with different design philosophies, provided comparable performance.

2.3.2.2   A total of 28 autopilot balked landings were flown in Toulouse by Airbus pilots. In Berlin, 87 autopilot balked landings were flown by nine different airline crews. The scenarios focused on low balked landing height and limiting ceiling and RVR conditions with significant crosswind.

2.4   FLIGHT DIRECTOR STUDY

2.4.1   NASA Ames full flight simulator sessions

2.4.1.1   Four flight simulator test sessions were conducted at the NASA Ames Boeing 747-400 full motion flight simulator to collect data supporting evaluation of OFZ standards with respect to modern NLA

performance. One hundred and twenty-five flight director approaches were flown with various wind and visibility settings at high and low altitude airports. Winds were generally near the maximum allowable crosswind component for conducting an approach.

2.4.1.2   Use of the full flight simulator assumes that the ILS signal has no irregularities; the calibration of the localizer receiving centring error is constant. The study assumed that the displacement of the centre-of-gravity would be an equivalent measure of the Flight Technical Error (FTE) and the means of guidance during the go-around phase of flight. The aeroplane guidance system was in "ground track hold" mode with the engagement of "go-around". The use of "ground track hold" mode is fundamental to the conclusion of the study. The absence of an ILS signal error in the guidance is to some extent offset by the fact that the aircraft is generally well into the visual segment of the approach before the balked landing is initiated. Small track errors introduced by the ILS would be masked by pilot-induced FTE.

2.4.1.3   FTE is an indicator of the capability of the pilot to follow the commands from the flight director pitch and roll bars. The study assumed that the FTE observed in the study, for the various environmental conditions, would be the same observed for an NLA with a design philosophy similar to that of the Boeing 747-400.

2.4.2   Berlin and Toulouse full flight simulator sessions

2.4.2.1   Full flight simulator flight director data were also collected in Toulouse and Berlin. The scenarios were modified from the NASA trials to include only the most difficult ceiling and visibility conditions, critically low balked landing heights and primarily high crosswinds. These conditions were where the track hold guidance would be perturbed and the largest deviations had been observed.

2.4.2.2   An additional balked landing trigger was introduced, namely, a loss of visual reference.

2.4.2.3   The matrix of scenarios included low and high airports and was also adjusted to provide sufficient variation in crosswind conditions to allow a reasonable conclusion to be drawn about the influence of crosswind on collision risk.

2.4.2.4   The scenarios matrix choice was influenced by the intended statistical treatment; that is, only the extreme cases of visual conditions and balked landing heights were used. The visual conditions for all approaches were set at a practical lower limit, by slightly raising the ceiling and RVR from a setting that caused uncommanded go-arounds. Trigger heights were all at 70 feet or below (40 and 10). The very low minima and simulator functional issues precluded the use of runway incursion triggers.

2.4.2.5   It is evident then that the resulting data set would be somewhat different to earlier sets. Details can be found in Part II, Chapter 3.

2.5   STUDY FINDING

2.5.1   The simulation studies for the NASA autoland approaches found that the maximum distance from the runway centre line which would be found on an aircraft wing tip was contained within ±50 m (164 ft) of either side of the centre line.

2.5.2   This result was contained within the dimensions of the balked landing surface found in Table A-1 in Appendix A where the code number is 4 and the code letter is E. To ensure ILS signal integrity for NLA operations using autoland, see Doc 9365 — *Manual of All-Weather Operations,* 5.2.13.

2.5.3   Subsequent analysis of the Airbus autopilot data by the FAA concluded that it was compatible; therefore, the conclusion that Code E OFZ surfaces are acceptable for autopilot NLA operations is also valid for A340/NLAs.

2.5.4   FAA analysis of the data from the Airbus A340-300 flight director trials found that the Toulouse and Berlin data were sufficiently statistically similar to be aggregated. The conclusion was reached that the collision risk was acceptable for an A340/NLA F/D flown approach in Cat I conditions to a runway with a Code E OFZ.

2.5.5   FAA analysis of the data from the Boeing 747-400 flight director trials similarly found that the collision risk was acceptable for a 747/NLA F/D flown approach in Cat I conditions to a runway with a Code E OFZ.

2.5.6   The analysis did not support a variation of OFZ dimensions with aerodrome altitude. Details of these analyses may be found in Part II, Chapter 7.

_____

Chapter 3
IMPLEMENTATION GUIDANCE
AT CODE LETTER E AERODROMES

3.1   INTRODUCTION

3.1.1   This chapter provides guidance on how to implement the findings of the balked landing study at existing code letter E aerodromes that anticipate operation of some code letter F aeroplanes, i.e. NLAs. The findings of the study focused on the OFZ balked landing surfaces. It suggests that the dimension of the code letter E OFZ balked landing surface would be adequate for protecting aircraft aborting a landing after passing the decision height (DH) when either the autopilot or flight director is in use and a "ground track hold" function is in use.

3.1.2   Specifically, the OFZ for a Code E aeroplane may be used to meet the OFZ requirements specified in Annex 14 and related documents for NLAs with these capabilities. Sections 3.2, 3.3 and 3.4 provide guidelines for the operation of NLAs at aerodromes.

3.1.3   If an autoland is intended, it is important that there be adequate protection of electronic signals from the ILS. This may require a determination of the dimension of the ILS-sensitive area for an NLA. Annex 10 — *Aeronautical Telecommunications*, Volume I — *Radio Navigation Aids*, provides the SARPs for determining this dimension.

3.2   OBSTACLE FREE ZONE (OFZ) DIMENSION

3.2.1   The OFZ can be used to assess the placement of obstacles or taxiing aeroplanes relative to the proximity of fixed or other appropriate obstacles to the runway. Table A-1 in Appendix A of this circular gives the dimensions for the balked landing surface used to define the OFZ. The dimension of primary interest is the width of the OFZ. For aerodromes designed to satisfy code letter F design requirements, the total width of the OFZ, as per an OCP/11 Recommendation, is 155 m (511 ft), whether the landing is conducted manually or with autopilot. The findings of the balked landing study support that the 155-m (511-ft) total strip width is adequate and conservative.

3.2.2   For aerodromes designed to satisfy code letter E design requirements, the total width of the OFZ within the runway strip is 120 m (390 ft) according to Table A-1. The balked landing study results found that when a modern digital autopilot or flight director with track hold guidance is used for the approach, a code letter F aeroplane would be contained within the code letter E OFZ. Consequently, the code letter E balked landing surface could be used to assess obstacles around the runway.

3.2.3   Both the total width of 120 m and the slope of 3:1 for the balked landing surface were found to be adequate.

3.3   TAXIING OPERATIONS

3.3.1   Annex 14 specifies that ground operations at existing aerodromes should be governed by the balked landing surfaces for code letter F described in Table A-1. However, the study findings suggest

that when the approaching NLA conducts an autoland or flight director approach, the balked landing surfaces for code letter E would be sufficient.

3.3.2   It is recommended that the aerodrome make a transition to a category II operational mode whenever it is necessary for any aircraft to conduct an autoland. This would require that all vehicles and aircraft on the ground remain outside the ILS critical and sensitive areas as described in Annex 10, Volume I, Part I, Attachment C, as they may cause reflection and possibly diffraction of the ILS signals[1]. Because the NLA geometric characteristics exceed the current reference aeroplane (i.e. the 747-400), to ensure ILS signal integrity, the dimensions of the ILS critical and sensitive areas require a reassessment on a case-by-case basis taking into account specific aerodrome layout, antenna characteristics and traffic density on the ground. For more details, see Doc 9365 — *Manual of All-Weather Operations,* 5.2.13.

3.3.3   It is also important that sufficient longitudinal separation be provided between landing aircraft so that the level of interference to the ILS signal from the tail of an aeroplane exiting the runway is acceptable. In this respect, 5.2.14 of Doc 9365 states the following:

> Diffraction and/or reflection may also be caused by large aeroplanes in the vicinity of the runway which may affect both the glide path and the localizer signals. This additional area, outside the critical area, is called the sensitive area. The extent of the sensitive areas will vary with the characteristics of the ILS and the category of operations. It is essential to establish the level of interference caused by aircraft and vehicles at various positions on the aerodrome so that the boundaries of the sensitive areas may be determined. Since it is obviously not practicable to develop precise criteria covering all cases, the size and shape of the sensitive areas for a particular category of operation must be determined by the State concerned.

3.4   AIR TRAFFIC SERVICES (ATS) SUPPORT

NLAs described in 3.1.1 operating at an existing aerodrome that does not meet the code letter F aerodrome design requirements are capable of operating on a runway with a code E OFZ using either an autopilot or flight director approach mode. A Memorandum of Understanding (MOU) between the local aerodrome authority, the air traffic services (ATS) facility and the airline operator of the NLA may be required for ATS. Specific approach and landing procedures for such NLAs should not be required unless noted in the Memorandum of Understanding.

_____

---

1. A reflection or diffraction of the ILS signal can induce disturbances to the guidance signals for the autopilot on the approach path. For more details, see Doc 9365 — *Manual of All-Weather Operations,* 5.2.13.

PART II

AERONAUTICAL STUDY DETAILS

Chapter 1

HISTORY AND DESCRIPTION OF THE
ICAO OBSTACLE LIMITATION SURFACES

1.1 GENERAL

1.1.1   Natural features and manmade constructions inside and outside its boundary may considerably influence the effective utilization of an aerodrome. These may result in limitation on the distances available for take-off and landing and on the range of meteorological conditions in which take-off and landing can be undertaken. For these reasons certain areas of the local airspace must be regarded as integral parts of the aerodrome environment. The degree of freedom from obstacles in these areas is as important to the safe and efficient use of the aerodrome as are the more obvious physical requirements of the runways and their associated strips.

1.1.2   The significance of any existing or proposed object within the aerodrome boundary in the vicinity of the aerodrome is assessed by the use of two separate sets of criteria defining airspace requirements. The first set comprises the obstacle limitation surfaces particular to a runway and its intended use as specified in Annex 14[1] — *Aerodromes,* Volume I — *Aerodrome Design and Operations*. The broad purpose of these surfaces is to define the volume of airspace that should ideally be kept free from obstacles in order to minimize the dangers presented to an aircraft, either during an entirely visual approach or during the visual segment of an instrument approach.

1.1.3   The second set of criteria comprises the surfaces described in Doc 8168 — *Procedures for Air Navigation Services — Aircraft Operations* (PANS-OPS), Volume II — *Construction of Visual and Instrument Flight Procedures*. The PANS-OPS surfaces are intended for use by procedure designers for the construction of instrument flight procedures and for specifying minimum safe altitudes and heights for each segment of the procedure.

1.1.4   The obstacle limitation surfaces are meant to be of a permanent nature. To be effective, they should, therefore, be enacted in local zoning laws or ordinances or as part of a national planning consultation scheme. The surfaces established should allow not only for existing operations but also for the ultimate development envisaged for each aerodrome.

1.1.5   The obstacle limitation surfaces are designed to protect a landing below the obstacle clearance height, or a balked landing executed with all engines operative and initiated below the obstacle clearance height. The requirements for obstacle limitation surfaces are specified on the basis of the intended use of the runway, i.e. take-off or landing and type of approach and the aeroplane performance characteristics (reference code number). The specifications and dimensions of the various obstacle limitation surfaces are contained in Chapter 4 of Annex 14 and guidance on the functions of these surfaces is given in Doc 9137 — *Airport Services Manual*, Part 6 — *Control of Obstacles*.

---

1. All references to Annex 14 are to Volume I (Fourth Edition).

1.2   THE OBSTACLE FREE ZONE (OFZ) — PHILOSOPHY
AND CONSIDERATIONS FOR ITS DEVELOPMENT

1.2.1   "See and avoid" was the concept behind obstacle clearance and avoidance before the development of the definition of OFZ. Obstacles were painted and striped so that the pilot could see and avoid them. However, as the approach speeds of jet aircraft became faster, this philosophy was no longer viable as pilots could not react in sufficient time to avoid collision with an obstacle.

1.2.2   For this reason, members of the ICAO OCP developed the notion of a zone free of obstacles during its second meeting in February 1970. The OFZ was intended to protect aircraft in the last visual stage of a precision approach and in a late missed approach with all engines operating normally. The Panel did not develop a precise definition then but decided to wait for the outcome of studies on this topic being conducted by Contracting States.

1.2.3   At the Third Meeting of the OCP (OCP/3) in October/November 1971, it was agreed that the priority consideration should be the development of requirements which, within established limitations, would provide additional protection from obstacles for aircraft obliged to execute a missed approach after the pilot had previously elected to continue a category II approach below the decision height (DH). Such a missed approach is referred to as a balked landing.

1.2.4   Figure 1-1 illustrates the difference between a traditional missed approach and a balked landing below the DH. Figure 1-2 illustrates the main concern about protecting the approaching aircraft from collision with fixed and/or mobile obstacles during a balked landing as a result of wing-tip displacements that may occur while the aircraft is in flight or in contact with the runway surface.

1.2.5   This protection was considered to be necessary for the following reasons:

   a)   In category II operations when the runway visual range (RVR) is low, a pilot would not have sufficient time to avoid an obstacle even if seen. It was necessary, therefore, to ensure that there was an OFZ that would allow a pilot to safely continue an approach below the DH and, if necessary, to overshoot from any height below it; and

   b)   It is accepted that certain obstacles have to be permitted within the strip, but in 1971 there was very little guidance on the siting of these objects.

1.2.6   For this purpose, it was assumed that the precision approach instrument guidance system and the operational procedures employed would position the aircraft at the 30-m (100-ft) DH and displace it horizontally from the runway centre line by a distance not exceeding 15 m (50 ft). This could be interpreted as meaning that the cockpit would be within the red barrettes of the precision approach category II lighting system at a distance of approximately 300 m (1 000 ft) from the runway threshold, if the pilot could be certain, by means of the visual cues available, that the approach could be continued. To this must be added an allowance for the largest aircraft likely to carry out the operation having a wingspan of about 60 m (200 ft) and a buffer area for wing tip and obstacle clearance of 15 m (50 ft) either side, making a total width of 120 m (400 ft) at origin, i.e. 60 m (200 ft) either side of the runway centre line.

1.2.7   From this "window" it was further assumed that the aircraft would continue the approach down to and along the runway such that the outer wheels of the aircraft could be flying over the runway edge. It was agreed that a missed approach might be initiated at any point below the 30-m (100-ft) DH, and that the OFZ should therefore extend to the upwind end of the runway. Full protection would be provided if the missed approach was initiated no later than the end of the touchdown zone lighting and thereafter executed in accordance with provisional acceptable means of compliance balked landing performance requirements. The missed approach climb profile would thereby originate not more than 1 800 m (6 000 ft) from the runway threshold.
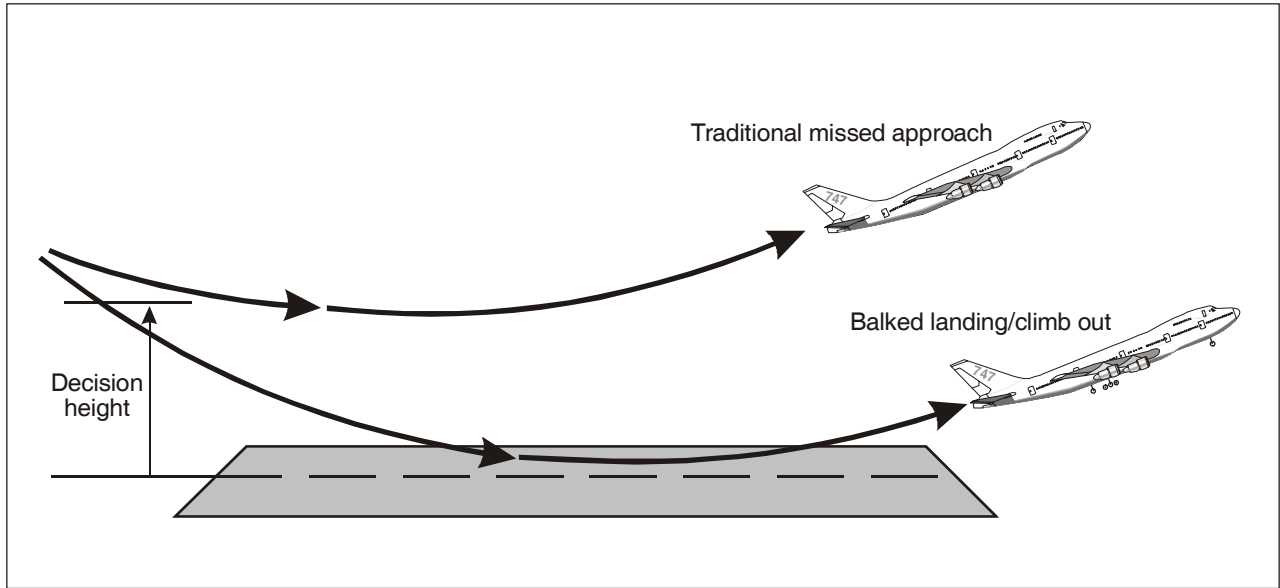
Figure 1-1.   Obstacle free zone (OFZ) critical events
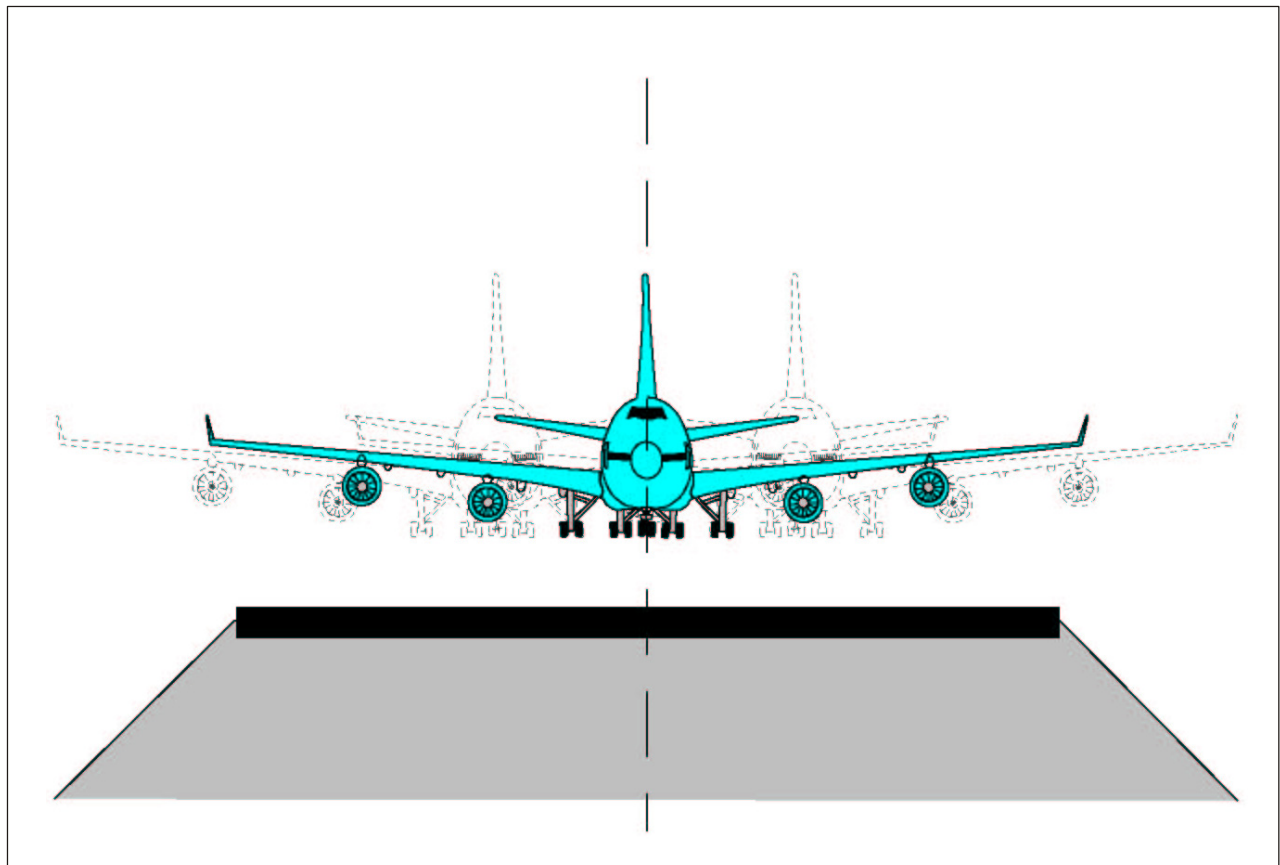
Figure 1-2.   Balked landing aircraft excursions

1.2.8   The Panel considered the advisability of limiting the length of the OFZ. A minority favoring this concept felt that 1 800 m (6 000 ft) represented adequate length and that extension of the OFZ to the end of the runway could impose unnecessarily stringent requirements, particularly in the case of very long runways. The majority considered that the advantages to be gained by such a limitation would be insufficient compared with the difficulties it would introduce. It also compromised the previously agreed concept of obstacle protection for the entire length of the runway. Furthermore, obstacle clearance in areas beyond the location of the missed approach plane was already provided by existing specifications relating to strips and take-off surfaces.

1.2.9   It was considered that a missed approach initiated below the DH would be a rare event. Consequently, the combined probability of such a missed approach and an engine failure occurring during the missed approach was too low as to be negligible and it was agreed that an all-engine missed approach could be assumed with an initial climb gradient of 3.2 per cent.

1.2.10   The Panel agreed that, with the operational limitations and parameters established in 1.2.8 and 1.2.9, it would be possible to specify an operational requirement for an OFZ for the Category II late missed approach case without requiring any change to the existing specifications in Annex 14, Chapter 4. In this regard it was recognized that the additional protection for aircraft envisaged in the OFZ also related to the following:

- Aircraft and vehicles on the ground in the vicinity of the runway, and

- Operationally essential facilities located within the runway strip, such as visual and radio aids

1.2.11   The majority felt that there was a valid differentiation between the tolerability adjacent to the OFZ of fixed obstacles, e.g. ILS glide path installations and mobile obstacles such as taxiing or holding aircraft. The minority felt that all obstacles, fixed and mobile, should be treated in the same way, i.e. there was no need for a specific surface for mobile obstacles. In developing its specification, the Panel considered the fin of a Boeing 747 aircraft as representing at that time the height of the critical mobile obstacle.

1.2.12   It was necessary to point out that the OFZ resulting from the above-mentioned assumptions and other criteria, e.g. aircraft performance, would relate to the existing environment. Therefore, the OFZ specifications would require review if larger aircraft types were introduced.

1.2.13   While the OFZ was limited to the category II operational situation, the dimensions might also be satisfactory in meeting the future requirements for category III operations, but this would require further study.

1.2.14   The Panel agreed that there should be total compliance with OFZ requirements and developed the following definitions and recommendations.

OCP/3 terminology and definitions

Mobile obstacle limitation surface. A specified surface, which defines a boundary above which no mobile obstacle or part thereof (e.g. an aeroplane) shall protrude.

Obstacle. All fixed and mobile objects, whether temporary or permanent, that extend above a defined surface intended to protect aeroplanes in flight or that are located on an area intended for the ground movement of aeroplanes.

Obstacle free zone (OFZ). A zone defined by surfaces which is kept clear of all fixed objects and, when operationally necessary, of all mobile objects. The OFZ is intended to afford aeroplanes protection from obstacles when approaches are continued below the DH and throughout a subsequent missed approach, with all engines operating normally, until a point is reached at which other prescribed obstacle clearance surfaces become effective.

OCP/3 Panel recommendations

OFZ application: An OFZ shall be established for each precision approach runway category I, II and III

OFZ general description: The limits of the OFZ shall be defined by:

- Surface A: a surface of specified dimensions coincident with a portion of the instrument approach surface

- Surface B: a surface which is coincident with a portion of the strip associated with a precision approach runway

- Mobile obstacle limitation surface

- Fixed obstacle limitation surface

OCP/3 OFZ dimensions

Surface A: Width is 60 m (200 ft) either side of the extended runway centre line
Length is 900 m (3 000 ft) from the inner edge of the approach surface

Surface B: Width is 60 m (200 ft) either side of the extended runway centre line
Length is equal to the length of the strip

Mobile obstacle limitation surface:

- Origin is 60 m (200 ft) either side of the runway centre line, to coincide as applicable with the outer edges of the surface B

- Limits are the inner horizontal surface

- Slope is 33.3 per cent (1:3)

- Length is equal to the length of the strip

Fixed obstacle limitation surface:

- Origin is the runway centre line

- Length is equal to the length of the strip

- Inner edge is the intersection of the mobile obstacle limitation plane

- Outer edge is the intersection of the transitional and inner horizontal surface

Note.— The dimensions result in an approximate slope of 10 per cent (1:10) for the fixed obstacle limitation plane.

1.2.15   The aim of the terminology and recommendations is to ensure that strips are clear of obstructions and that approach surfaces are not infringed. Only equipment essential to the conduct of an instrument approach, a landing or missed approach are permitted within the strip. It is also required that such objects be light and frangible as their design and function permit.

1.2.16   The proposed terminology and recommendations from OCP/3 were circulated to Contracting States and international organizations for comment. The responses suggested that there was a need for improvement; therefore, the Air Navigation Commission (ANC) agreed that the Panel should study the issue in more detail.

1.2.17   The Fourth Meeting of the OCP in November/December 1973, developed a revised proposal to incorporate the new obstacle clearance surfaces in Annex 14. It was also agreed that only frangible objects penetrating the zone would be permitted within the width of the strip. The revised proposal was accepted and incorporated in Amendment 30 to Annex 14, which became effective in June 1976. This was done for precision approach category II runway operations and became applicable to precision approach category III runway operations at the Fifth Meeting of the OCP in January 1976.

1.2.18   After developing a collision risk model (CRM) and new instrument approach-to-land procedures, the OCP at its Sixth Meeting in October 1978 gave attention to defining obstacle limitation surfaces for precision approach category I runway operations. This was necessary as the new approach procedures resulted in lower minima and the approach speed of jet transports resulted in reducing the pilot's "see and avoid" capability. Therefore, the concept of visual avoidance of obstacles was no longer practical.

1.2.19   Based on the recommendations of both the Sixth and Seventh Meetings of the OCP, it was decided at the ICAO Aerodromes, Air Routes and Ground Aids Divisional Meeting in April/May 1981, to include obstacle limitation surfaces for precision approach category I runway operations in Annex 14. Consequently, the OFZ was defined for all precision approach categories of operations.

1.2.20   In the Third Edition (1999) of Annex 14, the OFZ is defined to be the airspace above the inner approach surface, inner transitional surfaces and balked landing surface and that portion of the strip bounded by these surfaces which is not penetrated by any fixed obstacle other than a low-mass and frangibly mounted one required for air navigation purposes.

1.2.21   As stated in 1.2.2, the OFZ was originally intended to protect aircraft making an approach in conditions appropriate to precision approach category II when below the DH of 30 m (100 ft) and in the event of the need to execute a balked landing, i.e. a discontinued landing made with all engines operating and in the landing climb configuration. Due to the low visibility during these operations, pilots could not rely on visual reference to avoid any obstacle that may have been present within this zone. Thus, the former Annex 14 concept of permitting an obstacle to penetrate an obstacle limitation surface provided the obstacle was marked and lighted, was unacceptable for these operations.

1.2.22   In summary, the original inner approach surface, inner transitional surfaces and balked landing surface provided on a category II runway were designed to allow an aircraft with a wing span of up to 60 m (200 ft), below a DH of 30 m (100 ft), having been correctly aligned within the runway width and visual at that height, to climb at a gradient of 3.33 per cent and diverge from the runway centre line at a splay no greater than 10 per cent (due to heading/track hold). The gradient of 3.3 per cent was the lowest gradient permitted for an all-engines operating balked landing.

1.2.23   The horizontal distance of 1 800 m (6 000 ft) from a threshold to the beginning of the balked landing surface was based on the assumption that the latest point for initiating the missed approach would

be the end of the touchdown zone lighting, and that changes in aircraft configuration to obtain a positive climb gradient would normally require a further distance of 900 m (3 000 ft), equivalent to a maximum time of 15 s. The slope of 33.3 per cent for the inner transitional surfaces were the resultant surfaces using a climb gradient of 3.33 per cent with a splay of 10 per cent The splay of 10 per cent was based on the dispersion of recorded data found in research programmes conducted by two Contracting States.

Note.— The existing dimensions of the obstacle limitation surfaces along with other tables for pertinent aeroplane and aerodrome dimension data can be found in Appendix A. Illustrations of the obstacle limitation surfaces are found in Figures A-1 and A-2 in Appendix A.

1.2.24   When the dimensions of the wingspan and the outer main gear wheelspan of the Boeing 747-400 aeroplane are used for the maximum critical dimensions for the operating aeroplanes using the runway, the resulting OFZ dimension corresponds to that of code letter E. (The code letter E OFZ was originally based on an aircraft with 60 m wingspan, but this was subsequently increased to 65 m to accommodate the 747-400). Code letter F criteria refer to aerodromes where the wingspan of the largest aircraft using the runway is greater than that of the Boeing 747-400 but less than 80 m (262 ft). The balked landing study focused on code letter F aeroplane operations at existing aerodromes, i.e. aerodromes that were designed for code letter E operations.

1.3   THE DEVELOPMENT OF OFZ CRITERIA FOR CODE LETTER F AEROPLANE OPERATIONS

1.3.1   At the Eleventh Meeting of the OCP in March 1997, the following formula was used in the derivation of criteria for code letter F aeroplane operations, namely, the OFZ width along the runway strip:

Runway width – main gear outer tire edge to outer tire edge width + wingspan + buffer

The following dimensions were used in the calculation:

- Runway width: 60 m

- Main gear outer tire edge to outer tire edge: 15 m

- Wingspan: 80 m (code letter F)

- Buffer value: 30 m

1.3.2   Hence, the total OFZ strip width became 155 m. Figure 1-3 illustrates the horizontal view of the OFZ for both code letter E and code letter F aeroplanes. The figure also illustrates the OFZ definition used by the FAA. The FAA OFZ definition was dependent upon the airport elevation. At low elevation, it could be less restrictive than the ICAO OFZ, whereas, at higher airport elevation, the opposite could be true. The FAA minimum runway-to-taxiway design separation distance, as illustrated in Figure 1-3, may need to be increased with airport elevation to meet the runway OFZ standards. The ICAO minimum runway-to-taxiway design separation distance is based on the wingtip of the taxiing aircraft being clear of the runway strip.

1.3.3   The OCP felt that there was a need for a more scientifically driven derivation of the OFZ dimensions. This need was based primarily on the use of the size of the buffer value, which corresponded to how well the ILS system placed the aircraft on the approach relative to the runway centre line at DH. With accurate computer representations of modern aircraft, computer simulation methods could be used to better define a buffer value and estimate the dimensions of the OFZ. Furthermore, with thousands of computer

runs, a contour of equal probability could be statistically estimated to determine where to expect to find the location of the approaching aircraft if a given probability level were pre-defined. Such a probability level would be referred to as a target level of safety (TLS). The contour of equal probability would then be used to evaluate or define the dimensions of the OFZ based on the dimension of the critical aircraft.

1.3.4   Since the ICAO definition for the OFZ is designed to provide protection for aircraft executing a missed approach procedure below DH, it was agreed that there should be a data-collection effort focusing on the balked landing[2] scenario. Therefore, the simulation studies needed to examine this scenario in order to provide technical input to the definition for the OFZ dimension corresponding to future larger aeroplanes. Figure 1-4 illustrates the essential elements involved in an analysis of the dispersions involved in the study of the balked landing scenario. Study details are found in Part II, Chapters 2 to 7.
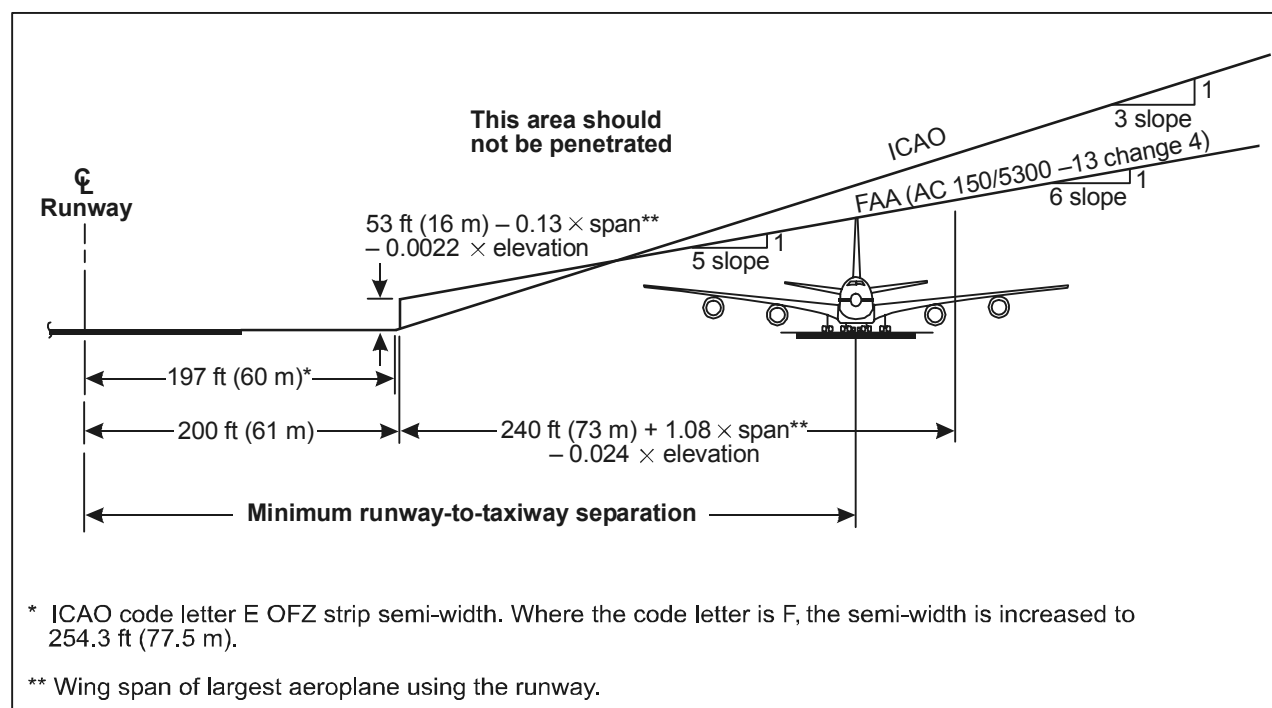
Figure 1-3.   ICAO and FAA obstacle free zone (OFZ) dimension criteria

---

2. The existing definition for Balked Landing was introduced at the 151st Session of the ICAO Air Navigation Commission in ICAO Memorandum C19-31/99-1 dated June 1999.

Critical factors:
• Pilot response
• Aeroplane performance
• Navigation aid
• Wind/weather

Rare events
performance
window

Iso-probability
contour and tunnel
for expected
aircraft position*

Missed approach
lateral displacement
distribution

Taxiway

Runway
₵

* The iso-probability contour corresponds to a given target level of safety
  and a given range position relative to the runway threshold.

Figure 1-4.   Balked landing dispersion analysis

_____

Chapter 2
BALKED LANDING ACCIDENT/INCIDENT DATA

2.1   INTRODUCTION

This chapter provides examples of actual balked landing-type events as recorded in ICAO and FAA database records. The database records and the FAA *Aviation Safety Statistical Handbook* were useful sources of information employed in the design of balked landing scenarios for the simulator trials and computer simulations. The scenarios are discussed in Part II, Chapter 3.

> *Note.*— *The following examples do not necessarily represent incidents directly applicable to the study. They should be viewed as demonstrating that balked landings do occur in a wide range of aircraft for a wide range of reasons. In some cases, the circumstances that produce the balked landing place them outside the intended scope of the OFZ protection.*

2.2   FAA DATA

2.2.1   The FAA publication, *Location of Commercial Aircraft Accidents/Incidents Relative to Runways* (DOT/FAA/AOV 90-1), Appendix 4 — *Listing of Landings Off the Runway*, documents only two balked landing incidents. The aircraft involved in both instances were DC-9s at small airports in the United States. The incident that occurred on 7 February 1983 in South Carolina is described as follows:

> Aircraft initially touched down partially on runway 1300′ from threshold, but continued rollout until it was entirely off runway. Aircraft became airborne at 1800′ from threshold and continued to Charlotte, North Carolina. Furthest distance from runway centerline was calculated to be 110′ (right of centerline). Instrument Meteorological Conditions. Missed approach delayed.

2.2.2   The record noted that the runway width was 46 m (150 ft), the length was 2 303 m (7 600 ft), and the surface conditions were dry. The remarks attribute the cause of the incident to a delay in the missed approach.

2.2.3   The second incident listed occurred on 10 February 1985 in Illinois as follows:

> X and Y distances are to the touchdown point. Instrument Meteorological Conditions. Aircraft attempting go around touched down then became airborne again and continued to St. Louis. Delayed directional control and improper use of procedure.

2.2.4   The record states that the touchdown point was at an X-distance of 274 m (900 ft) from runway threshold and a Y-distance of 28 m (91 ft) left of the runway centre line. The runway width was 46 m (150 ft), length of 2 469 m (8 100 ft), and the status was snow but dry. The cause of the incident was delay in directional control and improper use of procedure.

2.2.5   The FAA has developed a safety action plan for airport surface operations to reduce the occurrence of RIs. Nearly all RIs are caused by human error, i.e. the lapse of discipline or procedure. The

FAA is working with industry to find and implement RI techniques with prevention methods that act on pilots directly rather than those which require a controller to relay instructions to a pilot as a result of surveillance. According to these techniques, the risk of being involved in an RI is reduced by improving pilot and controller communication skills, pilot knowledge of airport taxiways and runways, and cockpit procedures.

2.3 ICAO DATA

2.3.1   From 1970 to 2004, the database in ICAO's Accident Investigation and Prevention Section contained about 600 reported accidents/incidents involving a missed approach and 60 reported accidents/incidents involving a balked (aborted) landing. Most of the aircraft documented were of an aircraft weight category of 5 700 kg (12 573 lb) or less. Almost 20 of the 60 records involved "heavy" or "large" aircraft, some of which were DC-10-10, B707-300,B737-500, B777-200, B747-400, A300, A320, A321, and an Antonov 12. A few of these events are summarized in 2.3.2 to 2.3.7.

2.3.2   In the incident involving the B707-300, the pilot missed the runway during the approach and executed a GA. During the GA, the aircraft touched the ground with the gear and number 1 and number 2 engines outside the runway. The aircraft diverted to another airport after another unsuccessful attempt to land. The record says that the approach was poorly executed and mismanaged and should have been aborted. In addition, the maximum landing weight was exceeded, pre-flight planning was incorrect, weather minima were ignored, and the DH procedure was not followed (28 November 1986).

2.3.3   In the incident involving the Boeing 747-400, as the aircraft descended through about 250 ft/76.2 m, it began to drift to the left. The pilot attempted to correct this but then decided to carry out a go-around. However, during this manoeuvre, the aircraft's number four engine struck the runway. The aircraft climbed away safely, but the oil pressure and quantity on the number four engine began to fall. The crew shut down the number four engine before returning for a safe landing. The accident happened in darkness (2230 London Time) with a runway visual range (RVR) of 3 000 m with the wind at 190° and 4 kt (6 January 1998).

2.3.4   An Airbus A320 was on final approach with strong, gusty surface winds in the forecast and present during the time of the approach, with the crew receiving frequent PIREPS (Pilot Weather Reports) and wind updates from ATC throughout the approach. There were no prior pilot reports of windshear. The autopilot was tracking the ILS until the captain manually flew (left side stick) from about 300 ft down. Manual tracking of the ILS was about as good as the autopilot. At approximately 200 ft, there was a strong gust followed by a significant increase in power from the autothrust (A/THR). The combination of these factors contributed to the crew's decision to go around. The aircraft reached about 15 ft AGL during the go-around. The flight diverted to a different airport (9 April 2000).

2.3.5   An Airbus A321 was cleared for an ILS approach with surface wind at 28 kt (maximum 40 kt). On short final, the aircraft encountered windshear. The pilot decided to go around and the tail hit the runway. After another approach and landing, inspection revealed the tail was scraped and the rear pressure bulkhead and nearby frame damaged (21 January 2002).

2.3.6   During the occurrence of a loss of separation incident, a close encounter between an arriving IFR flight (Airbus A319) and a departing IFR flight (MD80) occurred. Due to inadequate separation between the two aircrafts, ATC ordered a go-around procedure to the landing aircraft and a disruption of departure to the departing aircraft. Although the control tower called the departing aircraft several times, the pilot did not reply and the aircraft took off. The pilot of the overshooting aircraft had to initiate a visual avoidance action (1 March 2002).

2.3.7   A Boeing 777-200 performed a go-around because of a runway incursion with an Airbus A340 aircraft on departure. There was no aircraft damage (18 October 2003).

2.4   CONCLUSION

2.4.1   The review of the database records revealed that the following causal factors were involved in some of the aborted landings: fog, crosswind and horizontal gust, poor planning, improper operation, delayed decisions to abort the landing, lack of pilot experience on aircraft type, landing roll, collisions, distance misjudgement, excessive airspeed, improper landing flare, power loss, runway surface condition (wet), incorrect procedure, inadequate compensation for wind, excessive pilot self-confidence and excessive weight balance. Some of these factors were taken into consideration for the design of simulator trials that investigated the balked landing for this study.

_____

Chapter 3
BALKED LANDING
FLIGHT SIMULATOR TRIALS

OVERVIEW

To assess the risk of collision of an NLA operating to an aerodrome that does not meet Code F standards, an aeronautical study involving a series of full flight simulator trials and subsequent analysis was made. Simulator trials were flown at the NASA Ames facility in California, at the Airbus training centre in Toulouse and at the Zentrum für Flugsimulation Berlin. The trials examined the flight paths of aircraft conducting balked landings to assess the probability of infringement of the OFZ.

NASA AMES TRIALS

3.1   INTRODUCTION

3.1.1   A series of scenarios were designed to create situations where a pilot would abort a landing after descending below DH. These scenarios incorporated situations that actually occurred on landings with the intent to observe the flight track and measure pilot response times during the execution of a missed approach procedure. It was not possible to examine the loss of control experienced when there was a collision with an object; however, it was possible to observe the actions of the crew during a missed approach procedure to avoid collision with an object.

3.1.2   The FAA *Aviation Safety Statistical Handbook* lists surface deviation types under the category of pilot deviation as: take-off without clearance, take-off on wrong runway or taxiway, landing without clearance, landing or take-off below weather minimums, landing on wrong runway, airport or taxiway, entering taxiway or runway without clearance, careless or reckless aircraft operation. This information was referenced for possible causes of a balked landing while developing flight simulator scenarios.

3.1.3   The experimental scenarios, which took place in the NASA Ames FAA approved and certified Boeing 747-400 simulator, were designed to measure the pilot response times and observe aircraft simulator flight tracks during the occurrence of an RI, a VPD or a response to a simulated ATC command to abort a landing and execute a missed approach procedure.

3.1.4   The first part of this chapter summarizes some of the flight track data from the Boeing 747-400 NASA Ames simulator sessions based on the following: GA initiation mode (RI, VPD), height, flight mode (piloting with F/D or autopilot), runway surface condition (dry/wet), time of day (daytime/night-time), meteorological conditions, airport elevation and aircraft weight. The results provided input, understanding and design criteria for a Monte Carlo collision risk simulation conducted by the FAA.

3.2   BALKED LANDING SIMULATOR TRIALS
AT THE NASA AMES RESEARCH CENTER

3.2.1   Forty-five airline crew were used over a period of one year to conduct simulator sessions involving an aborted or balked landing as a result of RIs, VPDs or a response to simulated ATC commands to execute a missed approach after the crew descended below DH. A number of factors were included in the development of test scenarios as follows:

a)   GA initiation mode: RIs, VPDs, arrival/departure traffic on the runway, simulated ATC GA command;

b)   Pilot mode: with F/D or autopilot;

c)   GA initiation height for issuance of ATC GA command: 3 m (10 ft), 6 m (20 ft), 11 m (35 ft), 15 m (50 ft);

d)   Runway surface condition: dry/wet;

e)   Time of day: daytime/night-time;

f)   Meteorological conditions: ceiling, visibility, wind speed, wind direction, temperature;

g)   airport elevation: John F. Kennedy (JFK) in New York City, 3 m (12 ft); Guarulhos Intl. (GRU) in Sao Paulo, 762 m (2 500 ft); Denver Intl. (DEN) in Denver, 1.6 km (1 mi); Licenciado Benito Juárez Intl. (MMX) in Mexico City, 2 224 m (7 341 ft); and

h)   Aircraft weight (415 000 lb, 595 000 lb, 630 000 lb).

3.2.2   Each crew was given a pre-experimental briefing and informed that they would perform various test scenarios, such as landing, missed approach and departure, in random sequence under various conditions. There was a post-briefing at the conclusion of the test day to solicit the crew's comments on the experiments. In general, the crew felt that the scenarios were realistic and, in some instances, were previously experienced or reported by fellow pilots. The scenarios are briefly described in 3.2.3 to 3.2.9. The scenario lists are provided in the appendix to this chapter.

Description of test scenarios by GA initiation mode

3.2.3   The weather conditions were consistent with wind speed. The wind speed was 35-kt quarter wind from either left or right. Most scenarios were in daytime conditions; ten were in night. The meteorological conditions varied from category I to category III. Category II and III approaches had to be autocoupled. The pilot flying alternated between the captain and the co-pilot.

3.2.4   Some scenarios involved precipitation conditions and the friction coefficient in the simulator is 0.33 with medium breaking when the surface was wet; but most involved a dry runway. The aircraft weight was mainly fixed at 270 454 kg (595 000 lb) with a reference speed of 149 kt on final approach, which was selected so the Boeing 747-400 would have the weight characteristics of an NLA. This weight value was agreeable to and recommended by the two prime potential manufacturers of NLAs. The airport elevation varied from near sea level to that of Mexico City, which is 2 224 m (7 341 ft).

The simulated air traffic control (ATC) command

3.2.5   There was radio communication between the flight crew and the test crew in the experimental observers station (EOS) in the form of pilot/controller communications. At the EOS the flight

crew's avionics display was viewed by the test crew on a TV screen. The GA initiation height was experimentally controlled by the test controller observing the crew's radio altimeter readout. A command to "go-around" was given when the crew's radio altimeter displayed the height at which the approach was to be aborted. The controller addressed the crew with their call sign and issued GA commands at the following heights when required by the test scenario: 3 m (10 ft), 6 m (20 ft), 11 m (35 ft), or 15 m (50 ft). Most of the experiments were at either 3 m (10 ft) or 15 m (50 ft).

Runway incursion (RI)

3.2.6   All RIs involved the crew's decision to continue or abort landing. There were three types of RI events totaling 56 (some of which did not result in a balked landing). The majority of RIs involved an aircraft at the hold position encroaching on the runway for departure while the crew attempted to land. This event was triggered when the approaching aircraft crossed a certain height, which was set to 79 m (260 ft) with a small variation of 1.2 m (4 ft).

3.2.7   Another RI involved one aircraft at the runway threshold taking off while another attempted to land. The crew in the approaching aircraft continued to communicate with ATC while watching the departing aircraft on the runway for safe separation. The crew in the approaching aircraft expressed concern about executing a missed approach because they were not sure whether the departing aircraft might veer off into the flight path of the missed approach.

3.2.8   The other incursion event involved one aircraft arriving on the runway and stalling while exiting, leaving its tail sticking out over the runway. The other aircraft was attempting to land, but decided to abort when it realized the situation on the runway would not be resolved for some time.

Vehicle/pedestrian deviation (VPD)

3.2.9   This event involved an emergency vehicle located at a runway crossing. When the crew was at 79 m (260 ft) on the approach, the vehicle started to move towards the runway with its emergency light flashing. The pilot not flying noticed the moving vehicle and initiated a landing abort.

3.3   TEST RESULTS

3.3.1   The test scenarios were designed to result in a balked landing. Some balked landings resulted in a touchdown followed with a roll on the runway surface before initiating the climb. Touchdowns generally occurred when the crew responded to the simulated ATC GA command issued when the aircraft was 3 m (10 ft) above ground. (None of the RIs or VPDs resulted in a touchdown.) In those instances where there was a touchdown, the crew was about 1.5 m (5 ft) above ground when the TO/GA button was pressed; sometimes the TO/GA was pressed shortly after touchdown.

          Note.— Once the TO/GA button is pressed in a Boeing 747 aircraft, the navigation mode becomes track hold until lateral navigation (LNAV) is engaged. LNAV cannot be engaged before 120 m (400 ft) above the ground to avoid turning the aircraft before this height is reached.

3.3.2   The test scenario results are summarized in tabular form in Tables 3-1 to 3-4. Figures 3-1[1] to 3-3 provide information relating to the aircraft geometry and points of reference of the balked landings.

---

1.   All figures are located at the end of this chapter.

**Table 3-1.   NASA Ames Boeing 747-400 simulator
balked landing deviations at critical points — flight director data**

Event	Airport	Weather condition	Triggering event at height of aircraft on approach	TO/GA switch press coordinates at the start of GA μ/σ (feet)	Minimum airborne descent coordinates in the GA μ/σ (feet)	Maximum deviation from centre line during the GA μ/σ (feet)
Runway incursion (RI)						
900-ft ceiling	JFK RWY 4R		259 ft/4 ft	N = 16 X = −1368/355 |Y| = 19/11 Z = 98/17	N = 16 X = −766/319 |Y| = 20/13 Z = 79/15	N = 15 X = −785/600 |Y| = 24/12 Z = 92/10.6
300-ft ceiling	DEN RWY 35L		195 ft/4 ft	N = 8 X = −228/1311 |Y| = 18/15 Z = 133/81	N = 10 X = −353/289.5 |Y| = 15/10 Z = 77/14	N = 10 X = −710/448.4 |Y| = −20.4/12.1 Z = 94/3.8
Engine out on approaching aircraft	JFK RWY 4R		259 ft/4 ft	N = 9 X = −994/686 |Y| = 11/10 Z = 100/32	N = 9 X = −806/314 |Y| = 11/10.3 Z = 77/14	N = 10 X = −575/561 |Y| = 17/9.3 Z = 88/11.5
Traffic on runway						
Arrival	JFK RWY 4R		N/A	N = 6 X = −1004/1086 |Y| = 26/15 Z = 92.5/50	N = 6 X = −326/924 |Y| = 25/16.3 Z = 72/44	N = 5 X = −69/1066 |Y| = 30.3/17.1 Z = 87/8.3
Departure	DEN RWY 35L		685 ft/11.5 ft	N = 3 X = 783/1178 |Y| = 30/30 Z = 74/33	N = 3 X = 1147/1181 |Y| = 24/22 Z = 51/11.5	N = 3 X = 1820/1849 |Y| = 44/48.4 Z = 85/15
VPD	JFK RWY 4R		250 ft/4.5 ft	N = 17 X = −373/671 |Y| = 17/7.5 Z = 50/25	N = 17 X = 185/569 |Y| = 17/9 Z = 36/22.6	N =16 X = 114/1389 |Y| = 31.6/12.2 Z = 89.6/11
	DEN RWY 35L		330 ft/28 ft	N = 4 X = −355/587 |Y| = 14/3.7 Z = 78/23	N = 4 X = 323.5/470.6 |Y| = 11.3/5.1 Z = 58/25	N = 4 X = −658/173 |Y| = 15.5/2.5 Z = 93.3/1.8
ATC-commanded go-around (GA)						
GA at 20 ft	JFK RWY 4R		GA command issued at 20 ft	N = 5 X = 736/271 |Y| = 12/5.9 Z = 9.6/5.6	N = 5 X = 1227/364 |Y| = 15/12 Z = 3.6/2.6	N = 6 X = 1678/1906 |Y| = 36/22 Z = 65/25.7
GA at 35 ft	JFK RWY 4R		GA command issued at 50 ft	N = 6 X = 505/232 |Y| = 9.7/8.1 Z = 16/3.7	N = 6 X = 894/290 |Y| = 12.5/6.5 Z = 9.7/3.1	N = 6 X = 2186/312 |Y| = 49/17 Z = 82/31.5
GA at 50 ft	DEN RWY 35L		GA command issued at 50 ft	N = 6 X = 390/353 |Y| = 21/10 Z = 23/8.5	N = 7 X = 789/21.5 |Y| = 21.6/12.7 Z = 16/7.2	N = 8 X = 988/1669 |Y| = 52/30 Z = 81/25
R = right L = left N = number of data points (sample size)						

**Table 3-2.   NASA Ames Boeing 747–400 simulator
balked landing deviations at critical points — autopilot data**

Event	Airport	Weather condition	Triggering event at height of aircraft on approach	TO/GA switch press coordinates at the start of GA μ/σ (feet)	Minimum airborne descent coordinates in the GA μ/σ (feet)	Maximum deviation from centre line during the GA μ/σ (feet)
Runway incursion (RI)						
900-ft ceiling	JFK RWY 4R		261 ft/4 ft	N = 6 X = −1624/373 |Y| = 7.14/0.15 Z = 112/20	N = 6 X = −832.5/365.3 |Y| = 6.9/0.4 Z = 84.5/17.6	N = 5 X = −948/614 |Y| = 7.1/0.6 Z = 95/5
300-ft ceiling	DEN RWY 35L		195 ft/4 ft	N = 7 X = −802/239 |Y| = 7/0.5 Z = 90/11	N = 8 X = 213/227 |Y| = 6.2/0.4 Z = 54/10	N = 8 X = −500/746 |Y| = 7.4/0.6 Z = 94/8
Engine out on approaching aircraft	N/A	N/A	N/A	N/A	N/A	N/A
Traffic on runway						
Arrival	JFK RWY 4R		N/A	N = 6 X = −2078/999 |Y| = 7.9/1.5 Z = 136/52	N = 6 X = −1256.8/978.3 |Y| = 7.3/0.6 Z = 106/50.5	N = 3 X = −525/457 |Y| = 6.72/0.03 Z = 67/22
Departure	N/A	N/A	N/A	N/A	N/A	N/A
VPD	JFK RWY 4R		251 ft/3.6 ft	N = 16 X = −640/657 |Y| = 7.2/1.4 Z = 66/31	N = 16 X = 105/601 |Y| = 6.6/2.6 Z = 41/29	N = 15 X = −1107/381 |Y| = 7.4/1.0 Z = 89/16
	DEN RWY 35L	N/A	N/A	N/A	N/A	N/A
ATC-commanded go-around (GA)						
GA at 20 ft	JFK RWY 4R		GA command issued at 20 ft	N = 5 X = 652/54 |Y| = 5.05/0.89 Z = 11/1.2	N = 5 X = 1193/119.5 |Y| = 3.2/1.7 Z = 4.1/1.3	N = 6 X = −1079/403 |Y| =8/2.4 Z = 88/20.5
GA at 35 ft	JFK RWY 4R		GA command issued at 35 ft	N = 6 X = 377/123 |Y| = 6.6/0.49 Z = 17.6/2.3	N = 6 X =878/114 |Y| = 5.5/0.9 Z = 8.5/1.4	N = 6 X = −1275/59 |Y| = 8/0.6 Z = 97.5/2.2
GA at 50 ft	JFK RWY 4R		GA command issued at 50 ft	N = 7 X = 280/238 |Y| = 6.5/0.5 Z = 21.6/5.6	N = 7 X = 789/61 |Y| = 4.9/0.8 Z = 11/1.4	N = 7 X = −803/1197 |Y| = 15/18 Z = 95/5
R = right L = left N = number of data points (sample size)						

**Table 3-3. NASA Ames Boeing 747–400 ATC-commanded GAs at 10 ft
that resulted in ground roll — flight director data**

Aircraft landing weight condition	Airport	Weather condition	TO/GA switch press height μ/σ (feet)	Coordinates at start of ground roll touchdown μ/σ (feet)	Coordinates at end of ground roll lift-off μ/σ (feet)	Roll distance μ/σ (feet)	Maximum deviation from centre line during ground roll μ/σ (feet)
Heavy							
630 000 lb	MMX RWY 23L		N = 7 μ = 0.5 ft σ = 5.5 ft	N = 7 X = 1393/651 |Y| = 45.4/17	N = 7 X = 1908/566 |Y| = 53/18	N = 7 μ = 516 ft σ = 353 ft	N = 7 X = 1889/585 |Y| = 53/18.2
Light							
415 000 lb	MMX RWY 23L		N = 2 μ = 11 ft σ = 9.4 ft	N = 2 X = 1702/28 |Y| = 54/0.4	N = 2 X = 1892/57 |Y| = 57.4/2.7	N = 2 Max = 260 ft Min = 119 ft	N = 2 X = 1892/71.5 |Y| = 57.4/2.7
Typical							
595 000 lb	JFK RWY 4R		N = 12 μ = 1.9 ft σ = 3.5 ft	N = 12 X = 1324/636 |Y| = 15.1/9.0	N = 12 X = 1937/591 |Y| = 9.9/7.0	N = 12 μ = 614 ft σ = 364 ft	N = 12 X = 1406/678 |Y| = 16/8.2
595 000 lb	JFK RWY 4R	Wet runway	N = 2 μ = 0.0 ft σ = 0.0 ft	N = 2 X = 1014/3.7 |Y| = 11.4/3.5	N = 2 X = 2028/1252 |Y| = 12.7/2.3	N = 2 Max = 1897ft Min = 131 ft	N = 2 X = 1510/520 |Y| = 15.2/1.2
595 000 lb	DEN RWY 35L		N = 6 μ = 1.7 ft σ = 4.2 ft	N = 6 X = 1802/706 |Y| = 19.8/7.4	N = 6 X = 2506/676 |Y| = 12.1/7.7	N = 6 μ = 704 ft σ = 393 ft	N = 6 X = 1849/771 |Y| = 20.4/6.6
595 000 lb	MMX RWY 23L		N = 1 μ = 0.0 ft σ = N/A	N = 1 X = 1944 |Y| = 11	N = 1 X = 2250 |Y| = 6.1	N = 1 μ = 306 ft σ = N/A	N = 1 X = 1944 |Y| = 11
R = right　L = left　N = number of data points (sample size)							

Figure 3-1 is the top view of the Boeing 747-400 showing the aircraft reference point, i.e. the CG, at the intersection of the aeroplane centre line and the point 25 per cent along the mean aerodynamic chord (MAC). It also shows the horizontal distance from the centre line to the outer edge of the tire of the wing-mounted gear to be 6 m 10 cm (20 ft 4 in).

3.3.3　　　　Figure 3-2 gives correction equations for the location of wheel bottom in the aft assembly of the wing-mounted gear. This is a virtual wheel located in the vertical plane that divides the fuselage into two halves. It shows the location of the wheel in reference to the CG as a function of aircraft pitch and roll. This is the reference point for touchdown and wheel height in Figures 3-1 to 3-10D.

3.3.4　　　　Figure 3-3 shows the vertical and lateral track of an aircraft during a balked landing. The aircraft's CG denotes its lateral position, while the wheel height (bottom of the main landing gear) represents vertical position. Unless otherwise noted, these references are retained throughout the report. The upper graph shows the lateral deviation from the runway centre line as the aircraft CG approaches and then passes the runway threshold. The lower graph shows the corresponding height of the main landing gear above ground level (AGL). The abscissa is the same for both graphs; consequently, the graphs correspond to top and side views, respectively, of the aircraft path over the runway.

**Table 3-4.   NASA Ames Boeing 747–400 ATC-commanded GAs at 10 ft
that resulted in ground roll — autopilot data**

Aircraft landing weight condition	Airport	Weather condition	TO/GA switch press height μ/σ (feet)	Coordinates at start of ground roll touchdown μ/σ (feet)	Coordinates at end of ground roll lift off μ/σ (feet)	Roll distance μ/σ (feet)	Maximum deviation from centre line during ground roll μ/σ (feet)
Heavy							
630 000 lb	JFK RWY 4R			N = 6 X = –1624/373 |Y| = 7.14/0.15 Z = 112/20	N = 6 X = –1624/373 |Y| = 7.14/0.15 Z = 112/20	N = 6 X = –832.5/365.3 |Y| = 6.9/0.4 Z = 84.5/17.6	N = 5 X = –948/614 |Y| = 7.1/0.6 Z = 95/5
Light							
415 000 lb	N/A	N/A		N/A	N/A	N/A	N/A
Typical							
595 000 lb	JFK RWY 4R		N = 11 μ = 4.9 ft σ = 1.7 ft	N = 11 X = 1474/260 |Y| = 1.5/1.0	N = 11 X = 1916/335 |Y| = 3.6/1.5	N = 11 μ = 442 ft σ = 158 ft	N = 3 X = 1843/411 |Y| = 3.8/1.0
595 000 lb	JFK RWY 4R	Wet runway	N = 4 μ = 5.5 ft σ = 0.8 ft	N = 4 X = 1492/42 |Y| = 3.5/0.3	N = 4 X = 1822/226 |Y| = 1.3/1.2	N = 4 μ = 330 ft σ = 243 ft	N = 4 X = 1492/43 |Y| = 3.5/0.3
595 000 lb	GRU RWY 9R		N = 5 μ = 5.2 ft σ = 0.6 ft	N = 5 X = 1745/417 |Y| = 3.6/4.3	N = 5 X = 2157/431 |Y| = 5.2/3.1	N = 5 μ = 412 ft σ = 214 ft	N = 5 X = 2072/608 |Y| = 5.3/3.4
595 000 lb	DEN RWY 35L		N = 8 μ = 3.4 ft σ = 1.1 ft	N = 8 X = 1752/59 |Y| = 1.4/1.0	N = 8 X = 2451/234 |Y| = 7.8/2.9	N = 8 μ = 699 ft σ = 190 ft	N = 8 X = 2434/239 |Y| = 7.7/3.0
595 000 lb	JFK RWY 4R	Category III, no visibility	N = 3 μ = 5.5 ft σ = 0.7 ft	N = 3 X = 1547/188 |Y| = 1.9/0.7	N = 3 X =1894/156 |Y| = 3.0/1.9	N = 3 μ = 348 ft σ = 271 ft	N = 3 X = 1810/291 |Y| = 3.1/1.6
595 000 lb	MMX RWY 23L	Category III, no visibility	N = 4 μ = 4.0 ft σ = 0.8 ft	N = 4 X = 1699/84.6 |Y| = 1.2/0.4	N = 4 X = 2177/348 |Y| = 3.9/3.3	N = 4 μ = 480 ft σ = 376 ft	N = 4 X = 2141/407 |Y| = 4.3/2.8
R = right L = left N = number of data points (sample size)							

3.3.5   Figures 3-4 to 3-10 A, B, C and D illustrate the test scenario results. "A" and "B" figures show the mean (average) values of the data by event type while "C" and "D" figures show the data (scatter plots) for all crew. The "A" and "C" figures refer to scenarios in which the F/D was used during the approach, and the letters "B" and "D" figures refer to when the autopilot was used.

3.3.6   Figures 3-4A and B show the height at which the TO/GA switch was pressed for a variety of balked landing scenarios where there was no touchdown on the runway. Figures 3-5A and B show the corresponding minimum wheel height reached as a result of height loss before the start of climb, and Figures 3-6A and B show the lateral deviation from runway centre line at minimum height. Figures 3-7A and B show the maximum lateral deviation from centre line observed during the course of the balked landing above ground to a height of 30 m (100 ft) and Figures 3-8A and B show the mean height at which the maximum lateral deviation was observed.

3.3.7   Figures 3-9A and B, and 3-10A and B show the mean ground path when the aircraft executed a rollout before climb for a variety of conditions. These conditions involved dry and wet runway, heavy and light aircraft weight and different runway elevations. The deviations correspond to the absolute value and, therefore, are independent of wind direction. The auto-coupled approaches are close to the runway centre line.

3.3.8   Figures 3-10A and B show that at a high elevation (Mexico City), the crew deviated farthest from the runway centre line when the approach was made with the F/D — the average deviation was 16 m (53 ft). However, the autopilot kept the crew very close to centre line with an average deviation of about 1.2 m (4 ft). The touchdowns were hard upon contact at the high elevations.

3.3.9   As stated in 3.3.6, Figures 3-7A and B show the maximum lateral deviation from centre line observed during the approach/climb from the ground to 30 m (100 ft) for an RI or VPD. The value of 30 m (100 ft) was selected because the bottom of the wheel of the main gear in a Boeing 747-400 is about 6 m (20 ft) below the point of CG, and it was not expected that the top of the tail of an NLA would be much more than 24 m (80 ft) above the ground. Therefore, once an aircraft is above 30 m (100 ft), it is not likely to collide with the tail of any aircraft.

3.3.10   For example, in a VPD the figures suggest that, on average, the maximum lateral deviation occurs when the aircraft is 10 m (32 ft) from the runway centre line (Figure 3-7A) and at an average height of 27 m (90 ft) above ground (Figure 3-8A) when the approach is made with the F/D. When the approach is coupled with the autopilot, the lateral deviation, on average, is reduced to 2.4 m (8 ft) from the centre line (Figure 3-7B) at an average height of 25 m (85 ft) above the ground (Figure 3-8B). These observations suggest that when an RI is involved where there is no touchdown, the maximum deviation from centre line will occur in the air and is greatly reduced when the approach is coupled with the autopilot.

Additional observations

3.3.11   It was observed that when an ATC-commanded GA was issued after the aircraft had crossed the runway threshold, in some instances the aircraft touched down before it started to climb. When there was traffic on the runway, the delay in pressing the TO/GA switch was due to the fact that the crew was busy watching the traffic and communicating with the controller about a concern for loss of separation. RIs by aircraft at the holdbar resulted in earlier execution of the GA than incursions from aircraft on the runway.

3.3.12   Figure 3-4A illustrates this for approaches with the F/D. The incursion from the VPD resulted from the vehicle crossing the runway at an intersection further away from threshold; therefore, the crew was closer to the ground during a VPD than during an RI when TO/GA was pressed.

3.3.13   Figure 3-6A shows the mean lateral deviation from centre line at minimum wheel height. In all the causal events, the aircraft CG was no more than 11 m (35 ft) from the centre line at the point of minimum descent before the start of climb, even in the engine-out condition. Figure 3-6B shows that during the autoland condition, the aircraft CG was close to centre line.

3.4   CONCLUSION

3.4.1   The trials conducted at the NASA Ames Research Center on the Boeing 747-400 simulator suggest that any further study take into consideration the following:

          a)   The impact of the autopilot on reducing the lateral deviation from centre line during the occurrence of a balked landing;

   b)   The impact of airport elevation on the lateral deviation from centre line during the balked landing; and

   c)   The impact of when the TO/GA switch is pressed, especially close to the ground on the balked landing.

3.4.2   The subsequent collision risk analysis took into account the above considerations using the FAA ASAT as the analysis tool.

BERLIN AND TOULOUSE TRIALS

3.5   INTRODUCTION

3.5.1   The intent of the balked landing study has always been the development of information relative to a "generic" NLA with modern avionics (including track hold guidance during the go-around manoeuvre). The current study is broad in that it captures a range of design philosophies that may be employed in the development of New Larger Aeroplanes. It is not the intent of the study to compare the merits of the different design technologies.

3.5.2   A series of scenarios were designed to create situations where pilots could conduct a balked landing. The intent of these scenarios was to validate the existing study results for the autopilot and complete a flight director analysis well before the entry into service of the first NLA in order to allow States and individual airports the maximum time to consider the applicability of the results to their requirements. For the autopilot case, the method used was to verify that the results of the ASAT computations could be generalized to include the autoland and auto go-around performance of an A340/NLA. The verification process consisted of obtaining sufficient flight simulator data to assess the conformance of the Airbus results to the earlier 747-400 autopilot data to allow the generalization.

3.5.3   The A340/NLA autopilot and flight control systems would be an evolution of the A340 systems, and Airbus advised that the A340 results would be representative of A340/NLA flight paths during a balked landing. Therefore, trials on A340 full flight simulators were arranged, initially in Toulouse at the Airbus training centre, and subsequently at the independent Zentrum für Flugsimulation (ZFB) at the Technical University in Berlin.

3.5.4   The original plan for the investigation of flight director-guided balked landings expected to use a computer simulation of a human pilot steering the NLA model which could be used to perform Monte Carlo analysis as similarly planned for the autopilot study. Pilot models have been under development by two research organizations but could not be made available to meet the desired schedule. To collect data for the autopilot validation and for flight director studies, an intensive flight simulator study was initiated.

3.5.5   The OCP agreed that an Extreme Value Analysis (EVA) of the A340 full flight simulator data would be an acceptable alternative method for determining the probability of infringement of the OFZ. The EVA method required revision of the NASA Ames scenarios to focus on limiting cases of the parameters of ceiling, RVR and balked landing initiation height. Changes were also made to the scenario list to specifically examine the effect of wind on the go-around tracking performance and to ensure that the de-crabbing effects were properly addressed. The very low RVR precluded the use of runway conflicts (aircraft or other intrusions). The GA was commanded either by a controller call or by using a new method of forcing the GA by removing pilot visual reference with the ground.

3.6   BALKED LANDING SIMULATOR TRIALS
AT AIRBUS TRAINING FACILITY AND ZFB, TECHNICAL UNIVERSITY OF BERLIN

3.6.1   Simulator autoland approach trials took place at the manufacturer facilities on 2–3 April 2004. Sessions focusing on flight director approaches were then done in Toulouse from May to August 2004, with an intensive series from June to August. Subsequently, the major part of the F/D trials were flown from 24 August to 3 September 2004 at the Technical University of Berlin.

3.6.2   The flight crew for the flight director Toulouse trials involved an Austrian Airlines crew and Airbus Training Department staff with major airlines background (Lufthansa, Sabena, Middle East Airlines and Air Liberté). For the sessions with the Airbus crew, the right seat was occupied by a test pilot who performed the pilot non-flying tasks.

3.6.3   For the Berlin trials, complete crews (captain and first officer) were provided by Lufthansa and Air France. A total of 28 pilots took part in the data collection. Scenarios were randomized to counter the influence of familiarity or fatigue on the results. Normal crew procedures were used, except that pilots alternated approaches to reduce fatigue, whereas, for example, some company procedures precluded co-pilots flying autopilot approaches.

3.6.4   All the A340-300 full flight simulators were qualified at level D, with a maximum landing weight of 183 t (403 446 pounds) or 181 t (399 037 pounds). The engines simulated were CFM 56-5C4 at Toulouse and -5C2 at Berlin. The scenario weights were chosen to provide a similar thrust/weight ratio to that of an A380 (see Appendix A) at expected landing weights, and at Toulouse where the engine thrust was a higher rating; the weight was the maximum landing weight.

3.6.5   In order to allow subsequent analysis of the crosswind effect, a range of crosswinds were used in the scenarios. The balked landing heights were set at 70, 40 and 10 ft. In Toulouse, the GA controller call or activation of the loss of visual reference was managed from the instructor station in the rear of the simulator cab, whereas in Berlin they were managed by a computer at a specific radar altitude (RADALT), using prerecorded instructions for the controller call.

3.6.6   Some differences between the simulator numerical settings and the perceived weather were noted. A simulator RVR of 1000 m was assessed by a technical pilot as effectively being 600 m. This is significant as many operators have operational crosswind limits, often as low as 10 kt, that come into effect at RVRs down to 800 m. Such limitations will affect the probability of exposure to the higher wind scenarios.

3.6.7   The scenario lists at Berlin and Toulouse are provided in the appendix to this chapter.

3.7   TEST RESULTS

3.7.1   Over 500 approaches were flown in all the full flight simulator trials, with about 75% being flight director approaches.

3.7.2   The autopilot approaches were examined and found to be suitable for the generalization of the ASAT autopilot study results (to be discussed in Part II, Chapter 6) to include the A340/NLA.

3.7.3   The climb performance (for both autopilot and flight director GAs) significantly exceeded the assumed 3.3% used in selecting the slope of the OFZ. In some of the 10 ft GA cases, the GA was initiated after the pilot had retarded the thrust levers for landing. This led to a longer portion of the flight path at low altitude, or in some cases ground roll, while the engines accelerated.

          Note.— For Airbus A340 and later aircraft, when the pilot places the thrust levers in the TO/GA position for a go-around, the flight director commands the pitch GA and roll GA track modes automatically; if the autopilot is engaged, it follows the same orders.

3.7.4   The flight director results showed bigger variations in track with the different piloting techniques. A particular effect was for the GA executed at 40 and 10 ft, as the pilot may have de-crabbed the aircraft for touchdown. Depending on the accuracy of this manoeuvre, the stored track for the GA may have been disturbed.

3.7.5   The aim of the loss of visual reference was to obtain representative pilot rotation rates. In the event, large differences in rotation rates were noted due to other reasons, such as specific training on tail strike awareness on other types of aircraft. Conversely, it was noted that on the controller call GAs, a majority of pilots made a deliberate effort to visually align the track with the runway prior to losing visual reference during the GA.

3.7.6   The test scenario results are summarized in tabular form in Tables 3-5 to 3-7. Figures 3-11A illustrates the x-y position of the aircraft at the lowest point of the operation for the autopilot runs. For those tracks which involved ground rolls, the point plotted is the initial touchdown point. Figure 3-11B is the same data for the flight director runs. The maximum deviation from centre line for the autopilot is shown in Figure 3-12A and for the flight director in Figure 3-12B.

**Table 3-5.   Berlin and Toulouse Airbus A340-300 simulator
balked landing deviations at critical points — flight director data**

Event	Airport	Weather condition	Triggering event at height of aircraft on approach	"GA initiation" coordinates μ/σ (feet)	Minimum airborne descent coordinates in the GA μ/σ (feet)	Maximum deviation from centre line in the GA μ/σ (feet)
ATC-commanded go-around (GA)						
GA at 10 ft			GA command issued at 10 ft	N = 45 X = 427/247 |Y| = 15/13 Z = 8/9	N = 45 X = 683/156 |Y| = 18/17 Z = 7/7	N = 45 X = 1673/1043 |Y| = 28/17 Z = 67/51
GA at 40 ft			GA command issued at 40 ft	N = 29 X = 16/387 |Y| = 14/10 Z = 37/16	N = 29 X = 550/274 |Y| = 12/11 Z = 20/13	N = 29 X = 1479/1025 |Y| = 25/13 Z = 90/40
GA at 70 ft			GA command issued at 70 ft	N = 31 X = −367/177 |Y| = 16/12 Z = 50/7	N = 31 X = 221/184 |Y| = 16/12 Z = 29/8	N = 31 X = 712/827 |Y| = 13/86 Z = 86/38
Visual loss go-around (GA)						
GA at 10 ft			GA command issued at 10 ft	N = 36 X = 422/293 |Y| = 15/10 Z = 11/10	N = 36 X = 942/304 |Y| = 14/8 Z = 6/6	N = 36 X = 1761/1013 |Y| = 34/20 Z = 63/51
GA at 40 ft			GA command issued at 40 ft	N = 48 X = −7/200 |Y| = 15/9 Z = 28/8	N = 48 X = 524/187 |Y| = 12/9 Z = 11/8	N = 48 X = 996/974 |Y| = 25/19 Z = 68/48
GA at 70 ft			GA command issued at 70 ft	N = 50 X = −375/297 |Y| = 14/9 Z = 52/14	N = 50 X = 326/355 |Y| = 13/10 Z = 30/15	N = 50 X = 856/1041 |Y| = 25/15 Z = 79/42
N = number of data points (sample size)						

**Table 3-6.   Berlin Airbus A340-300 simulator
balked landing deviations at critical points — autopilot data**

Event	Airport	Weather condition	Triggering event at height of aircraft on approach	"GA initiation" coordinates μ/σ (feet)	Minimum airborne descent coordinates in the GA μ/σ (feet)	Maximum deviation from centre line in the GA μ/σ (feet)
ATC-commanded go-around (GA)						
GA at 10 ft			GA command issued at 10 ft	N = 0	N = 0	N = 0
GA at 40 ft			GA command issued at 40 ft	N = 15 X = 186/67 |Y| = 11/0.5 Z = 28/2.7	N = 15 X = 722/55 |Y| = 10/0.5 Z = 13/1.8	N = 15 X = 231/110 |Y| = 11/0.5 Z = 26/4.3
GA at 70 ft			GA command issued at 70 ft	N = 29 X = −374/108 |Y| = 12/1.0 Z = 52/4.4	N = 29 X = 256/122 |Y| = 11/0.9 Z = 28/3.2	N = 29 X = −306/143 |Y| = 12/1.0 Z = 48/6.6
Visual loss go-around (GA)						
GA at 10 ft			GA command issued at 10 ft	N = 12 X = 568/173 |Y| = 6/0.5 Z = 11/4.7	N = 12 X = 983/141 |Y| = 5/0.4 Z = 4/2.6	N = 12 X = 985/913 |Y| = 7/1.9 Z = 35/47
GA at 40 ft			GA command issued at 40 ft	N = 14 X = 6/55 |Y| = 11/0.5 Z = 30/2.5	N = 14 X = 492/43 |Y| = 11/0.5 Z = 16/1.5	N = 14 X = 79/84 |Y| = 11/0.4 Z = 28/2.9
GA at 70 ft			GA command issued at 70 ft	N = 0	N = 0	N = 0
N = number of data points (sample size)						

3.7.7   The flight director tracks generated from the simulator trials provided input data for the Extreme Value Analysis (EVA). The EVA will evaluate the risk of an NLA, while conducting a balked landing, infringing upon the airspace protected by the OFZ. The details of this analysis and its conclusions are found in Part II, Chapter 7.

3.7.8   The balked landing rate was not adjusted for the distribution between autopilot and flight director approaches. Another technique was mentioned by some of the test crews but was not used in the trials. Some operators advocate, in adverse conditions that are short of category II or III, the use of the autopilot down to the category I minima followed by disconnection and manual landing. This does not require that special procedures be implemented, but it is conceived that this technique would produce a smaller lateral deviation relative to an all manual-flown approach.

3.8   CONCLUSIONS

The data collected at Berlin and Toulouse for the scenarios discussed were subsequently analysed by the FAA using the methodology of Extreme Value Analysis. Details of the analysis (which also includes the data set from NASA Ames) are found in Part II, Chapter 7.

**Table 3-7.   Berlin and Toulouse Airbus A340-300 simulator
balked landing deviations during ground roll**

Event	Airport	Weather condition	Coordinates at start of ground roll touchdown μ/σ (feet)	Coordinates at end of ground roll touchdown μ/σ (feet)	Roll distance μ/σ (feet)	Maximum deviation from centre line during ground roll μ/σ (feet)
Flight director data						
			N = 84 X = 709/321 |Y| = 13/8.9	N = 84 X = 1083/331 |Y| = 12/8.3	N = 84 X = 373/16.5	N = 84 |Y| = 15/8.4
Autopilot data						
			N = 3 X = 1189/165 |Y| = 5.1/1.3	N = 3 X = 1267/106 |Y| = 4.7/1.0	N = 3 X = 79/108	N = 20 |Y| = 5.1/1.3
N = number of data points (sample size)						

— — — — — — — —
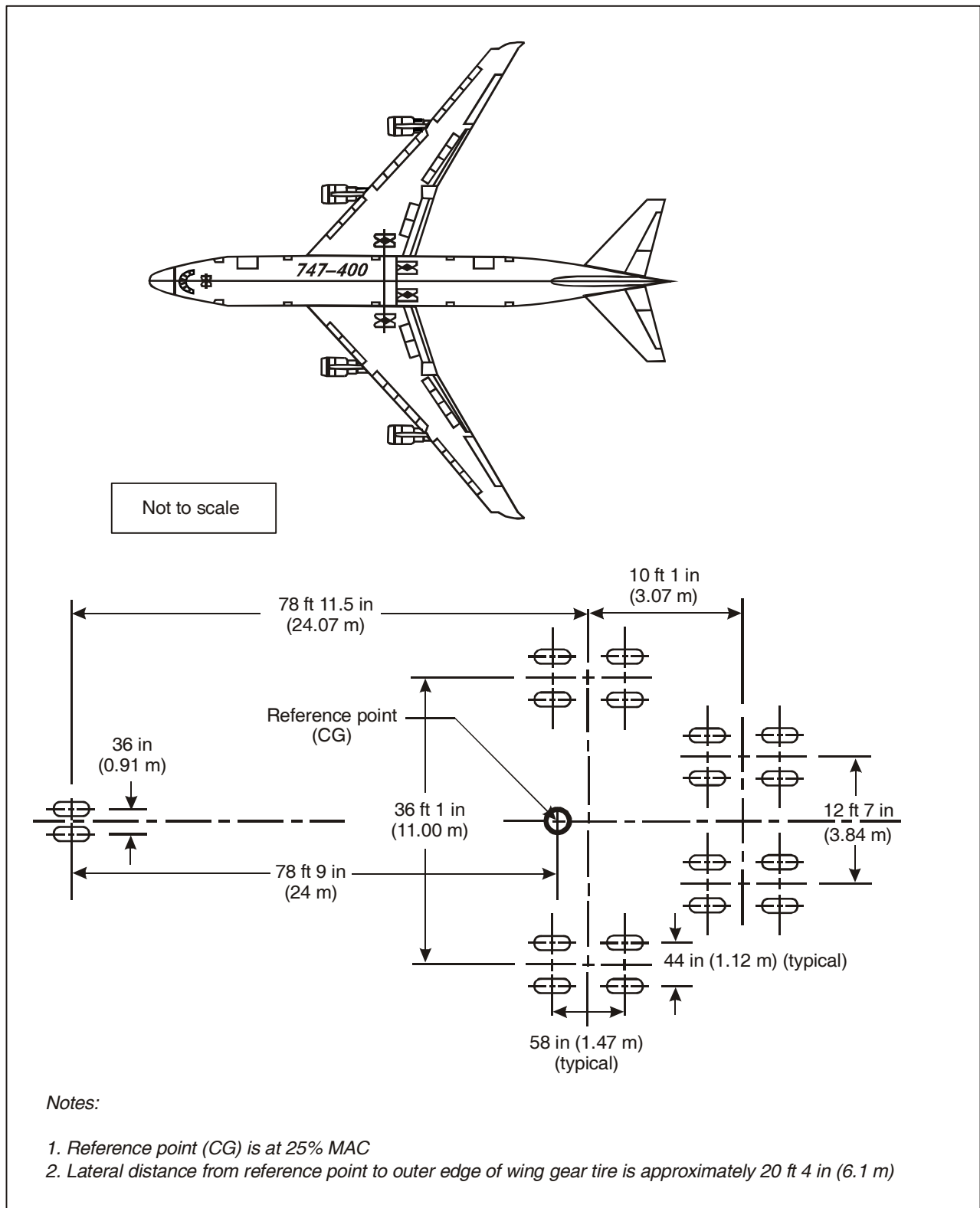
Figure 3-1.   Location of aeroplane reference point for 747-400 aircraft
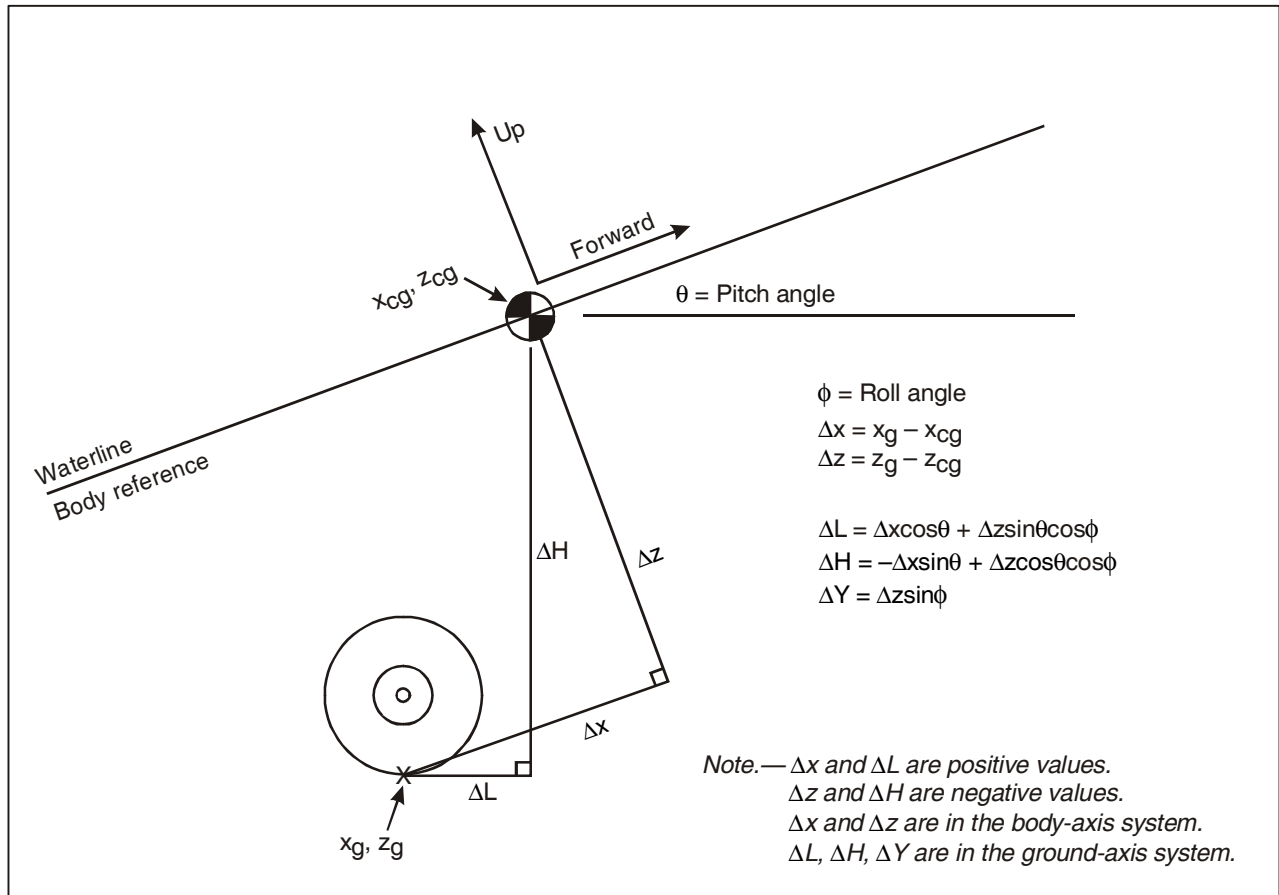
Figure 3-2.   Correction equations calculated from centre of gravity (CG) to lowest tire point
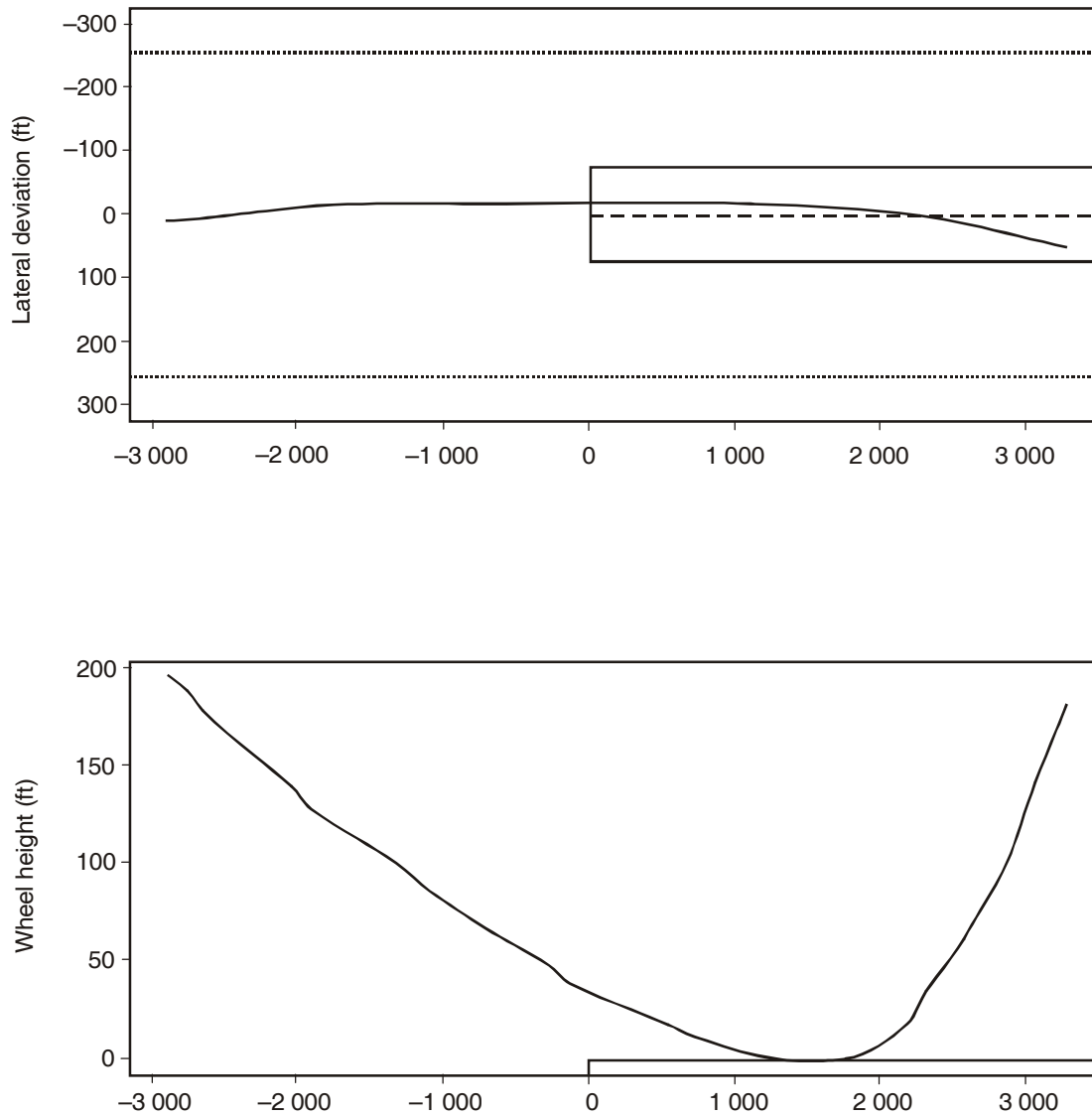
**Figure 3-3.   Aircraft trajectory for balked landing — distance from threshold (ft)
(Example from a NASA Ames scenario)**
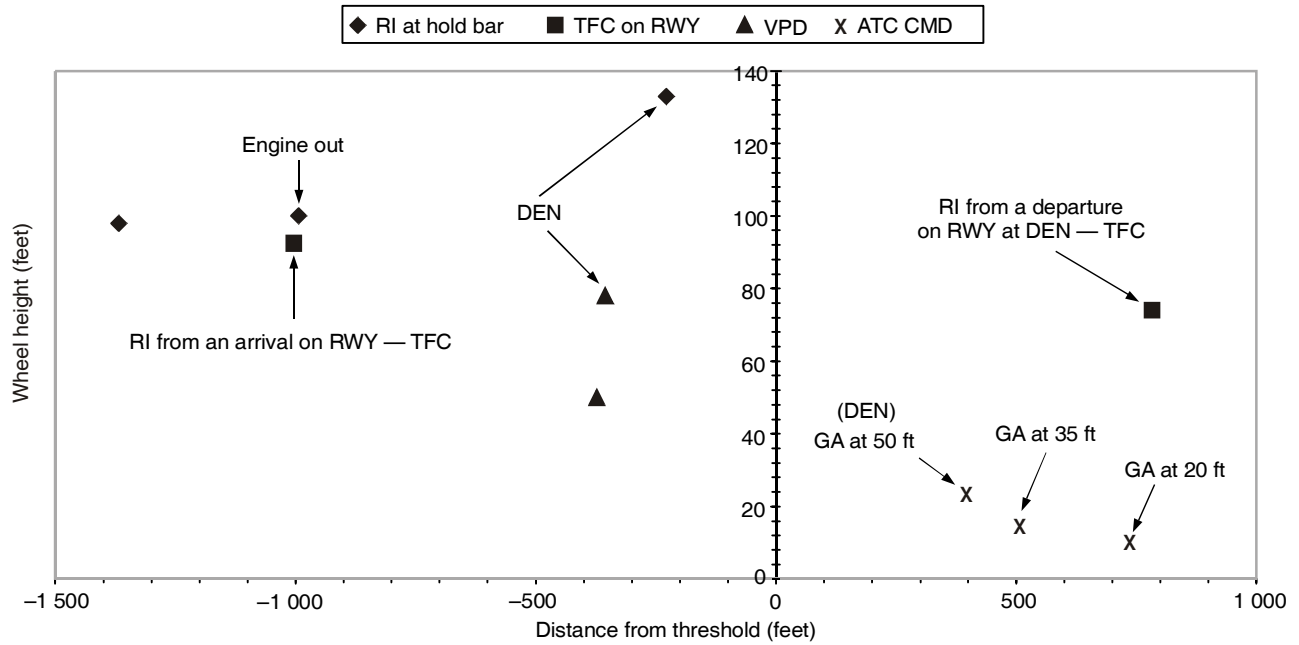
Note.— *The mean absolute lateral deviation at CG is 19 ft.*

**Figure 3-4A.   (Mean) wheel height at TO/GA switch press (JFK/DEN)
during a balked landing with use of *Flight Director* in NASA Ames B747-400 simulator**
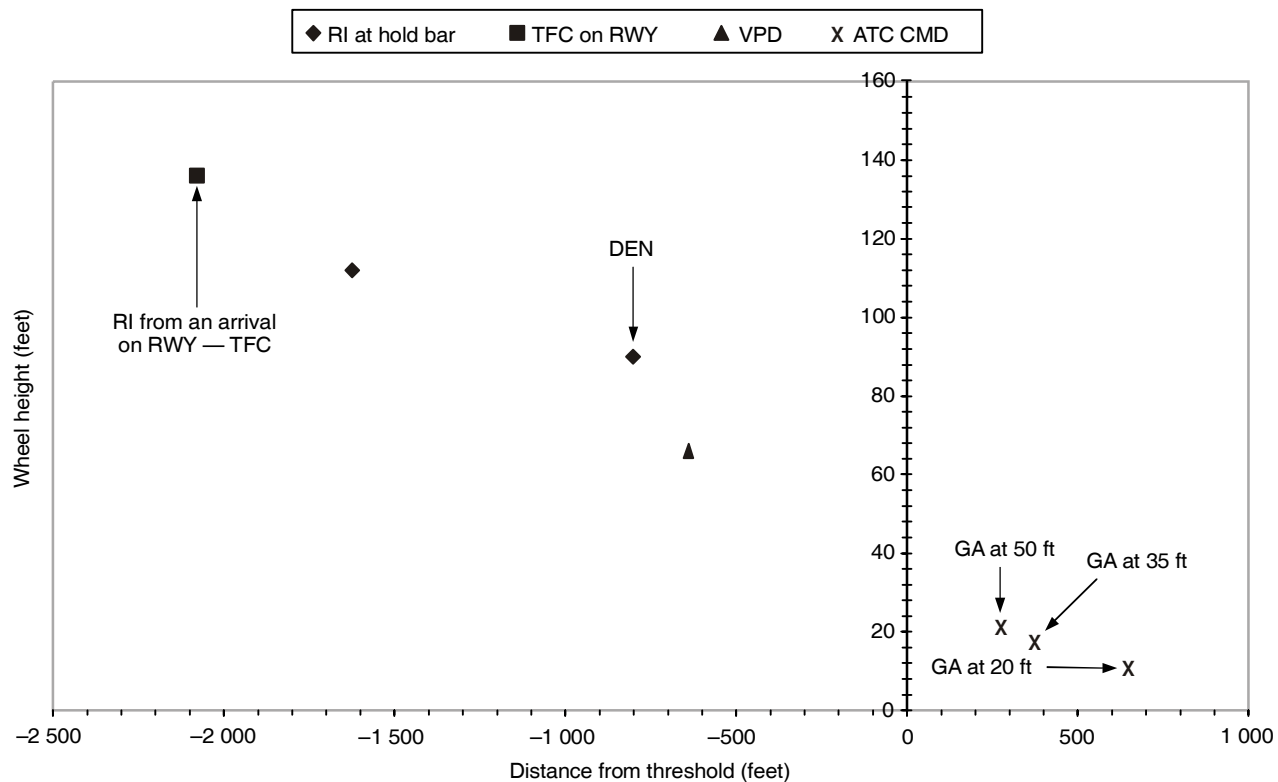
**Figure 3-4B.   (Mean) wheel height at TO/GA switch press (JFK/DEN)
during a balked landing with use of *Autopilot* in NASA Ames B747-400 simulator**
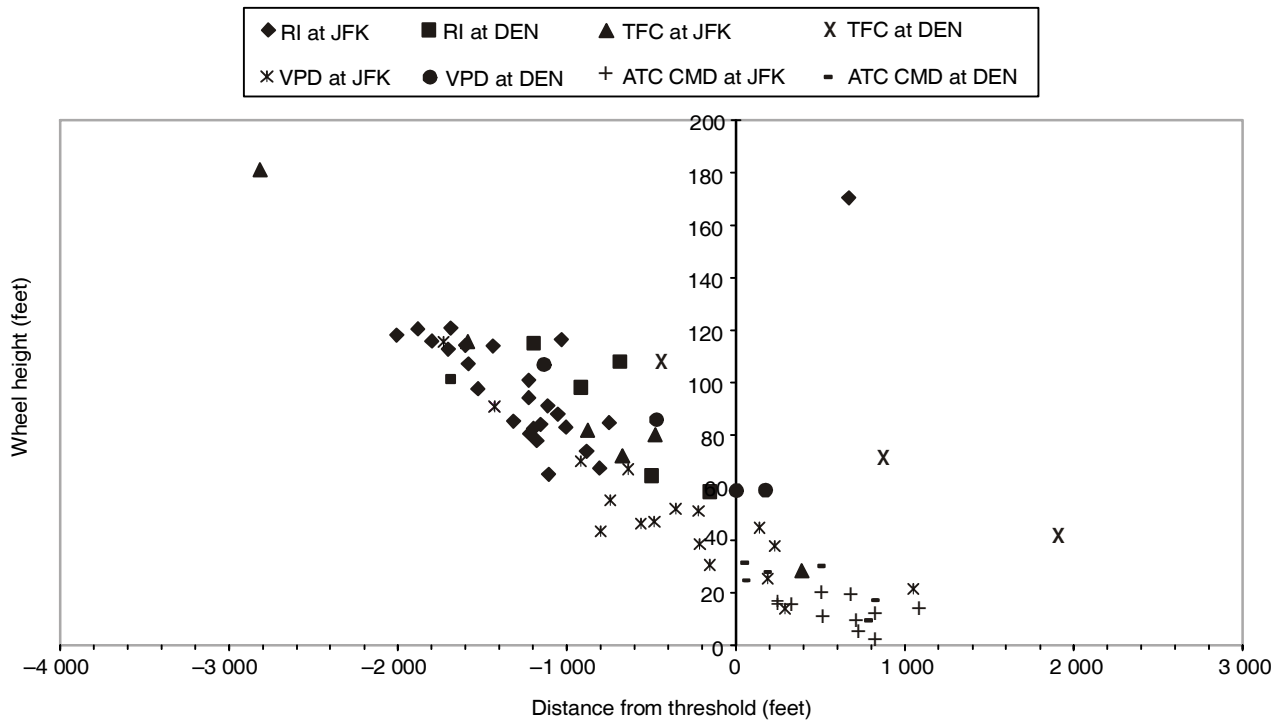
**Figure 3-4C.   Wheel height at TO/GA switch press (JFK/DEN)
during a balked landing with use of *Flight Director* in NASA Ames B747-400 simulator**
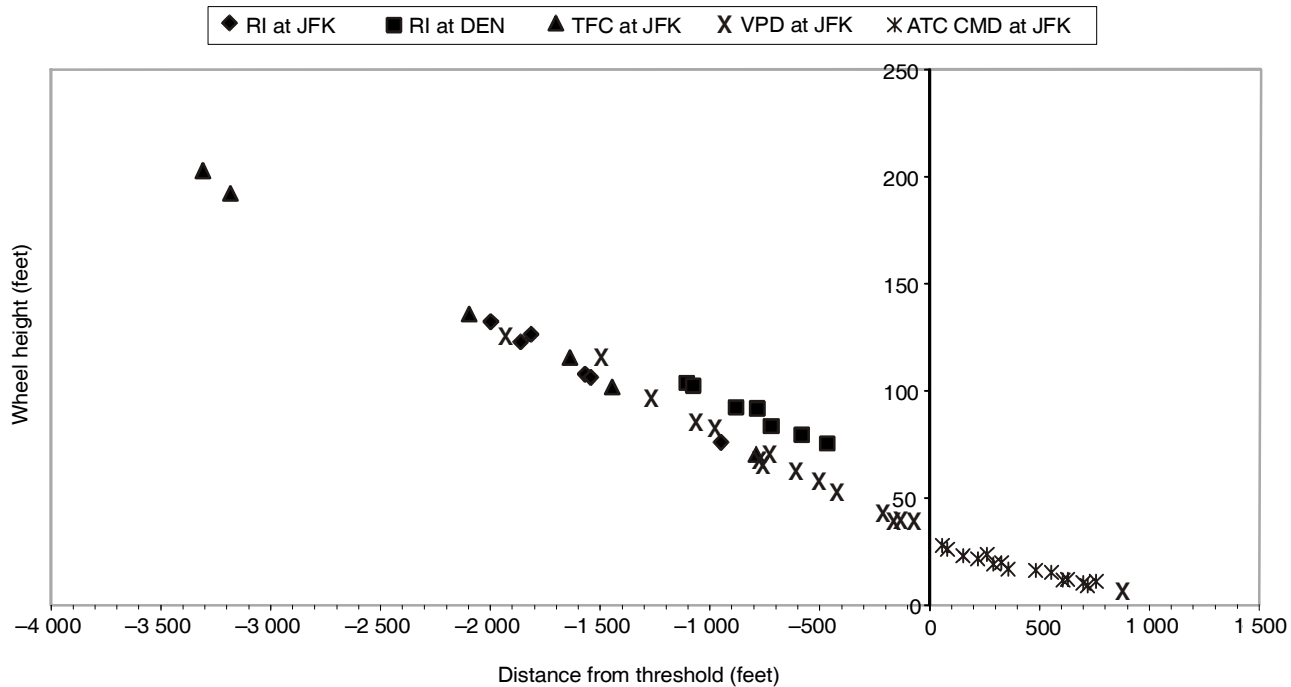
**Figure 3-4D.   Wheel height at TO/GA switch press (JFK/DEN)
during a balked landing with use of *Autopilot* in NASA Ames B747-400 simulator**

◆ RI at hold bar   ■ TFC on RWY   ▲ VPD   X ATC CMD

DEN

Engine out

RI from an arrival
on RWY — TFC

DEN

RI from a departure on
RWY at DEN — TFC

Wheel height (feet)

(DEN)
GA at 50 ft

GA at 20 ft

GA at 35 ft

90

80

70

60

50

40

30

20

10

0

−1 000   −500   0   500   1 000   1 500

Distance from threshold (feet)
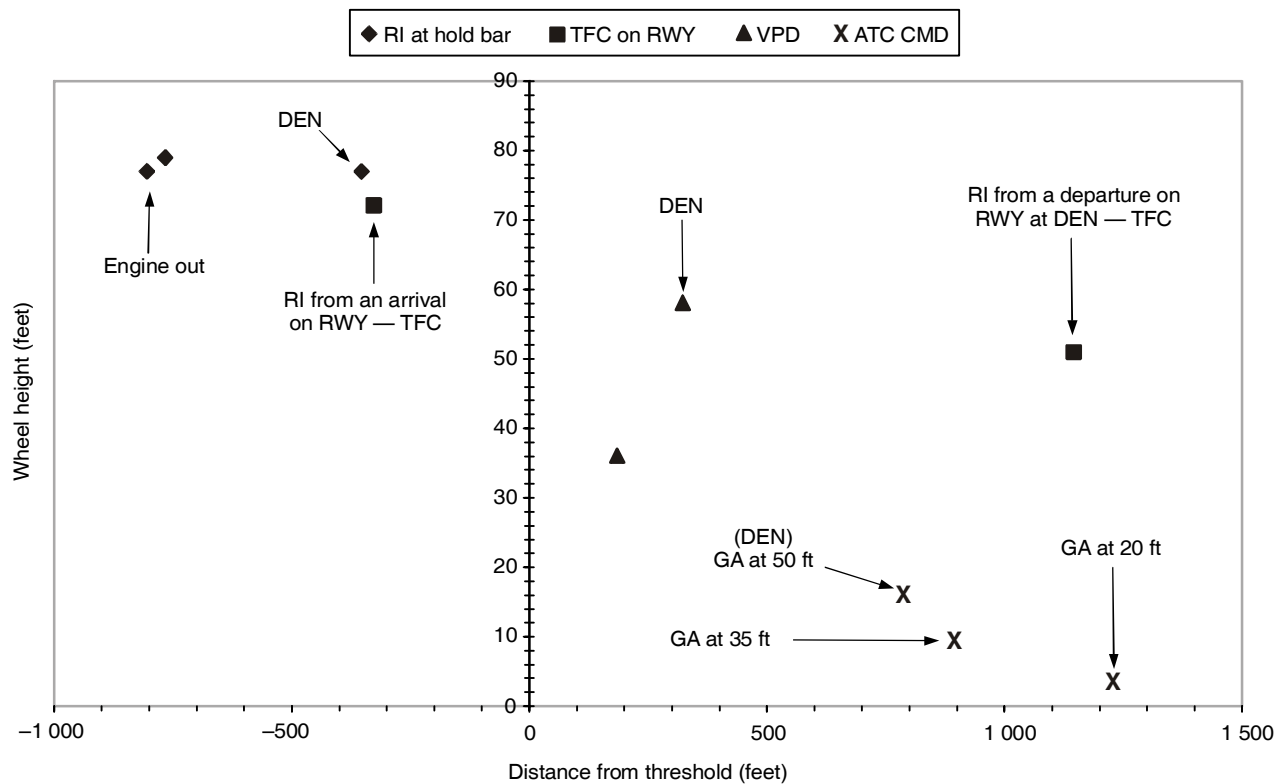
Note.— The mean absolute lateral deviation at CG is 18 ft.

Figure 3-5A.   (Mean) minimum wheel height at JFK/DEN
during a balked landing with use of *Flight Director* in NASA Ames B747-400 simulator
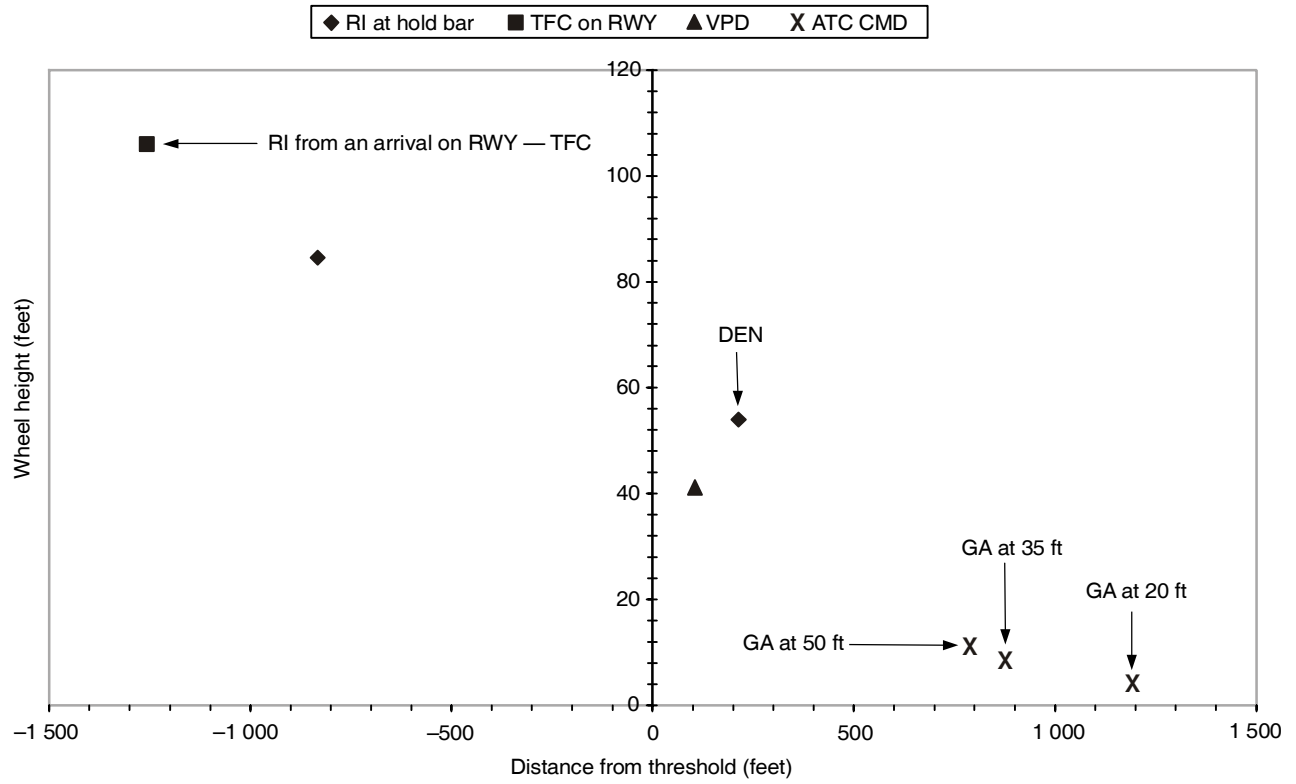
**Figure 3-5B.   (Mean) minimum wheel height at JFK/DEN
during a balked landing with use of *Autopilot* in NASA Ames B747-400 simulator**
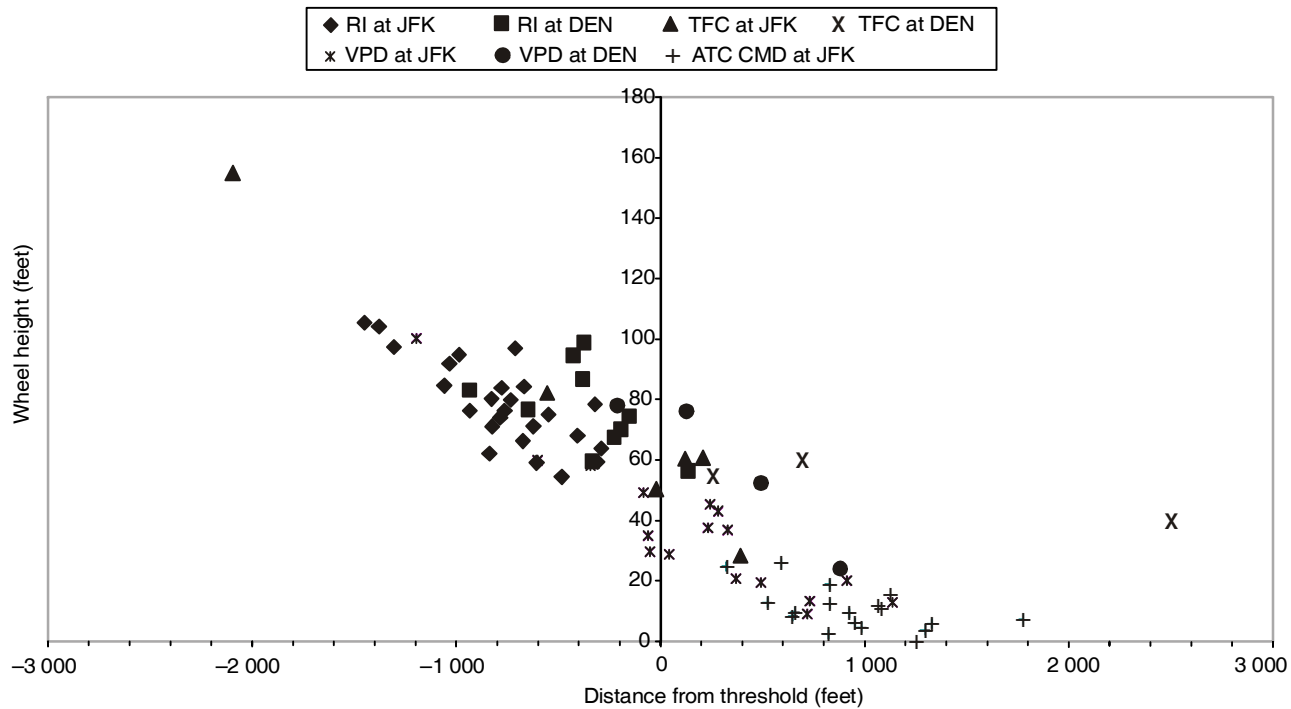
Note.— *Data do not include balked landings that touched down on the RWY.*

**Figure 3-5C.   Minimum (airborne) wheel height at JFK/DEN
during a balked landing with use of *Flight Director* in NASA Ames B747-400 simulator**
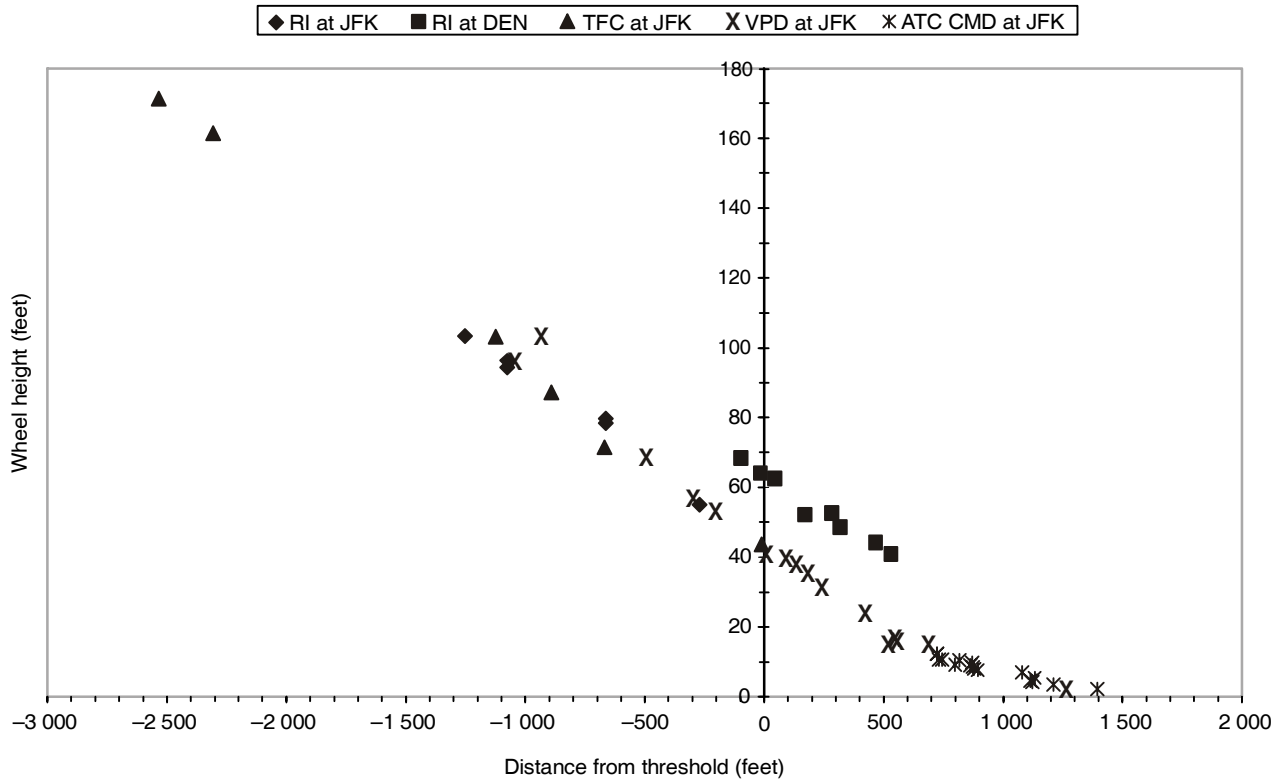
Note.— *Data do not include balked landings that touched down on the RWY.*

**Figure 3-5D.   Minimum (airborne) wheel height at JFK/DEN
during a balked landing with use of *Autopilot* in NASA Ames B747-400 simulator**

**Figure 3-6A.   (Mean) lateral deviation at minimum wheel height at JFK/DEN
during a balked landing with use of *Flight Director* in NASA Ames B747-400 simulator**
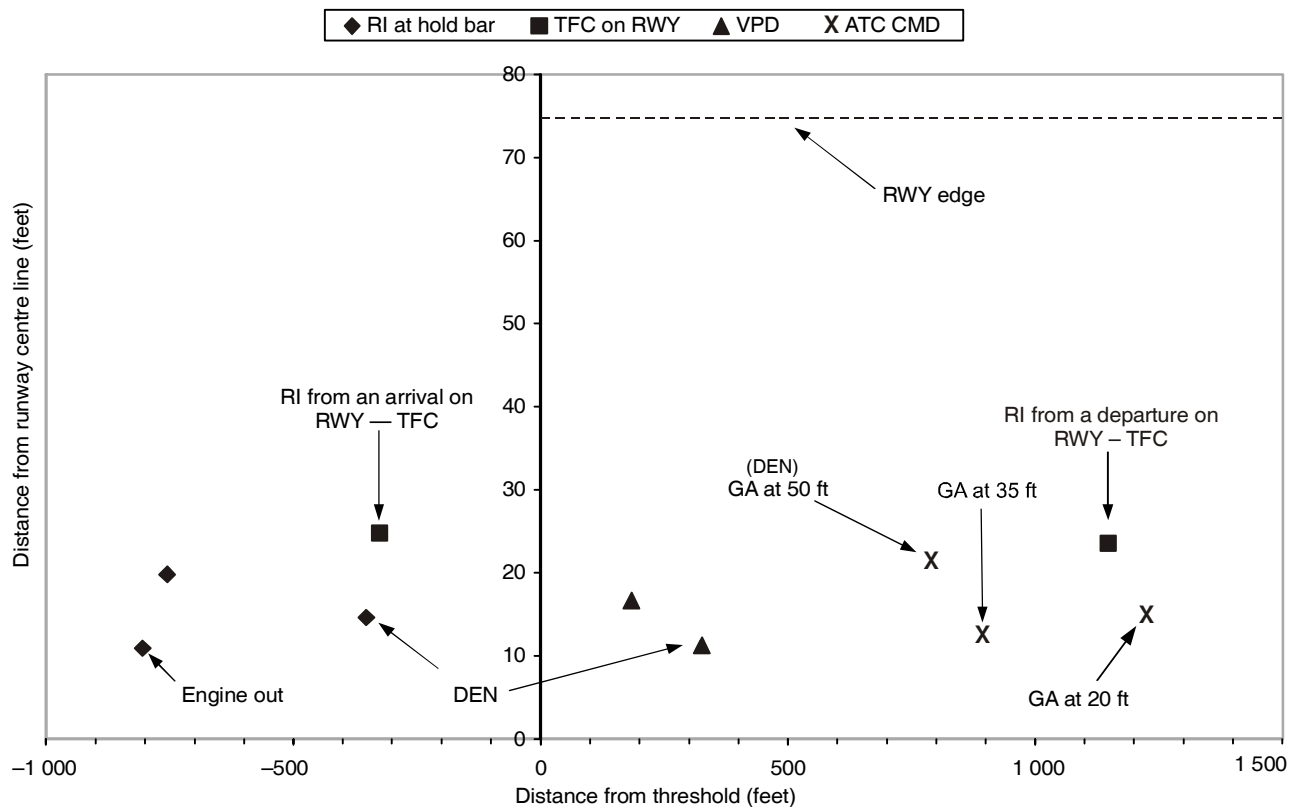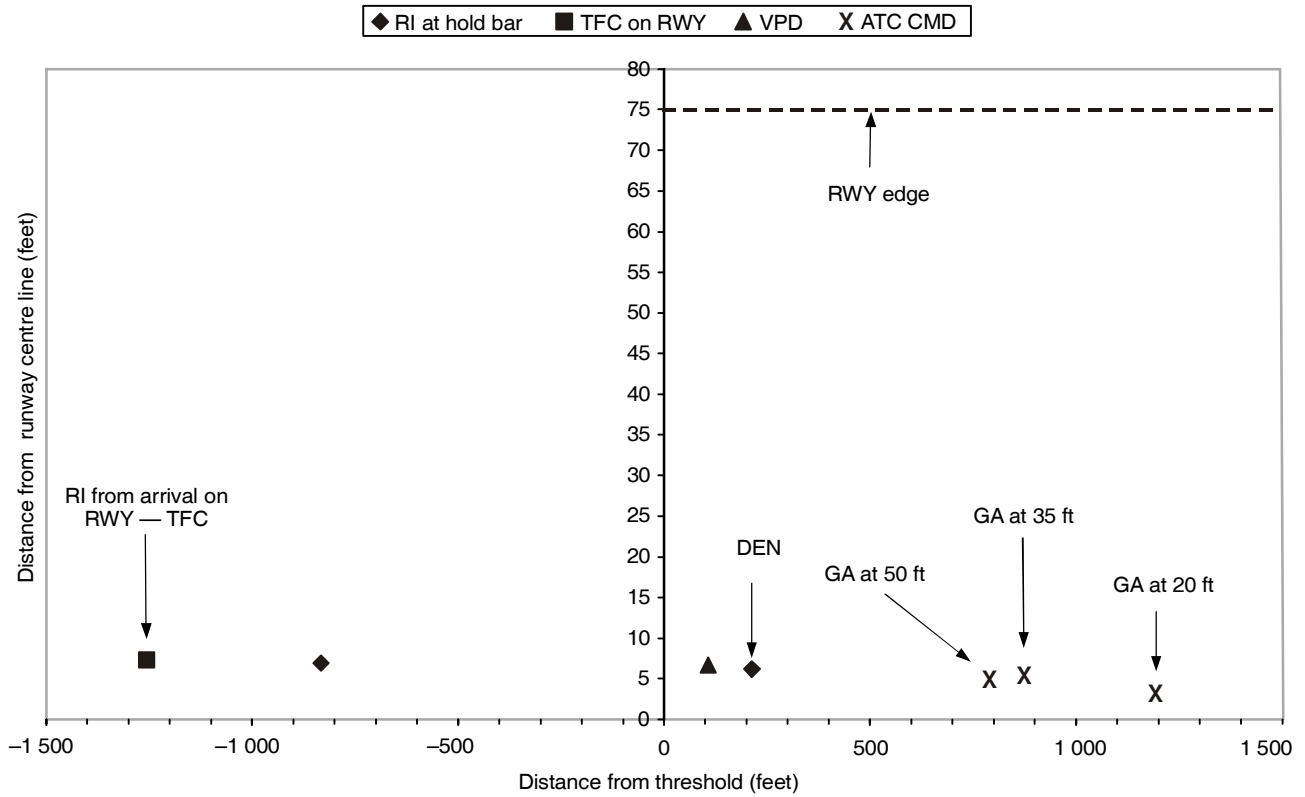
Notes:
– *The (mean) minimum wheel height above ground is 44 ft.*
– *All lateral deviations are positive (i.e. the absolute value).*
– *The symbols correspond to the CG point of 747-400. Add 20 ft to the CG point to locate main gear outer tire edge.*

**Figure 3-6B.   (Mean) lateral deviation at minimum wheel height at JFK/DEN
during a balked landing with use of *Autopilot* in NASA Ames B747-400 simulator**
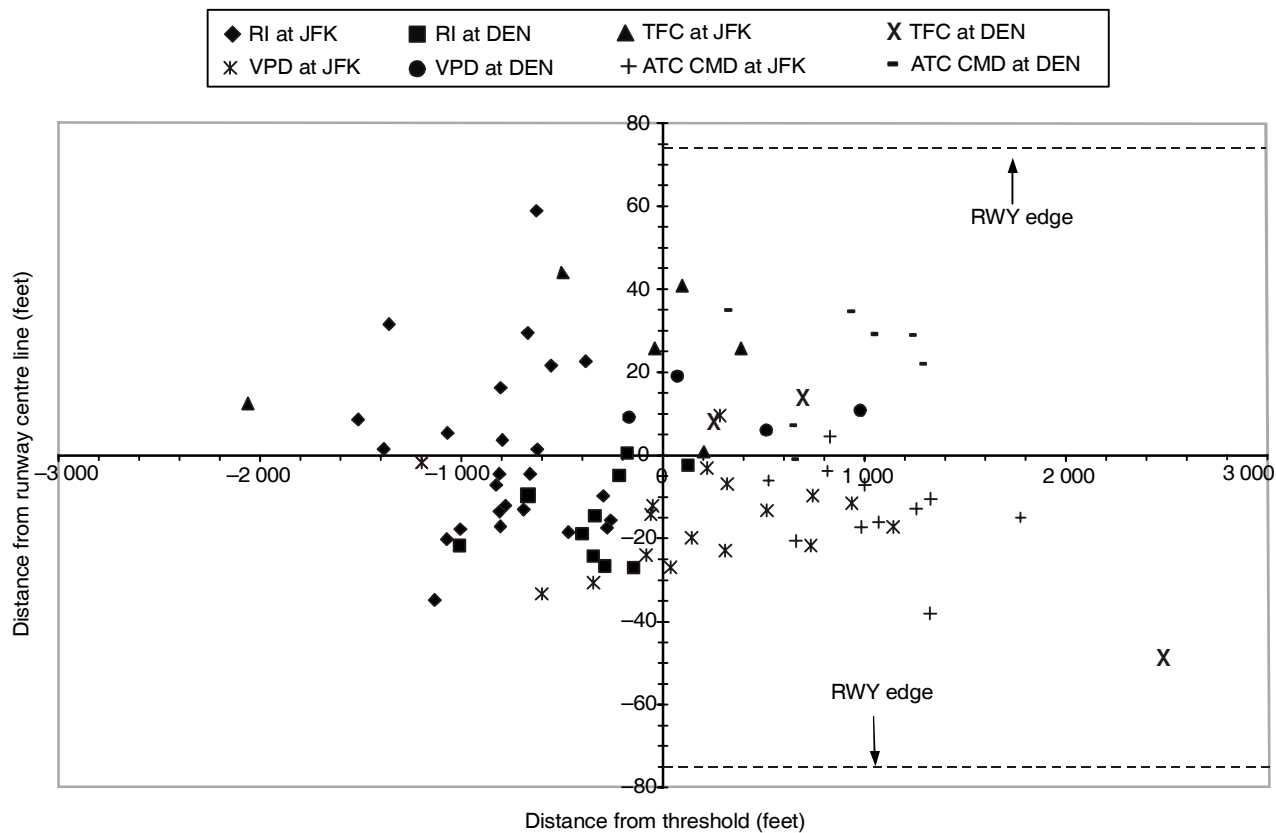
Notes:
– The (mean) minimum wheel height above ground is 49 ft.
– Runway width is 150 ft.

**Figure 3-6C.   Lateral deviation at minimum wheel height at JFK/DEN
during a balked landing with use of *Flight Director* in NASA Ames B747-400 simulator**
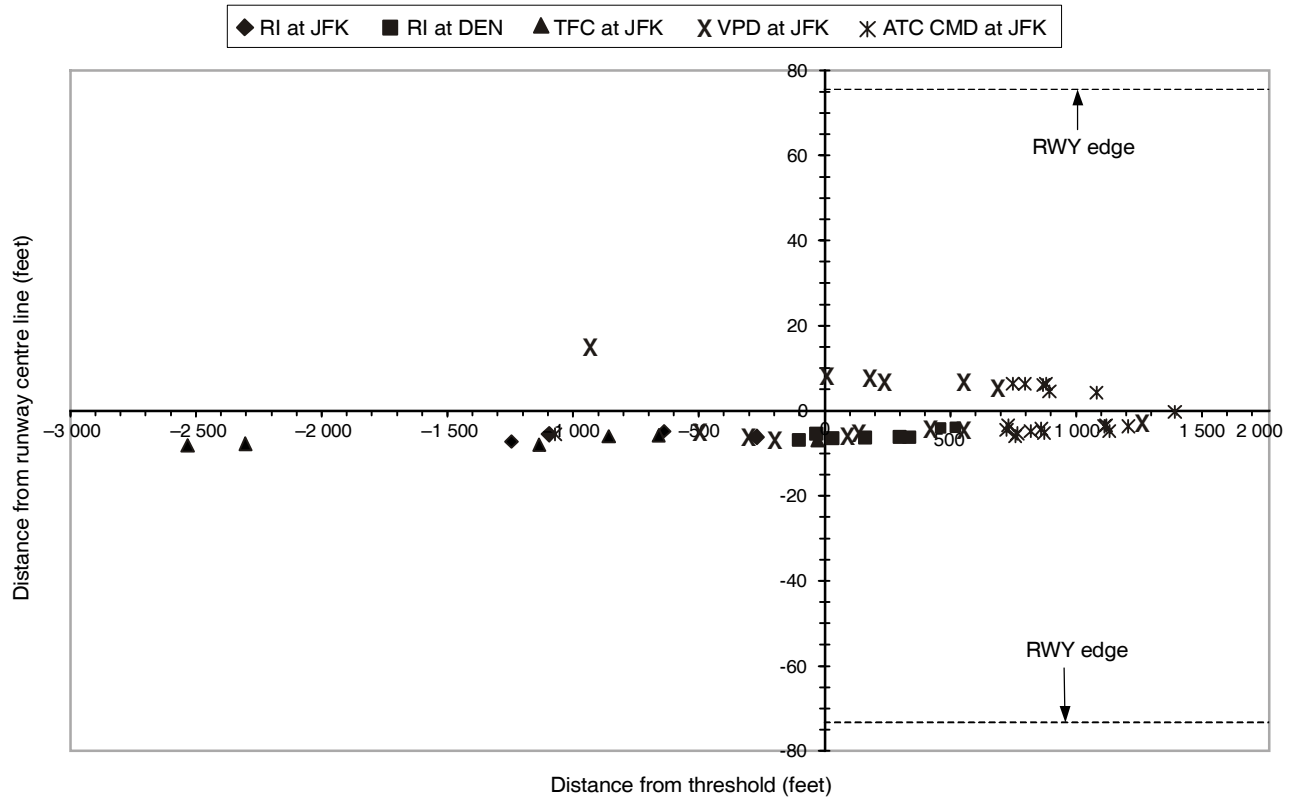
**Figure 3-6D.   Lateral deviation at minimum wheel height at JFK/DEN
during a balked landing with use of *Autopilot* in NASA Ames B747-400 simulator**

Figure 3-7A.   (Mean) maximum lateral deviation from runway centre line at JFK/DEN during a balked landing with use of *Flight Director* in NASA Ames B747-400 simulator

◆ RI at hold bar ■ TFC on RWY ▲ VPD ✕ ATC CMD

Figure 3-7B.   (Mean) maximum lateral deviation from runway centre line at JFK/DEN during a balked landing with use of *Autopilot* in NASA Ames B747-400 simulator

**Figure 3-7C.   Maximum lateral deviation from runway centre line at JFK/DEN
during a balked landing with use of *Flight Director* in NASA Ames B747-400 simulator**

Figure 3-7D. Maximum lateral deviation from runway centre line at JFK/DEN during a balked landing with use of *Autopilot* in NASA Ames B747-400 simulator
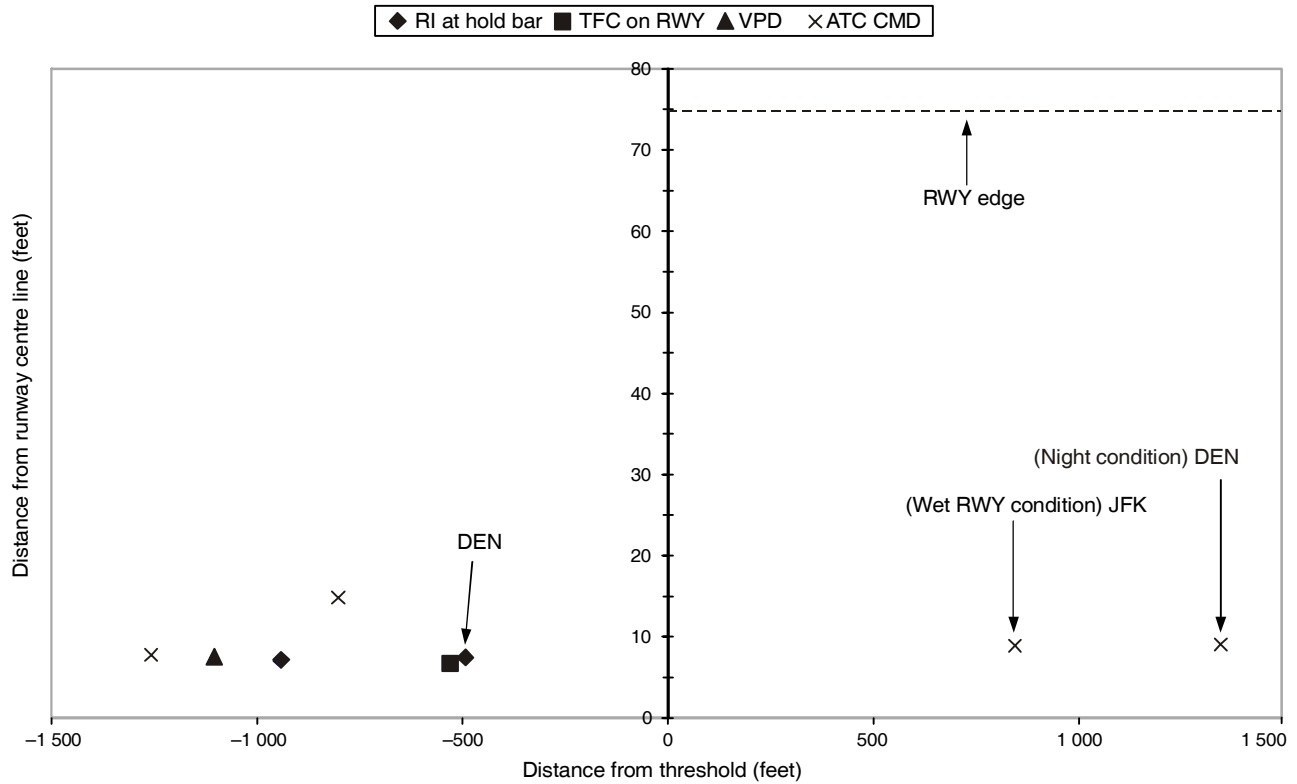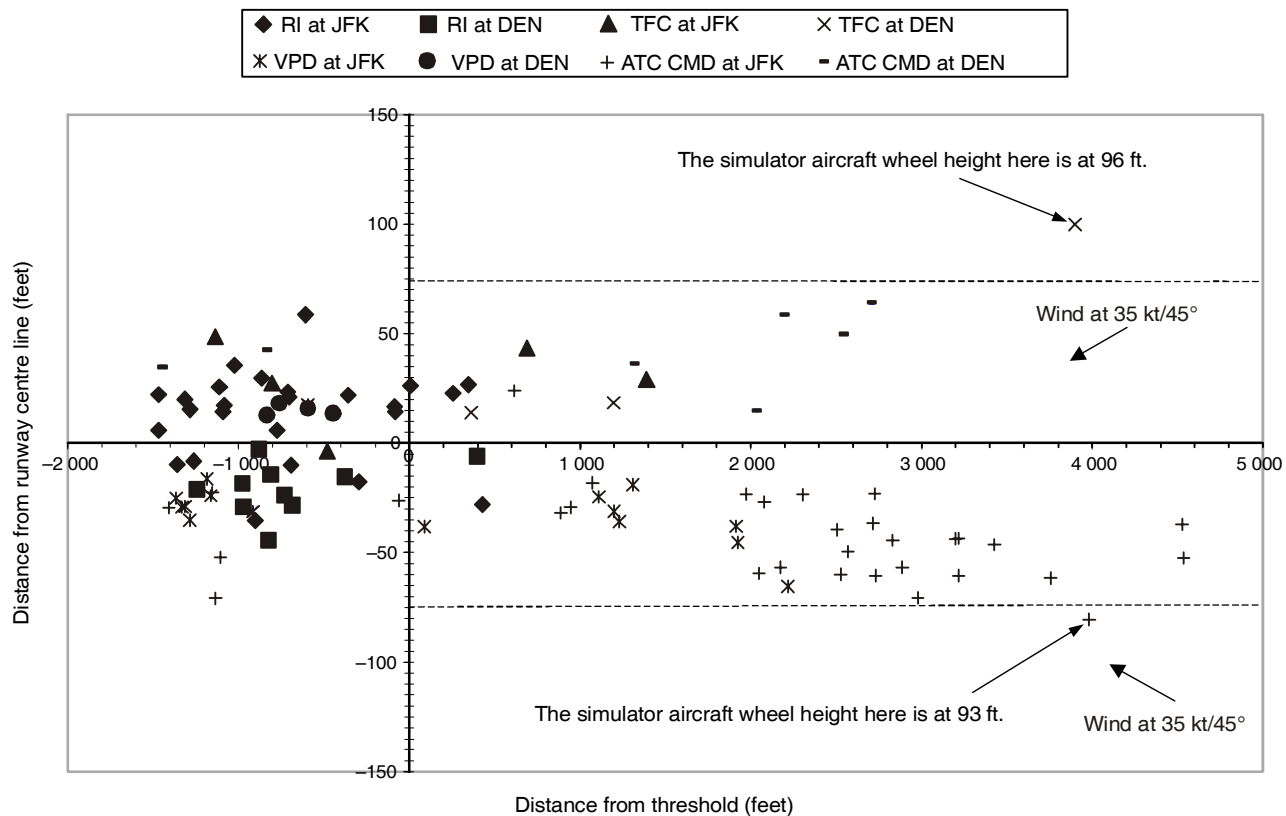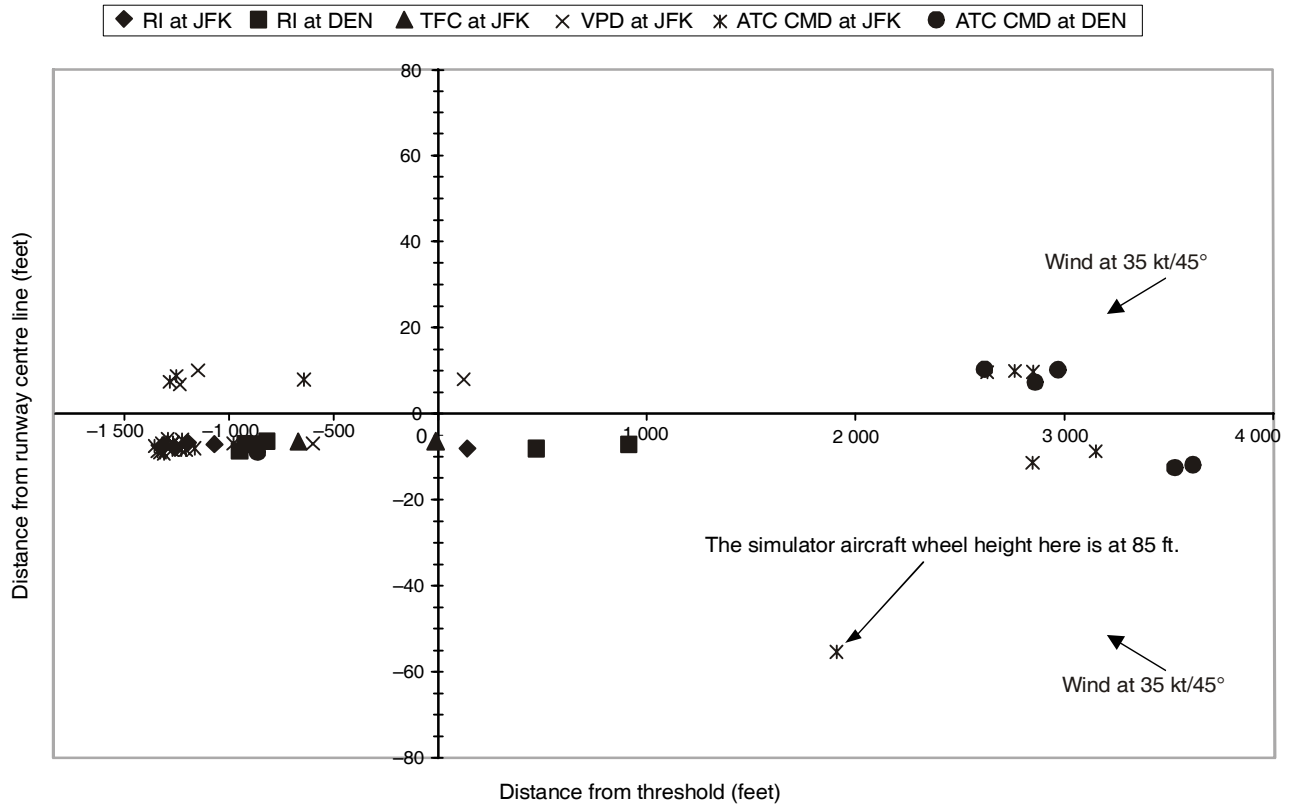
Notes:
– The mean (simulator aircraft) wheel height is 88 ft above ground level.
– Add 20 ft to either side of CG point to locate main gear outer tire edge.
– Each symbol corresponds to the CG point.
– Winds are at 35 kt and at 45° from right or left.
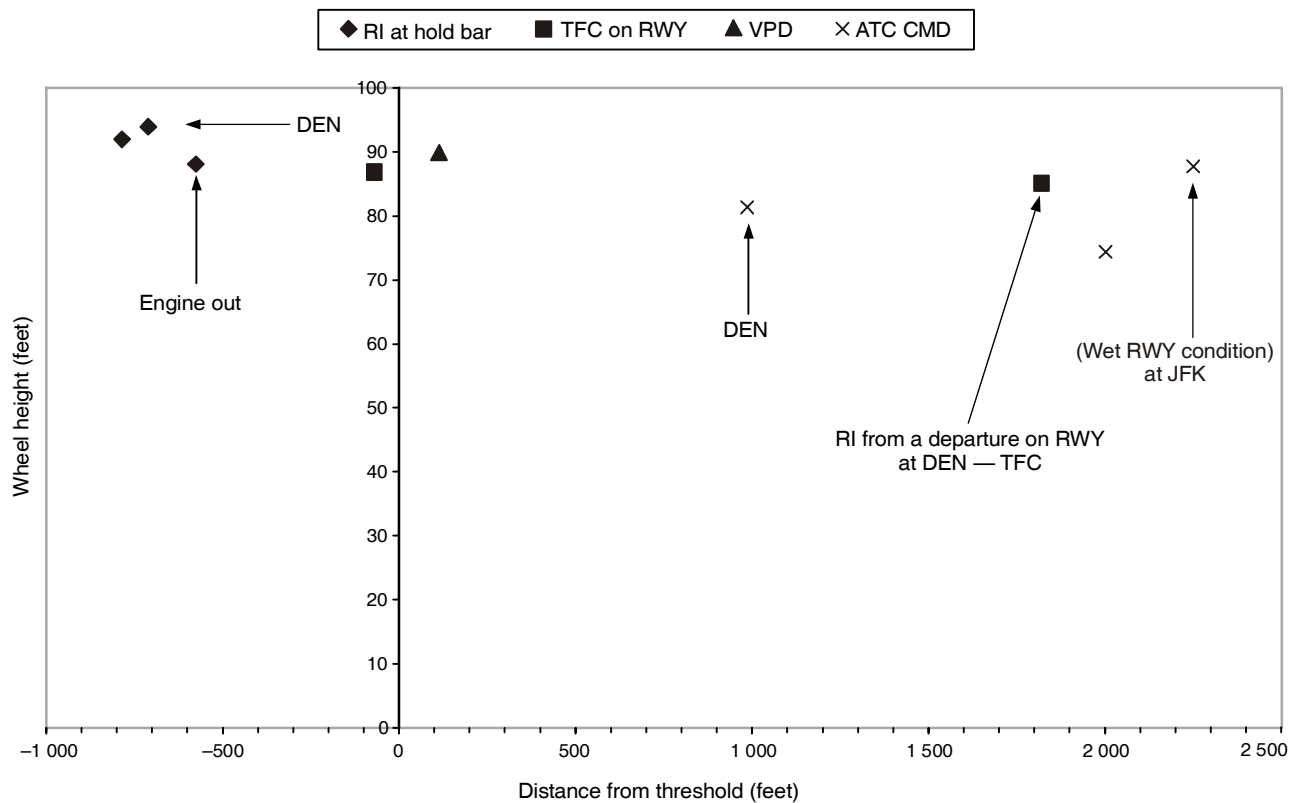
Note.— *The mean (absolute) lateral deviation is 33 ft.*

Figure 3-8A.   (Mean) wheel height at maximum lateral deviation from runway centre line at JFK/DEN during a balked landing with use of *Flight Director* in NASA Ames B747-400 simulator

Figure 3-8B.   (Mean) wheel height at maximum lateral deviation from runway centre line at JFK/DEN
during a balked landing with use of *Autopilot* in NASA Ames B747-400 simulator
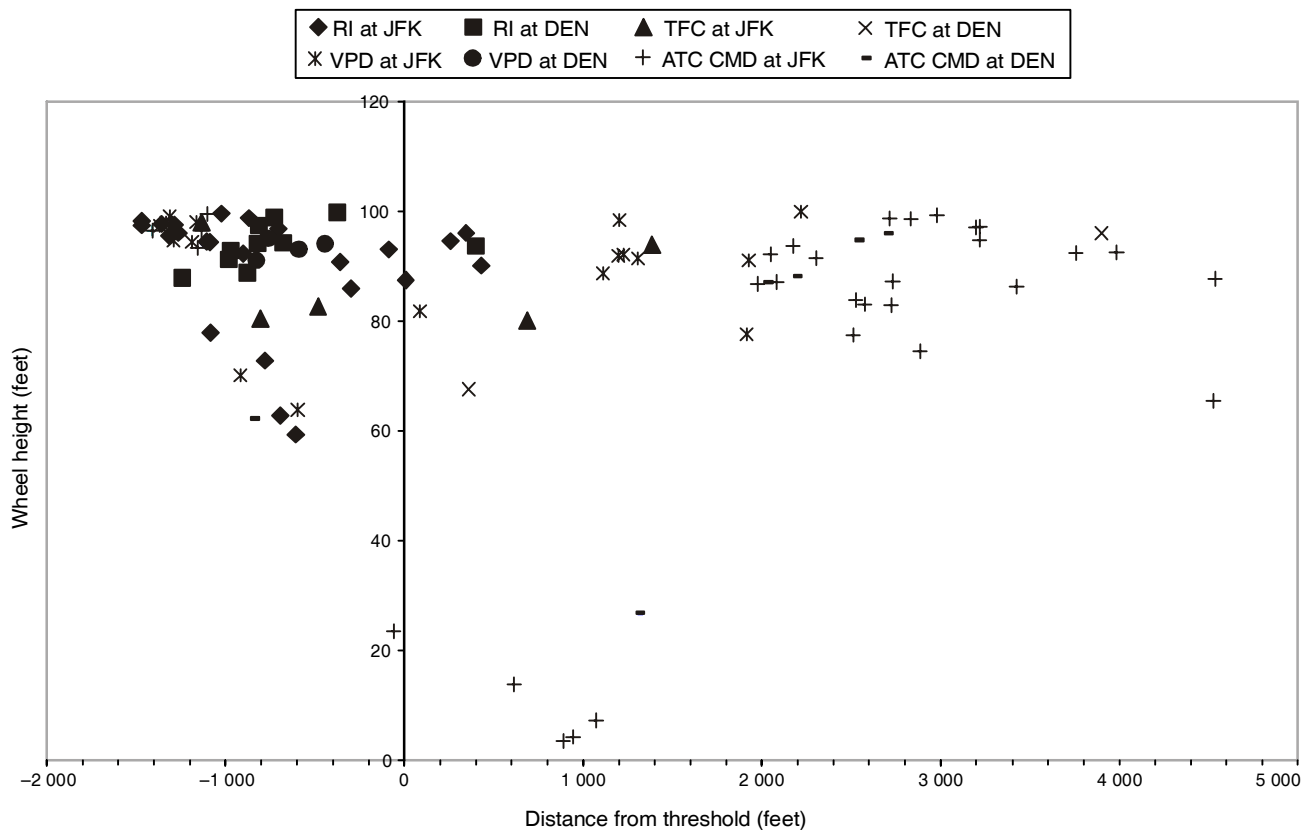
Note.— The mean (absolute) lateral deviation is 33 ft.

**Figure 3-8C.   Wheel height at maximum deviation from runway centre line at JFK/DEN
during a balked landing with use of *Flight Director* in NASA Ames B747-400 simulator**
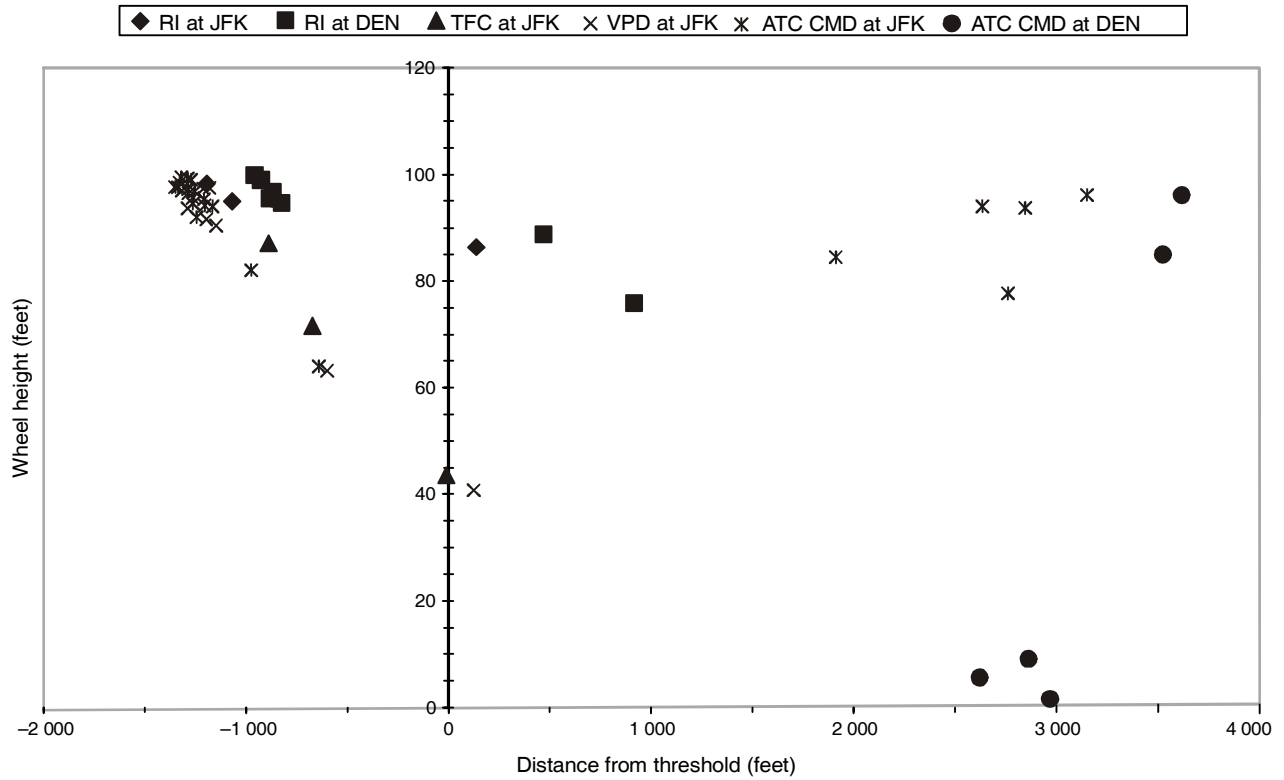
Note.— *The mean (absolute) lateral deviation is 8 ft.*

Figure 3-8D.   Wheel height at maximum deviation from runway centre line at JFK/DEN during a balked landing with use of *Autopilot* in NASA Ames B747-400 simulator
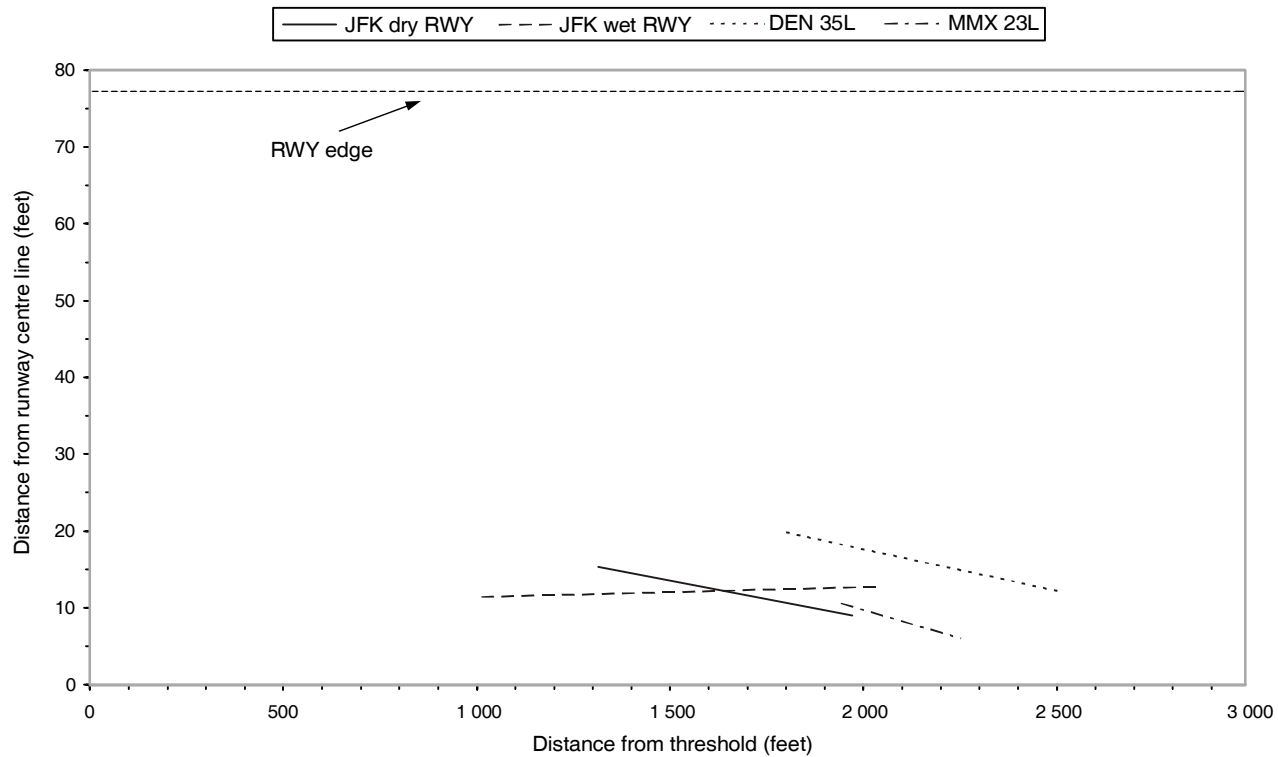
Notes:
– Ground roll corresponds to the aircraft CG point.
– All lateral deviations are positive (i.e. the absolute value).

**Figure 3-9A.   (Mean) ground path in touchdown roll during a balked landing
with use of *Flight Director* in NASA Ames B747-400 simulator**
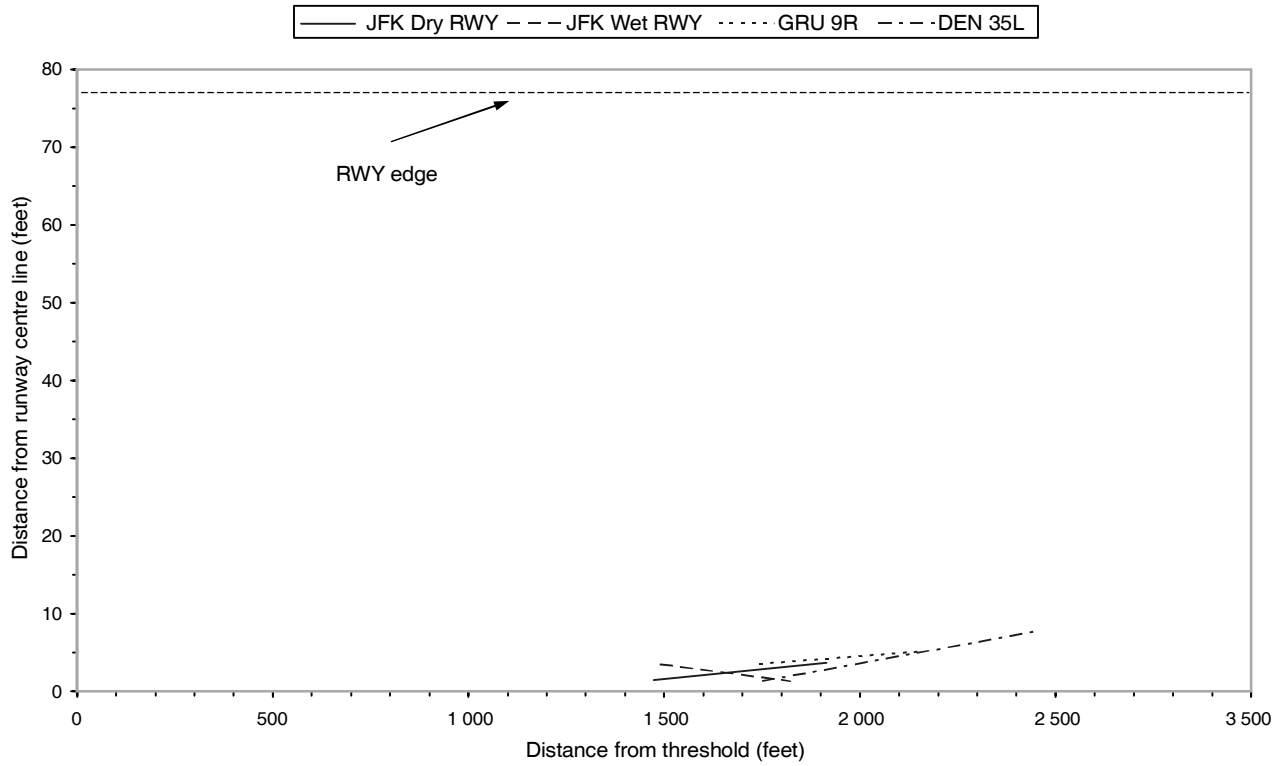
Notes:
– Ground roll corresponds to the aircraft CG point.
– All lateral deviations are positive (i.e. the absolute value).

**Figure 3-9B.   (Mean) ground path in touchdown roll during a balked landing
with use of *Autopilot* in NASA Ames B747-400 simulator**
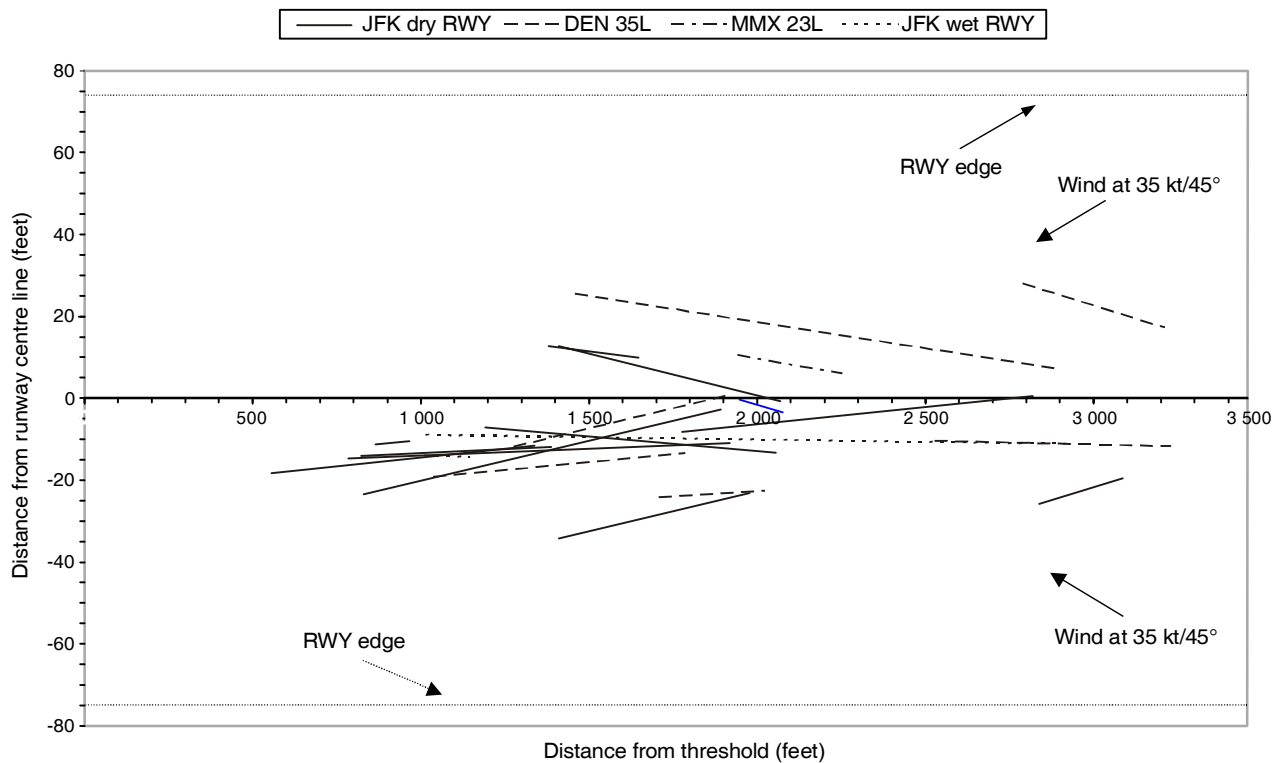
Notes:
– The winds are at 35 kt and at 45°.
– Ground paths correspond to the movement of the simulator aircraft CG point.

**Figure 3-9C.   Ground paths in touchdown roll during a balked landing
with use of *Flight Director* in NASA Ames B747-400 simulator**
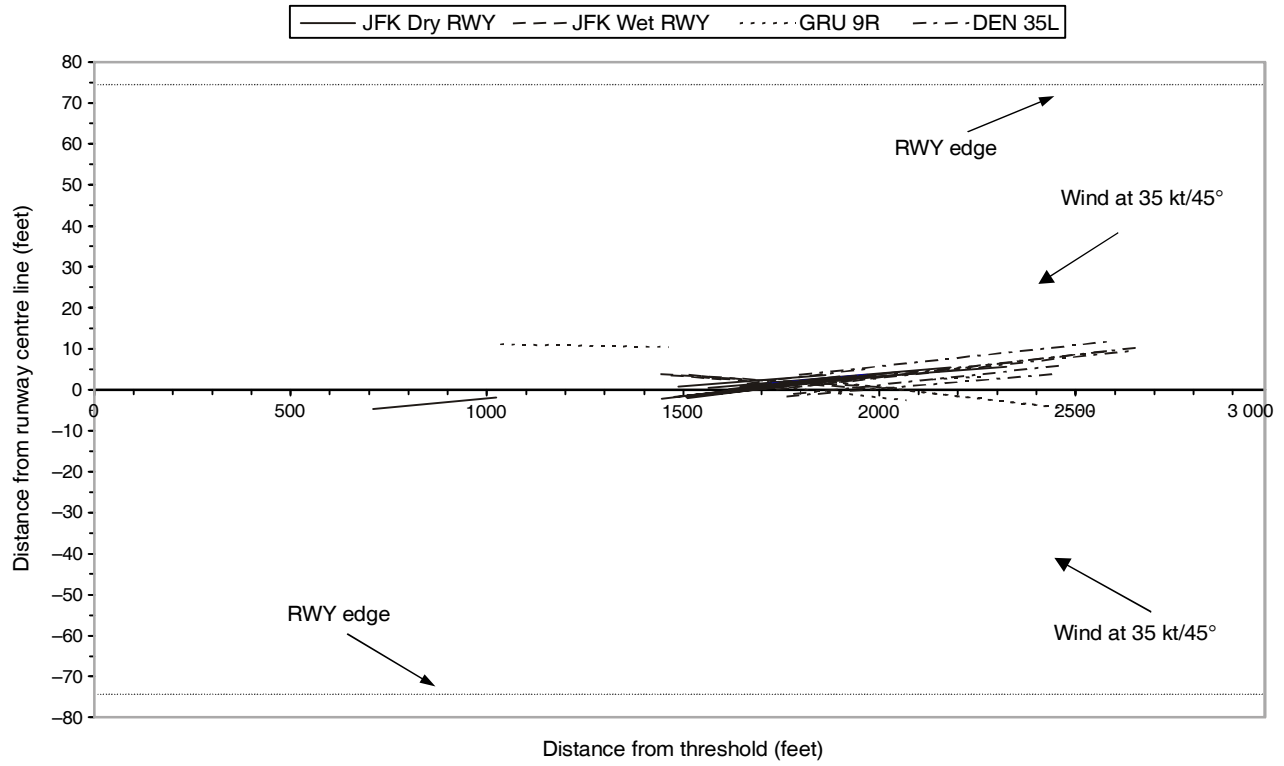
Notes:
– The winds are at 35 kt and at 45° from right or left.
– Ground paths correspond to the movement of the simulator aircraft CG point.

**Figure 3-9D.   Ground paths in touchdown roll during a balked landing
with use of *Autopilot* in NASA Ames B747-400 simulator**
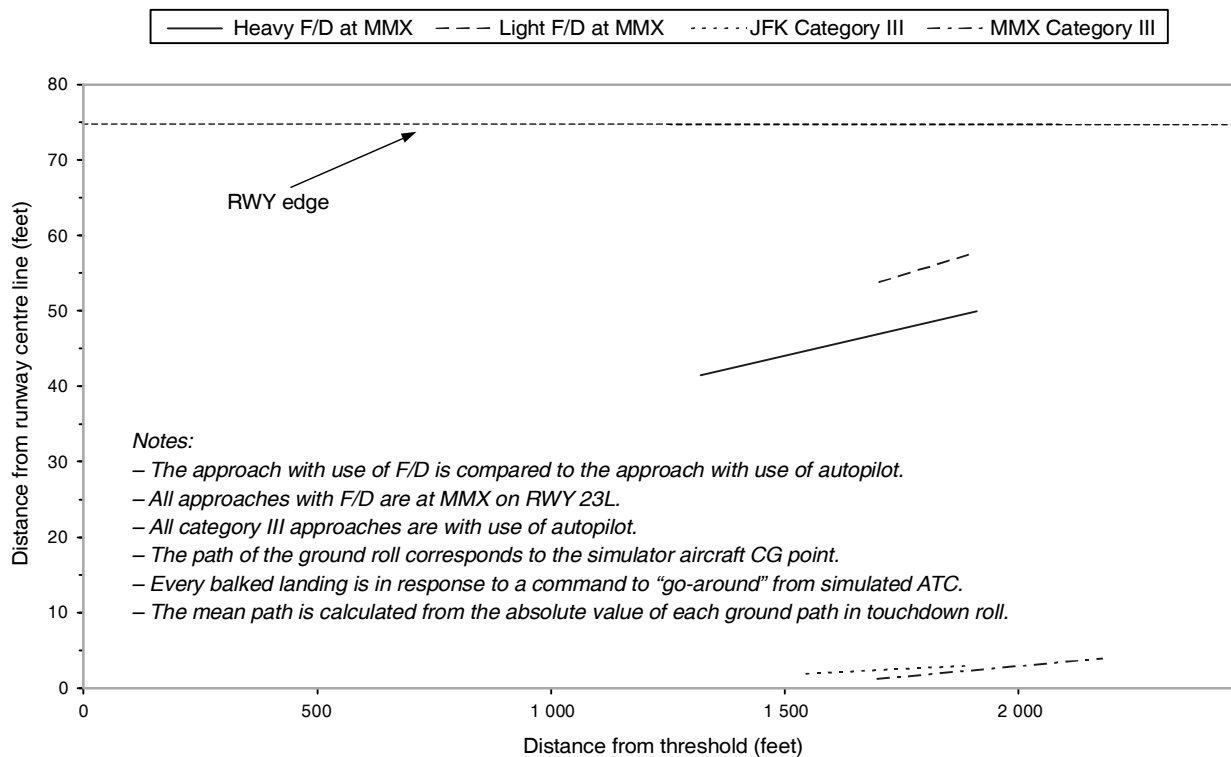
**Figure 3-10A and 3-10B.   (Mean) ground path in touchdown roll during a balked landing
in NASA Ames B747-400 simulator: Impact of high elevation (7 341 ft) and aircraft weight**
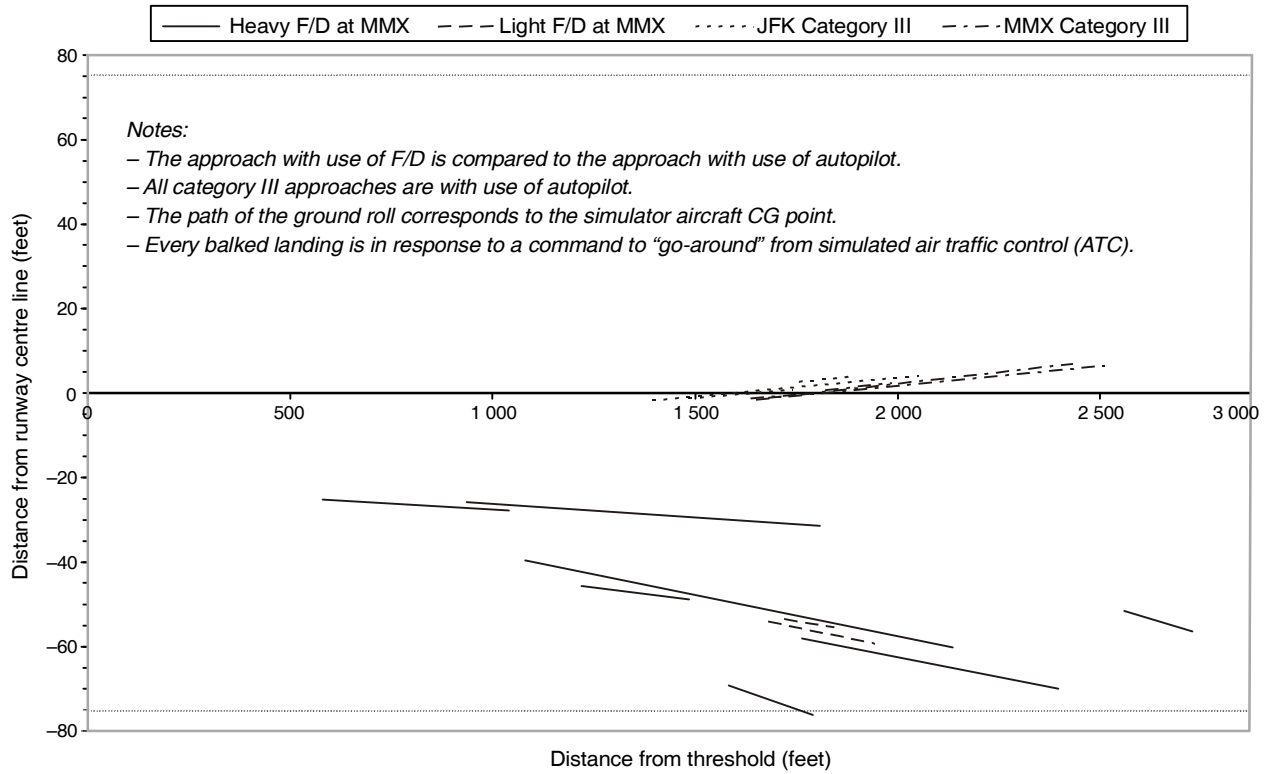
**Figure 3-10C and 3-10D.   Ground paths in touchdown roll during a balked landing
in NASA Ames B747-400 simulator: Impact of high elevation (7 341 ft) and aircraft weight**
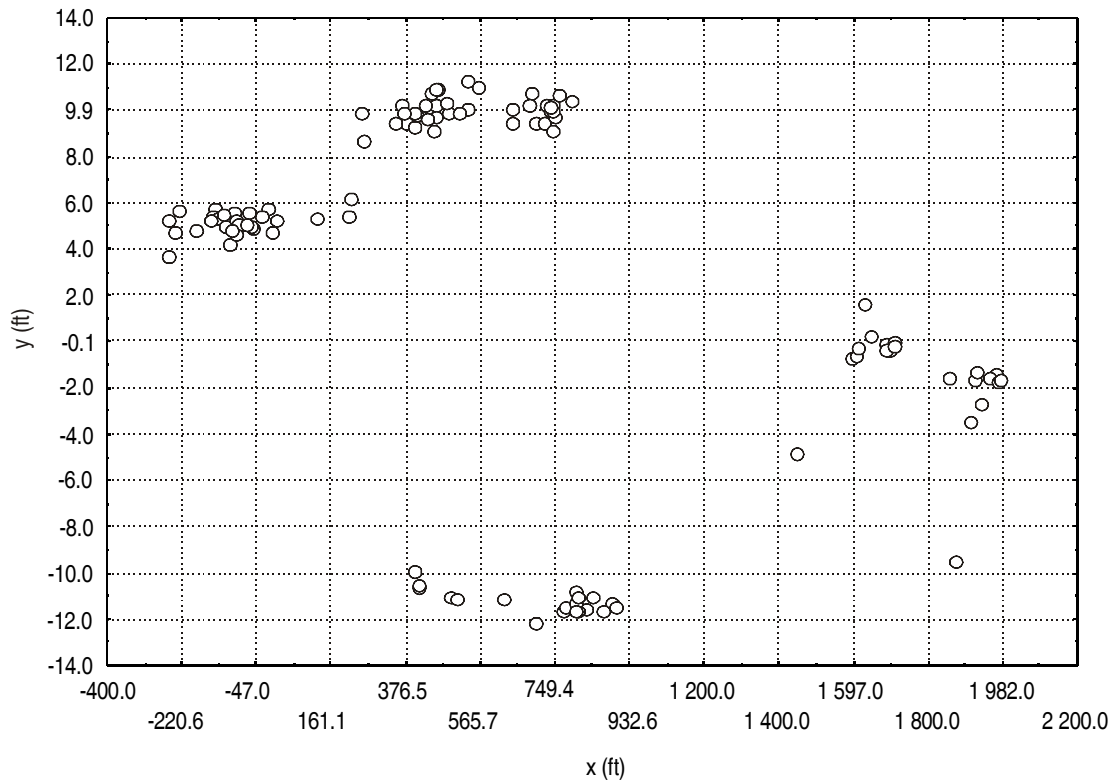
**Figure 3-11A.   Berlin balked landing Autopilot test runs —
Points at minimum height**
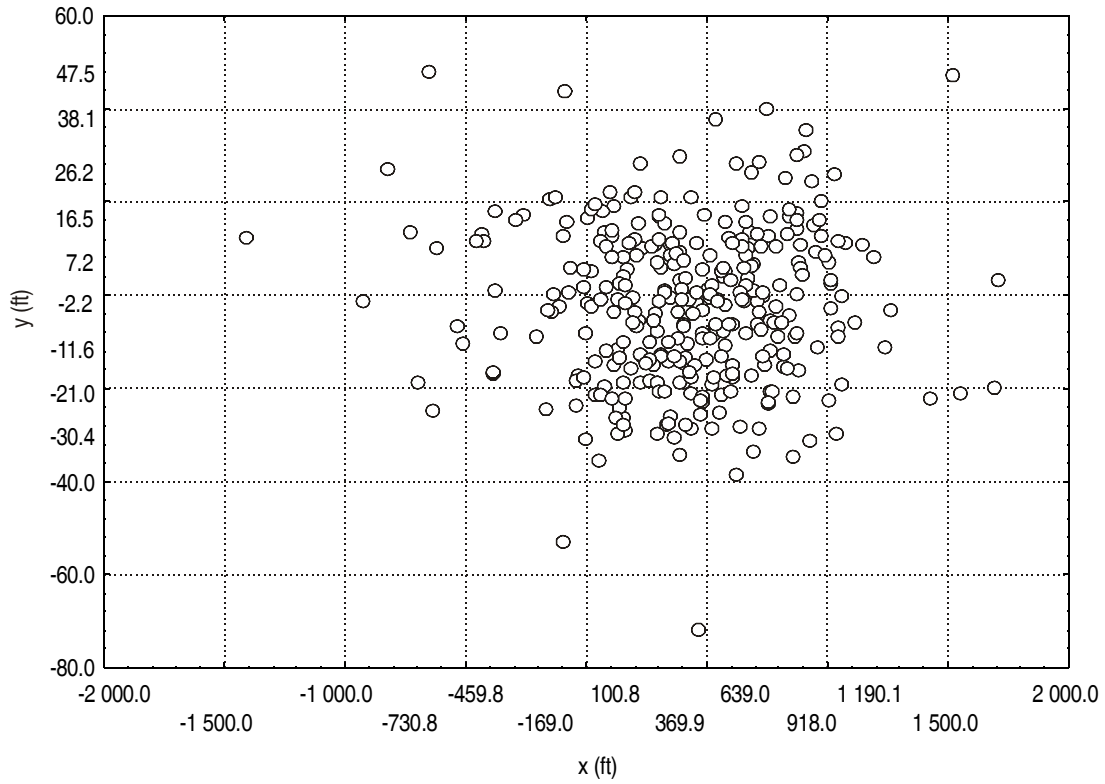
**Figure 3-11B.   Berlin & Toulouse balked landing Flight Director test runs —
Points at minimum height**
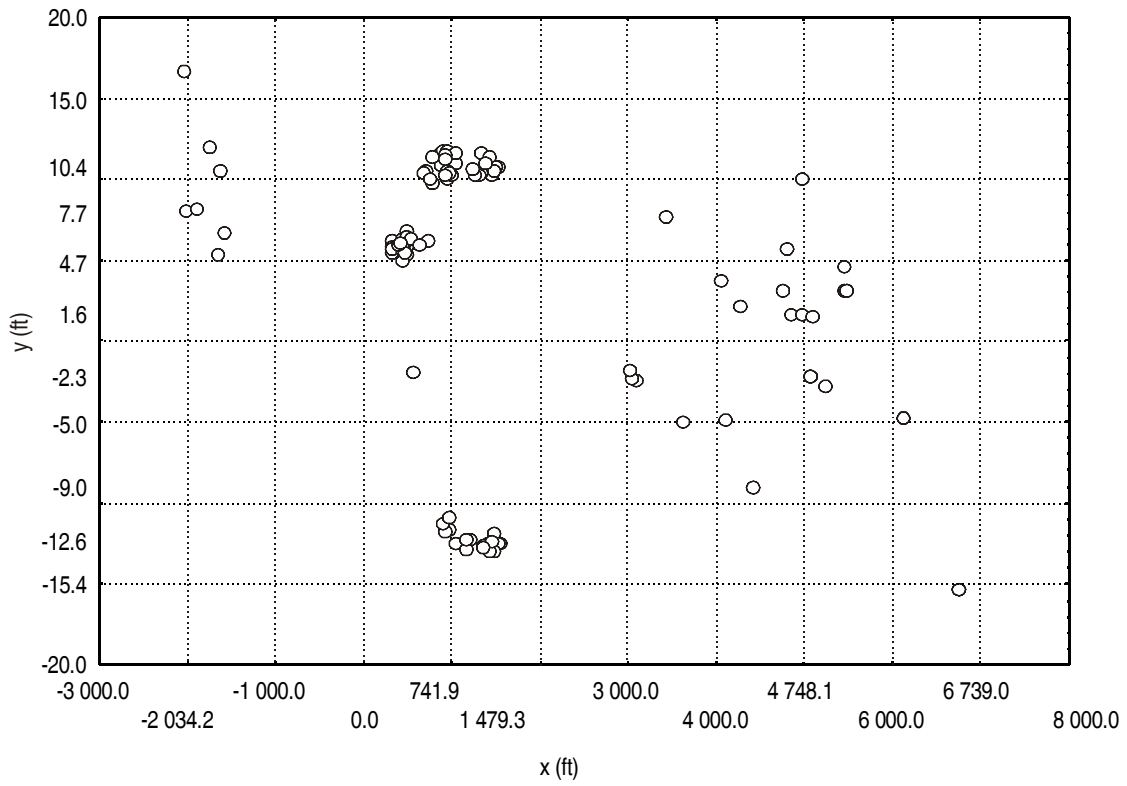
**Figure 3-12A.   Berlin balked landing Autopilot test runs —
Maximum lateral deviation points**
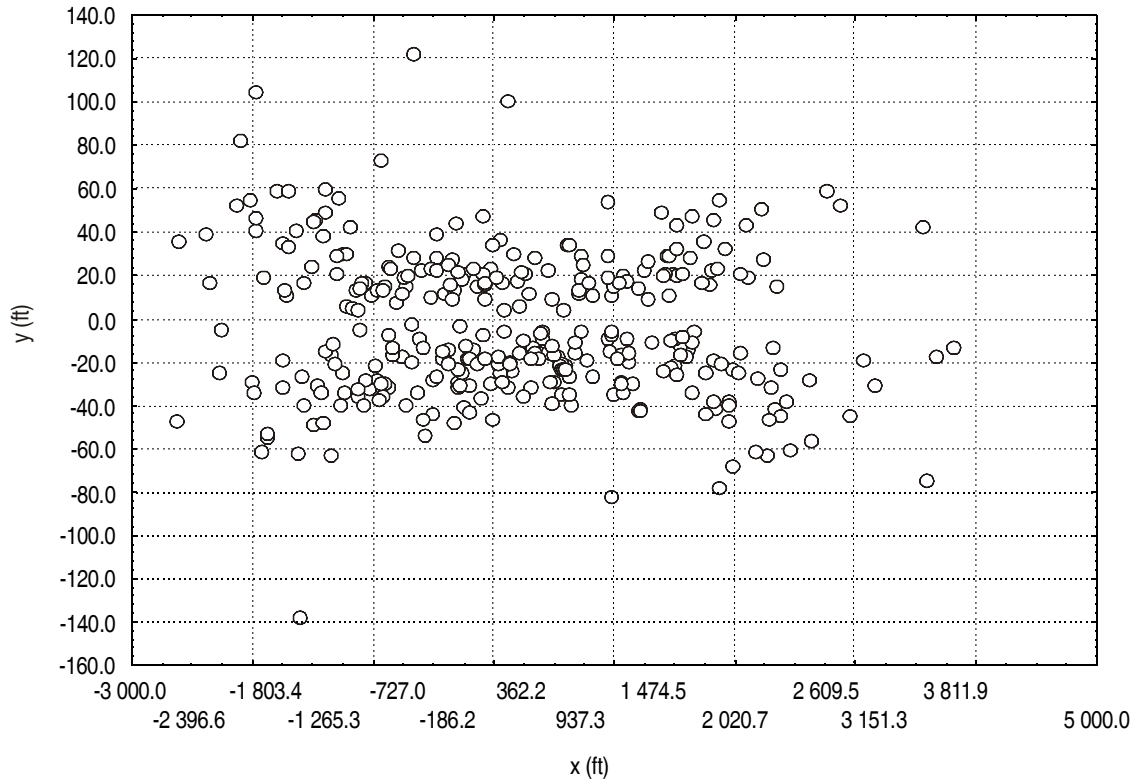
**Figure 3-12B.   Berlin & Toulouse balked landing Flight Director test runs —
Points of maximum lateral (y) deviation**

— — — — — — — —

Appendix to Chapter 3

Table 3-A-1. NASA Ames scenario listing for the May 1997 trial

Scenario #	Go-around altitude (AGL feet)	Airport/runway/category	Autopilot/flight director mode	Go-around initiation mode	Simulator weather	Crosswind component	Gust (%)
1	LAND (595 000 lb)	JFK, 04R, CAT I	FLIGHT DIRECTOR	N/A	300 ft ceiling, ½ mile visibility, wind 085/14	10	4
2	LAND (595 000 lb)	DEN, 35L, CAT I	FLIGHT DIRECTOR	N/A	900 ft ceiling, 2 mile visibility, wind 360/40 at 8 000 ft decreasing linearly to 305/35 (25 kt headwind) at the surface	25	4
3	LAND (595 000 lb)	DEN, 35L, CAT II	AUTOPILOT	N/A	100 ft ceiling, RVR 1 200 ft, wind 360/40 at 8 000 ft decreasing linearly to 035/35 (25 kt headwind) at the surface	25	4
4	10 (595 000 lb)	JFK, 04R, CAT I	FLIGHT DIRECTOR	ATC Command	300 ft ceiling, ½ mile visibility, wind 085/28	20	4
5	10 (595 000 lb)	JFK, 04R, CAT II	AUTOPILOT	ATC Command	100 ft ceiling, RVR 1 200 ft, wind 085/28, 59 ft BARO	20	4
6	10 (595 000 lb)	DEN, 35L, CAT I	FLIGHT DIRECTOR	ATC Command	300 ft ceiling, ½ mile visibility, wind 080/40 at 8 000 ft decreasing linearly to 035/35 (25 kt headwind) at the surface, 54 ft BARO	25	4
7	10 (595 000 lb)	DEN, 35L, CAT II	AUTOPILOT	ATC Command	100 ft ceiling, RVR 1 200 ft, wind 080/40 at 8 000 ft decreasing linearly to 035/35 (25 kt headwind) at the surface, 54 ft BARO	25	4
8	50 (595 000 lb)	JFK, 04R, CAT II	AUTOPILOT	ATC Command	100 ft ceiling, RVR 1 200 ft, wind 085/28 (20 kt headwind)	20	4
9	Take-off (Normal)	DEN, 35L, CAT I	MANUAL	N/A	500 ft ceiling, 2 mile visibility, wind 040/30, 870 000 lb take-off weight	21	4

Scenario #	Go-around altitude (AGL feet)	Airport/runway/category	Autopilot/flight director mode	Go-around initiation mode	Simulator weather	Crosswind component	Gust (%)
10	Take-off (Engine #4 failed at 130 kt)	DEN, 35L, CAT I	MANUAL	N/A	500 ft ceiling, 2 mile visibility, wind 040/30, 870 000 lb take-off weight	21	4
11	Take-off (Normal)	JFK, 04L, CAT I	MANUAL	N/A	500 ft ceiling, 2 mile visibility, wind 090/20, 870 000 lb take-off weight	14	4
12	Take-off (Engine #4 failed at 125 kt)	JFK, 04L, CAT I	MANUAL	N/A	500 ft ceiling, 2 mile visibility, wind 090/20, 870 000 lb take-off weight	14	4
13	Take-off (Engine #4 failed at 50 KIAS kt — seized engine)	DEN, 35L, CAT I	MANUAL	N/A	500 ft ceiling, 2 mile visibility, wind 040/30, medium braking	21	4

Table 3-A-2. NASA Ames scenario listing for the June/July 1997 trial

Scenario #	Go-around altitude (AGL feet)	Airport/runway/category	Autopilot/flight director mode	Go-around initiation mode	Simulator weather	Crosswind component	Gust (%)
1	LAND (595 000 lb)	JFK, 04R, CAT I	FLIGHT DIRECTOR	N/A	300 ft ceiling, ½ mile visibility, wind 085/14	10	4
2	LAND (595 000 lb)	DEN, 35L, CAT I	FLIGHT DIRECTOR	N/A	900 ft ceiling, 2 mile visibility, wind 360/40 at 8 000 ft decreasing linearly to 305/35 (25 kt headwind) at the surface	25	4
14	LAND 10 m low bias (-626 ft from normal GPI) (595 000 lb)	DEN, 35L, CAT I	MANUAL	N/A	250 ft ceiling, RVR 2 400, wind 160/5, altimeter = 29.55 Hg, PAPI Off	3.5	–
15	LAND 10 m low bias (-626 ft from normal GPI) (595 000 lb)	DEN, 35L, CAT I	MANUAL	N/A	250 ft ceiling, RVR 2 400, wind 070/5, altimeter = 29.55 Hg, PAPI Off	3.5	–
16	LAND 10 m low bias (-626 ft from normal GPI) (595 000 lb)	DEN, 35L, CAT I	MANUAL	N/A	250 ft ceiling, RVR 4 000, wind 160/5, altimeter = 29.55 Hg, PAPI Off	3.5	–
17	LAND 10 m low bias (-626 ft from normal GPI) (595 000 lb)	DEN, 35L, CAT I	MANUAL	N/A	250 ft ceiling, RVR 4 000, wind 070/5, altimeter = 29.55 Hg, PAPI Off	3.5	–
17	Event-driven/ crew-based decision (595 000 lb)	DEN, 35L, CAT I	FLIGHT DIRECTOR	RI (Aircraft rolls onto runway for take-off)	300 ft ceiling, ½ mile visibility, wind 080/40 at 8 000 ft decreasing linearly to 035/35 (25 kt headwind) at the surface	25	4

Scenario #	Go-around altitude (AGL feet)	Airport/runway/category	Autopilot/flight director mode	Go-around initiation mode	Simulator weather	Crosswind component	Gust (%)
18	Event-driven/ crew-based decision (595 000 lb)	DEN, 35L, CAT II	AUTOPILOT	RI (Aircraft rolls onto runway for take-off)	300 ft ceiling, ½ mile visibility, wind 080/40 at 8 000 ft decreasing linearly to 035/35 (25 kt headwind) at the surface	25	4
19	Event-driven/ crew-based decision (595 000 lb)	DEN, 35L, CAT I	FLIGHT DIRECTOR	VPD (Emergency vehicle crosses runway)	900 ft ceiling, 2 mile visibility, wind 360/40 at 8 000 ft decreasing linearly to 305/35 (25 kt headwind) at the surface	25	4
20	10 (595 000 lb)	DEN, 35L, CAT II	AUTOPILOT	ATC Command	Night-time, 100 ft ceiling, RVR 1 200 ft, wind 080/40 at 8 000 ft decreasing linearly to 035/35 (25 kt headwind) at the surface. ATC at 10 ft AGL radar altitude, 5 404 ft BARO	25	4
21	Event-driven/ crew-based decision (595 000 lb)	DEN, 35L, CAT	FLIGHT DIRECTOR	Departure traffic on runway	Clear, 20 mile visibility, wind 360/40 at 8 000 ft decreasing linearly to 305/25 kt (25 kt headwind) at the surface. Active ATC results in landing aircraft too close to departing aircraft	25	

Table 3-A-3.   NASA Ames scenario listing for the November 1997 trial

Note.— Unless otherwise noted, the temperature was at 59° F, runway was dry, braking action was good, altimeter setting was 29.55 Hg at JFK, New York, USA, and 29.92 Hg at MMX, Mexico City, Mexico.

Scenario #	Go-around altitude (AGL feet)	Airport/runway/category	Autopilot/flight director mode	Go-around initiation mode	Simulator weather	Crosswind component	Gust (%)
22	LAND (595 000 lb)	JFK, 04R, CAT I	FLIGHT DIRECTOR	N/A	900 ft ceiling, 4 nautical mile visibility, wind 085/35	25	4
23	LAND (595 000 lb)	JFK, 04R, CAT I	FLIGHT DIRECTOR	N/A	900 ft ceiling, 4 nautical mile visibility, wind 360/35	25	4
24	LAND (595 000 lb)	MMX, 23L, CAT I	FLIGHT DIRECTOR	N/A	900 ft ceiling, 4 nautical mile visibility, wind 277/35	25	4
25	Event-driven/ crew-based decision (595 000 lb)	JFK, 04R, CAT I	FLIGHT DIRECTOR	RI (Aircraft rolls onto runway for take-off)	900 ft ceiling, 4 nautical mile visibility, wind 365/35	25	4
26	Event-driven/ crew-based decision (595 000 lb)	JFK, 04R, CAT II	AUTOPILOT	RI (Aircraft rolls onto runway for take-off)	900 ft ceiling, 4 nautical mile visibility, wind 085/35	25	4
27	10 (595 000 lb)	JFK, 04R, CAT I	FLIGHT DIRECTOR	ATC Command	350 ft ceiling, RVR 4 000 ft, wind 085/35	25	4
28	10 (595 000 lb)	JFK, 04R, CAT II	AUTOPILOT	ATC Command	200 ft ceiling, RVR 1 800 ft, wind 085/35	25	4
29	20 (595 000 lb)	JFK, 04R, CAT I	FLIGHT DIRECTOR	ATC Command	350 ft ceiling, RVR 4 000 ft, wind 085/35	25	4
30	20 (595 000 lb)	JFK, 04R, CAT II	AUTOPILOT	ATC Command	200 ft ceiling, RVR 1 800 ft, wind 085/35	25	4
31	Event-driven/ crew-based decision (595 000 lb)	JFK, 04R, CAT I	FLIGHT DIRECTOR	VPD (Emergency vehicle crosses runway)	900 ft ceiling, 4 nautical mile visibility, wind 085/35	25	4

Scenario #	Go-around altitude (AGL feet)	Airport/runway/category	Autopilot/flight director mode	Go-around initiation mode	Simulator weather	Crosswind component	Gust (%)
32	Event-driven/ crew-based decision (595 000 lb)	JFK, 04R, CAT II	AUTOPILOT	VPD (Emergency vehicle crosses runway)	900 ft ceiling, 4 nautical mile visibility, wind 360/35	25	4
33	35 (595 000 lb)	JFK, 04R, CAT I	FLIGHT DIRECTOR	ATC Command	350 ft ceiling, RVR 4 000 ft, wind 085/35	25	4
34	35 (595 000 lb)	JFK, 04R, CAT II	AUTOPILOT	ATC Command	200 ft ceiling, RVR 1 800 ft, wind 360/35	25	4
35	10 (595 000 lb)	JFK, 04R, CAT I	FLIGHT DIRECTOR	ATC Command	350 ft ceiling, RVR 4 000 ft, wind 085/35, temperature 38°F, rain on, wet runway with fair braking action	25	4
36	10 (595 000 lb)	JFK, 04R, CAT II	AUTOPILOT	ATC Command	350 ft ceiling, RVR 4 000 ft, wind 360/35, temperature 38°F, rain on, wet runway with fair braking action	25	4
37	10 (595 000 lb)	JFK, 04R, CAT III	AUTOPILOT	ATC Command	100 ft ceiling, RVR 1 000 ft, wind 085/35	25	4
38	Event-driven/ crew-based decision (595 000 lb)	JFK, 04R, CAT I	FLIGHT DIRECTOR	Arrival traffic on runway	900 ft ceiling, 4 nautical mile visibility, wind 360/35	25	4
39	Event-driven/ crew-based decision (595 000 lb)	JFK, 04R, CAT II	AUTOPILOT	Arrival traffic on runway)	900 ft ceiling, 4 nautical mile visibility, wind 085/35	25	4
40	10 (595 000 lb)	MMX, 23L, CAT I	FLIGHT DIRECTOR	ATC Command	350 ft ceiling, RVR 4 000 ft, wind 277/35	25	4
41	10 (595 000 lb)	MMX, 23L, CAT III	AUTOPILOT	ATC Command	100 ft ceiling, RVR 1 000 ft, wind 277/35	25	4

Table 3-A-4. NASA Ames scenario listing for the January/February 1998 trial

Note.— Unless otherwise noted, the temperature was at 59° F, runway was dry, braking action was good, altimeter setting was of 29.55 Hg at JFK New York, U.S.A., and 29.92 Hg at MMX, Mexico City, Mexico, and GRU, Sao Paulo, Brazil.

Scenario #	Go-around altitude (AGL feet)	Airport/runway/category	Autopilot/flight director mode	Go-around initiation mode	Simulator weather	Crosswind component	Gust (%)
42	Event-driven/ crew-based decision (595 000 lb)	JFK, 04R, CAT I	FLIGHT DIRECTOR	RI (Aircraft starts rolling onto runway for take-off when approaching aircraft reaches 250 ft AGL)	900 ft ceiling, RVR at maximum, 4 nautical mile visibility, wind 365/35	25	4
43	Event-driven/ crew-based decision with Outboard Engine #4 failed on approach (595 000 lb)	JFK, 04R, CAT I	FLIGHT DIRECTOR	RI (Aircraft starts rolling onto runway for take-off when approaching aircraft reaches 250 ft AGL)	900 ft ceiling, RVR at maximum, 4 nautical mile visibility, wind 085/35	25	4
44	10 (595 000 lb)	JFK, 04R, CAT I	FLIGHT DIRECTOR	ATC Command	350 ft ceiling, 0.8 mile visibility, wind 085/35	25	4
45	10 (415 000 lb)	JFK, 04R, CAT I	FLIGHT DIRECTOR	ATC Command	350 ft ceiling, 0.8 mile visibility, wind 085/35	25	4
46	10 (630 000 lb)	JFK, 04R, CAT I	FLIGHT DIRECTOR	ATC Command	350 ft ceiling, 0.8 mile visibility, wind 085/35	25	4
47	10 (415 000 lb)	MMX, 23L, CAT I	FLIGHT DIRECTOR	ATC Command	350 ft ceiling, 0.8 mile visibility, wind 275/35	25	4
48	10 (630 000 lb)	MMX, 23L, CAT I	FLIGHT DIRECTOR	ATC Command	350 ft ceiling, 0.8 mile visibility, wind 275/35	25	4
49	Event-driven/ crew-based decision (595 000 lb)	JFK, 04R, CAT I	FLIGHT DIRECTOR	VPD (Emergency vehicle starts to cross runway when approaching aircraft reaches 250 ft AGL)	900 ft ceiling, RVR at maximum, 4 nautical mile visibility, wind 085/35	25	4

Scenario #	Go-around altitude (AGL feet)	Airport/runway/category	Autopilot/flight director mode	Go-around initiation mode	Simulator weather	Crosswind component	Gust (%)
50	Event-driven/ crew-based decision (595 000 lb)	JFK, 04R, CAT II	AUTOPILOT	VPD (Emergency vehicle starts to cross runway when approaching aircraft reaches 250 ft AGL)	900 ft ceiling, RVR at maximum , 4 nautical mile visibility, wind 360/35	25	4
51	10 (595 000 lb)	GRU, 04R, CAT I	AUTOPILOT	ATC Command	200 ft ceiling, .8 mile visibility, wind 045/35	25	4
52	10 (595 000 lb)	GRU, 04R, CAT II	FLIGHT DIRECTOR	ATC Command	350 ft ceiling, 0.8 mile visibility, wind 045/35, temperature 38°F, rain on, wet runway with fair braking action, 300 ft fog top	25	4
53	Take-off (Engine #4 failed at VMCg - 111 kt)	JFK, 04R, CAT I	FLIGHT DIRECTOR	N/A	350 ft ceiling, 0.8 mile visibility, wind 085/35, temperature 38°F, Precipitous rain, wet runway with fair braking action, 700 000 lb is aircraft take-off weight.	25	4
54	LAND (595 000 lb)	JFK, 04R, CAT I	FLIGHT DIRECTOR	N/A	300 ft ceiling, ½ mile visibility, wind 085/35 (25 kt headwind)	25	4
55	LAND (414 000 lb)	MMX, 23L, CAT I	FLIGHT DIRECTOR	N/A	300 ft ceiling, ½ mile visibility, wind 275/35	25	4
56	LAND (595 000 lb)	GRU, 09R, CAT I	FLIGHT DIRECTOR	N/A	400 ft ceiling, ½ mile visibility, wind 045/35 (25 kt headwind)	25	4

Table 3-A-5.   ZFB (Berlin) trial scenario listing

Scenario #	Go-around altitude (AGL feet)	Airport/runway/category	Autopilot/flight director mode	Controller call or loss of visual ref.	Simulator weather[1]	Crosswind component	Turbulence (%)
1	10	DEN, 35R, CAT I	AUTOPILOT	CC	150 ft ceiling, 1 000 m RVR & VIS, wind 035/14	10	10
2	10	DEN, 35R, CAT I	FLIGHT DIRECTOR	CC	150 ft ceiling, 1 000 m RVR & VIS, wind 305/14	10	10
3	10	DEN, 35R, CAT I	FLIGHT DIRECTOR	VL	150 ft ceiling, 1 000 m RVR & VIS, wind 305/25	18	10
4	10	DEN, 35R, CAT I	FLIGHT DIRECTOR	VL	150 ft ceiling, 1 000 m RVR & VIS, wind 035/35	25	20
5	40	DEN, 35R, CAT I	FLIGHT DIRECTOR	VL	150 ft ceiling, 1 000 m RVR & VIS, wind calm	0	0
6	40	DEN, 35R, CAT I	FLIGHT DIRECTOR	VL	150 ft ceiling, 1 000 m RVR & VIS, wind 080/10	10	10
7	40	DEN, 35R, CAT I	FLIGHT DIRECTOR	CC	150 ft ceiling, 1 000 m RVR & VIS, wind 305/35	25	20
8	70	DEN, 35R, CAT I	FLIGHT DIRECTOR	VL	150 ft ceiling, 1 000 m RVR & VIS, wind 260/10	10	10
9	70	DEN, 35R, CAT I	FLIGHT DIRECTOR	VL	150 ft ceiling, 1 000 m RVR & VIS, wind 305/25	18	10
10	70	DEN, 35R, CAT I	FLIGHT DIRECTOR	CC	150 ft ceiling, 1 000 m RVR & VIS, wind 035/35	25	20
11	LAND	DEN, 35R, CAT I	AUTOPILOT	N/A	150 ft ceiling, 1 000 m RVR & VIS, wind 035/14	10	10
12	LAND	DEN, 35R, CAT I	FLIGHT DIRECTOR	N/A	150 ft ceiling, 1 000 m RVR & VIS, wind 080/10	10	10
13	LAND	DEN, 35R, CAT I	FLIGHT DIRECTOR	N/A	150 ft ceiling, 1 000 m RVR & VIS, wind 305/25	18	10

1. Due to an elevation error in the ground model at DEN, the tabulated ceiling setting needed adjustment. The tabulated ceiling setting gave CAT I visual conditions to the pilots.

Scenario #	Go-around altitude (AGL feet)	Airport/runway/category	Autopilot/flight director mode	Controller call or loss of visual ref.	Simulator weather[1]	Crosswind component	Turbulence (%)
14	40	DEN, 35R, CAT II	AUTOPILOT	CC	150 ft ceiling, 1 000 m RVR & VIS, wind 035/25	18	10
15	70	DEN, 35R, CAT II	AUTOPILOT	CC	150 ft ceiling, 1 000 m RVR & VIS, wind 035/25	18	10
16	LAND	DEN, 35R, CAT II	AUTOPILOT	N/A	300 ft ceiling, 1 000 m RVR & VIS, wind calm	0	0
17	10	JFK, 04R, CAT I	FLIGHT DIRECTOR	CC	300 ft ceiling, 1 000 m RVR & VIS, wind calm	0	0
18	10	JFK, 04R, CAT I	AUTOPILOT	VL	300 ft ceiling, 1 000 m RVR & VIS, wind 085/14	10	10
19	10	JFK, 04R, CAT I	FLIGHT DIRECTOR	CC	300 ft ceiling, 1 000 m RVR & VIS, wind 355/14	10	10
20	10	JFK, 04R, CAT I	FLIGHT DIRECTOR	VL	300 ft ceiling, 1 000 m RVR & VIS, wind 355/25	18	10
21	10	JFK, 04R, CAT I	FLIGHT DIRECTOR	CC	300 ft ceiling, 1 000 m RVR & VIS, wind 355/35	25	20
22	40	JFK, 04R, CAT I	FLIGHT DIRECTOR	VL	300 ft ceiling, 1 000 m RVR & VIS, wind 130/10	10	10
23	40	JFK, 04R, CAT I	FLIGHT DIRECTOR	VL	300 ft ceiling, 1 000 m RVR & VIS, wind 355/25	18	10
24	40	JFK, 04R, CAT I	AUTOPILOT	VL	300 ft ceiling, 1 000 m RVR & VIS, wind 085/25	18	10
25	40	JFK, 04R, CAT I	FLIGHT DIRECTOR	VL	300 ft ceiling, 1 000 m RVR & VIS, wind 085/35	25	20
26	70	JFK, 04R, CAT I	FLIGHT DIRECTOR	VL	300 ft ceiling, 1 000 m RVR & VIS, wind calm	0	0
27	70	JFK, 04R, CAT I	FLIGHT DIRECTOR	CC	300 ft ceiling, 1 000 m RVR & VIS, wind 130/10	10	10
28	70	JFK, 04R, CAT I	AUTOPILOT	CC	300 ft ceiling, 1 000 m RVR & VIS, wind 355/25	18	10

Scenario #	Go-around altitude (AGL feet)	Airport/runway/category	Autopilot/flight director mode	Controller call or loss of visual ref.	Simulator weather[1]	Crosswind component	Turbulence (%)
29	70	JFK, 04R, CAT I	FLIGHT DIRECTOR	CC	300 ft ceiling, 1 000 m RVR & VIS, wind 085/25	18	10
30	LAND	JFK, 04R, CAT I	FLIGHT DIRECTOR	N/A	300 ft ceiling, 1 000 m RVR & VIS, wind 085/35	25	20
31	LAND	JFK, 04R, CAT II	AUTOPILOT	N/A	300 ft ceiling, 1 000 m RVR & VIS, wind 355/25	18	10
32	LAND	JFK, 04R, CAT II	AUTOPILOT	N/A	300 ft ceiling, 1 000 m RVR & VIS, wind calm	0	0

Table 3-A-6. Toulouse trial scenario listing

Scenario #	AP/F/D	Rwy	Controller call or loss of visual reference	GA height (AGL feet)	Wind	X Wind	Simulator weather	Turbulence (%)
1	AP	JFK, 04R	n/a	LAND	Calm wind	0	Dusk 300 ft ceiling, RVR 1 000 m	0
2	F/D	JFK, 04R	VL	70	Wind 085/33	23	Dusk 300 ft ceiling, RVR 1 000 m	10
3	F/D	JFK, 04R	VL	40	Wind 085/25	18	Dusk 300 ft ceiling, RVR 800 m	10
4	F/D	JFK, 04R	CC	10	Wind 355/25	18	Dusk 300 ft ceiling, RVR 800 m	20
5	F/D	JFK, 04R	n/a	LAND	Wind 355/33	23	Dusk 300 ft ceiling, RVR 1 000 m	10
6	F/D	JFK, 04R	VL	10	Wind 085/30	21	Dusk 300 ft ceiling, RVR 800 m	20
7	F/D	JFK, 04R	CC	40	Wind 085/14	23	Dusk 300 ft ceiling, RVR 1 000 m	10
8	F/D	JFK, 04R	VL	70	Wind 355/25	18	Dusk 300 ft ceiling, RVR 800 m	20
9	F/D	JFK, 04R	VL	40	Wind 355/30	21	Dusk 300 ft ceiling, RVR 800 m	20
10	AP	MEX, 23L	n/a	LAND	Calm wind	0	Dusk 300 ft ceiling, visibility 1 000 m	0
11	F/D	MEX, 23L	CC	40	Wind 185/33	23	Dusk 300 ft ceiling, visibility 1 000 m	10
12	F/D	MEX, 23L	VL	10	Wind 185/25	18	Dusk 300 ft ceiling, visibility 800 m	10
13	F/D	MEX, 23L	VL	70	Wind 275/33	23	Dusk 300 ft ceiling, visibility 1 000 m	20
14	F/D	MEX, 23L	n/a	LAND	Wind 275/25	18	Dusk 300 ft ceiling, visibility 1 000 m	20
15	F/D	MEX, 23L	VL	70	Wind 185/25	18	Dusk 300 ft ceiling, visibility 800 m	10
16	F/D	MEX, 23L	CC	40	Wind 275/25	18	Dusk 300 ft ceiling, visibility 800 m	10
17	F/D	MEX, 23L	VL	10	Wind 185/14	10	Dusk 300 ft ceiling, visibility 800 m	20
18	F/D	MEX, 23L	CC	40	Wind 275/14	10	Dusk 300 ft ceiling, visibility 1 000 m	20
19	F/D	MEX, 23L	VL	70	Wind 185/14	10	Dusk 300 ft ceiling, visibility 1 000 m	10

Chapter 4
PILOT RESPONSE TIME ANALYSIS OF NASA AMES STUDY

4.1   INTRODUCTION

4.1.1   The FAA, in cooperation with aeroplane manufacturers, conducted a series of piloted simulator studies to investigate OFZ requirements for airports to accommodate NLAs. The studies assisted in establishing operational requirements for airports not designed to meet code letter F criteria. These studies evaluated pilot response time and aircraft position during balked landings. Part II, Chapter 3 summarizes the effects of wind, GA height, aircraft landing weight, airport elevation and flight control mode on aircraft position during the balked landing procedure. This chapter reports how these experimental conditions affected pilot response times.

4.1.2   All these tests employed a strong crosswind component during landing approach. By testing airline pilots under extreme operational conditions, it was hoped knowledge would be gained in generalizing the balked landing study results outside the testing environment.

Pilot response time results

4.1.3   The term "pilot response time" is used to denote the time required for the crew to perform specific procedures of a balked landing manoeuvre. The variables under study were time delays from the following:

   a)   GA initiation (TO/GA switch press) to flaps handle in the 20-detent position (flaps time); and

   b)   Flaps handle in 20-detent to landing gear handle "up" (gear time).

4.1.4   The mean and standard deviations of these variables are summarized in Table 4-1. These data were analysed to identify factors that influence pilot response time, which are useful for constructing input distributions for the Monte Carlo simulation. The key results with regard to pilot response time are as follows:

   • The data indicate a small but statistically significant correlation between flaps time and gear time $(r = -0.16; p = 0.006; n = 285)$.[1]

      — The estimated correlation coefficient and additional analysis indicate only a weak relationship between these variables. Therefore, in spite of the observed correlation, it may be sufficient to independently sample flaps and gear times in the Monte Carlo simulation.

---

1. r is used to denote the sample correlation coefficient; p denotes the p-value from a statistical hypothesis test; n denotes sample size.

- The data exhibit substantial crew-to-crew variability in flaps time $(F_{33,\ 214} = 2.1;$ $p < 0.001).$[2] Estimates indicate that crew-to-crew differences account for about 30 per cent of the observed variability in flaps time. This suggests that a "crew effect" should be explicitly included in Monte Carlo simulation to reflect the observed variability. Gear time does not indicate significant "between crew" variability.

- Flaps time and gear time do not appear to be affected by flight control mode.

- GA initiation height and airport elevation do not appear to significantly affect pilot response time.

- The type of event initiating the GA (GA initiation) does not appear to affect pilot response time.

- Balked landings occurring at night exhibit a longer flaps time. The data indicate the delay is between 0.6 and 3.2 s for night GAs. Gear time is not affected by night-time balked landings.

- For GAs initiated at low altitude 3-m (10-ft) AGL, touchdown results in an increase in flaps time ($p = 0.02$). In 81 of 146 low-altitude balked landings that touched down, the mean flaps time was 5.76 s. This is about 0.75 s longer (95 per cent confidence interval is 0.10 to 1.45 s longer) than those that do not touch down (mean 4.99 s). Touchdown does not appear to affect gear time.

- The response time data do not indicate a "surprise" effect for flaps time or gear time. That is, the first GA presented to a flight crew does not appear to influence the response times when crew follow recommended procedure. Earlier studies suggest that the time from ATC command to TO/GA switch press may have been influenced by a surprise effect. However, departures from recommended balked landing procedure may be associated with a surprise effect ($p = 0.01$). In 4 of 32 (0.125) first GAs, flight crew raised the landing gear before changing the flaps position, which is counter to recommended procedure. However, in later GAs this departure occurred in only 4 of 277 (0.014) approaches.

4.1.5   A more complete description related to the pilot response time analysis of the simulator study is in 4.2 (see Part II, Chapter 3, Figures 3-4A to 3-10D for graphical details). Section 4.3 provides an analysis and quantitative summary of the results of the pilot response time analysis, and 4.4 summarizes these findings.

4.2   STUDY DESCRIPTION

4.2.1   The studies included four test sessions[3], which were conducted in May, June/July, November 1997, and January/February 1998, at the NASA Ames Research Center on a Boeing 747-400 full-motion flight simulator. The studies evaluated pilot response times during balked landing GA procedures.

---

2. *F*33, 214 denotes an *F*-distribution with 33 numerator degrees of freedom (df) and a 214 denominator *Df*.

3. In addition to the four test sessions described in 4.2.1, eight flight crew were tested in January 1997. The test procedure for this preliminary session was not as well defined as in subsequent sessions. Furthermore, a number of additional variables, such as time at thrust lever advance (TLA), were added in later experiments. Due to these changes and some uncertainty about a touchdown occurrence, the January 1997 data were omitted from this analysis.

Airline flight crew were asked to fly landing approaches and balked landing manoeuvres under experimentally controlled conditions in order to evaluate the effects of varying flight conditions on aircraft track and pilot responses during balked landings.

4.2.2   The GAs were initiated by simulated ATC instructions, RI by another aircraft, VPD or by active traffic (TFC) on the runway. In addition, the flight control mode (auto-coupled or F/D), aircraft weight and airport elevation, as well as other factors were explored to evaluate their effects on the response variables. Tables 4-2 to 4-5 summarize the four test sessions.

4.2.3   For the balked landing trials conducted in May 1997, airport elevation was incorporated as an experimental factor. Nine volunteer airline crew of two pilots each flew six different balked landing scenarios. The landing weight of 240 454 kg (595 000 lb) was selected to represent the approach speed of an NLA. All approaches to JFK were performed in 28-kt quartering head wind (direction 085, 20-kt right crosswind component, 20-kt head-wind component).

4.2.4   For all DEN approaches, the wind direction and magnitude changed (linearly) with decreasing altitude. In all cases the wind direction shifted 45 degrees and magnitude was reduced 5 kt, with the change beginning 2 438 m (8 000 ft) AGL. For scenarios 3 and 4, the quartering head wind was 35 kt (035/35, 25-kt right crosswind component, 25-kt head wind component) at ground level.

4.2.5   For DEN approach scenario 6, the quartering head wind was from the left (not the right as with scenarios 3 and 4). For manually flown approaches, the ceiling was at 91 m (300 ft) and visibility was 0.8 km (0.5 miles). Autopilot/autoland approaches had a 30-m (100-ft) ceiling and RVR of 364 m (1 200 ft).

4.2.6   The flight control mode and GA call height were experimentally controlled factors. The GA was initiated by verbal instruction via a simulated ATC radio transmission. The "GA" command was given when the aircraft reached either 15 m (50 ft) or 3-m (10-ft) AGL.

4.2.7   Ten crew completed five balked landing tests in June/July 1997 as shown in Table 4-3. For these, as well as all remaining test sessions, there was a 35-kt quartering head wind for all GAs. Unless otherwise noted, the atmospheric and aircraft weight conditions were as described in 4.2.3 to 4.2.6. ATC 3 m (10 ft)/night denotes a test scenario in which the landing approach and GA occurred at night.

4.2.8   In November 1997, six crew completed the balked landing tests. Each crew performed 17 balked landings. The test scenarios are described in Table 4-4. The ATC 3 m (10 ft)/III code denotes a category III landing approach. Similarly, ATC 3 m (10 ft)/wet denotes wet runway conditions.

4.2.9   Eleven crew were tested in January/February 1998. The test scenarios are summarized in Table 4-5. The RI/EO code indicates a runway incursion with one engine out. For heavy-weight scenarios the aircraft weight was set to 286 000 kg (630 000 lb) and for light-weight scenarios to 188 636 kg (415 000 lb).

4.3   RESULTS

4.3.1   Test results were summarized for two key responses:

a)   Flaps time (time from GA initiation, i.e. the take-off/go-around (TO/GA) switch press, to flaps handle in 20 detent); and

b)   Gear time (time from flaps handle in 20 detent to landing gear handle in "up" position).

4.3.2   Both flaps and gear handle positions were monitored during the simulation. Hence, the time at which they reached their designated positions was easy to determine. Conversely, identifying the time at which the GA was initiated was more difficult since the GA could begin with either the TO/GA switch press or the thrust lever advance (TLA) by the pilot-in-command. TLA presented further complication since small advances in the thrust levers might occur during normal landing procedures and not necessarily indicate the initiation of a GA. After examination of the data, it was specified that TLA occurs (associated with GA initiation) when the thrust levers advance two degrees above the minimum recorded value for each landing approach. A summary table of the thrust lever advance is provided in Table 4-6.

4.3.3   The TO/GA switch press time was used to indicate GA initiation whenever it preceded the time at which the aircraft reached minimum altitude. However, in about 20 per cent of GAs, TO/GA switch press occurred after the minimum altitude was reached; therefore, the pilot must have advanced the thrust lever first. In those cases, the following rules were used to identify GA initiation:

a)   If TO/GA switch press time preceded minimum altitude and followed ATC command time (for those balked landings induced by ATC), TO/GA switch press began the GA;

b)   If TO/GA switch press followed minimum altitude, and TLA met the conditions of rule a), TLA began the GA; and

c)   If TLA preceded ATC command time, and TO/GA followed minimum altitude, the GA start time was recorded as missing.

This scheme resulted in 281 GAs initiated at TO/GA switch press, 18 initiated at TLA and 30 that could not be resolved; as a consequence, the total was 329 GAs.

4.3.4   Flaps and gear times were calculated according to the following formulae:

Flaps time = time for flaps handle at 20 detent – GA initiation time

Gear time = time for gear handle "up" – time for flaps handle at 20 detent

4.3.5   A summary of the data revealed the following general results:

a)   In 183 of 307 runs (60 per cent) the thrust levers advanced before TO/GA switch press. A summary of the difference (TLA – TO/GA) is time in seconds. Therefore, TLA can precede TO/GA by more than 30 s and never trails by more than 1.1 s. Part of this discrepancy may be explained by small advances in the thrust levers during normal landing procedures;

b)   Of 15 landings, five indicated a TLA before 3-m (10-ft) AGL because the pilot did not execute a GA. The times were 51.2, 46.1, 14.9, 13.3 and 1.3 s before 3 m (10 ft). This suggests it is not unusual for pilots (or autopilots) to advance the thrust levers at low altitudes during landings, which further supports the conjecture in a) above; and

c)   There were eight balked landings (2.6 per cent) where gear time was negative, i.e. landing gear raised before flaps change. The recommended procedure is first to change the flaps, then raise the landing gear. Retaining these negative observations produces a negative correlation between flaps and gear times (correlation coefficient $r = -0.44$, p-value $p < 0.001$). However, omitting the negative flaps observations results in a correlation of smaller magnitude ($r = -0.16$, $p = 0.006$). Although a statistically significant correlation is present, the relationship appears weak. For Monte

Carlo simulation, it may be reasonable to model flaps time and gear time as independent. The operational significance of this correlation could be evaluated through ASAT testing.

Note.— The data contain eight negative values for gear time. These values result from trials where crew raised the landing gear before changing the flaps to 20 degrees, which is contrary to recommended missed approach procedure. Unless otherwise noted, the negative values are withheld from further analyses since they reduce the estimated mean and increase the reported variability.

Flaps time results

4.3.6   Factors affecting the pilot response for flaps time were evaluated. Since the data would be used to define Monte Carlo inputs, initial analyses focused on subsets of the data most pertinent to the simulation. When no differences appear, subsets are then combined to achieve a large enough sample to estimate an input distribution. First, how crew-to-crew variability influences the dependence structure of the data was investigated. Second, how experimentally controlled factors influence the pilot response were reviewed. Third, the association between flaps time and touchdown — an uncontrolled experimental outcome — was examined.

4.3.7   Experimentally controlled factors were examined one at a time (by comparison with observations from a reference condition) and the results are displayed in Figures 4-1 to 4-7. When a more quantitative comparison was necessary, *t* or *F*-tests (for one-way analysis of variance) were used. These tests were interpreted informally since it was unlikely that the data would meet the distributional assumptions associated with the procedures. However, because the tests procedures were robust to moderate departures from the assumptions, they provided useful guidance for interpreting factors.

Crew-to-crew variability

4.3.8   Time for flaps to detent 20 shows significant crew-to-crew variability in all the above-mentioned experiments, $p < 0.001$, (see the appendix to this chapter for an analysis of variance (ANOVA) partitioning). Substantial variability between crew (crew-to-crew variability) as well as variation in the repeatability of responses for a given crew (within crew variability) was observed.

4.3.9   Figure 4-1[4] shows the range of flaps time observations for the 34 flight crew participating in the study. Heuristically, we interpret inter-crew variability as "some crews are faster than others" in changing flaps position. Technically, the observations from a given crew are positively correlated with one another. This implies that naïve estimation of flaps time variance will underestimate the true variability.

4.3.10   The observed flaps time mean was 5.49 s, and naive estimation of the variance is 3.77 ($n = 285$). Estimating the separate components of variance results in values of 1.26 for between crew variance and 2.70 for within crew variance.[5] Therefore, inter-crew differences account for about 30 per cent of the variability in flaps time observations.

4.3.11   Using the estimates above, naive estimation of flaps time variance results in an underestimation of about 5 per cent ((1.26 + 2.70)/3.77). This suggests that a "crew effect" in the Monte

---

4.   All figures are located at the end of this chapter.

5.   These values were obtained from a robust estimation procedure. The data were "cleaned" using an initial robust estimate and the restricted maximum likelihood (REML) procedure was used for the cleaned data.

Carlo simulation algorithm may be included. However, it is unclear whether this degree of underestimation has any operationally significant consequences.

Airport elevation

4.3.12   ATC 3-m (10-ft) initiated GAs performed in auto-coupled mode were considered the reference set of observations. Figure 4-2 summarizes the distribution of flaps time for three airports that differ in elevation (JFK in New York City, GRU in Sao Paulo and DEN in Denver).

4.3.13   There is little difference in mean flaps time for these three airports. The variability of values at GRU appears smaller than at either of the other two airports, estimated variance = 0.85 versus 6.0 – 7.0 for JFK and DEN. The variance ratio test[6,7] indicates a significant difference in variability (p = 0.004). It is unclear why the variability at this (simulated) elevation should be smaller. Furthermore, variance for flight director balked landings at GRU does not appear to be smaller than that at other airports. Due to the relatively small sample sizes and the fact that Bartlett's test is not robust to non-normal data, the test result may not be reliable and may not hold in repeated sampling of the data. Except for the reduced variability at GRU, the data do not indicate that auto-coupled flaps time at 3 m (10 ft) differs for different elevations.

Flight control mode

4.3.14   Figure 4-3 summarizes the flaps time distributions for auto-coupled and manual F/D controlled balked landings. F/D GAs at 3 m (10 ft) do not substantially differ from autopilot GAs at the three airports. ANOVA indicates that neither airport elevation nor flight control mode nor their interaction significantly affects flaps time ($F_{5, 66}$ = 1.2, p = 0.30) (see the appendix to this chapter).

Other ATC 3-m (10-ft) GAs

4.3.15   Figure 4-4 shows the flaps time distributions for other ATC 3-m (10-ft) GAs. The figure suggests that night balked landings may exhibit longer flaps time than the other groups. Heavy- and light-weight, and wet runway balked landings do not appear to differ from ATC 3-m (10-ft) GAs. ANOVA ($F_{4, 129}$ = 4.1, p = 0.004) indicates that night balked landings differ significantly from other ATC 3-m (10-ft) GAs. Night GAs averaged 7.1 s, while other GAs averaged 5.2 s. A 95-per cent confidence interval for the difference is 0.6, 3.2.

          Note.— Heavy-weight, light-weight, wet runway and night GAs were all initiated by ATC command at 3-m (10-ft) AGL.

GA initiation altitude

4.3.16   Flaps time for balked landings initiated by ATC call at 6-m (20-ft), 11-m (35-ft) and 15-m (50-ft) AGL are shown in Figure 4-5. The graph shows that flaps time does not differ substantially from 3-m (10-ft) GAs. GA initiation height (AGL) does not appear to affect flaps response time.

---

6.   The variance ratio test evaluates the null hypothesis that the variances of two independent normal distributions are equal. Under the null hypothesis, the ratio of sample variances, s_1^2/s_2^2 exhibits an F-distribution with $n_1 – 1$ and $n_2 – 1$ *Df*. The symbols n_1 and n_2 denote the number of observations in samples 1 and 2, respectively.

7.   Brownlee, K. A. Statistical Theory and Methodology in Science and Engineering. Wiley, New York, 1965.

Other GA initiators

4.3.17   Other GA initiators (VPD, RI, RI/EO, TFC arriving and departing) do not appear to affect flaps time, (when compared with ATC command). Figure 4-6 summarizes the observations from the balked landing studies.

Aircraft touchdown

4.3.18   Flaps time appears to be longer for 3-m (10-ft) GAs that touch down (81 of 146) than for those that do not. Figure 4-7 shows back-to-back histograms of flaps time for touchdowns and non-touchdowns. The mean for touchdowns is 5.76 s versus 4.99 s for non-touchdowns ($p = 0.023$; 95 per cent confidence interval is 0.10 to 1.45). The graph also shows a more dispersed distribution for touchdowns.

4.3.19   A test of equality of variances ($F_{81, 65} = 2.37$, $p < 0.001$) indicates that the dispersion difference is statistically significant (variance of 5.63 for touchdowns, 2.37 for GAs that do not). The *F*-test results should be interpreted cautiously since this test is not robust to non-normality. However, graphical analysis suggests the difference in distributions cannot be adequately described by simple location shift.

4.3.20   For GAs initiated at 6 m (20 ft) and above, only 4 of 139 touched down. These observations also indicate that touchdown delays flaps time, 7.7 versus 5.5 s; $p = 0.014$; 95 per cent confidence interval is 0.46 to 4.0.

        Note.— Aircraft touchdown is a response and not an experimentally controlled variable. Therefore, it cannot be distinguished whether touchdown causes delayed flaps, slow flaps causes touchdown or whether both result from the action of some other factors.

4.3.21   In summary, flaps time shows significant crew-to-crew variability (some crews are faster than others). However, no other tested factors, e.g. flight control mode, differing GA height, aircraft weight, airport elevation, cause of GA initiation, appear to substantially influence flaps time. Flaps time appears to be between 0.6 and 3.2 s slower for night balked landings. For low-altitude balked landings initiated at 3 m (10 ft) or less aircraft touchdown is associated with flaps time averaging up to 1.5 s longer than those that do not.

Gear time results

Crew-to-crew variability

4.3.22   As with flaps time, time to gear "up" exhibits statistically significant variability between flight crew ($F_{33, 228} = 1.71$, $p = 0.013$). However, the magnitude of the crew-to-crew differences is much smaller for gear time than for flaps time. Crew variability accounts for only about 6 per cent of the total variation in gear time observations. This produces a negligible difference in the estimate of total variability when compared with a naïve estimation procedure — both procedures yield an estimate of variance of 2.59. Although it is statistically significant, crew variability does not appear to be an important source of variability in gear time. Figure 4-8 shows the range of gear time for the 34 flight crew participating in the study.

Airport elevation

4.3.23   Balked landings initiated by ATC command at 3-m (10-ft) AGL do not exhibit differing gear times at airports of differing elevation ($p = 0.24$). Gear times for ATC 3-m (10-ft) GAs with coupled approach are summarized in Figure 4-9.

Flight control mode and GA initiation altitude

4.3.24   For 3-m (10-ft) GAs the data indicate that flight control mode significantly affects gear time (t_{69} = 2.1; p = 0.04). Auto-coupled approaches average about 4.09 s, while F/D GAs require only 3.39 s (95 per cent confidence interval is 0.02 to 1.39 s for the difference in mean). Conversely, for GAs initiated at 6, 11 and 15 m (20, 35 and 50 ft) and for GA 3 m (10 ft)/wet and GA 3 m (10 ft)/III, there is no significant difference between auto-coupled and F/D gear times. Since the flight control mode difference is not repeated at any height other than 3 m (10 ft), nor for 3-m (10-ft) GAs with wet runway, night or category III GAs), this difference is attributed to random sampling error. The data does not provide sufficient evidence to conclude a difference in gear time based on flight control mode.

Other ATC 3-m (10-ft) GAs

4.3.25   Neither aircraft weight (heavy, light) nor changing atmospheric conditions (wet runway, night and category III conditions) affect gear time for ATC-initiated GAs ($F_{5, 150}$ = 0.52; p = 0.76). Figure 4-10 summarizes the gear time observations for these scenarios.

Other GA initiators

4.3.26   Figure 4-11 displays the gear response times for RI, VPD and active runway traffic initiated balked landings. Analysis of variance indicates that the mean gear time for balked landings initiated by active arriving traffic (TFC-Arr mean 4.7 s) differs significantly (p = 0.04) from that for an RI (RI mean 2.8 s). However, neither of these initiators differs significantly from ATC-initiated GAs.

Aircraft touchdown

4.3.27   Gear time for 3-m (10-ft) GAs does not show a significant difference between balked landings that touchdown and those that do not (p = 0.10) (see Figure 4-12). The graph indicates that the gear time distributions are similar for the two different conditions.

4.3.28   In summary, gear times do not exhibit substantial crew-to-crew variability. Hypothesis testing suggests that auto-coupled balked landings result in slower gear times than F/D (manual) approaches only for GAs initiated at 3-m (10-ft) AGL. Since the data do not demonstrate this result under any other test conditions, it is attributed to random variation. Aircraft weight and airport elevation do not appear to substantially influence gear time. Gear times for balked landings initiated by a VPD appear slightly shorter than those from arriving traffic. However, neither condition significantly differs from any other balked landing initiator. Unlike flaps time, aircraft touchdown is not associated with increased gear time.

4.4   FLIGHT CONTROL MODE, GO-AROUND (GA)
AND AIRPORT ELEVATION RESULTS

The FAA study explored the effects of flight control mode, GA height and airport elevation on pilot response times during balked landings. The primary results of this study are as follows:

        a)   Flaps time and gear time exhibit a negative correlation (r = –0.16). However, the relationship between these variables appears weak. In spite of the observed correlation, it may be sufficient to independently sample flaps and gear times in the Monte Carlo simulation;

b)   The flaps time response exhibits substantial crew-to-crew variability, suggesting that a "crew effect" should be explicitly included in Monte Carlo simulation for this variable. Gear time does not indicate substantial "between crew" variability;

c)   Flight control mode, GA initiation height and airport elevation do not appear to significantly affect any of the pilot response time variables;

d)   The type of event initiating the GA (GA initiation) has little influence on pilot response time;

e)   GAs that touchdown exhibit an increase in flaps time over those that do not. The mean flaps time is about 0.75 s longer for touchdown; and

f)   The response time data do not indicate a "surprise" effect for flaps time or gear time. However, flight crew are more likely to deviate from recommended procedure for their first balked landing than for subsequent GAs.

4.5   IMPLEMENTATION OF
THE PILOT RESPONSE TIME ANALYSIS

4.5.1   As suggested in 4.4 a), independent sampling of flaps time and gear time would be adequate in Monte Carlo simulations. Therefore, there was a separate distribution fit for incremental time from TO/GA switch press time to flaps time and another distribution fit for the incremental time from flaps time to gear time.

Note.— For the purposes of simulation, incremental times subsequent to gear time were not deemed essential as the changing the gear lever position normally occurred well above the height for OFZ, which was 45 m (150 ft).

4.5.2   As noted in 4.4 d), the type of event initiating a GA has little influence on pilot response time. Furthermore, analysis of data that differed from responses to ATC commands to execute the GA procedure showed that the data could be combined for further statistical analysis. Therefore, it was decided to curve-fit the data to a statistical family of distributions that utilizes the first, second, third and fourth moments, namely, the Johnson family of statistical distributions[8]. The flaps time for GAs initiated at 3-m (10-ft) AGL was adjusted with an additional mean flaps time of about 0.75 s in anticipation of a touchdown, as mentioned in 4.4 e).

4.5.3   Figure 4-13 illustrates the family of Johnson statistical distributions utilized in the Monte Carlo simulations. The first plot in the figure illustrates the statistical distribution corresponding to the incremental time from pressing the TO/GA switch and moving the flaps handle into the 20-detent position. The second plot illustrates the statistical distribution describing incremental time from moving the flaps handle into the 20-detent position to moving the gear lever to the "up" position.

— — — — — — — —

---

8. A detailed discussion on the Johnson family of statistical distributions can be found in N. L. Johnson's *"Systems of Frequency Curves Generated by Methods of Transition"*. *Biometrika*, Volume 36, pp. 149–176, 1949. Also, an algorithm for fitting Johnson distributions is in the article by I. D. Hill, R. Hill and R. L. Holder, *"Algorithm AS 99: Fitting Johnson Curves by Moments"*. *Applied Statistics,* Volume 25, Number 2, pp. 180–189, 1976. See also Chapter 6 of *Statistical Models in Engineering* by Gerald J. Hahn and Samuel S. Shapiro, published by John Wiley and Sons, 1994 (reprint).

Table 4-1.   Numeric summary of flaps and gear time (in seconds)

Response	n (sample size)	Mean	Standard deviation
Flaps time	285	5.49	1.94
Gear time	300	3.61	1.61

Table 4-2.   May 1997 balked landing test scenarios

Scenario	Approach	Wind	Flight control mode	GA initiation
1	JFK 4R	085/28	Manual	ATC 3 m (10 ft)
2	JFK 4R	085/28	Auto	ATC 3 m (10 ft)
3	DEN 35L	035/35	Manual	ATC 3 m (10 ft)
4	DEN 35L	035/35	Auto	ATC 3 m (10 ft)
5	JFK 4R	085/28	Auto	ATC 15 m (50 ft)
6	DEN 35L	0305/35	Manual	ATC 15 m (50 ft)
L = left				

Table 4-3.   June/July 1997 balked landing test scenarios

Scenario	Approach	Flight control mode	GA initiation
1	DEN 35L	Autopilot	ATC 3 m (10 ft)/night
2	DEN 35L	Autopilot	RI
3	DEN 35L	F/D	RI
4	DEN 35L	F/D	TFC-departure
5	DEN 35L	F/D	VPD
L = left			

Table 4-4.   November 1997 balked landing test scenarios

Scenario	Approach	Flight control mode	GA initiation
1	JFK 4R	Autopilot	ATC 3 m (10 ft)
2	JFK 4R	Autopilot	ATC 3 m (10 ft)/III
3	JFK 4R	Autopilot	ATC 3 m (10 ft)/wet
4	JFK 4R	Autopilot	ATC 6 m (20 ft)
5	JFK 4R	Autopilot	ATC 11 m (35 ft)
6	JFK 4R	Autopilot	RI

Scenario	Approach	Flight control mode	GA initiation
7	JFK 4R	Autopilot	TFC-arrival
8	JFK 4R	Autopilot	VPD
9	JFK 4R	F/D	ATC 3 m (10 ft)
10	JFK 4R	F/D	ATC 3 m (10 ft)/wet
11	JFK 4R	F/D	ATC 6 m (20 ft)
12	JFK 4R	F/D	ATC 11 m (35 ft)
13	JFK 4R	F/D	RI
14	JFK 4R	F/D	TFC-arrival
15	JFK 4R	F/D	VPD
16	MMX	Autopilot	ATC 3 m (10 ft)/III
17	MMX	F/D	ATC 3 m (10 ft)
R = right			

Table 4-5.   January/February 1998 balked landing test scenarios

Scenario	Approach	Flight control mode	GA initiation
1	GRU 9R	Autopilot	ATC 3 m (10 ft)
2	GRU 9R	F/D	ATC 3 m (10 ft/wet)
3	JFK 4R	Autopilot	VPD
4	JFK 4R	F/D	ATC 3 m (10 ft)
5	JFK 4R	F/D	ATC 3 m (10 ft)/H
6	JFK 4R	F/D	ATC 3 m (10 ft)/L
7	JFK 4R	F/D	RI
8	JFK 4R	F/D	RI/EO
9	JFK 4R	F/D	VPD
10	MMX 23L	F/D	ATC 3 m (10 ft)/H
11	MMX 23L	F/D	ATC 3 m (10 ft)/L
ATC 3 m (10 ft)/H — denotes heavy-weight balked landings ATC 3 m (10 ft)/L — denotes light-weight balked landings			

Table 4-6.   Summary of thrust lever advance (TLA) — TO/GA difference

Minimum	1st quartile	Median	Mean	3rd quartile	Maximum
−32.54	−4.398	−0.8008	−3.261	0.5352	1.07

— — — — — — — —
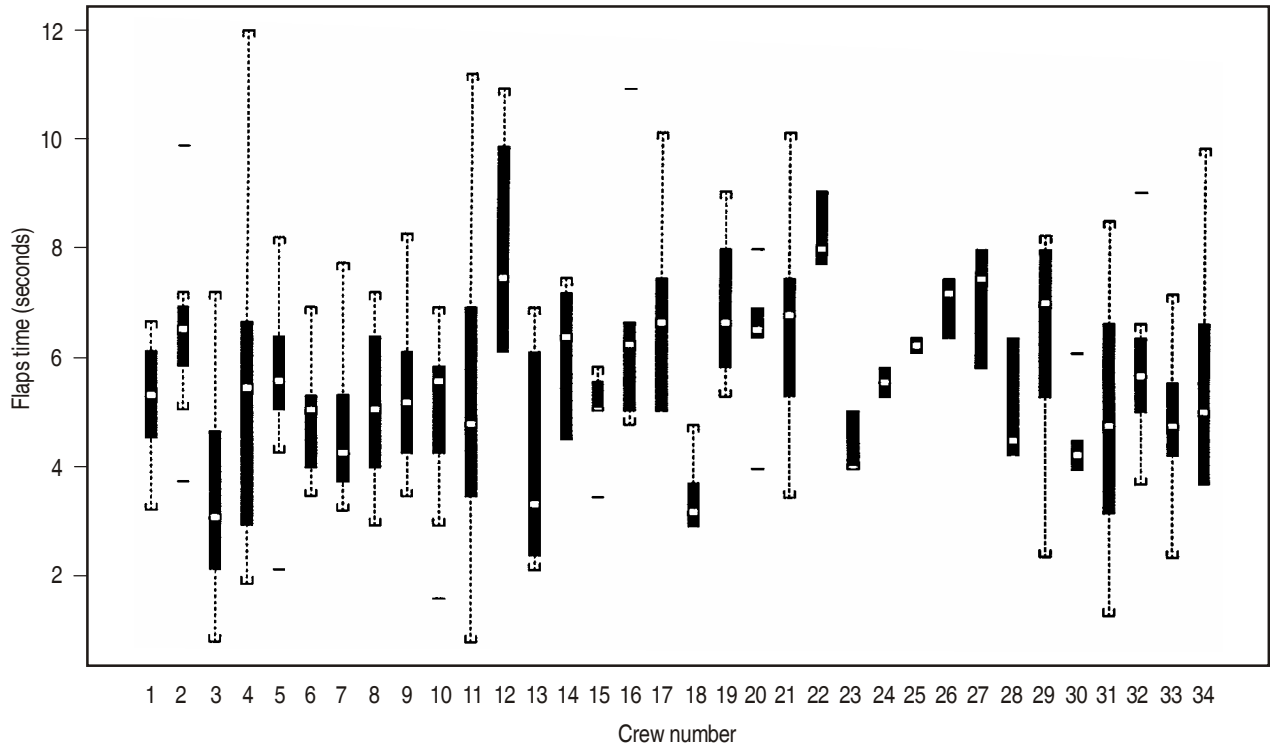
Figure 4-1.   Crew variability for flaps time
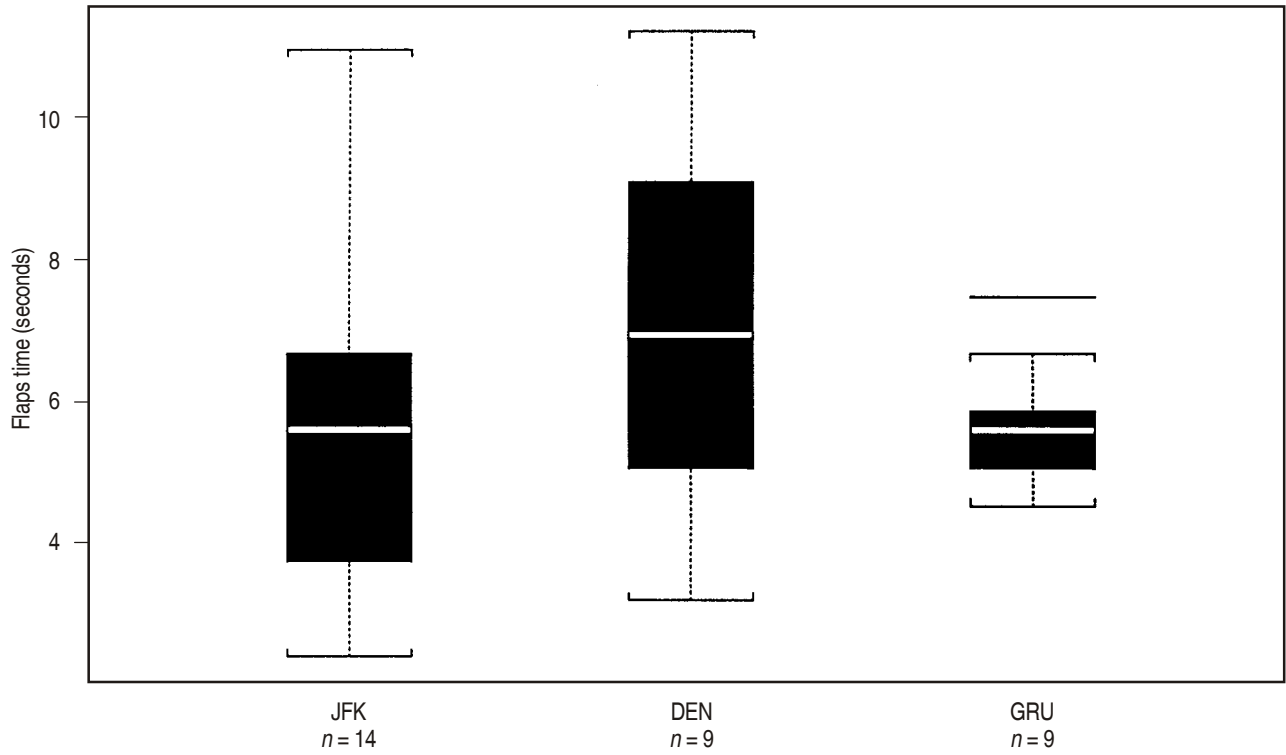
Note.— "n" denotes sample size.

Figure 4-2.   Flaps time for airports with differing elevations
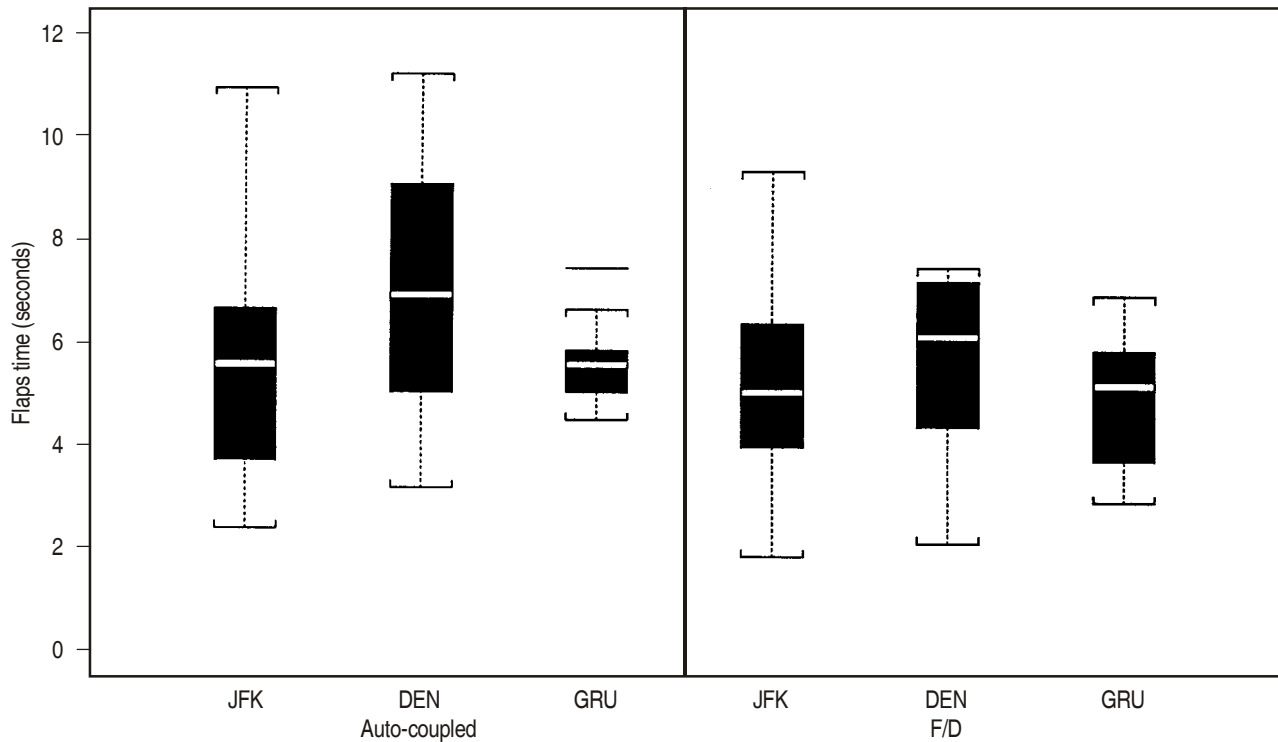
Figure 4-3.   Effect of control mode for flaps time
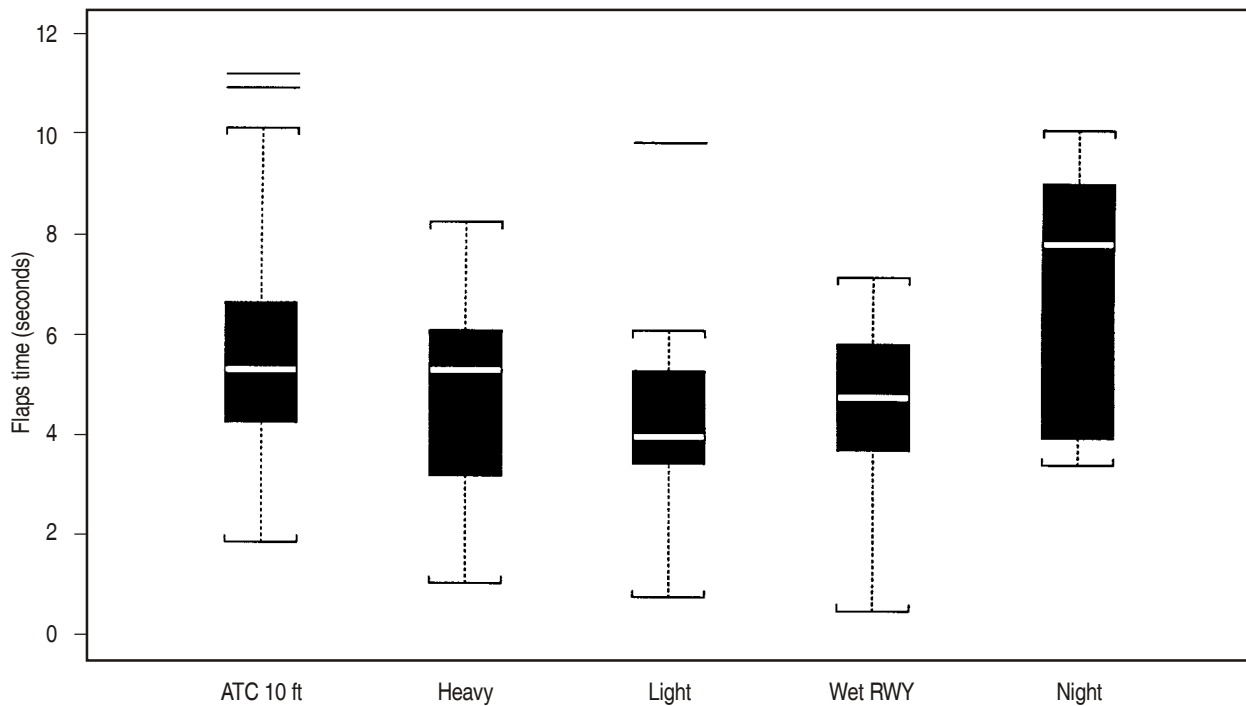
Figure 4-4.   Flaps time for other ATC 10 ft GAs
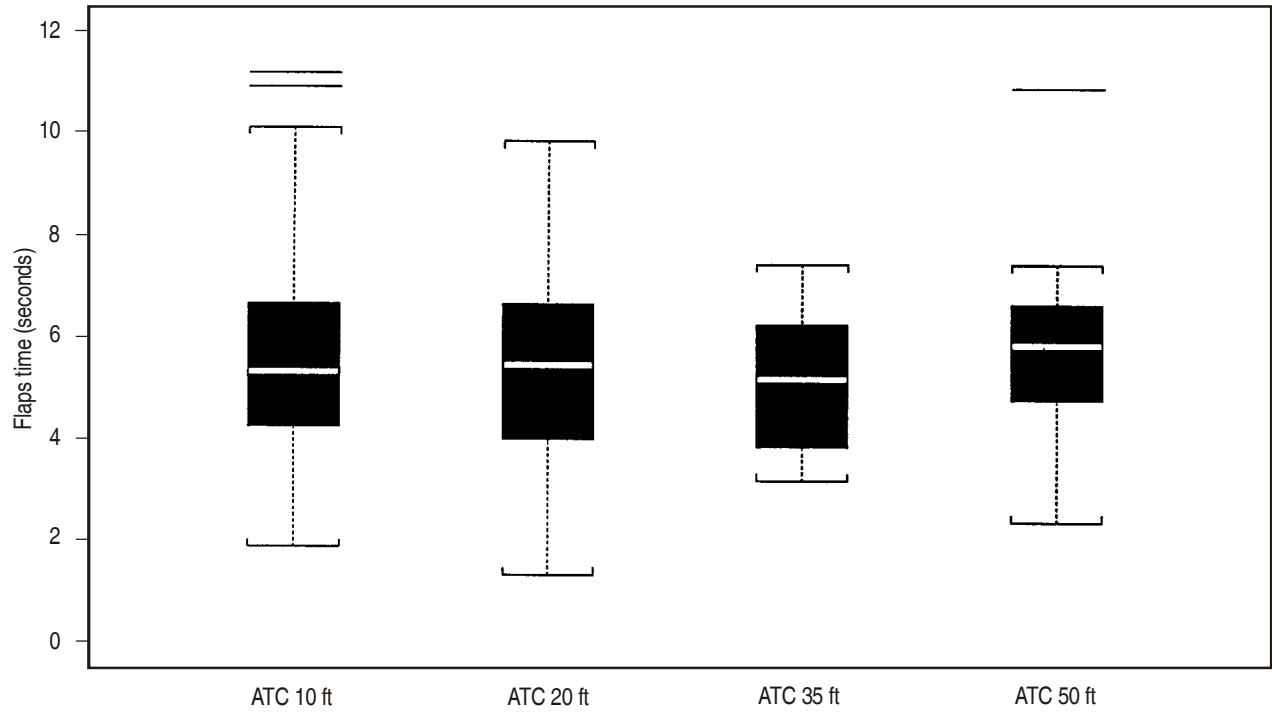
Figure 4-5.　Flaps time for GA initiation height
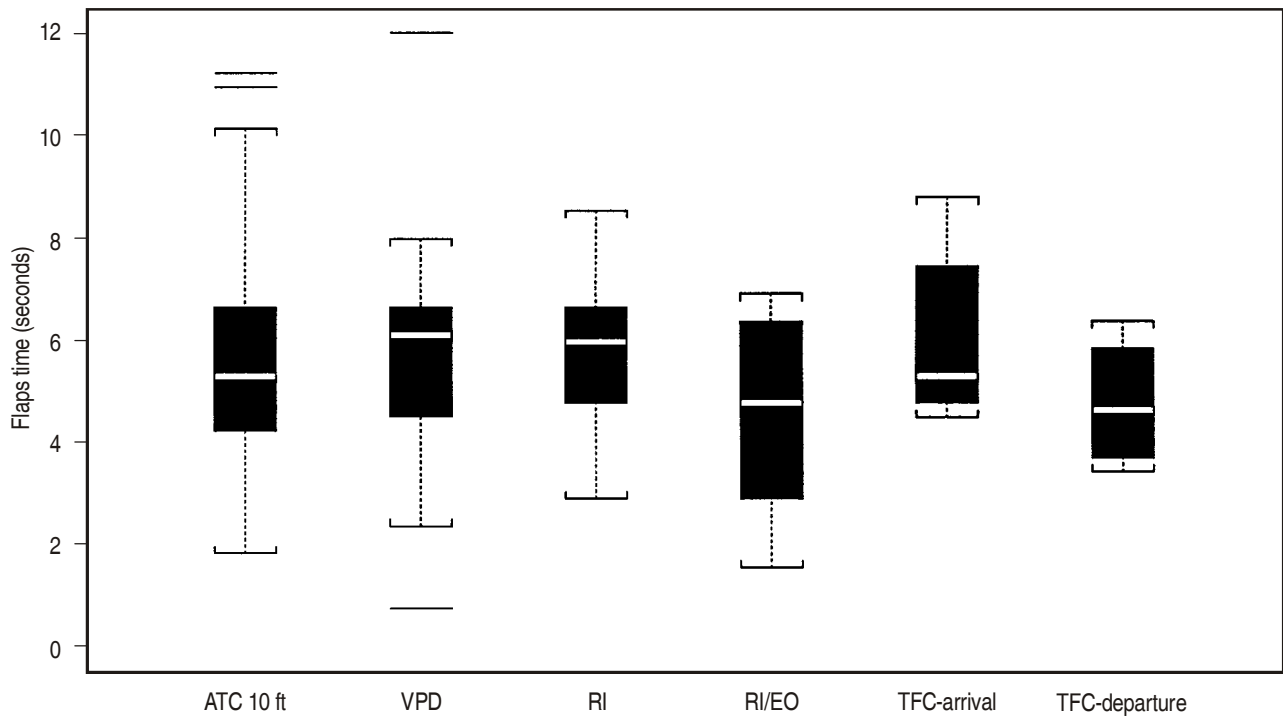
Figure 4-6.　Flaps time for non-ATC initiators
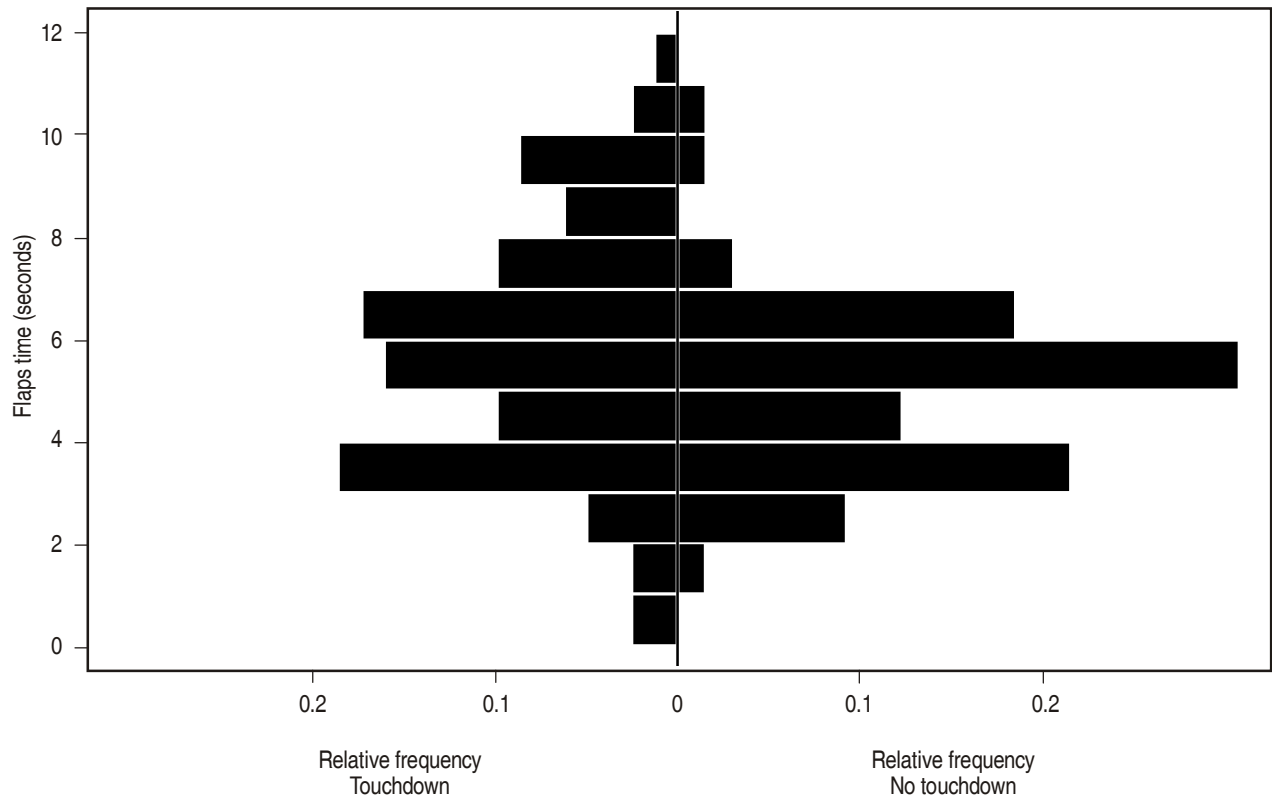
Figure 4-7.   Effect of touchdown on flaps time
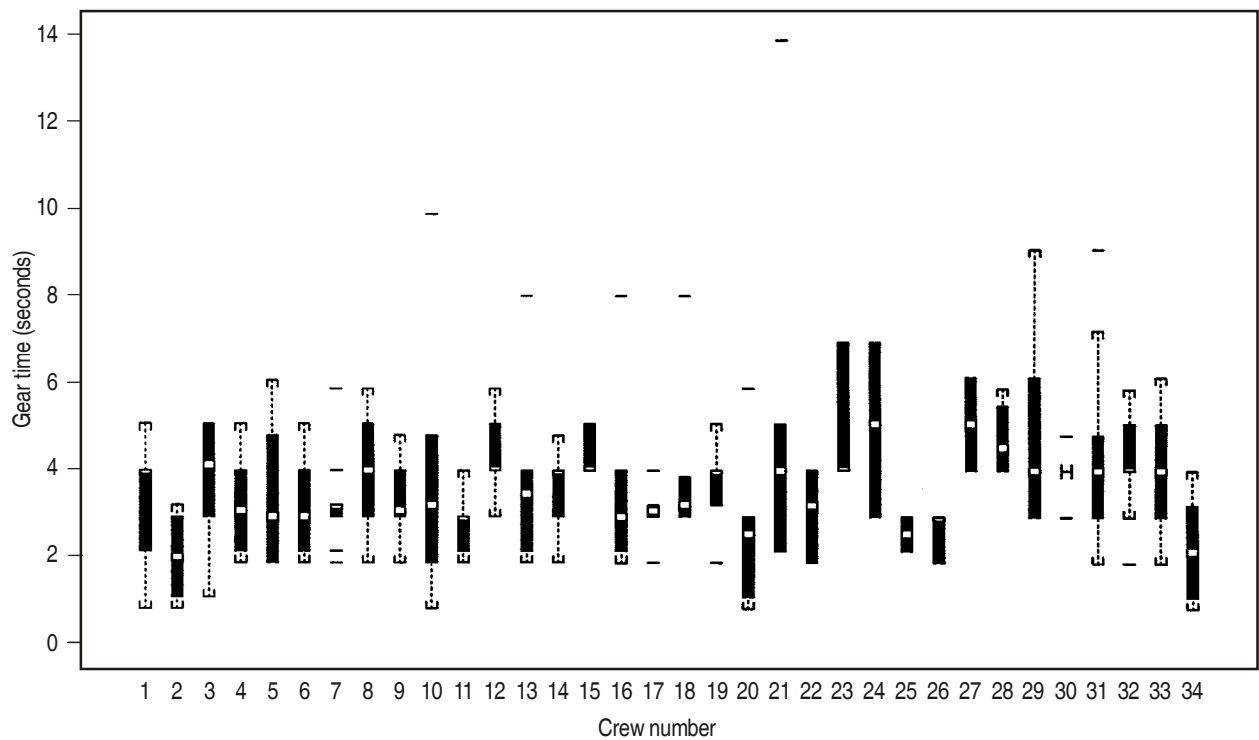
Figure 4-8.   Crew variability for gear time
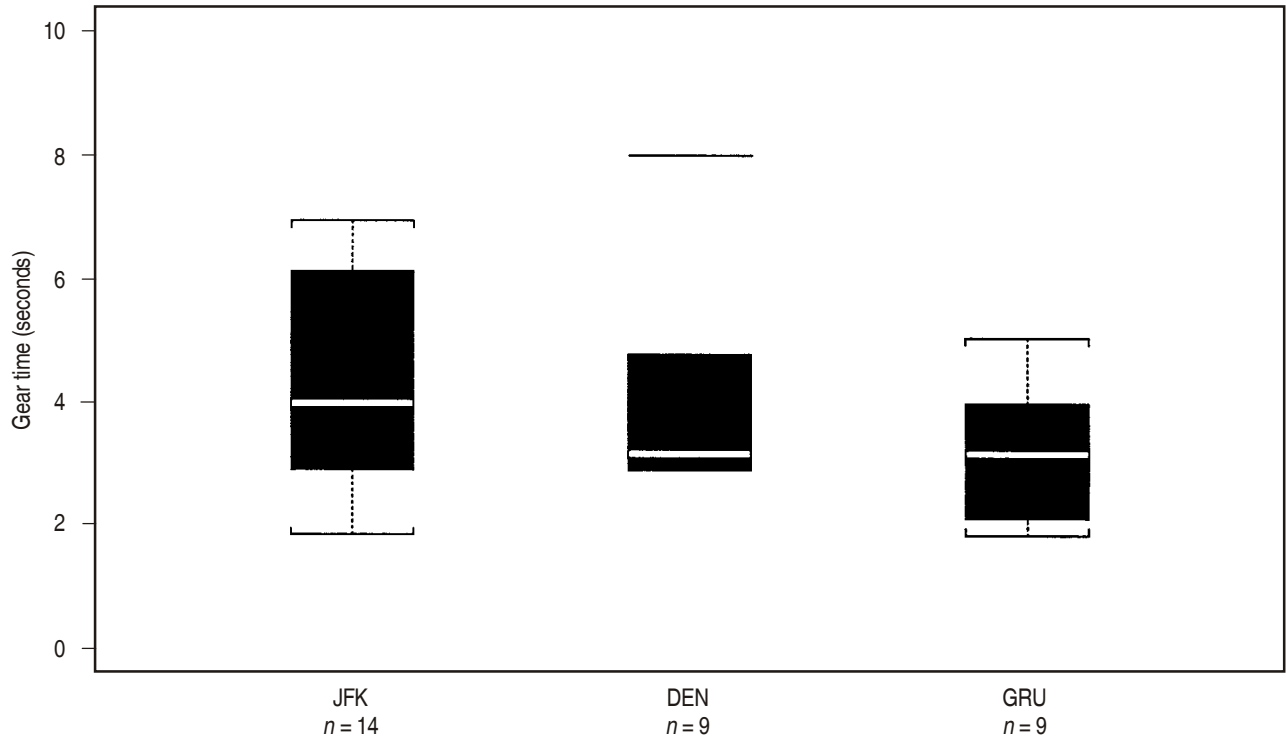
Note.— "n" denotes sample size.

Figure 4-9.   Gear times for ATC 10 ft GAs with coupled approach
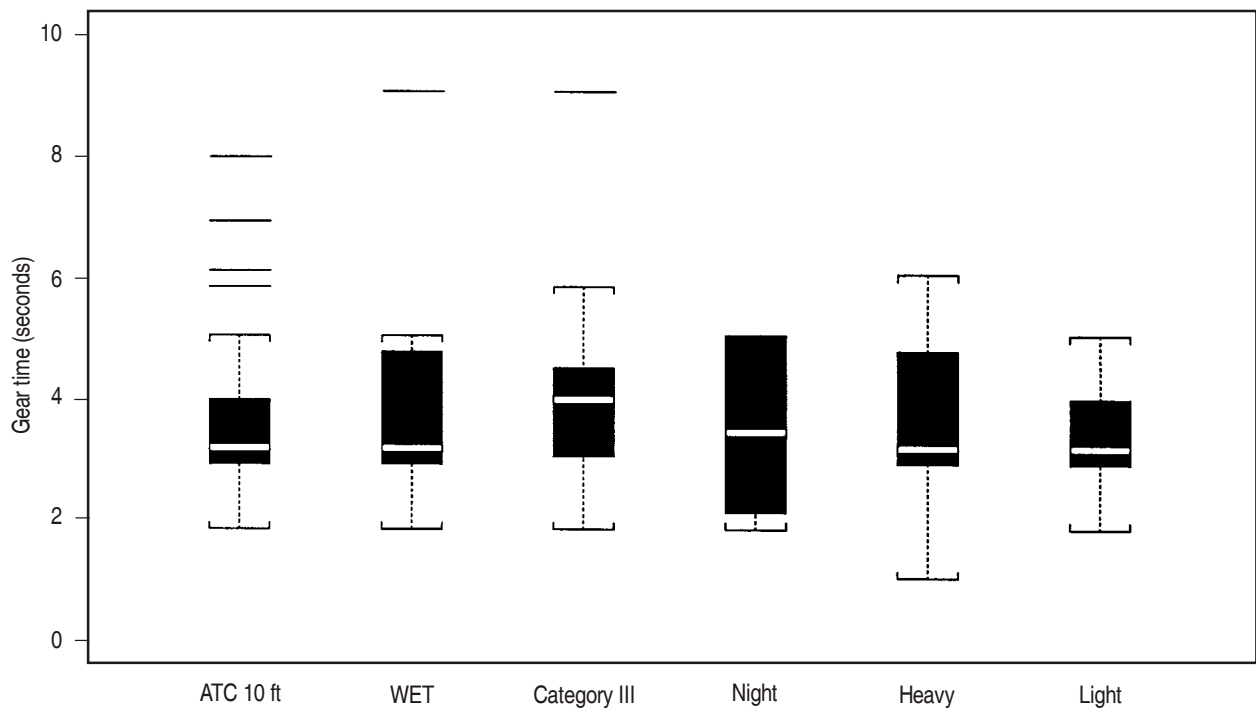
Figure 4-10.   Gear times for other ATC 10 ft GAs
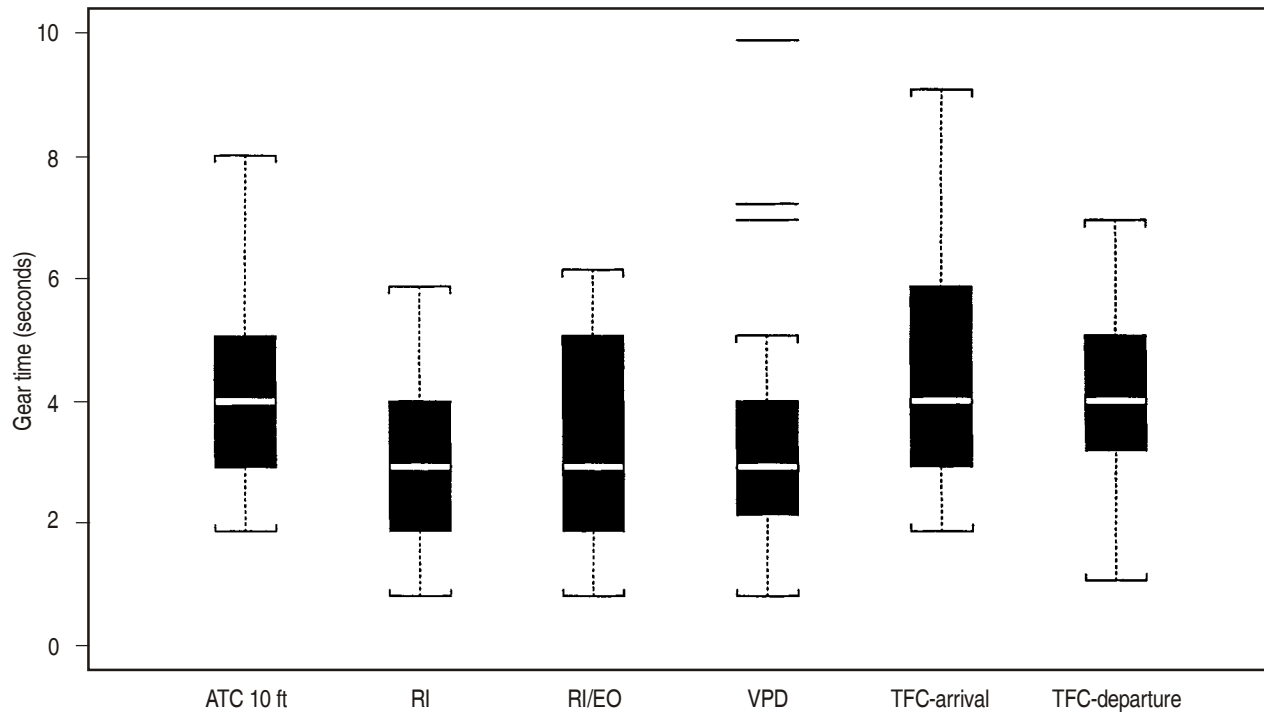
Figure 4-11.   Gear times for other GA initiators
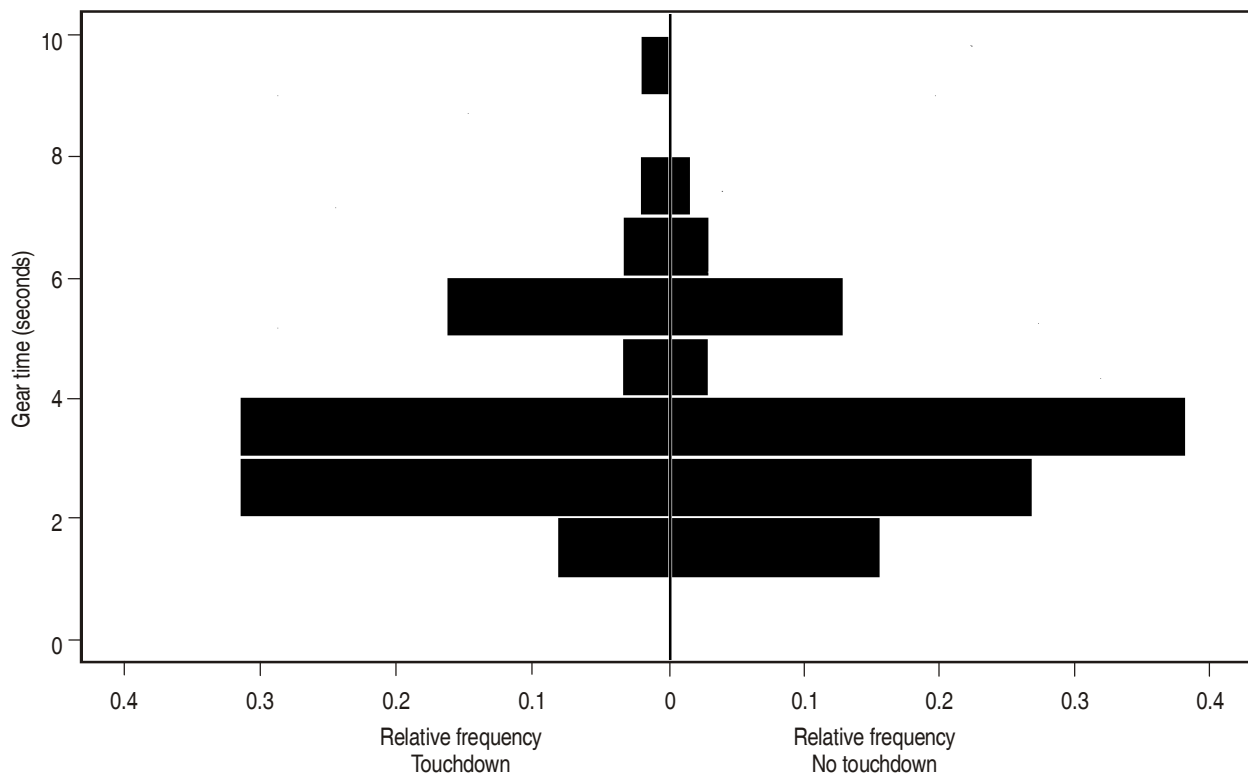
Figure 4-12.   Effect of touchdown on gear time

Johnson type: SU
Min: +0.53
Max: +17.30

Xi: +0.4122730e+01
Lambda: +0.2842432e+01
Delta: +0.1669656e+01
Gamma: −0.7159748e+00

0.4

0.0

To/GA to flaps 20 (seconds)   20.0

Johnson type: SU
Min: +0.80
Max: +13.87

Xi: +0.1610582e+01
Lambda: +0.1948067e+01
Delta: +0.1931568e+01
Gamma: −0.1489220e+01

0.4

0.0

Flaps 20 to gear up (seconds)   20.0
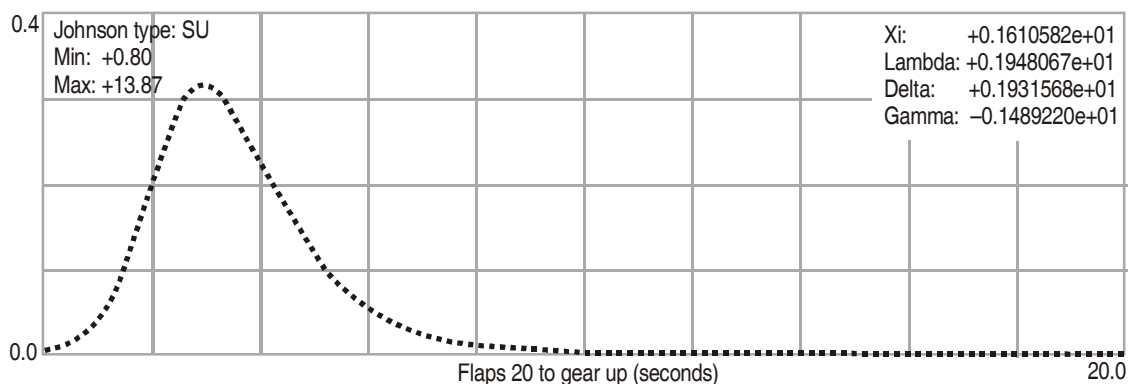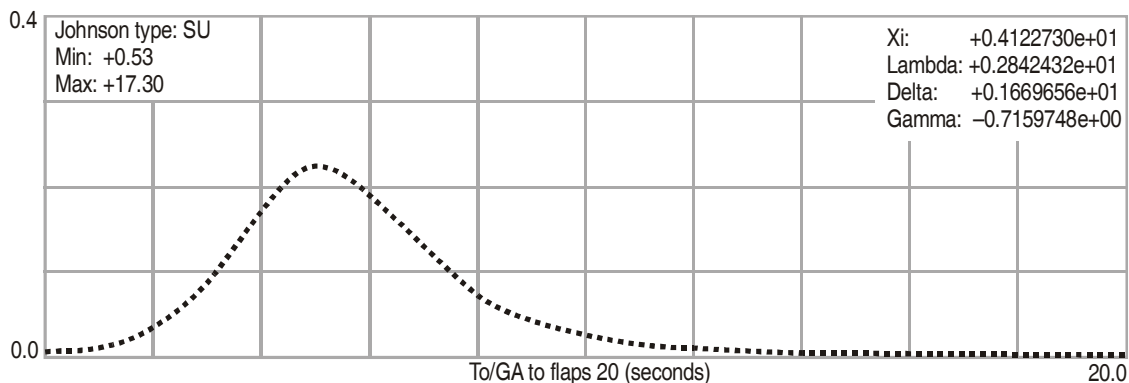
Jc.Xi[0]	= +0.4122730e+01;	LocMin [Deg]...................................: −0.15
Jc.Lambda[0]	= +0.2842432e+01;	LocMax [Deg]...................................: 0.15
Jc.Delta[0]	= +0.1669656e+01;	LocSigma [−]....................................: 0.05
Jc.Gamma[0]	= −0.7159748e+00;	
Jc.BoundMin[0]	= +0.53;	GsMin [Deg]....................................: −0.075
Jc.BoundMax[0]	= +17.3;	GsMax [Deg]...................................: 0.075
		GsSigma [−]....................................: 0.025
Jc.Xi[1]	= +0.1610582e+01;	
Jc.Lambda[1]	= +0.1948067e+01;	
Jc.Delta[1]	= +0.1931568e+01;	
Jc.Gamma[1]	= −0.1489220e+01;	
Jc.BoundMin[1]	= +0.79883;	
Jc.BoundMax[1]	= +13.867;	

Figure 4-13.   NASA Ames B747-400 balked landing pilot response time distributions using the (unbounded) Johnson distribution function

— — — — — — — —

Appendix to Chapter 4
ANALYSIS OF VARIANCE (ANOVA) RESULTS

Table 4-A-1.   ANOVA for flaps time — crew-to-crew variability

Source	Df	Sum of square	Mean square	F value	Pr(F)
Crew	35	397.3	11.35	4.2	0.001
Residuals	249	673.4	2.70		
Df = degree of freedom *F* = (distribution) statistic Pr(*F*) = *F*-statistic probability					

Table 4-A-2.   ANOVA for flaps time — airport and flight control

Source	Df	Sum of square	Mean square	F value	Pr(F)
Scenario	5	14.46	2.89	1.24	0.30
Residuals	66	154.36	2.34	*n*	*n*
Df = degree of freedom *F* = (distribution) statistic Pr(*F*) = *F*-statistic probability					

Table 4-A-3.   ANOVA for gear time — crew-to-crew variability

Source	Df	Sum of square	Mean square	F value	Pr(F)
Crew	33	137.53	4.17	1.71	0.013
Residuals	228	55.97	2.44	*n*	*n*
Df = degree of freedom *F* = (distribution) statistic Pr(*F*) = *F*-statistic probability					

_____

Chapter 5
WIND MODEL CLIMATOLOGICAL DATA

5.1   INTRODUCTION

5.1.1   The (former) Atmospheric Physics group at The Boeing Company has assisted the FAA in the development of a global wind model for use in the FAA Airspace Simulation and Analysis Tools (ASAT) in support of the NLA OFZ study. The wind model described in *Wind Models for Flight Simulator Certification of Landing and Approach Guidance and Control Systems* (FAA-RD-74-206, December 1974) has been revised to include wind statistics from 40 international airports selected on the basis of a marketing forecast for future NLA activity (see Table 5-1).

5.1.2   The marketing forecast was based on the examination of the frequency of Boeing 747 operations published in the *Official Airline Guide (OAG)* in September 1993. The revision to the empirical wind model is based on annual wind statistics derived from historical wind data for the 40 international airports. Appendix B contains details concerning the turbulence, gust and wind shear models used respectively by the FAA (Wind Model A) and the Joint Aviation Authorities – JAA (Wind Model B).

5.2   DISCUSSION

Wind database

5.2.1   Hourly wind observations are available in the International Surface Weather Observations (ISWO) database for major, worldwide airports. This ISWO CD-ROM (version 1.0) was developed jointly by the United States Department of Commerce and the United States Air Force at the Federal Climate Complex in Asheville, North Carolina.

5.2.2   Monthly and annual wind statistics were developed for the 40 international airports using 16 years of hourly wind observations (1982–1997) and an analysis programme developed by the atmospheric physics group[1]. The annual wind distribution statistics were compiled into a matrix format that depicts the percent frequency of occurrence of wind direction versus wind speed (see sample annual wind statistics from San Francisco in Table 5-2).

5.2.3   Wind direction is summarized for 16 compass points, i.e. N (0.0 degrees), NNE (22.5 degrees), NE (45.0 degrees), ENE (67.5 degrees), E (90.0 degrees). Wind speed is summarized for small speed intervals, i.e. 13 kt, 4–6 kt. The per cent frequency of each wind direction is summarized for all speed intervals; the percent frequency of each speed interval and the mean wind speed is summarized for all 16 wind directions. In addition, the per cent frequency of calm (no direction and zero speed) and variable winds (variable direction) is included.

---

1. The ISMCS 48-year record (1948–1996) was also examined for the NLA OFZ study but was later replaced with the 16-year continuous record (1982–1997) in order to obtain data on extreme value winds. Extreme value winds are omitted from the 48-year record due to truncation within the database.

5.2.4   The 40 airports selected represent 10 major climatic regions, from the tropics to the sub-arctic; providing a global wind database. Although no airports in the Russian Federation were used to develop the global wind model, wind statistics were available from one airport, e.g. Moscow. Wind sensor or anemometer information was available from the National Climatic Data Center for United States airports.

Wind normalization for 40 individual airports

5.2.5   Since the prevailing wind direction and runway alignments vary considerably among the 40 airports, the winds for each airport first had to be normalized to a common direction. The primary active runway was selected to be the normalized direction and designated to be zero degrees; therefore the annual wind statistics for each airport were normalized to the primary active runway for NLA operations (see Table 5-3). Furthermore, since wind direction is reported with respect to the geographic coordinate system, and runways directions are specified with respect to the geomagnetic coordinate system, the geomagnetic declination from true to magnetic was also applied in normalizing the winds. After correcting for the magnetic declination at each airport and normalizing the winds to zero degrees along the primary active runway, the normalized results were ready for development of the wind model (see Table 5-4).

Composite wind normalization for 40 airports

5.2.6   The overall wind model was developed by simply adding the 40 individual airport values for each wind direction and speed interval condition within the matrix and dividing by 40 to obtain the average value. Therefore, the composite matrix is of the same format as each airport (see Table 5-5). The wind direction and wind speed were charted and are depicted in Figures 5-1 and 5-2, respectively.

Wind model format and development

5.2.7   The revised global wind model is in the same format developed in previous models. Both the global wind direction and speed are presented as cumulative probabilities (see Tables 5-6 and 5-7, and Figures 5-3 and 5-4).

5.3   SUMMARY

Boeing Atmospheric Physics assisted in the development of a revised wind model for NLA OFZ studies. The revised, global wind model is an empirical model that was based on annual wind statistics for 40 international airports selected from a marketing forecast for future NLA activity. The model was used with one of the two turbulence models described in Appendix B (Wind Model A), for which it supplied the value of the parameter there called "mean wind velocity at 20 feet above ground level". The model could also be used with the other turbulence model (Wind Model B) described in Appendix B, for which it would also supply the value of the parameter there called "mean wind velocity at 10 m (33 ft)".

— — — — — — — —

Table 5-1. Large aeroplane preliminary design (LAPD) destination airports

No.	Airport Code	Airport/Country	9/93 OAG	No.	Airport Code	Airport/Country	9/93 OAG
1	AKL	Auckland International, New Zealand	26	21	LGW	London Gatwick, United Kingdom	38
2	AMS	Amsterdam Schiphol, Netherlands	17	22	LHR	London Heathrow, United Kingdom	7
3	ATH	Athens Hellenikon, Greece	73	23	MAD	Madrid Barajas, Spain	24
4	BKK	Bangkok Don Muang International, Thailand	9	24	MEL	Tullamarine International, Melbourne, Australia (VI)	4
5	BOM	Bombay Santa Cruz International, India	25	25	MIA	Miami International, Florida, U.S.A.	47
6	CDG	Paris Charles de Gaulle, France	14	26	MNL	Manila Nioy Aquino International, Philippines	29
7	CGK	Jakarta International, Indonesia	42	27	NRT	Tokyo Narita/New Tokyo Apt, Japan	31
8	CTS	Sapporo New Chitose, Japan	16	28	ORD	Chicago O'Hare, Ilinois, U.S.A.	27
9	EZE	Buenos Aires Ministro Pistarini, Argentina	49	29	PEK	Beijing China-Capital	1
10	FCO	Rome Fiumicino, Italy	28	30	RUH	Riyadh King Khaled International, Saudi Arabia	20
11	FRA	Frankfurt Rhein Main, Germany	8	31	GRU	Sao Paulo Guarulhos, Brazil	23
12	GIG	Rio De Janeiro Galeao International, Brazil	57	32	SEL	Kimpo International, Seoul, Republic of Korea	34
13	HKG	Hong Kong International, Hong Kong		33	SFO	San Francisco International, California, U.S.A.	
14	HNL	Honolulu International, Hawaii (Oahu), U.S.A.	18	34	SHA	Shanghai Hongqiao, China	12
15	IAD	Washington Dulles International, U.S.A.	35	35	SIN	Singapore Changi International, Singapore	19
16	JFK	New York John F. Kennedy, U.S.A.	5	36	SYD	Sydney Kingsford Smith International, Australia (NSW)	45
17	JNB	Johannesburg Jan Smuts International, South Africa	32	37	TPE	Taipei Chiang Kai Shek, Taiwan	6
18	KIX	Osaka Kansai International, Japan	[11]	38	YVR	Vancouver International, British Columbia, Canada	13
19	KUL	Kuala Lumpur Subang International, Malaysia	38	39	YYZ	Toronto Lester B. Pearson, Ontario, Canada	10
20	LAX	Los Angeles International, California, U.S.A.	7	40	ZRH	Zurich Kloten, Switzerland	36

Table 5-2. San Francisco annual wind distribution statistics (1982–1997)

16-point direction	Speed (kt)											Total (%)	Mean wind speed (kt)
	1–3	4–6	7–10	11–16	17–21	22–27	28–33	34–40	41–47	48–55	>56		
N	0.2697	1.5855	1.0684	0.4603	0.2045	0.0943	0.0191	0.0040	0.0000	0.0000	0.0000	3.7059	
NNE	0.2480	1.7523	0.9688	0.1128	0.0224	0.0119	0.0053	0.0020	0.0000	0.0007	0.0000	3.1242	6.3333
NE	0.2658	1.7748	0.7215	0.1148	0.0132	0.0026	0.0000	0.0000	0.0000	0.0000	0.0000	2.8927	5.9528
ENE	0.2077	1.4021	0.6285	0.2196	0.0244	0.0026	0.0007	0.0000	0.0000	0.0000	0.0007	2.4864	6.4971
E	0.2196	1.3085	0.7308	0.1695	0.0171	0.0026	0.0000	0.0007	0.0000	0.0000	0.0000	2.4488	6.4218
ESE	0.1820	0.8508	0.6648	0.2223	0.0297	0.0059	0.0007	0.0000	0.0007	0.0000	0.0000	1.9568	7.0637
SE	0.2387	1.1766	0.9636	0.5573	0.1167	0.0284	0.0007	0.0007	0.0000	0.0000	0.0007	3.0833	8.0357
SSE	0.3199	1.3474	0.7743	0.3733	0.0765	0.0297	0.0046	0.0007	0.0000	0.0000	0.0000	2.9263	7.1922
S	0.6556	2.1487	1.0117	0.7420	0.2559	0.1372	0.0561	0.0099	0.0013	0.0000	0.0000	5.0183	8.0728
SSW	0.3759	1.3395	0.7096	0.5777	0.2249	0.1134	0.0455	0.0145	0.0026	0.0000	0.0000	3.4038	8.8436
SW	0.4234	1.3942	0.9418	0.7011	0.2018	0.0805	0.0290	0.0119	0.0033	0.0007	0.0000	3.7876	8.4752
WSW	0.4511	2.0340	1.8783	1.4298	0.3357	0.1049	0.0198	0.0013	0.0000	0.0007	0.0000	6.2556	8.8176
W	0.4214	2.7251	5.2676	7.2996	2.9217	0.8574	0.1266	0.0106	0.0000	0.0000	0.0000	19.6300	12.0638
WNW	0.2895	2.2984	5.6818	7.7764	3.5680	0.9398	0.1444	0.0132	0.0013	0.0000	0.0007	20.7136	12.5325
NW	0.1906	1.4061	2.9685	3.9466	1.9271	0.3185	0.0224	0.0020	0.0000	0.0013	0.0000	10.7832	12.0779
NNW	0.1161	0.6819	0.6932	0.6556	0.1728	0.0290	0.0059	0.0007	0.0000	0.0007	0.0000	2.3558	9.4678
Calm/variable	0.0798	0.0838	0.0000	0.0000	0.0000	0.0000	0.0000	0.0000	0.0000	0.0000	0.0000	5.4279	3.8871
All	4.9550	25.3098	25.6732	25.3586	10.1124	2.7588	0.4808	0.0719	0.0092	0.0040	0.0020	100.0000	9.6632

Table 5-3.   Airports on international surface weather observations (ISWO) CD-ROM (version 1.0)

Station name	Location	Runway	Station name	Location	Runway
Auckland International AP	37:01S 174:48E	23	London (Gatwick) AP	51:09N 000:11W	08
Amsterdam	52:18N 004:46E	06	London (Heathrow)	51:29N 000:27W	27
Athens	37:54N 023:44E	33	Madrid	40:27N 003:33W	33
Bangkok	13:55N 100:36E	21	Melbourne	37:40S 144:50E	16
Bombay	19:07N 072:51E	27	Miami AP	25:49N 080:17W	09
Paris (Charles de Gaulle)	49:01N 002:32E	27	Manila	14:35N 120:59E	06
Jakarta (Hamlin AFB)	06:15S 106:54E	25	Tokyo International	35:46N 140:23E	34
Sapporo	43:03N 141:20E	01	Chicago (O'Hare)	41:59N 087:54W	32
Buenos Aires	34:49S 058:32W	11	Bejing	39:56N 116:17E	18
Rome (Fiumicino)	41:48N 012:14E	16	Riyadh	24:43N 046:43E	15
Frankfurt Main AP	50:03N 008:36E	25	Sao Paulo (Congonhas)	23:37S 046:39W	09
Rio De Janeiro (Galeao)	22:49S 043:15W	28	Seoul (Kimpo)	37:33N 126:48E	32
Hong Kong International AP	22:20N 114:11E	13	San Francisco AP	37:37N 122:23W	28
Honolulu International AP	21:21N 157:56W	04	Shanghai	31:10N 121:26E	36
Washington Dulles AP	38:51N 077:02W	01	Singapore (Changi)	01:22N 103:59E	20
New York Kennedy AP	40:39N 073:47W	31	Sydney AP	33:57S 151:11E	16
Johannesburg (Jan Smuts)	26:08S 028:14E	21	Taipei	25:04N 121:33E	05
Osaka International AP (Itami)	34:47N 135:27E	24	Vancouver International	49:11N 123:10W	08
Kuala Lumpur	03:07N 101:33E	33	Toronto International AP	43:40N 079:38W	15
Los Angeles AP	33:56N 118:24W	25	Zurich	47:23 008:34E	34

Table 5-4. Normalized wind statistics for San Francisco International Airport (Runway 28)

Median direction (deg)	Wind speed intervals											Heading frequency (%)	Average speed (kt)
	1–3 (kt)	4–6 (kt)	7–10 (kt)	11–16 (kt)	17–21 (kt)	22–27 (kt)	28–33 (kt)	34–40 (kt)	41–47 (kt)	48–55 (kt)	>=56 (kt)		
0.0	0.2895	2.2984	5.6818	7.7764	3.5680	0.9398	0.1444	0.0132	0.0013	0.0000	0.0007	20.7136	
22.5	0.1906	1.4061	2.9685	3.9466	1.9271	0.3185	0.0224	0.0020	0.0000	0.0013	0.0000	10.7832	12.0779
45.0	0.1161	0.6819	0.6932	0.6556	0.1728	0.0290	0.0059	0.0007	0.0000	0.0007	0.0000	2.3558	9.4678
67.5	0.2697	1.5855	1.0684	0.4603	0.2045	0.0943	0.0191	0.0040	0.0000	0.0000	0.0000	3.7059	8.1849
90.0	0.2480	1.7523	0.9688	0.1128	0.0224	0.0119	0.0053	0.0020	0.0000	0.0007	0.0000	3.1242	6.3333
112.5	0.2658	1.7748	0.7215	0.1148	0.0132	0.0026	0.0000	0.0000	0.0000	0.0000	0.0000	2.8927	5.9528
135.0	0.2077	1.4021	0.6285	0.2196	0.0244	0.0026	0.0007	0.0000	0.0000	0.0000	0.0007	2.4864	6.4971
157.5	0.2196	1.3085	0.7308	0.1695	0.0171	0.0026	0.0000	0.0007	0.0000	0.0000	0.0000	2.4488	6.4218
180.0	0.1820	0.8508	0.6648	0.2223	0.0297	0.0059	0.0007	0.0000	0.0007	0.0000	0.0000	1.9568	7.0637
202.5	0.2387	1.1766	0.9636	0.5573	0.1167	0.0284	0.0007	0.0007	0.0000	0.0000	0.0007	3.0833	8.0357
225.0	0.3199	1.3474	0.7743	0.3733	0.0765	0.0297	0.0046	0.0007	0.0000	0.0000	0.0000	2.9263	7.1922
247.5	0.6556	2.1487	1.0117	0.7420	0.2559	0.1372	0.0561	0.0099	0.0013	0.0000	0.0000	5.0183	8.0728
270.0	0.3759	1.3395	0.7096	0.5777	0.2249	0.1134	0.0455	0.0145	0.0026	0.0000	0.0000	3.4038	8.8436
292.5	0.4234	1.3942	0.9418	0.7011	0.2018	0.0805	0.0290	0.0119	0.0033	0.0007	0.0000	3.7876	8.4752
315.0	0.4511	2.0340	1.8783	1.4298	0.3357	0.1049	0.0198	0.0013	0.0000	0.0007	0.0000	6.2556	8.8176
337.5	0.4214	2.7251	5.2676	7.2996	2.9217	0.8574	0.1266	0.0106	0.0000	0.0000	0.0000	19.6300	12.0638
Calm/variable												5.4277	
Wind speed frequency	4.8750	25.2259	25.6732	25.3587	10.1124	2.7587	0.4808	0.0722	0.0092	0.0041	0.0021		
Exceedence probability	94.5723	89.6973	64.4714	38.7982	13.4395	3.3271	0.5684	0.0876	0.0154	0.0062	0.0021		

Table 5-5.   Normalized wind statistics for 40 international airports

Median direction (deg)	Wind speed intervals											Heading frequency (%)	Average speed (kt)
	1–3 (kt)	4–6 (kt)	7–10 (kt)	11–16 (kt)	17–21 (kt)	22–27 (kt)	28–33 (kt)	34–40 (kt)	41–47 (kt)	48–55 (kt)	>=56 (kt)		
000.0	1.1002	2.5096	2.6641	1.7842	0.3781	0.0996	0.0124	0.0016	0.0003	0.0003	0.0005	8.5509	
022.5	1.0495	2.0759	2.0976	1.5179	0.3071	0.0708	0.0092	0.0022	0.0003	0.0004	0.0010	7.1321	7.4516
045.0	0.9056	1.7267	1.7810	1.1616	0.2004	0.0551	0.0082	0.0016	0.0004	0.0002	0.0002	5.8410	7.1842
067.5	0.8243	1.4993	1.3883	0.7977	0.1533	0.0443	0.0077	0.0013	0.0002	0.0002	0.0001	4.7168	7.1267
090.0	0.9612	1.7009	1.3667	0.6718	0.1284	0.0363	0.0057	0.0015	0.0003	0.0002	0.0002	4.8731	6.9256
112.5	0.9990	1.7074	1.4139	0.7155	0.1327	0.0347	0.0071	0.0026	0.0003	0.0003	0.0004	5.0139	6.7577
135.0	0.9255	1.5533	1.3291	0.6982	0.1361	0.0333	0.0096	0.0038	0.0001	0.0002	0.0006	4.6897	6.7255
157.5	0.9134	1.6406	1.4029	0.7368	0.1491	0.0461	0.0118	0.0040	0.0003	0.0004	0.0004	4.9058	6.7779
180.0	0.9565	1.8473	1.6400	0.9440	0.2476	0.1146	0.0303	0.0075	0.0006	0.0003	0.0007	5.7896	7.0339
202.5	0.9063	1.6690	1.4360	0.8536	0.1915	0.0641	0.0115	0.0050	0.0001	0.0001	0.0005	5.1377	7.1687
225.0	0.7639	1.4617	1.1792	0.6405	0.1238	0.0306	0.0043	0.0004	0.0002	0.0002	0.0004	4.2052	6.8138
247.5	0.7589	1.4056	1.1901	0.6431	0.1058	0.0227	0.0039	0.0009	0.0002	0.0003	0.0003	4.1318	6.5661
270.0	0.7623	1.5080	1.2284	0.6047	0.1006	0.0206	0.0034	0.0010	0.0001	0.0002	0.0004	4.2297	6.5700
292.5	0.8517	1.6064	1.3411	0.6789	0.1186	0.0282	0.0047	0.0011	0.0002	0.0004	0.0002	4.6315	6.7558
315.0	0.7382	1.6849	1.8057	1.2100	0.2109	0.0424	0.0063	0.0008	0.0002	0.0002	0.0004	5.6998	7.3655
337.5	0.8976	2.0271	2.2799	1.4193	0.2788	0.0669	0.0087	0.0012	0.0001	0.0002	0.0006	6.9806	7.6544
Calm/variable												13.4708	
												100.0000	
Wind speed frequency	14.3142	27.6238	25.5439	15.0778	2.9628	0.8104	0.1448	0.0365	0.0039	0.0042	0.0070		
Exceedence probability	86.5292	72.2149	44.5912	19.0473	3.9695	1.0067	0.1964	0.0516	0.0151	0.0112	0.0070		

**Table 5-6.   Global wind direction cumulative probabilities
as implemented in ASAT**

Wind direction	Cumulative probability
0.0	0.0000
22.5	0.0988
45.0	0.1812
67.5	0.2487
90.0	0.3033
112.5	0.3596
135.0	0.4175
157.5	0.4717
180.0	0.5284
202.5	0.5953
225.0	0.6547
247.5	0.7033
270.0	0.7510
292.5	0.7999
315.0	0.8535
337.5	0.9193
360.0	1.0000

**Table 5-7.   Global wind speed cumulative probabilities
as implemented in ASAT**

Wind speed	Cumulative probability
>55.5	0.0001
47.5	0.0001
40.5	0.0002
33.5	0.0005
27.5	0.0020
21.5	0.0101
16.5	0.0397
10.5	0.1905
6.5	0.4459
3.5	0.7221
0.5	0.8653
0.0	1.0000

— — — — — — — —
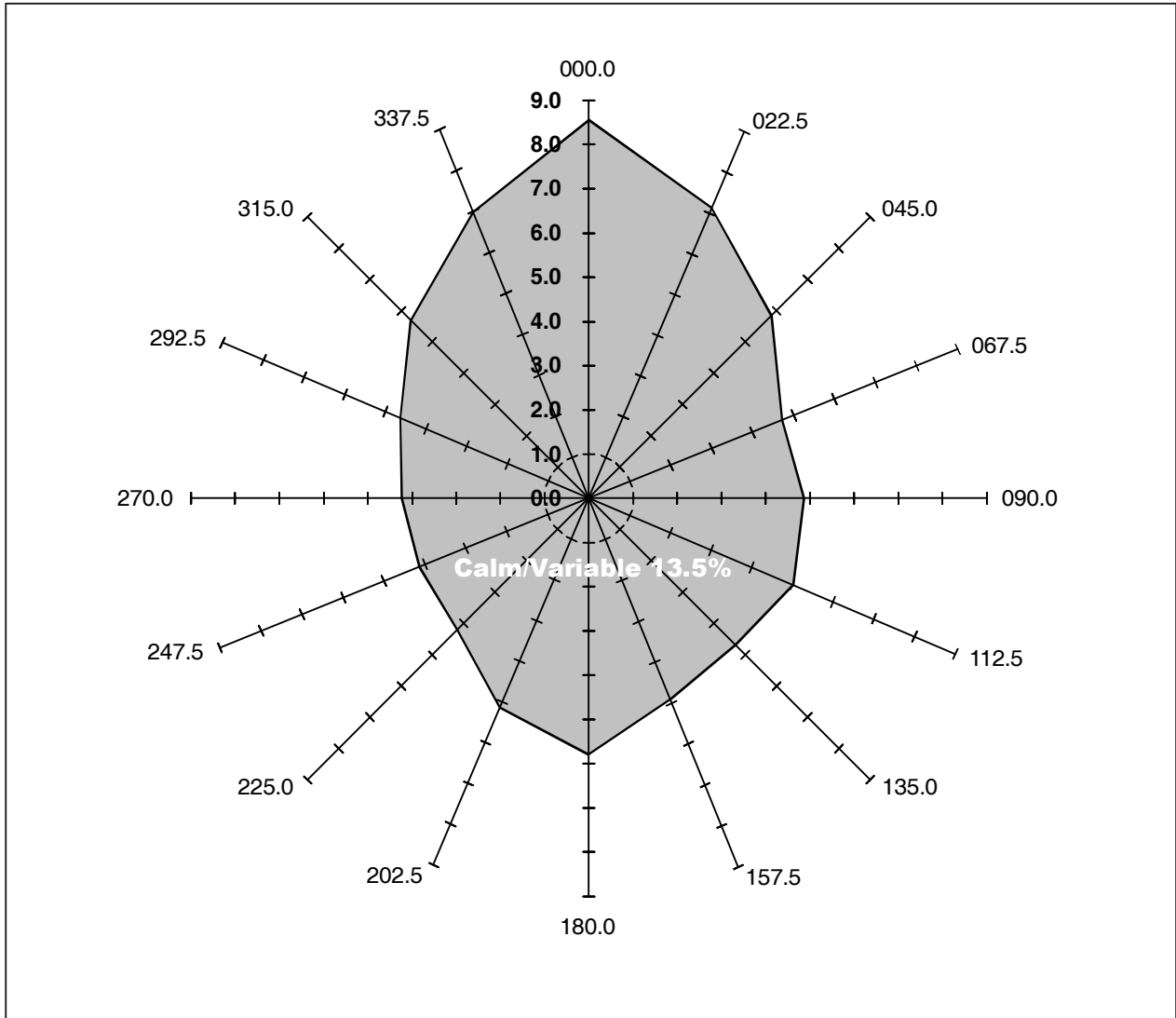
**Figure 5-1.   Global wind model direction distribution
depicted as per cent occurrence for each of 16 directions**

Calm/Variable

>56 kt

2.0 kt

51.5 kt

5.0 kt

44.0 kt

8.5 kt

37.0 kt

13.5 kt

30.5 kt

19.0 kt

24.5 kt
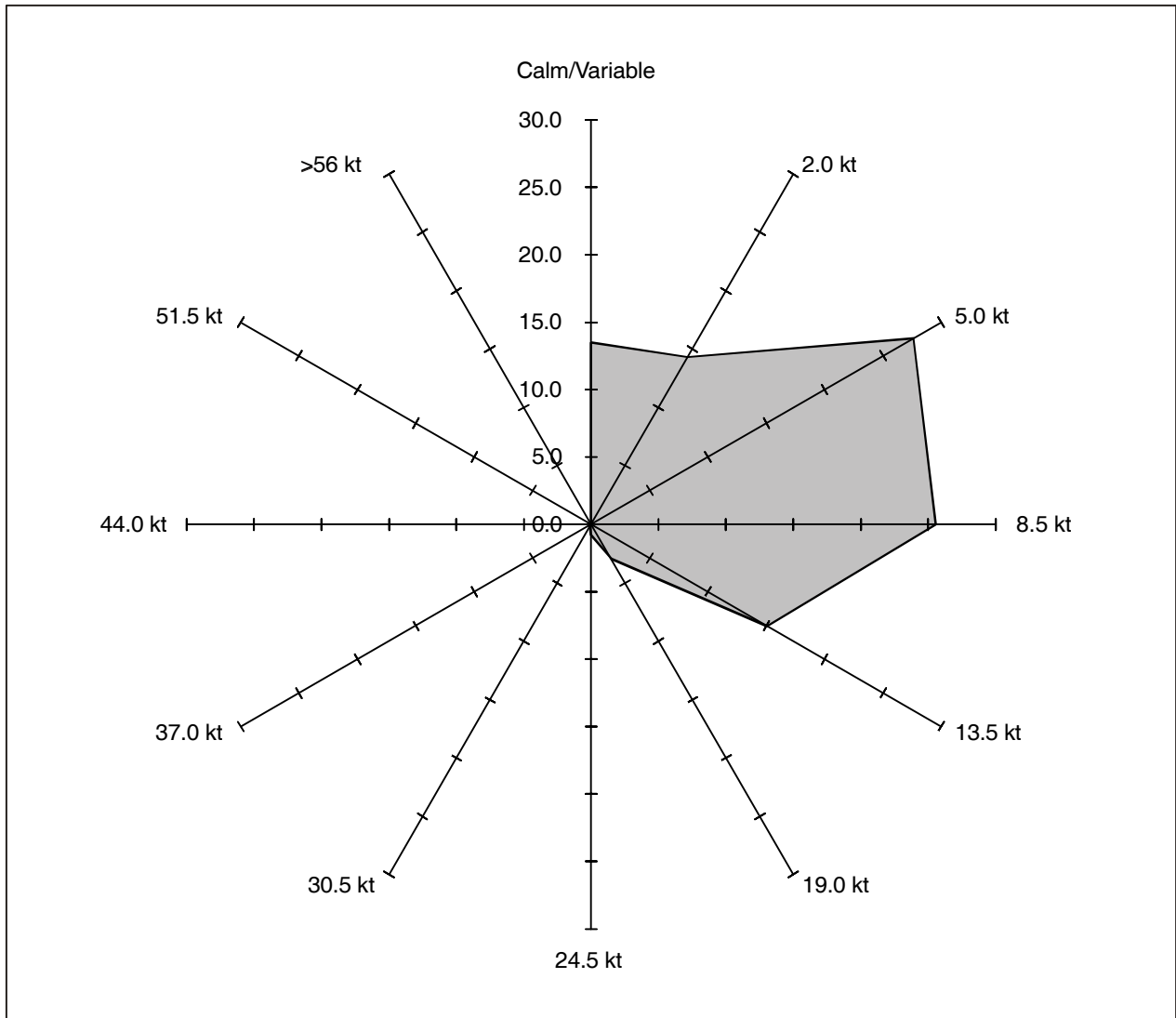
**Figure 5-2.   Global wind model speed distribution
depicted as per cent occurrence for specific wind speeds**
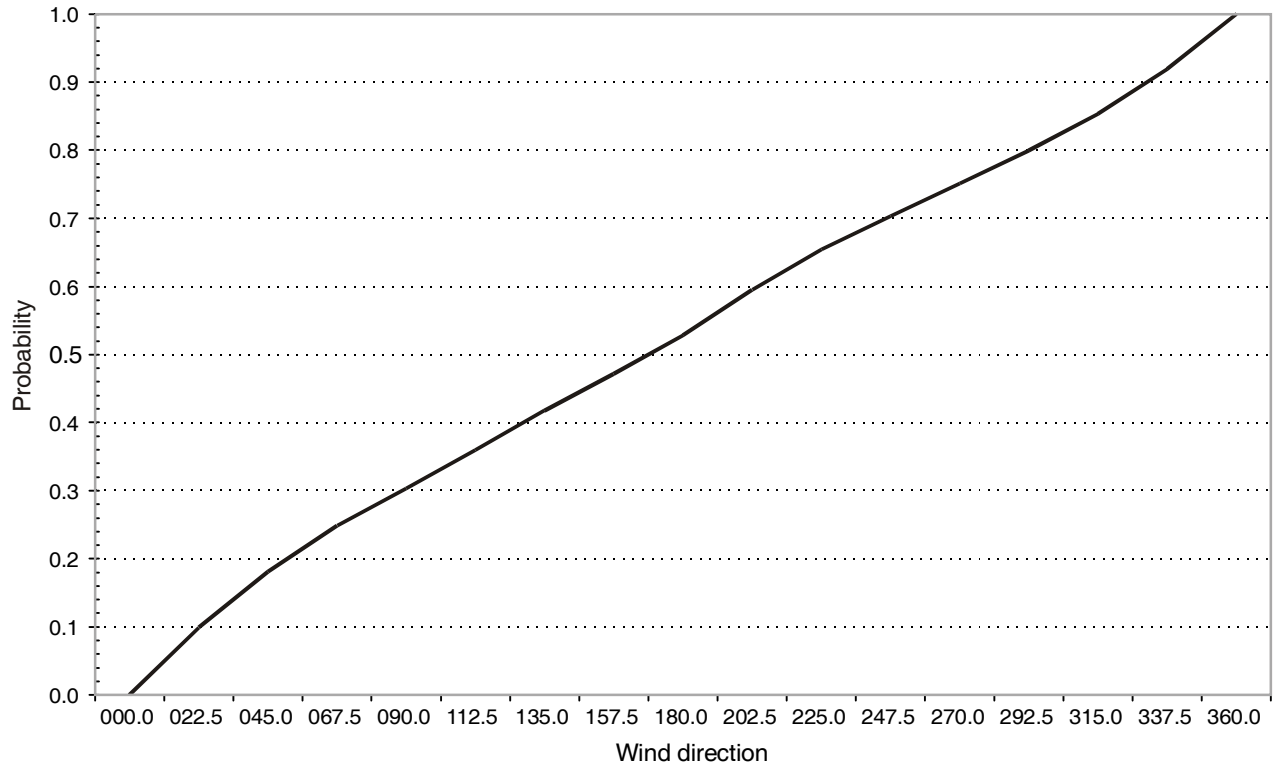
Figure 5-3.   Global wind model wind direction cumulative probability
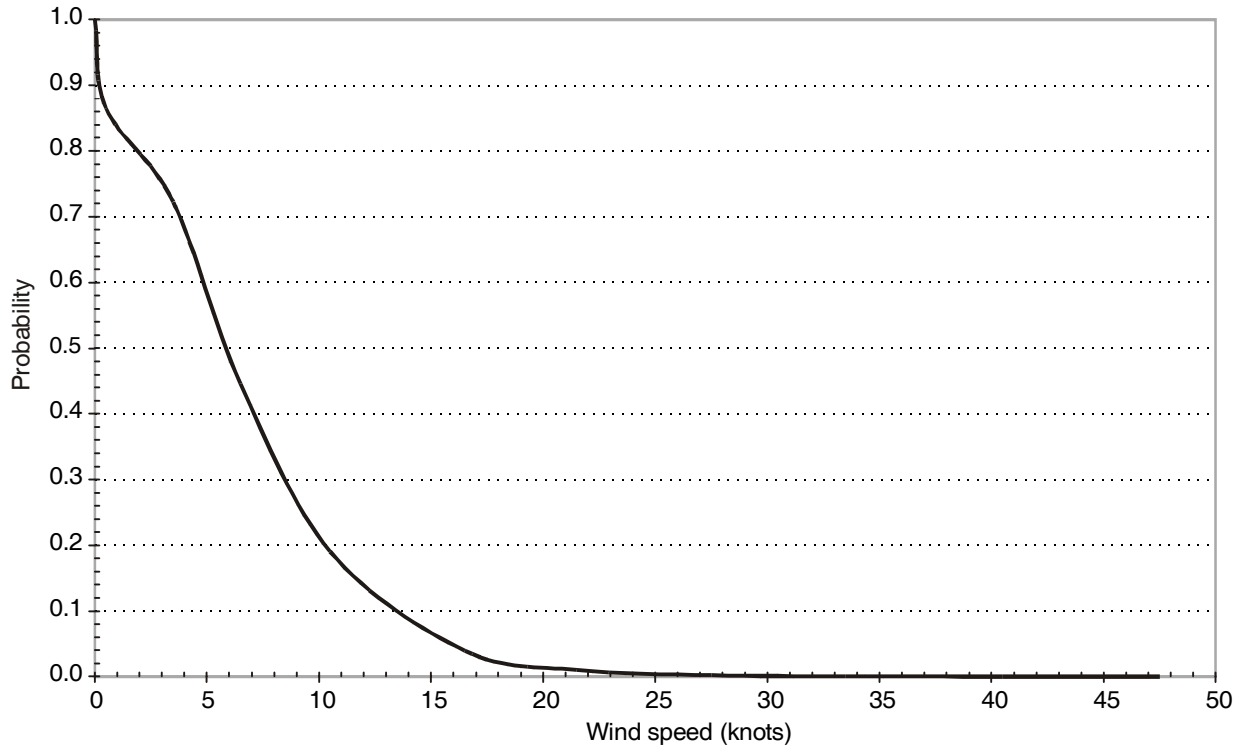
Figure 5-4.   Global wind model wind speed cumulative probability

———————————

Chapter 6

NEW LARGER AEROPLANE (NLA) BALKED LANDING SIMULATIONS WITH AUTOPILOT

6.1   DESCRIPTION OF THE
ASAT COMPUTER OFZ SIMULATION STUDY

ASAT was used to simulate various types of balked landings for the construction of 10^{-7} iso-probability contours along the length of a runway. The iso-probability contours served as a basis for the development of an OFZ definition for NLAs with similar characteristics in flight technical error (FTE). The value of 10^{-7} defined the target level of safety (TLS) was used as the criterion for the risk of collision between an aircraft on the approach and another aircraft, vehicle or object on the ground and was consistent with ICAO CRM.

6.2   PROCEDURE

6.2.1   ASAT incorporated certified and flight-validated simulation models of the Boeing 737-500, 767-300 and 747-400 aircraft. The Boeing 747-400 aircraft simulation was used to represent the performance of an NLA on the approach. The standard ILS configuration[1] as described in ICAO Doc 9274 — *Manual on the Use of the Collision Risk Model (CRM) for ILS Operations* was used initially in the study.

6.2.2   The computer simulation was initialized by placing the approaching aircraft at a point in space about 8.15 km (4.4 NM) before the runway threshold using statistical distributions from the existing ICAO ILS CRM. Pilot response time model inputs were used to conduct a missed approach procedure or balked landing according to standard missed approach procedures in the flight crew training manual for a 747-400[2]. The models were based on data obtained from commercial airline pilots conducting missed approaches and balked landings in the simulator.

6.2.3   A comprehensive statistical analysis of pilot response times showed that only one model was necessary to reflect pilot responses to a balked landing and to approaches with autopilot or F/D.

6.2.4   The aircraft position in each run was recorded at fixed points along the length of the runway as it passed through planes "planar tiles" perpendicular to the runway centre line, as in the ICAO ILS CRM. Statistical tests were used to position the tiles to ensure independence, i.e. no correlation. If placement of

---

1.   Standard ILS parameters include: 3-degree glide path; 3.22-degree localizer course width, etc.

2.   The published procedure requires initiation of a GA by pressing the TO/GA switch, followed by moving the flaps lever to the 20-detent position once positive rate of climb is established, followed by moving the gear lever to the "up" position. When the aircraft is 120 m (400 ft) or more above ground, LNAV can be engaged and when the aircraft is 305 m (1 000 ft) or more above ground, vertical navigation (VNAV) can be engaged. For this study, only pilot actions from TO/GA button press to gear up were considered. The NASA Ames Boeing 747-400 simulator is an FAA certified and approved simulator.

the planar tiles at 100 m (328 ft) was satisfactory, the statistical distributions could be substituted directly into the ICAO ILS CRM. Otherwise, additional data manipulation would be necessary. The sources of random variation used in the simulation included wind direction and speed[3], turbulence, ILS error sources, FTE, etc.

6.2.5   The next step in the procedure was to analyse the flight track intercept points at each planar tile. The dispersion of intercept points were resolved into lateral and vertical component distributions with appropriate probability density functions (PDF) determined. If required, Johnson distributions, which are transformations of normal distributions, would be used as in the CRM. The number of Monte Carlo runs that would be necessary to obtain good parameter estimates to fit the data for the estimation of skewness and kurtosis had to be determined. The programme was being continued to accumulate data on simulated "actual" collisions between the aircraft doing the GA and aircraft on the taxiways or with other ground obstacles. The procedure was repeated for varying runway elevations for the OFZ study.

6.2.6   The following assumptions were made for using the Boeing 747-400 integrated aircraft configuration (IAC) in simulating NLAs:

- The speed of the Boeing 747-400 on the approach was representative of NLA speeds, and a weight of 270 455 kg (595 000 lb) was used to set the approach speed and produce appropriate wing loading and inertia values.

- The guidance system was expected to be ground track hold with the engagement of GA.

- The lateral displacement behavior of NLAs was represented in the use of proper distributions for the localizer alignment and localizer receiver centring error.

- The roll control mode authority of NLAs was expected to be as good or better than the current Boeing 747-400.

6.2.7   Given the above assumptions, the Boeing 747-400 IAC simulation was used to construct iso-probability contours that represented NLAs as a limiting behavior.

6.3   SIMULATION INPUTS

6.3.1   A summary of the deterministic and random input variables used in the simulation is given in 6.3.2 and 6.3.3.

Aeroplane-related type variables

6.3.2   The aeroplane-related type variables were based on recommendations from the manufacturer.

- Weight*:* the weight would be constant at 595 000 lb. This was determined by the approach speed of an NLA, which was estimated to be around 149 kt.

- Centre of gravity (CG)*:* the CG would remain constant at 25 per cent mean aerodynamic chord (MAC).

- Airspeed: the airspeed might vary from Vref 149 kt (171 mph) to Vref + 10 kt (12 mph).

---

3. The NASA Ames simulator studies utilized 35 kt winds from an angle of 45 degrees left or right.

ILS-type variables

6.3.3   The ILS-type variables were primarily determined by the FAA Flight Procedure Standards branch, AFS-420. Where available, data from the 40 airports worldwide that were likely to service an NLA (according to a Boeing forecast) were considered.

- Glideslope angle: the glideslope angle would remain constant at three degrees

- ILS reference datum: 17 m (55 ft)

- Glideslope transmitter: fixed location

- Glideslope alignment error: Gaussian

- Glideslope receiver centring error: Gaussian

- Glideslope beam noise: Gaussian

- Localizer alignment at the threshold: Gaussian (μa, $0\mu a$, $\sigma = 5\mu a$; max/min = +/−12μa)

- Localizer receiver centring error: Gaussian

- Radio altitude noise: random, Gaussian and continuous variable with a zero mean and standard deviation of 0.2 m (0.06 ft)

Airport runway-related inputs

- Runway slope: the runway slope would remain level at 0.0 per cent.

- Runway length: the average runway length for the 40 airports was about 3 656 m (12 065 ft) with a standard deviation, σ_n, of 345 m (1 138 ft). For simulation purposes, two runway lengths were used for each elevation, 2 560 m (8 400 ft) and 3 048 m (10 000 ft) for the near sea level airport 4-m (13-ft) threshold elevation and 3 048 m (10 000 ft) and 3 658 m (12 000 ft) for the high-altitude airport 2 000-m (6 500-ft) threshold elevation. These runway lengths were mixed uniformly, i.e. about 50 per cent each.

- Runway elevation: the study would investigate the influence of runway elevation at the following breakpoints: sea level 408 m (1 345 ft) and 1 988 m (6 560 ft). These values corresponded to the FAA Airplane Design Group V standard for runway centre line to parallel taxiway centre line separation distances depending on the aerodrome elevation described in Table 2-2 in FAA Advisory Circular AC 150/5300-13, Change 2 (see Appendix A, Table A-6). The simulation to date had only examined the sea level and high-altitude cases using 4 m (13 ft) for the sea level case and 2 000 m (6 500 ft) for the high elevation.

- Runway surface condition: the runway surface condition would remain dry.

Atmospheric-related inputs
(see Chapter 5, Tables 5-5 and 5-6, and Figures 5-1 and 5-2)

- Wind magnitude: a table look-up random variable based on wind data corresponding to the 40 airports. The average wind speed was 7.2 kt.

- Wind heading: a table look-up random variable based on wind data corresponding to the list of 40 airports.

Balked landing-related inputs

- Spatial coordinate initiation point: the simulation would be initiated at a point in space determined from the random distribution used in the CRM for the range value of 4.2 NM (7.8 km) before the runway threshold.

- GA initiation height: Gaussian with a mean of 9 m (30 ft) above the ground and a standard deviation of 3 m (10 ft). The distribution was truncated at 3 m (10 ft) and 15 m (50 ft).

- Pilot mode: all approaches would be auto-coupled, utilizing pilot response time characteristics as determined from experiments conducted at the NASA Ames Crew Vehicle Systems Research Facility in a Boeing 747-400 FAA certified simulation (see Part II, Chapter 4, Figure 4-3).

6.4   SIMULATION RESULTS

6.4.1   The final simulation results include a large amount of track data and charts generally falling into the following categories:

a)   Distribution of maximum lateral deviations on the ground: Figures 6-1[4] and 6-2 show the maximum lateral excursions of those balked landings that did touch down;

b)   Maximum lateral deviation under 30 m (100 ft) and above the ground: Figures 6-3 and 6-4 show the maximum lateral excursions of those balked landings that did not touch down; and

c)   Tiles: Figure sets 6-5 and 6-6 show the 10^{-7} iso-probability contours as based on the lateral and vertical distributions of penetration for each planar tile located at various ranges relative to runway threshold.

Touchdown dispersion data from balked landings
(see Figures 6-1 and 6-2)

6.4.2   In low-threshold elevation, the simulation results show touchdowns dispersed from 333 m (1 100 ft) to slightly over 490 m (1 600 ft), which agrees with observations from airline crew flying the Boeing 747-400 simulator. At the high elevation of 2 000 m (6 500 ft), the aircraft flies faster and touchdowns occur further away from threshold than they do in the low-elevation case. The touchdowns at the CG point were contained within +/–9 m (30 ft) of the runway centre line.

6.4.3   Of 59 273 simulations in the low-elevation case, 3.15 per cent or 1 865 resulted in a touchdown, whereas in the high-elevation case, of 69 684 simulations, 6.14 per cent or 4 279 resulted in

---

4. All figures are located at the end of this chapter.

touchdowns. Therefore, a touchdown was more likely at higher elevation than at lower for the distribution of TO/GA switch mode activation used in the study. The figures also show that, in the low-elevation case, the touchdown ranged from about 333 m (1 100 ft) to slightly over 490 m (1 600 ft). In the high-elevation case, the touchdowns ranged from a little more than 300 m (1 000 ft) to 549 m (1 800 ft).

6.4.4　　　　The simulation runs that resulted in touchdown were primarily due to the very low height above ground at which the TO/GA mode was activated. In the majority of runs, it happened past threshold. This resulted in the tracks at sea level and at high elevation being very similar up to that point. Since aircraft in the high-elevation runs were flying faster, they covered more range until the start of climb, resulting in lesser altitude dispersion past the threshold, compared to that low elevation.

　　　　Note.— The symmetry in the wind distribution influenced the symmetry observed in the data around the centre line. Also, the dispersion around the centre line was influenced by the variation in localizer alignment. The simulator studies were conducted with a perfectly aligned (simulated) localizer.

Maximum lateral dispersion — no touchdowns
(see Figures 6-3 and 6-4)

6.4.5　　　　The point of maximum lateral dispersion in the simulations occurred at a range between 212 m (700 ft) and 818 m (2 700 ft) past the threshold for the low-elevation condition and at a range between 212 m (700 ft) and 970 m (3 200 ft) past threshold for the high-elevation condition. In the low-elevation case, the points are clustered between 545 to 670 m (1 800 to 2 200 ft), whereas in the high-elevation case, the points are clustered between 609 and 762 m (2 000 and 2 500 ft). The difference can be accounted for by the higher speed of the aircraft at the higher elevation.

　　　　Note.— Once the TO/GA mode is activated, the aircraft maintains track until a height of 121 m (400 ft) is reached in executing the GA so it is unlikely that the aircraft will maintain centre line, which may explain why so few points are on centre line.

6.4.6　　　　All data points were contained within +/–9 m (30 ft) around the centre line for both low and high elevation simulation conditions. In the studies, the point of maximum lateral deviation was within +/–3 m (9 ft) of runway centre line when approaches were flown with the autopilot. The major difference in the studies was the localizer alignment. In the simulations the alignment was +/–6 m (21 ft) around centre line. Therefore, the +/–3 m (9 ft) lateral deviations with maximum misalignments of 6 m (21 ft) would be comparable to what is observed in the simulation data.

The iso-probability contour plots
(see Figure sets 6-5A to 6-5P and 6-6A to 6-6P)

6.4.7　　　　Notes regarding the iso-probability contour plots are as follows:

　　　　a)　　The plots in set 6-5 are for a field elevation of 4 m (13 ft), and those in 6-6 are for a field elevation of 1 970 m (6 500 ft);

　　　　b)　　The first two tiles, 4 200 and 1 200 m (13 860 and 3 960 ft) correspond to the nominal tiles found in the CRM;

　　　　c)　　There is a tile at 900 and 600 m (2 950 and 1 968 ft) before threshold — on the approach side of threshold starting at 300 m (984 ft) there are tiles at 50-m (164-ft) increments to 250 m (820 ft) past threshold — the missed approach side;

d)   The origin is set at the height of the median of the vertical distribution AGL. The median of a distribution is the value y such that $P(Y \leq y) = 0.5$;

e)   The oval-shaped curve encloses the CG of the aircraft. It is drawn so that the probability of being outside the curve is 2×10^{-7}. The lower curve is the lower half of the oval curve corrected for semi-span and wheel location of the aircraft. The value of semi-span used is 40 m (131 ft), i.e. a total span of 80 m (262 ft) with the flight path of the bottom of the wheel located 7 m (24 ft) below the horizontal plane of the CG point. The lower half of the curve is that part below the median of the vertical distribution. Therefore, the probability of some part of the aircraft being below the lower curve is one half of 2×10^{-7} or 1×10^{-7};

f)   The line that depicts the ground plane is at the height of the runway surface at threshold. It has not been corrected for earth curvature, but for the distances used, the curvature correction is insignificant;

g)   In several plots the ground plane crosses the lower curve. This indicates that some aircraft are expected to touch wheels on the runway. It does not indicate that they have impacted the ground or crashed; and

h)   The ends of the lower curve indicate the maximum distance from runway centre line for a probability of 1×10^{-7}, which would be found on an aircraft wing tip.

6.5   CONCLUSIONS

The simulations indicate that an NLA performing an autopilot-handled "normal" balked landing (one not driven by aircraft system failures) were fully contained within the current ICAO code letter E OFZ protection surfaces.

— — — — — — — —
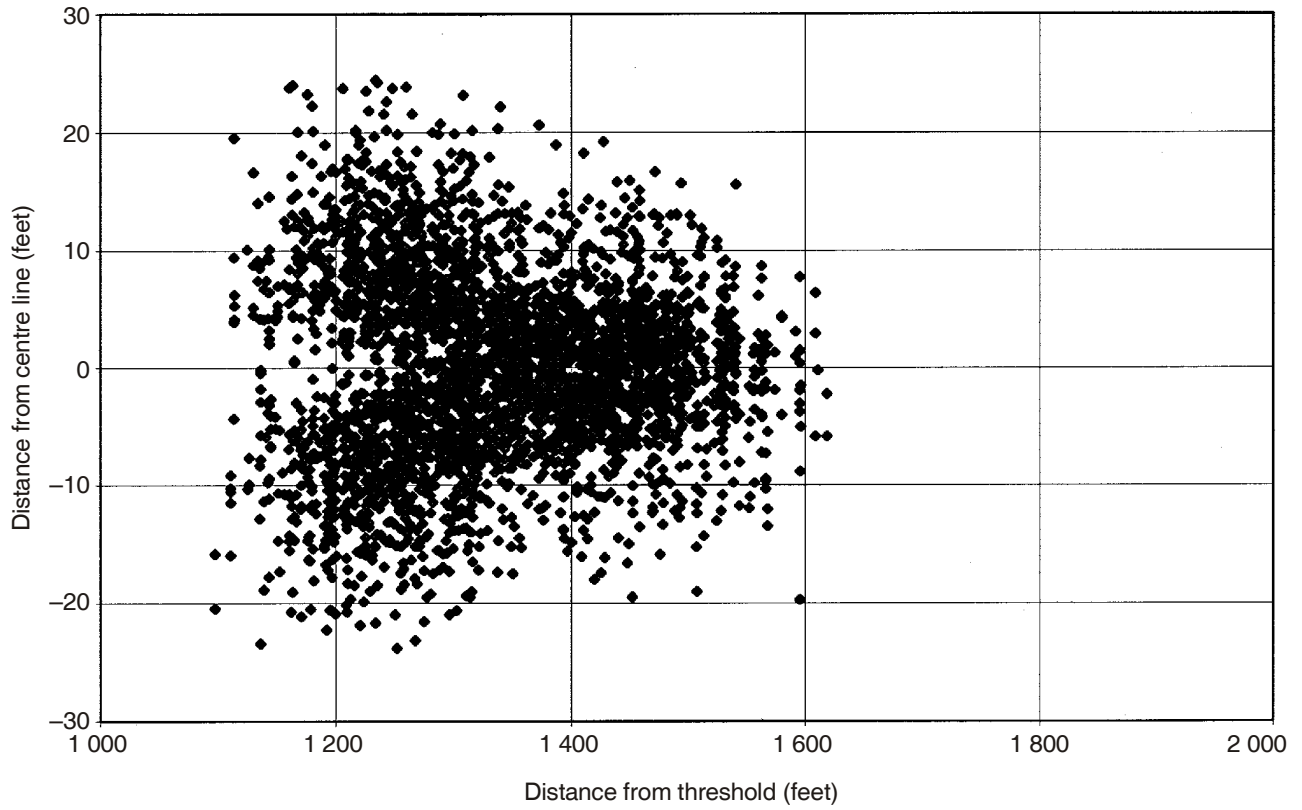
**Figure 6-1.   NLA touchdown dispersion during balked landing —
Threshold elevation: 13 ft**
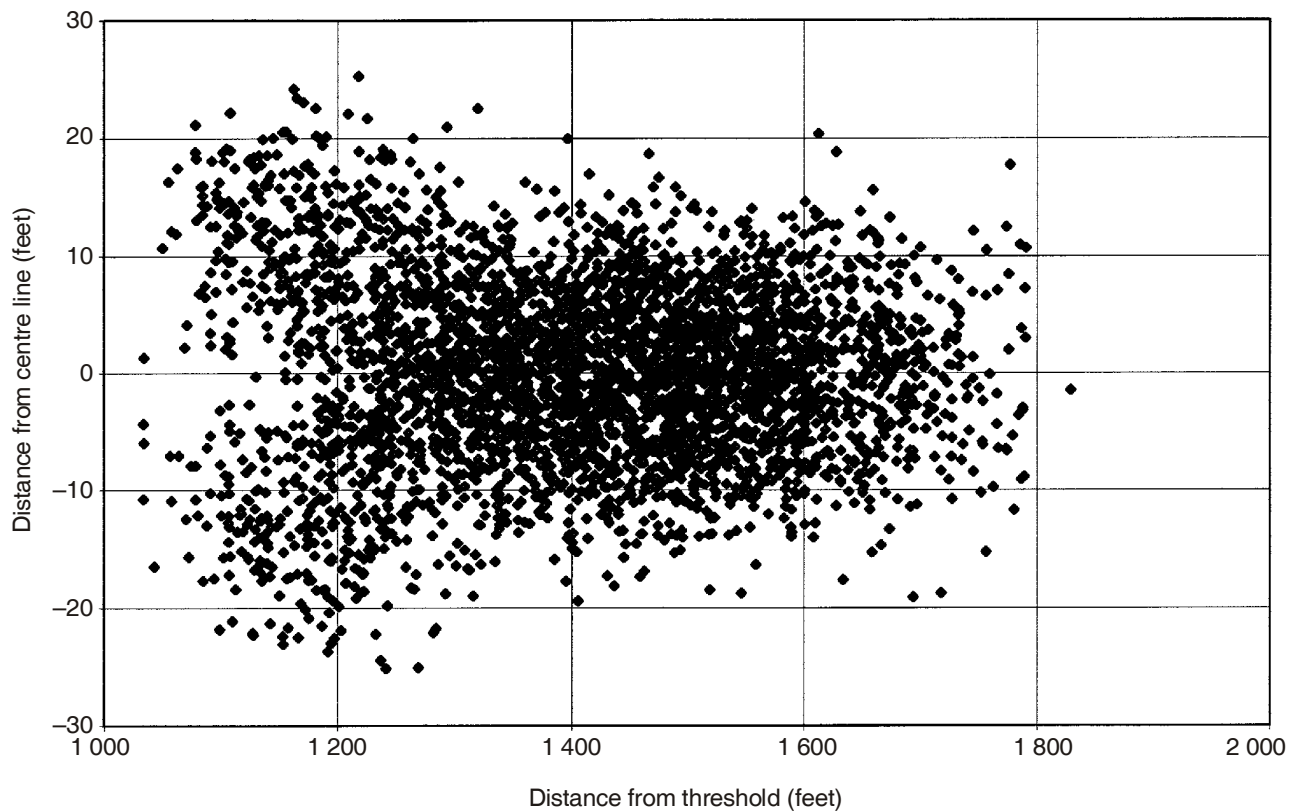
**Figure 6-2.   NLA touchdown dispersion during balked landing —
Threshold elevation: 6 500 ft**
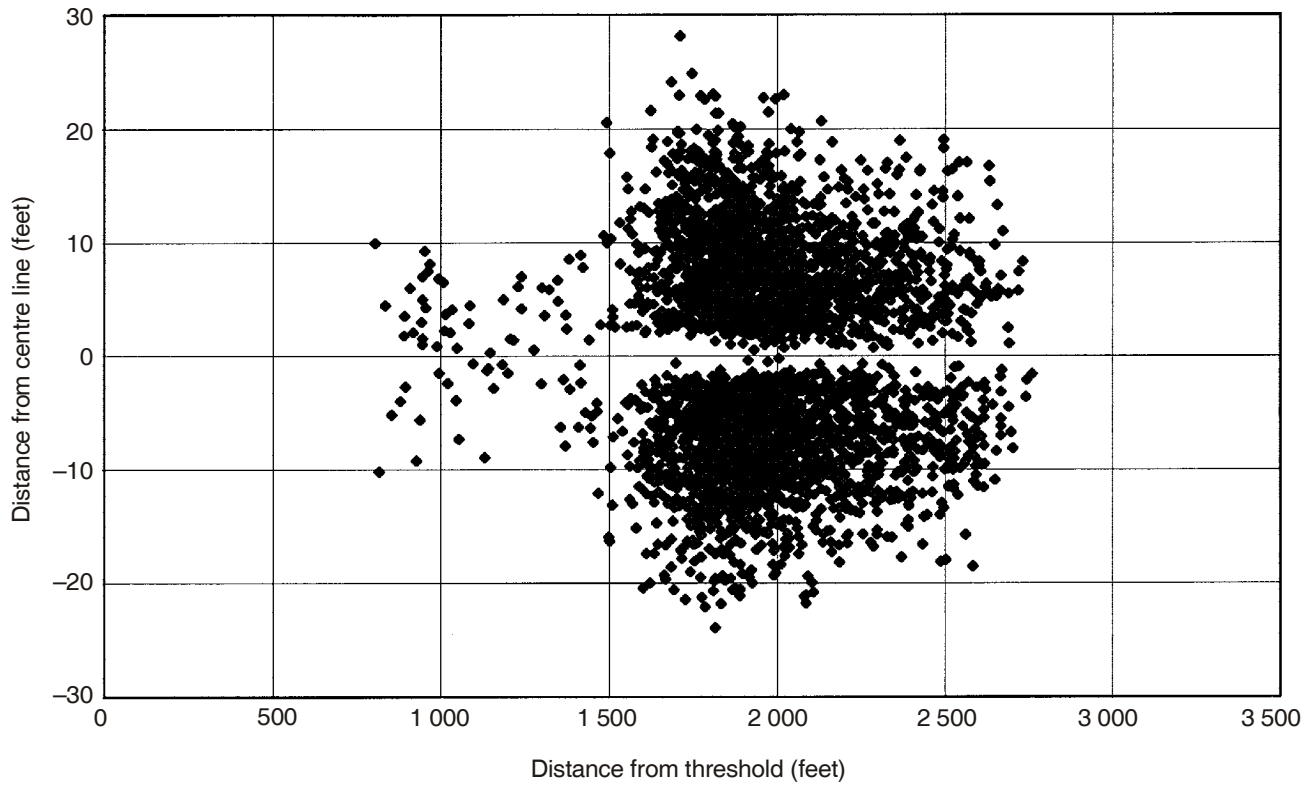
**Figure 6-3.   NLA maximum lateral dispersion during balked landing
without touchdown — Threshold elevation: 13 ft**
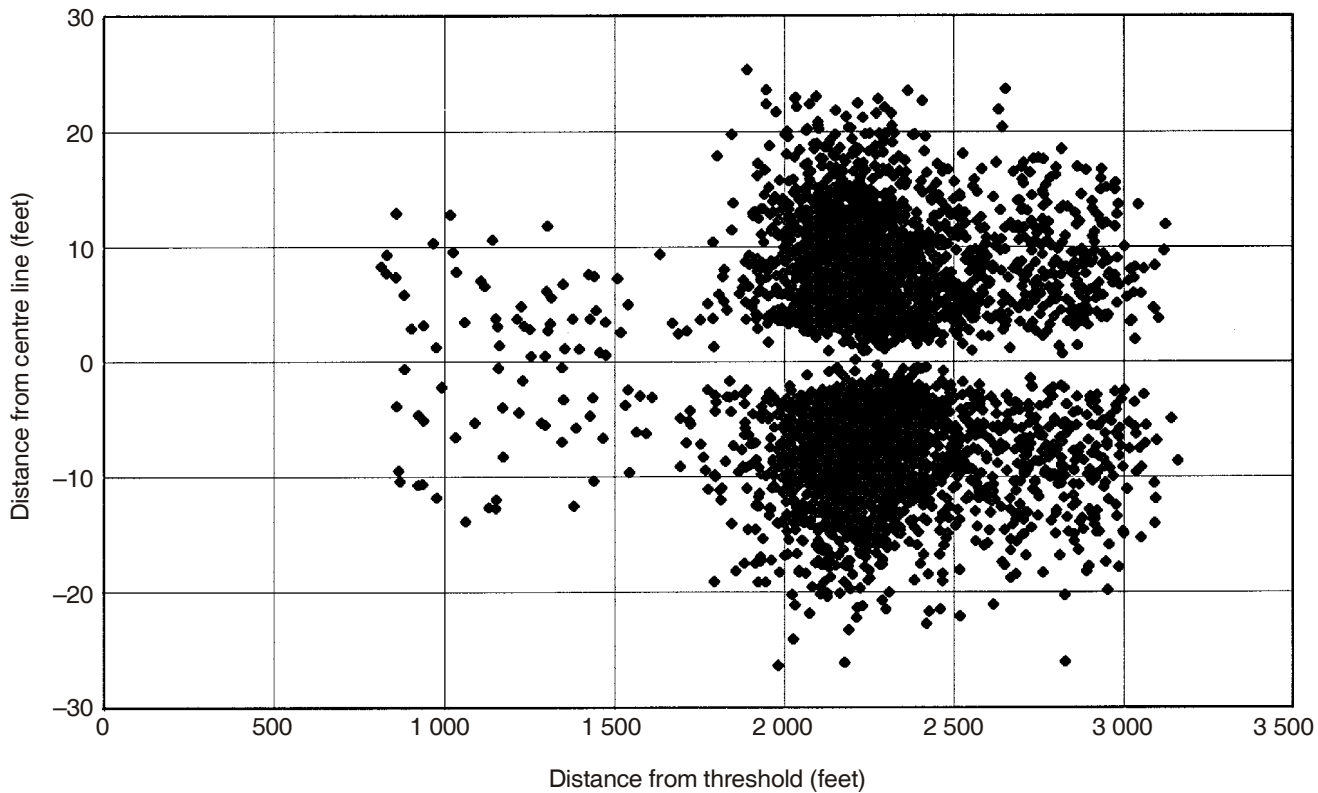
**Figure 6-4.   NLA maximum lateral dispersion during balked landing
without touchdown — Threshold elevation: 6 500 ft**

FIGURE SET 6-5 (A TO P)

10^{-7} Iso-probability contour plots (low threshold elevation of 13 ft)

Range:

— before threshold: 4 200 m, 1 200 m, 900 m, 600 m, 300 m, 250 m, 200 m, 150 m, 100 m, 50 m

— threshold: 0 m

— after threshold: 50 m, 100 m, 150 m, 200 m, 250 m

Figure 6-5A.   4 200 m before threshold at elevation of 13 ft

The oval-shaped curve is the curve that encloses the centre of gravity of the aircraft. The lower curve is the lower half of the oval curve corrected for semi-span and wheel height of the aircraft. The value of semi-span used is 40 m/131 ft; the wheel height is 7.3 m/24 ft.

Probability under curve is 10^{-7}
Metres before threshold = 1 200
Airport elevation is 13 ft
Maximum X is 51.6 m
Minimum X is –51.6 m
Minimum Y is 68.4 m
Origin is 78 m above ground

Figure 6-5B.   1 200 m before threshold at elevation of 13 ft

The oval-shaped curve is the curve that encloses the centre of gravity of the aircraft. The lower curve is the lower half of the oval curve corrected for semi-span and wheel height of the aircraft. The value of semi-span used is 40 m/131 ft; the wheel height is 7.3 m/24 ft.

Figure 6-5C.   900 m before threshold at elevation of 13 ft

The oval-shaped curve is the curve that encloses the centre of gravity of the aircraft. The lower curve is the lower half of the oval curve corrected for semi-span and wheel height of the aircraft. The value of semi-span used is 40 m/131 ft; the wheel height is 7.3 m/24 ft.

Probability under curve is 10^{-7}
Metres before threshold = 600
Airport elevation is 13 ft
Maximum X is 50.0 m
Minimum X is –50.0 m
Minimum Y is 37.7 m
Origin is 46 m above ground

Ground plane

Figure 6-5D.   600 m before threshold at elevation of 13 ft

The oval-shaped curve is the curve that encloses the centre of gravity of the aircraft. The lower curve is the lower half of the oval curve corrected for semi-span and wheel height of the aircraft. The value of semi-span used is 40 m/131 ft; the wheel height is 7.3 m/24 ft.
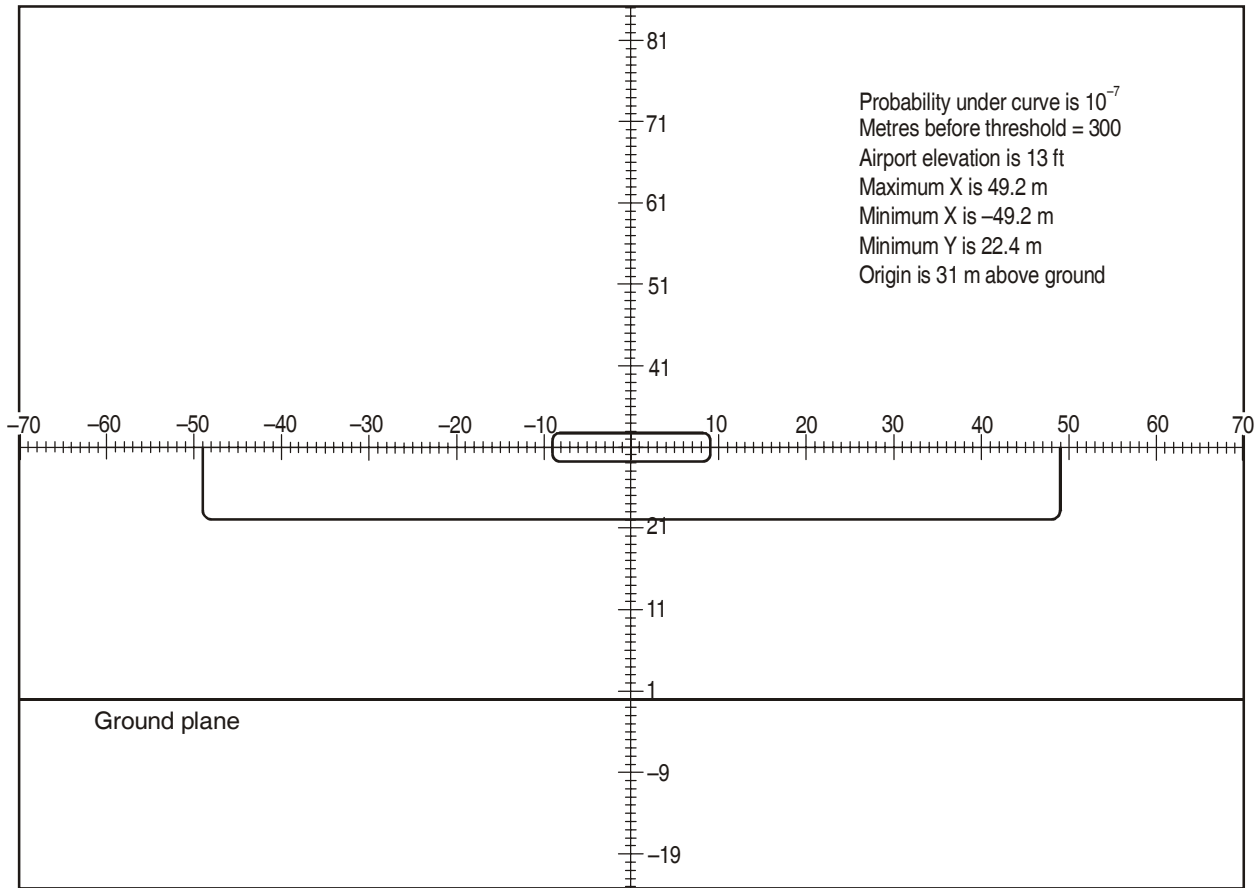
Figure 6-5E.   300 m before threshold at elevation of 13 ft

The oval-shaped curve is the curve that encloses the centre of gravity of the aircraft. The lower curve is the lower half of the oval curve corrected for semi-span and wheel height of the aircraft. The value of semi-span used is 40 m/131 ft; the wheel height is 7.3 m/24 ft.

78

Probability under curve is 10^{-7}
Metres before threshold = 250
Airport elevation is 13 ft
Maximum X is 49.1 m
Minimum X is –49.1 m
Minimum Y is 19.5 m
Origin is 28 m above ground

68

58

48

38

−70   −60   −50   −40   −30   −20   −10   10   20   30   40   50   60   70

18

8

Ground plane   −2

−12

−22

Figure 6-5F.   250 m before threshold at elevation of 13 ft

The oval-shaped curve is the curve that encloses the centre of gravity of the aircraft. The lower curve is the lower half of the oval curve corrected for semi-span and wheel height of the aircraft. The value of semi-span used is 40 m/131 ft; the wheel height is 7.3 m/24 ft.
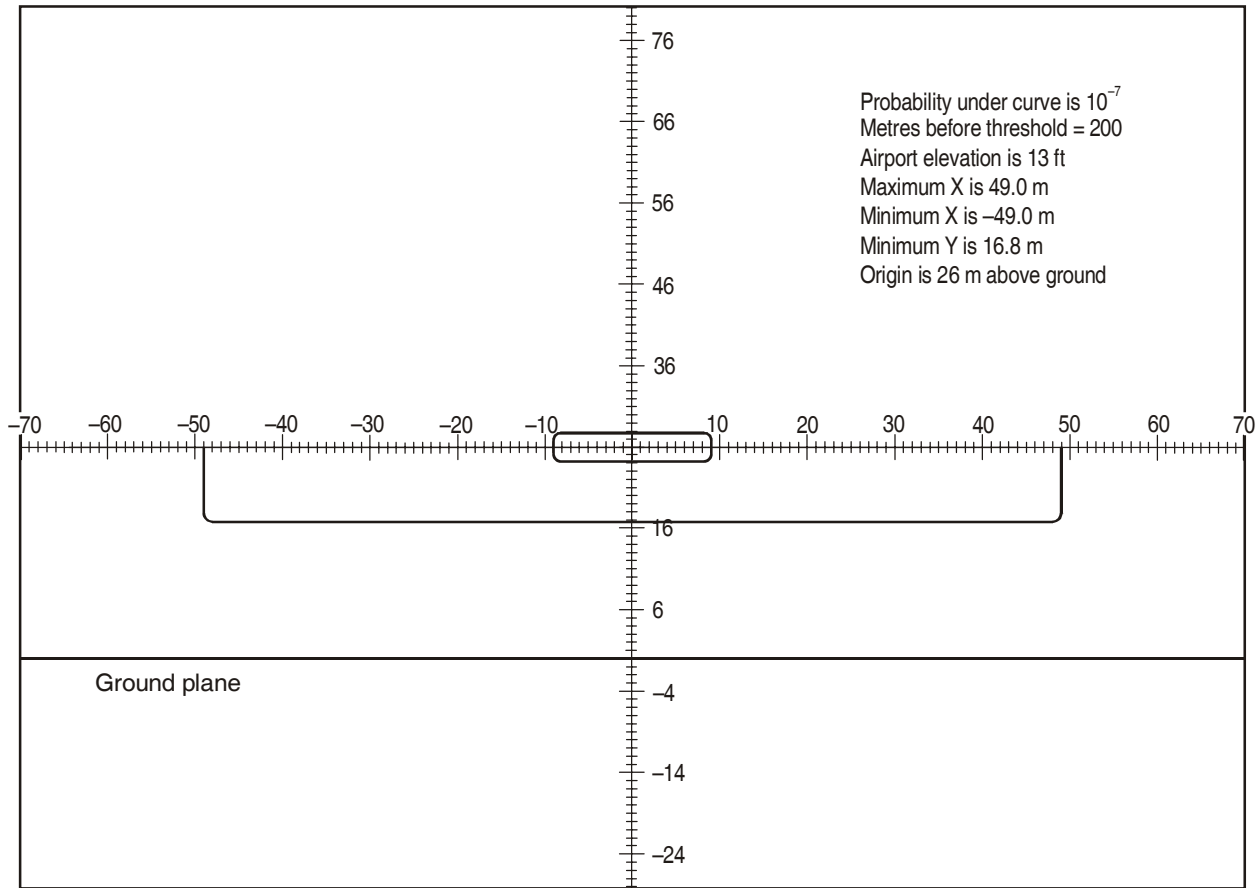
Figure 6-5G.   200 m before threshold at elevation of 13 ft

The oval-shaped curve is the curve that encloses the centre of gravity of the aircraft. The lower curve is the lower half of the oval curve corrected for semi-span and wheel height of the aircraft. The value of semi-span used is 40 m/131 ft; the wheel height is 7.3 m/24 ft.

Probability under curve is 10^{-7}
Metres before threshold = 150
Airport elevation is 13 ft
Maximum X is 48.8 m
Minimum X is –48.8 m
Minimum Y is 14.0 m
Origin is 23 m above ground

Ground plane

Figure 6-5H.   150 m before threshold at elevation of 13 ft

The oval-shaped curve is the curve that encloses the centre of gravity of the aircraft. The lower curve is the lower half of the oval curve corrected for semi-span and wheel height of the aircraft. The value of semi-span used is 40 m/131 ft; the wheel height is 7.3 m/24 ft.

71

Probability under curve is 10^{-7}
Metres before threshold = 100
Airport elevation is 13 ft
Maximum X is 48.7 m
Minimum X is –48.7 m
Minimum Y is 12.4 m
Origin is 21 m above ground

61

51

41

31

−70   −60   −50   −40   −30   −20   −10   10   20   30   40   50   60   70

11

1

Ground plane

−9

−19

−29

Figure 6-5l.   100 m before threshold at elevation of 13 ft

The oval-shaped curve is the curve that encloses the centre of gravity of the aircraft. The lower curve is the lower half of the oval curve corrected for semi-span and wheel height of the aircraft. The value of semi-span used is 40 m/131 ft; the wheel height is 7.3 m/24 ft.

Probability under curve is 10^{-7}
Metres before threshold = 50
Airport elevation is 13 ft
Maximum X is 48.5 m
Minimum X is –48.5 m
Minimum Y is 9.9 m
Origin is 18 m above ground

Ground plane

Figure 6-5J.   50 m before threshold at elevation of 13 ft

The oval-shaped curve is the curve that encloses the centre of gravity of the aircraft. The lower curve is the lower half of the oval curve corrected for semi-span and wheel height of the aircraft. The value of semi-span used is 40 m/131 ft; the wheel height is 7.3 m/24 ft.
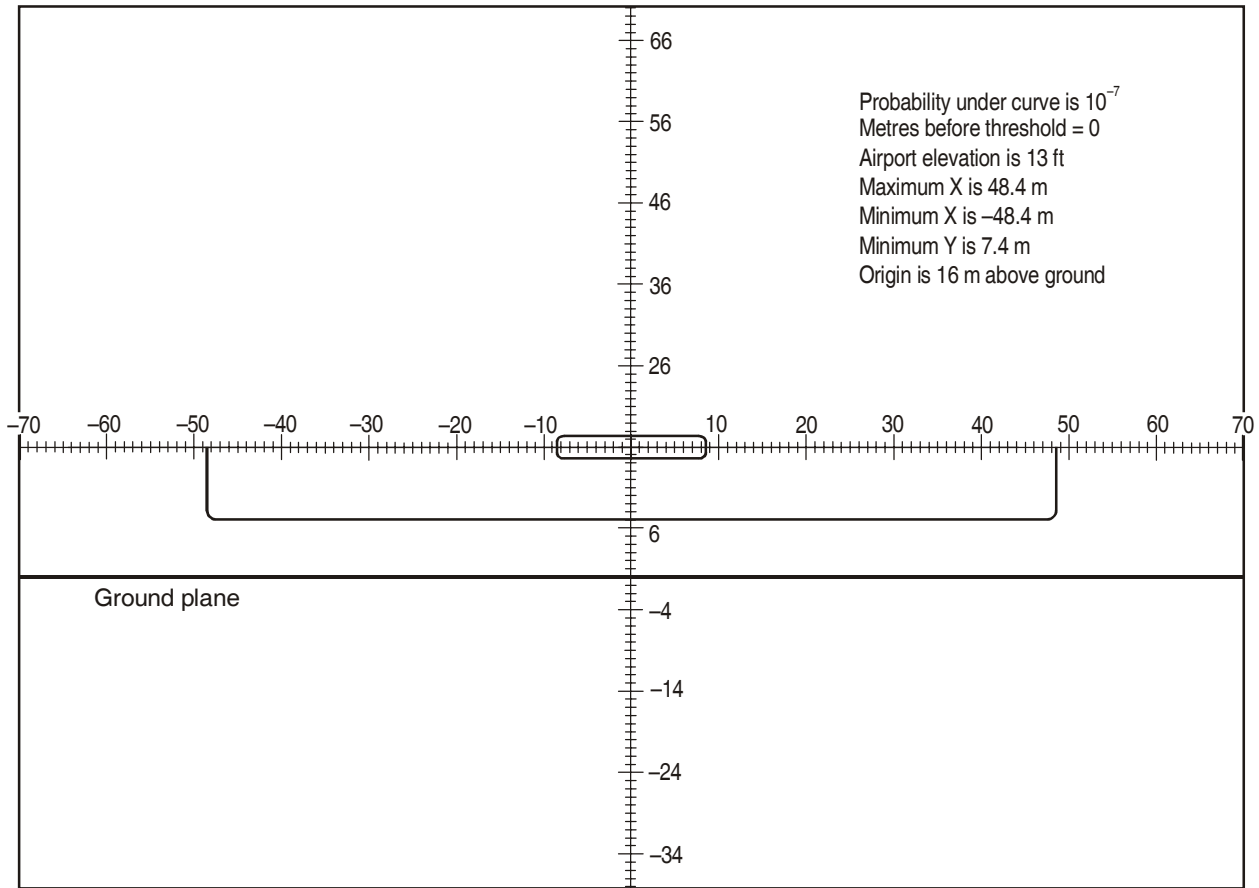
Figure 6-5K.   0 m before threshold at elevation of 13 ft

The oval-shaped curve is the curve that encloses the centre of gravity of the aircraft. The lower curve is the lower half of the oval curve corrected for semi-span and wheel height of the aircraft. The value of semi-span used is 40 m/131 ft; the wheel height is 7.3 m/24 ft.

Probability under curve is 10^{-7}
Metres after threshold = 50
Airport elevation is 13 ft
Maximum X is 48.3 m
Minimum X is –48.3 m
Minimum Y is 5.1 m
Origin is 13 m above ground

Ground plane

Figure 6-5L.   50 m after threshold at elevation of 13 ft

The oval-shaped curve is the curve that encloses the centre of gravity of the aircraft. The lower curve is the lower half of the oval curve corrected for semi-span and wheel height of the aircraft. The value of semi-span used is 40 m/131 ft; the wheel height is 7.3 m/24 ft.
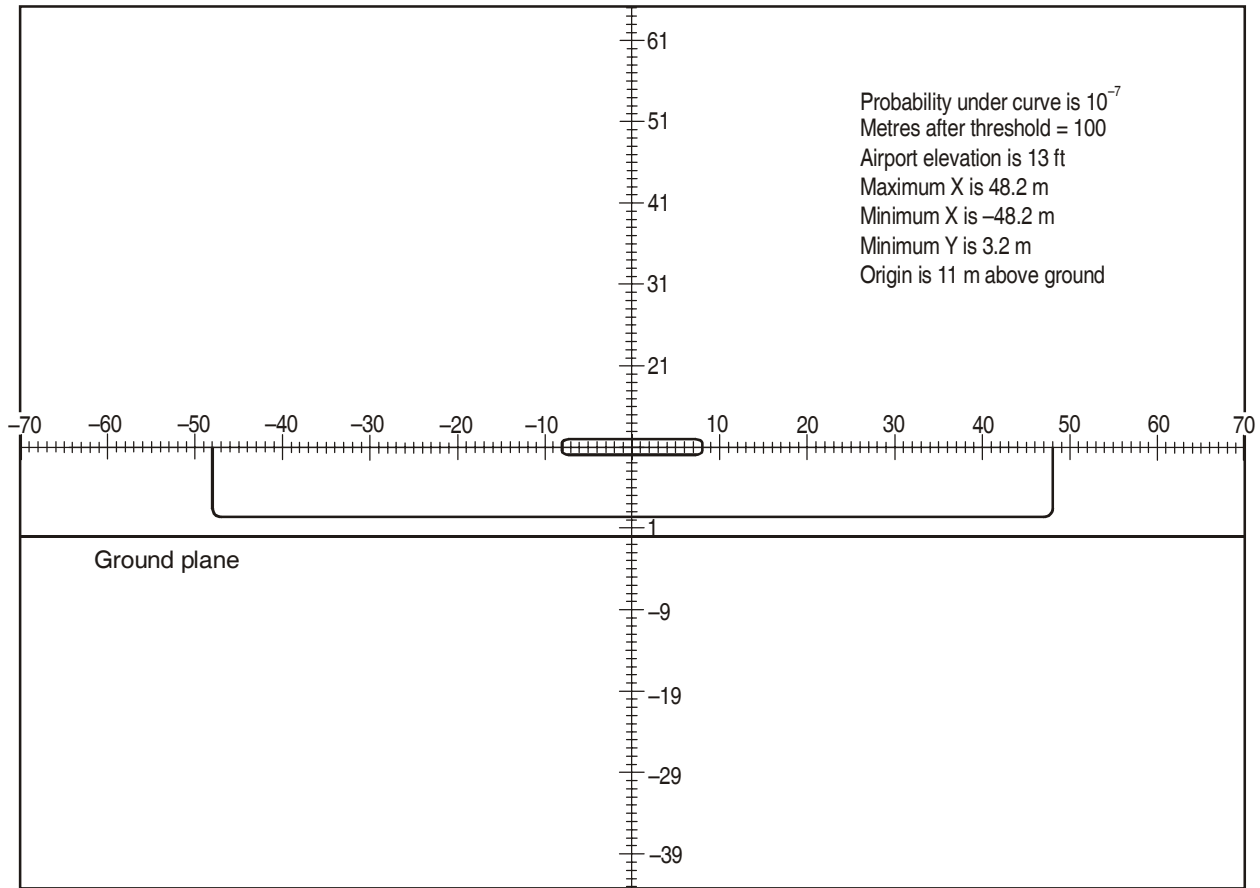
Figure 6-5M.   100 m after threshold at elevation of 13 ft

The oval-shaped curve is the curve that encloses the centre of gravity of the aircraft. The lower curve is the lower half of the oval curve corrected for semi-span and wheel height of the aircraft. The value of semi-span used is 40 m/131 ft; the wheel height is 7.3 m/24 ft.

Probability under curve is 10^{-7}
Metres after threshold = 150
Airport elevation is 13 ft
Maximum X is 48.1 m
Minimum X is –48.1 m
Minimum Y is –1.8 m
Origin is 9 m above ground

Ground plane
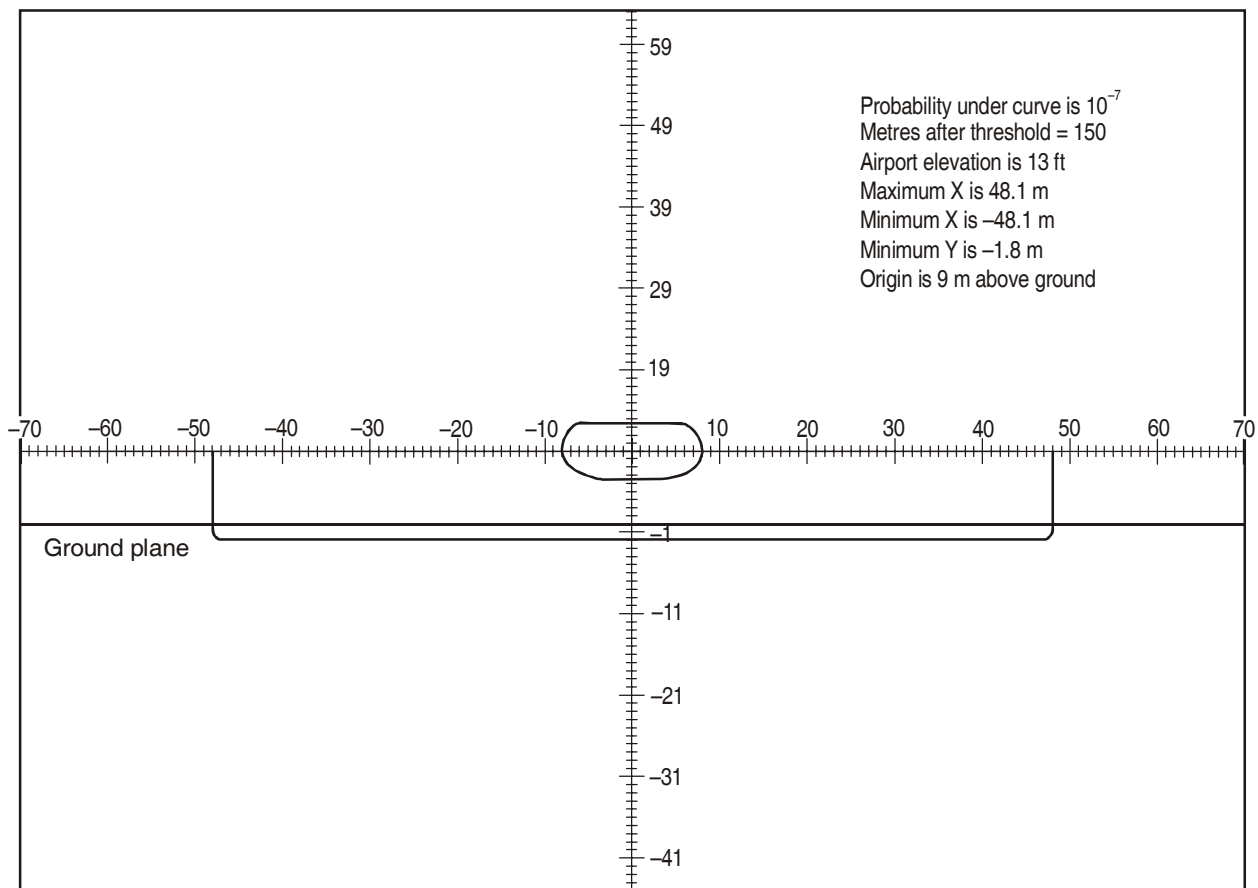
Figure 6-5N.   150 m after threshold at elevation of 13 ft

The oval-shaped curve is the curve that encloses the centre of gravity of the aircraft. The lower curve is the lower half of the oval curve corrected for semi-span and wheel height of the aircraft. The value of semi-span used is 40 m/131 ft; the wheel height is 7.3 m/24 ft.

Probability under curve is 10^{-7}
Metres after threshold = 200
Airport elevation is 13 ft
Maximum X is 48.1 m
Minimum X is –48.1 m
Minimum Y is –2.8 m
Origin is 11 m above ground

Ground plane
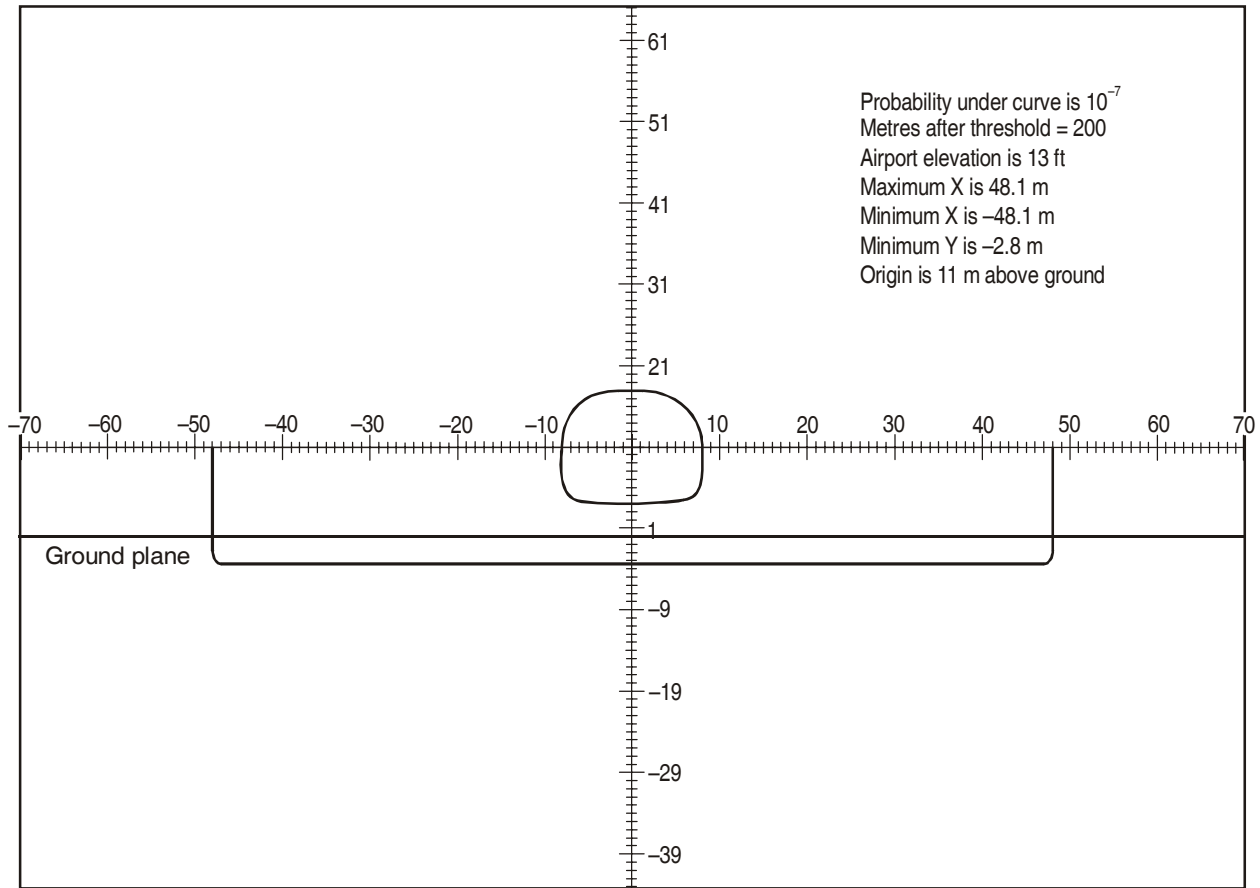
Figure 6-5O.   200 m after threshold at elevation of 13 ft

The oval-shaped curve is the curve that encloses the centre of gravity of the aircraft. The lower curve is the lower half of the oval curve corrected for semi-span and wheel height of the aircraft. The value of semi-span used is 40 m/131 ft; the wheel height is 7.3 m/24 ft.
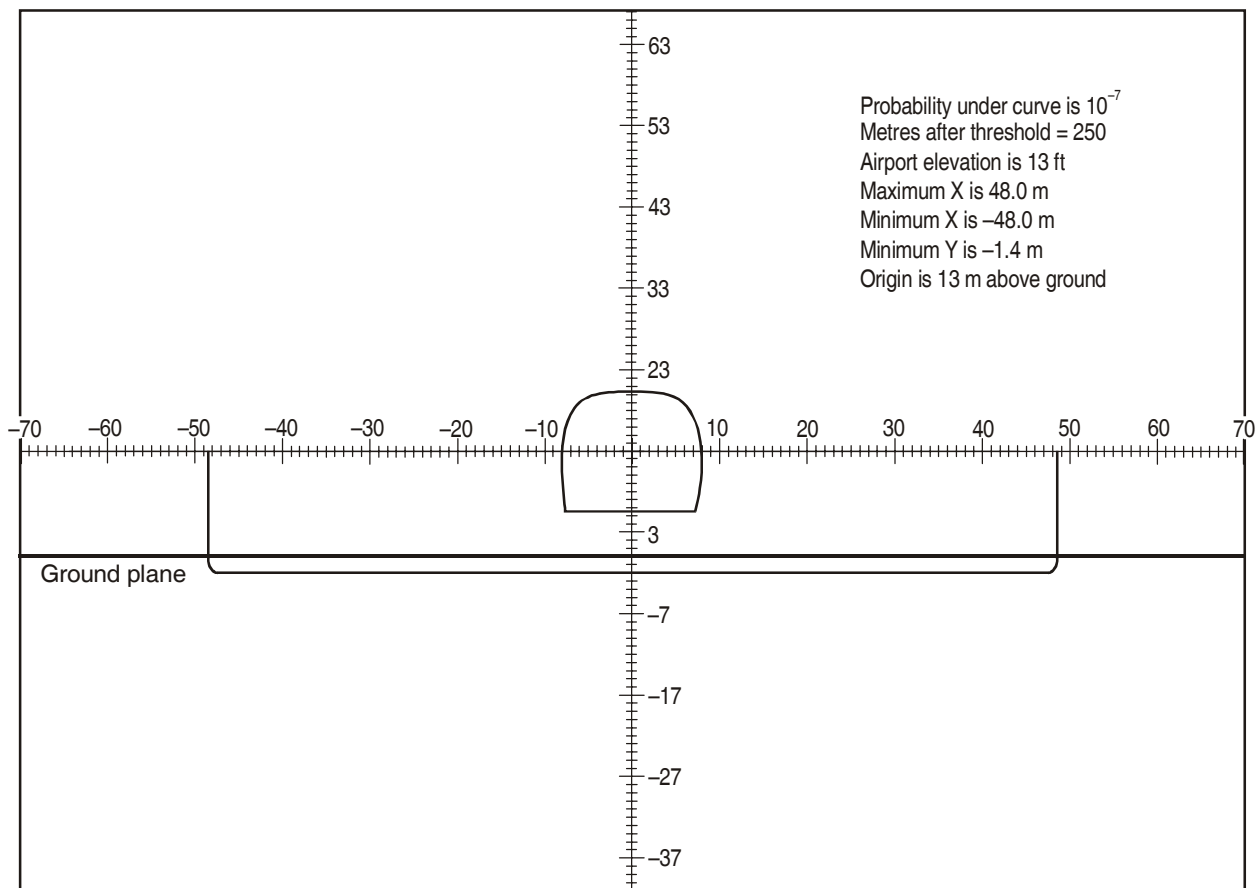
Figure 6-5P.   250 m after threshold at elevation of 13 ft

The oval-shaped curve is the curve that encloses the centre of gravity of the aircraft. The lower curve is the lower half of the oval curve corrected for semi-span and wheel height of the aircraft. The value of semi-span used is 40 m/131 ft; the wheel height is 7.3 m/24 ft.

FIGURE SET 6-6 (A TO P)

10^{-7} Iso-probability contour plots (high threshold elevation of 6 500 ft)

Range:

— before threshold: 4 200 m, 1 200 m, 900 m, 600 m, 300 m, 250 m, 200 m, 150 m, 100 m, 50 m

— threshold: 0 m

— after threshold: 50 m, 100 m, 150 m, 200 m, 250 m
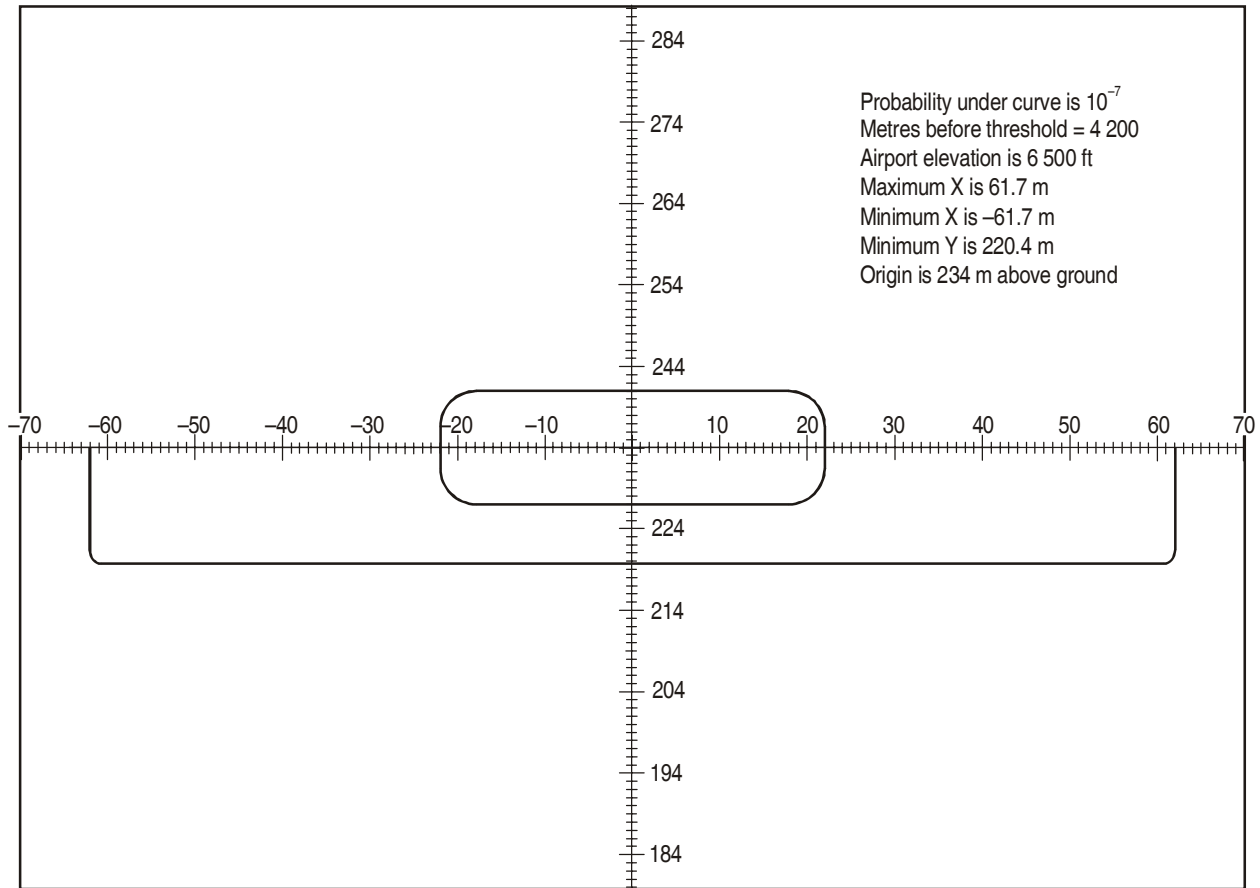
Figure 6-6A.   4 200 m before threshold at elevation of 6 500 ft

The oval-shaped curve is the curve that encloses the centre of gravity of the aircraft. The lower curve is the lower half of the oval curve corrected for semi-span and wheel height of the aircraft. The value of semi-span used is 40 m/131 ft; the wheel height is 7.3 m/24 ft.

Probability under curve is 10^{-7}
Metres before threshold = 1 200
Airport elevation is 6 500 ft
Maximum X is 52.3 m
Minimum X is –52.3 m
Minimum Y is 68.3 m
Origin is 78 m above ground
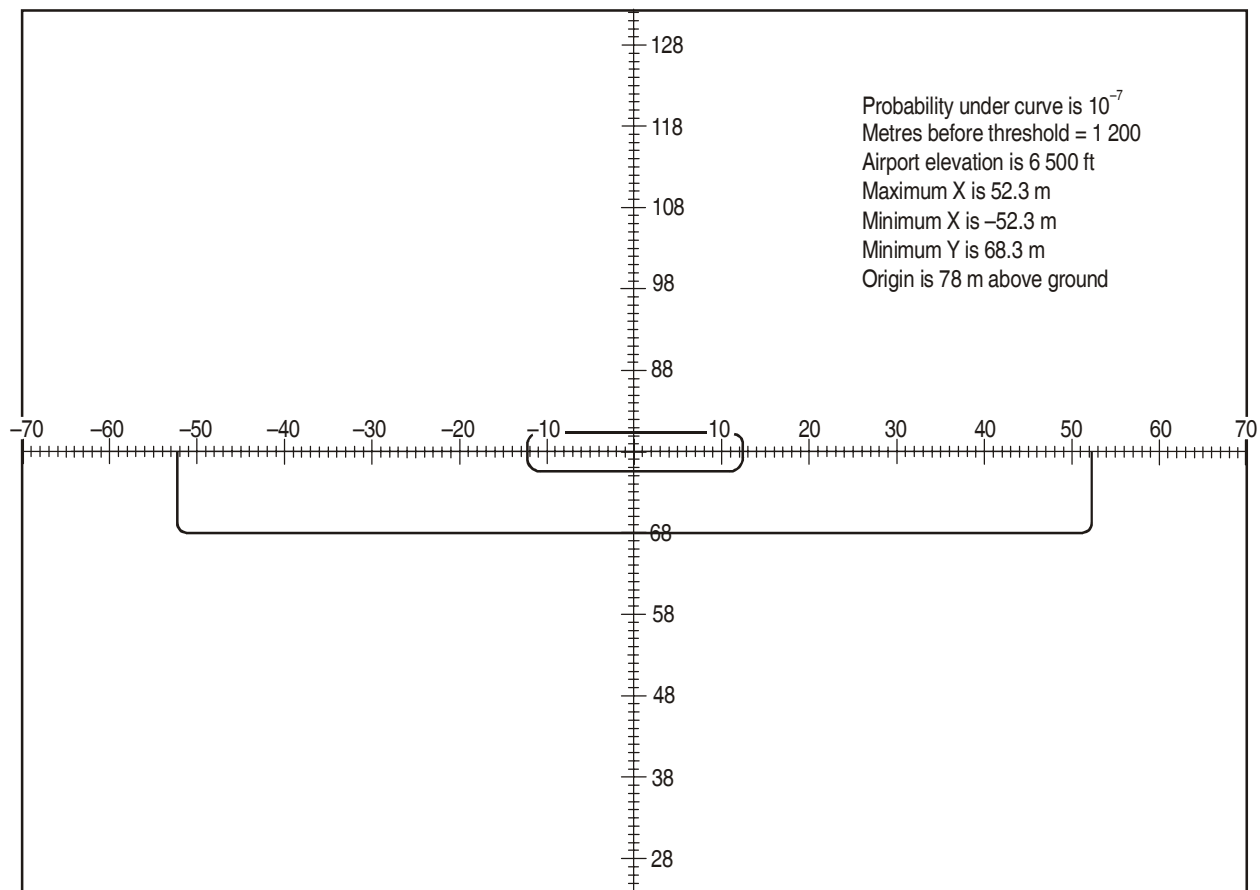
Figure 6-6B.   1 200 m before threshold at elevation of 6 500 ft

The oval-shaped curve is the curve that encloses the centre of gravity of the aircraft. The lower curve is the lower half of the oval curve corrected for semi-span and wheel height of the aircraft. The value of semi-span used is 40 m/131 ft; the wheel height is 7.3 m/24 ft.
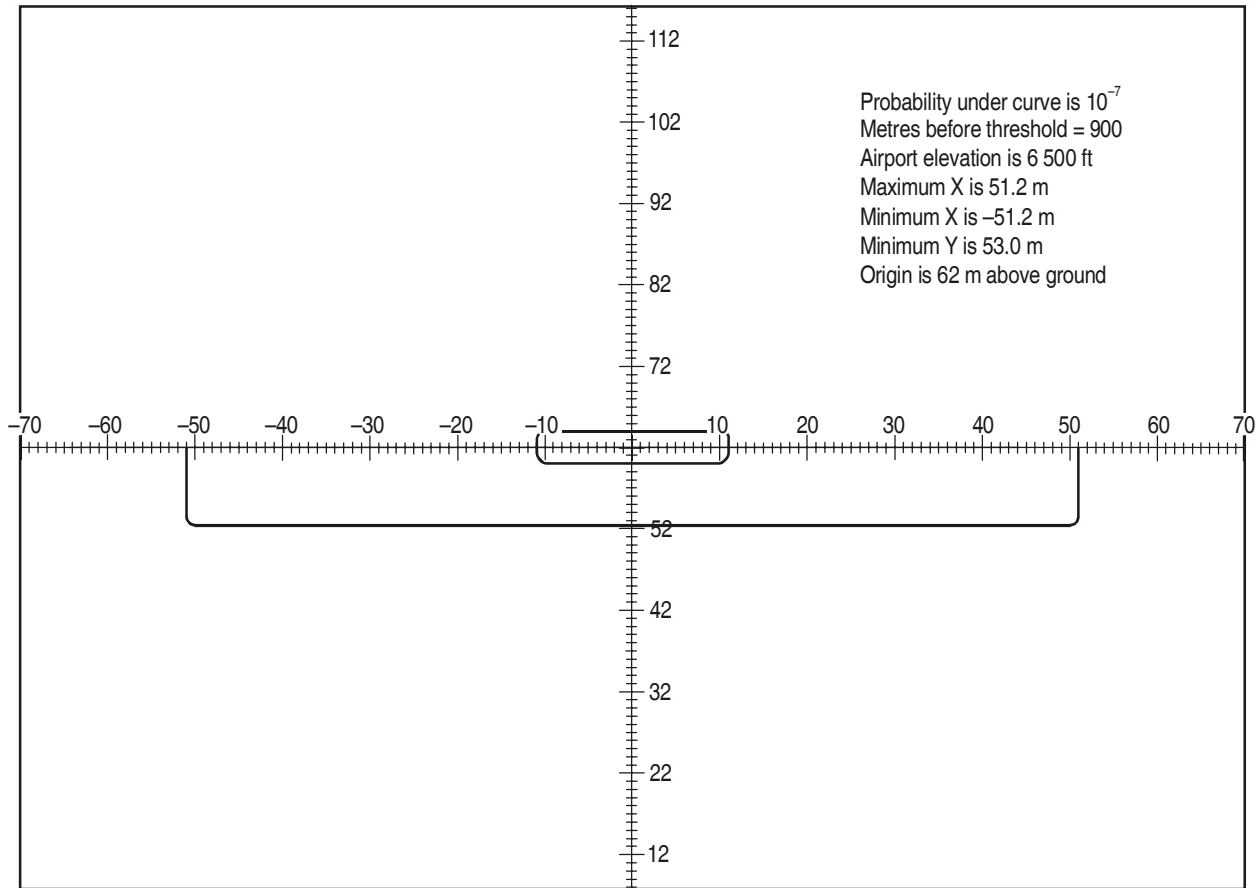
Figure 6-6C.   900 m before threshold at elevation of 6 500 ft

The oval-shaped curve is the curve that encloses the centre of gravity of the aircraft. The lower curve is the lower half of the oval curve corrected for semi-span and wheel height of the aircraft. The value of semi-span used is 40 m/131 ft; the wheel height is 7.3 m/24 ft.
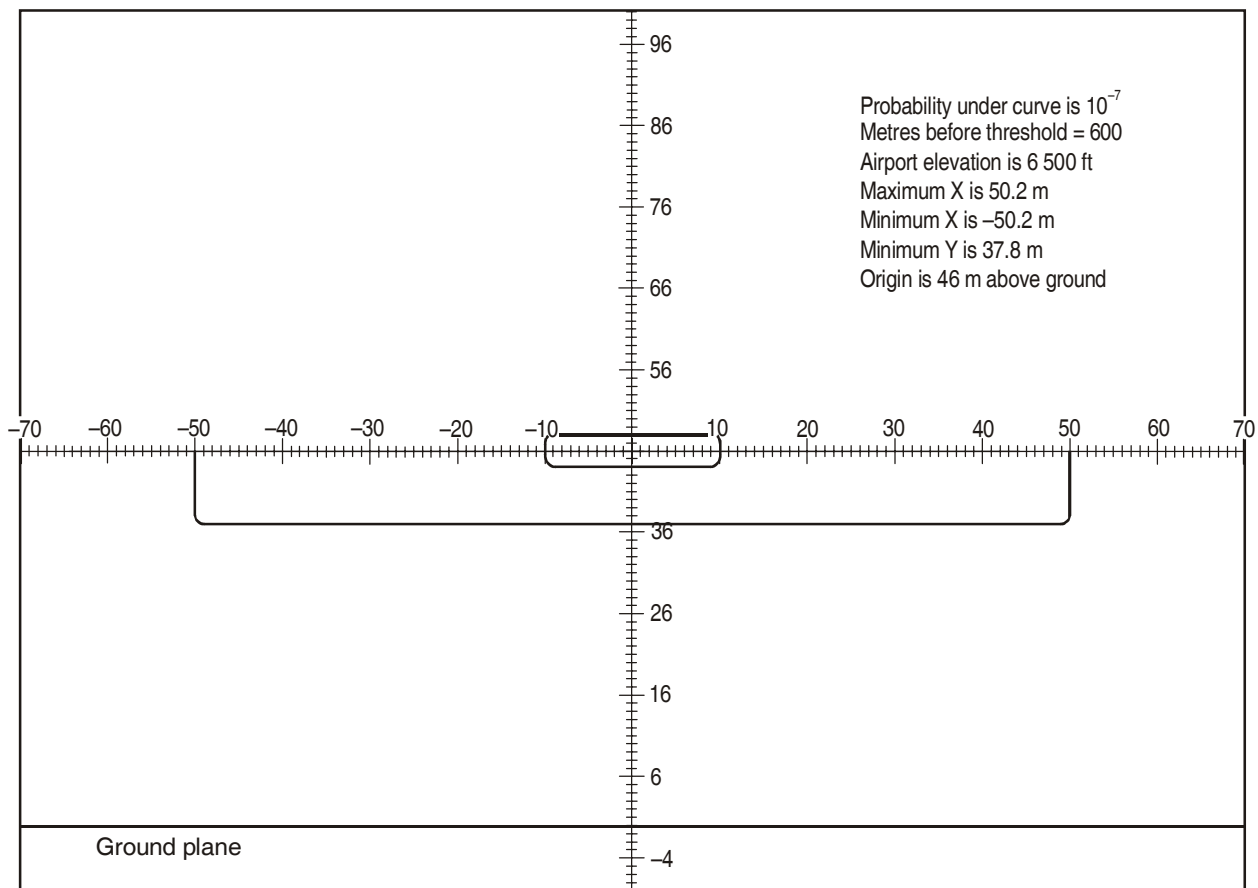
Figure 6-6D.   600 m before threshold at elevation of 6 500 ft

The oval-shaped curve is the curve that encloses the centre of gravity of the aircraft. The lower curve is the lower half of the oval curve corrected for semi-span and wheel height of the aircraft. The value of semi-span used is 40 m/131 ft; the wheel height is 7.3 m/24 ft.
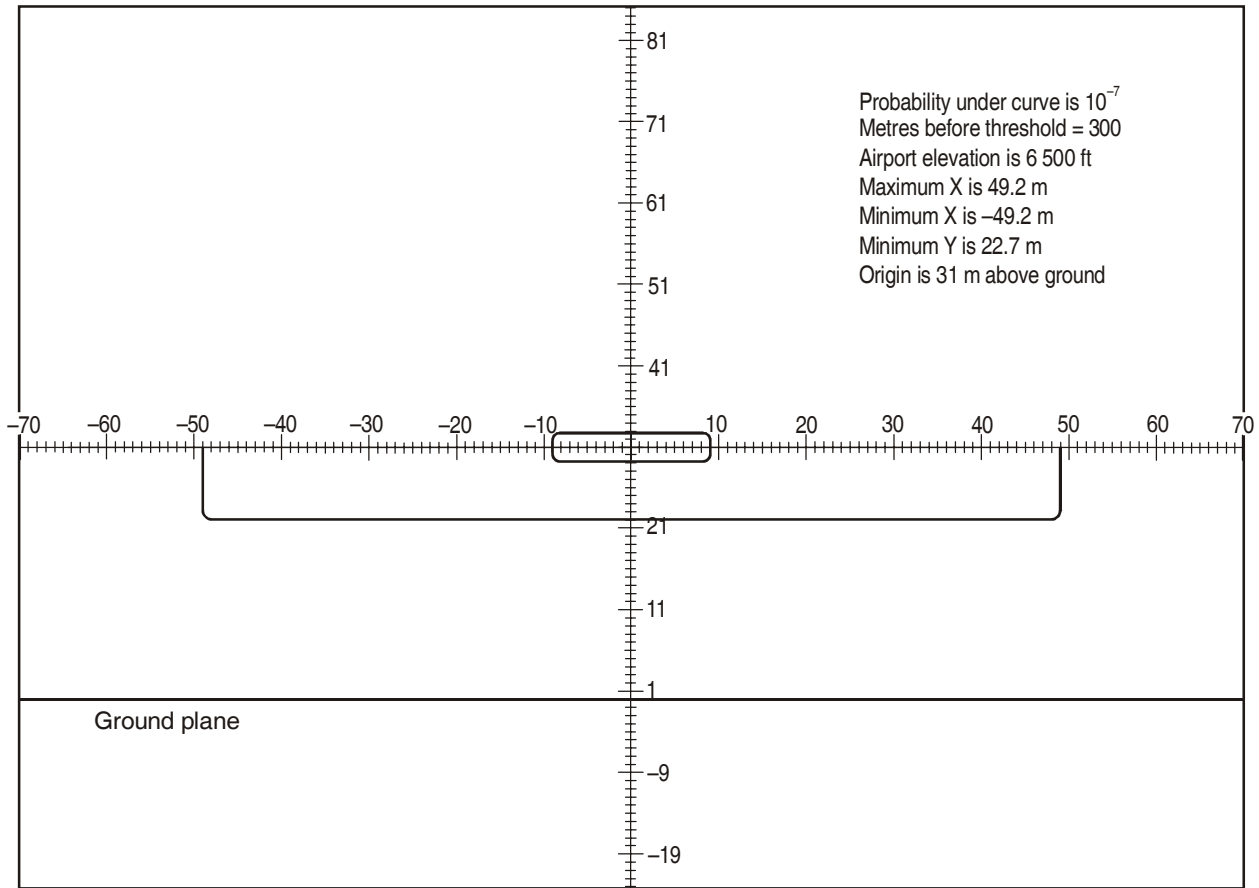
Figure 6-6E.   300 m before threshold at elevation of 6 500 ft

The oval-shaped curve is the curve that encloses the centre of gravity of the aircraft. The lower curve is the lower half of the oval curve corrected for semi-span and wheel height of the aircraft. The value of semi-span used is 40 m/131 ft; the wheel height is 7.3 m/24 ft.

Probability under curve is 10^{-7}
Metres before threshold = 250
Airport elevation is 6 500 ft
Maximum X is 49.1 m
Minimum X is –49.1 m
Minimum Y is 20.2 m
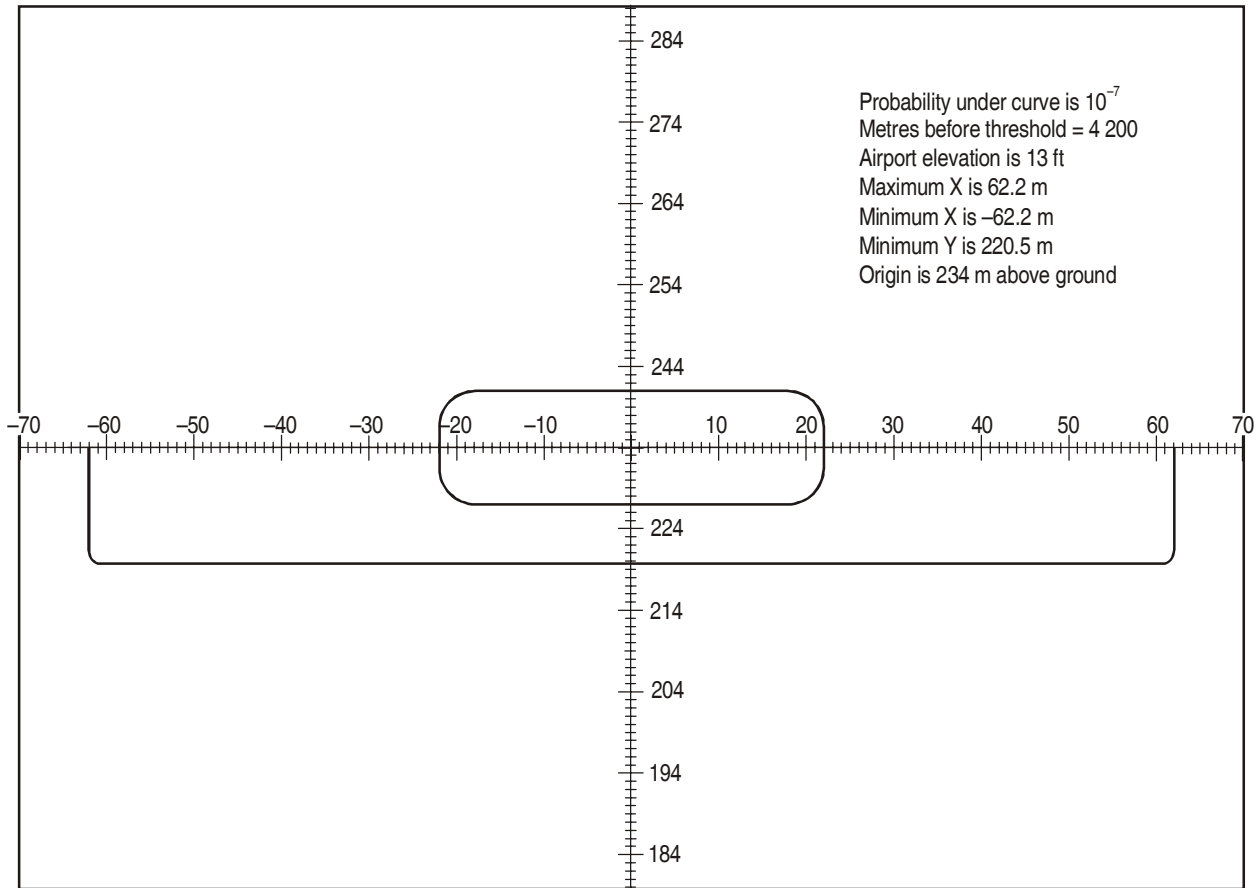Origin is 29 m above ground

Ground plane
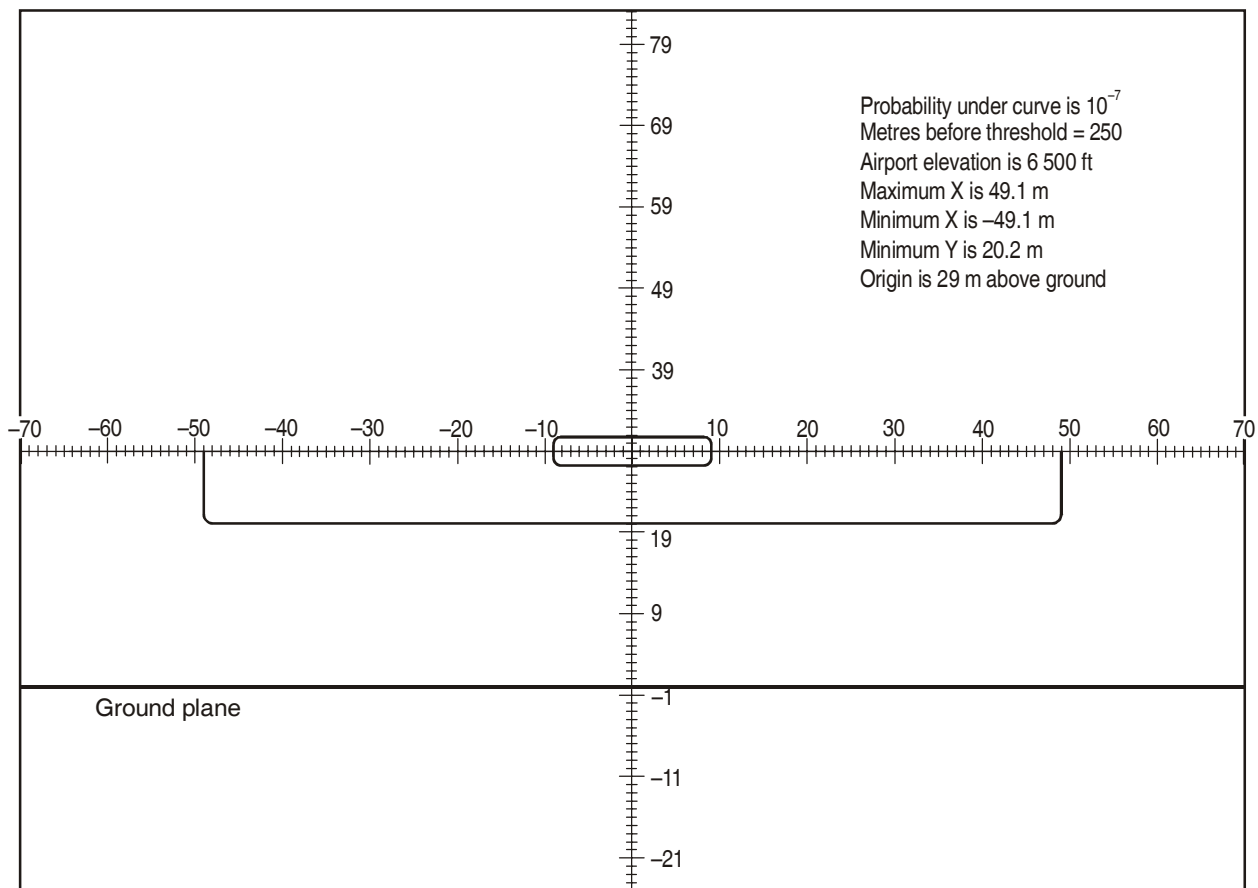
Figure 6-6F.   250 m before threshold at elevation of 6 500 ft

The oval-shaped curve is the curve that encloses the centre of gravity of the aircraft. The lower curve is the lower half of the oval curve corrected for semi-span and wheel height of the aircraft. The value of semi-span used is 40 m/131 ft; the wheel height is 7.3 m/24 ft.
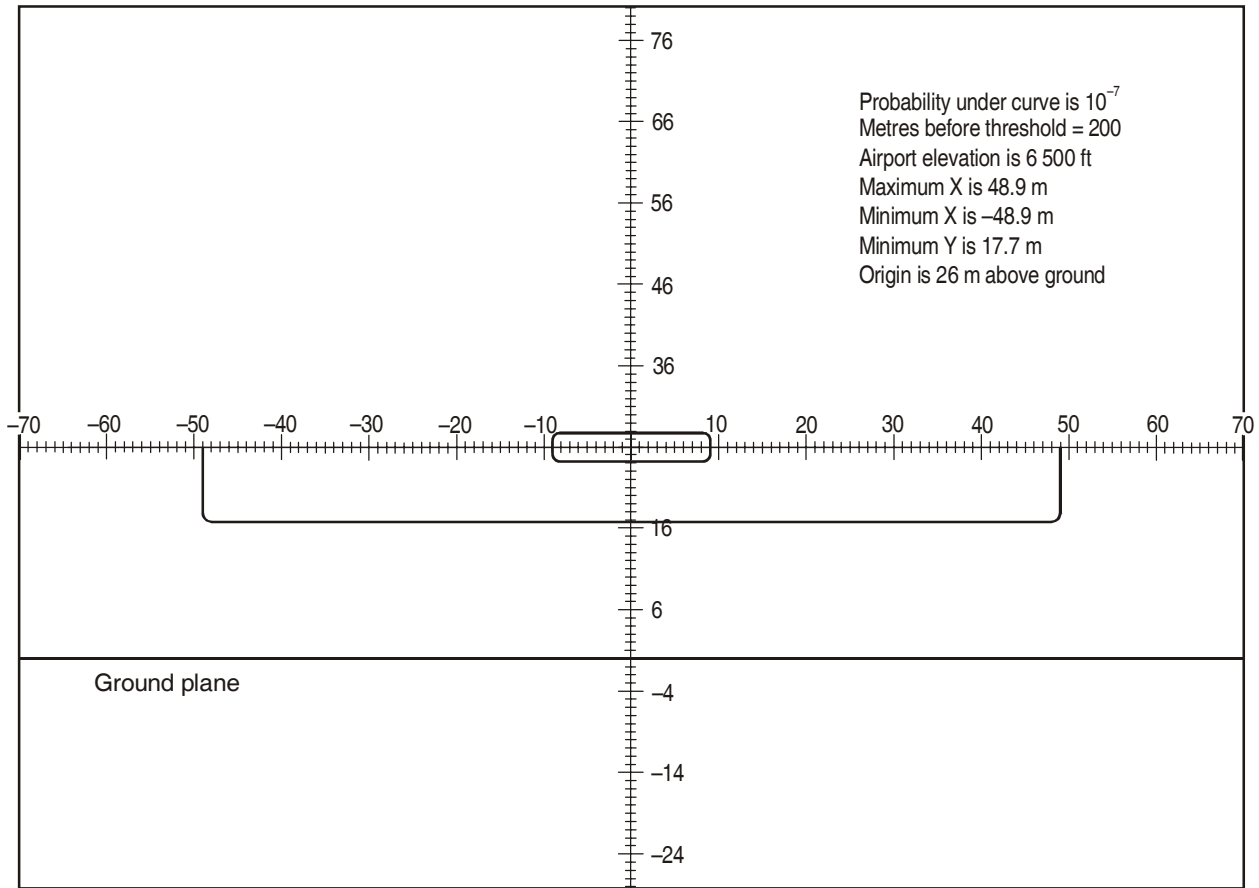
Figure 6-6G.   200 m before threshold at elevation of 6 500 ft

The oval-shaped curve is the curve that encloses the centre of gravity of the aircraft. The lower curve is the lower half of the oval curve corrected for semi-span and wheel height of the aircraft. The value of semi-span used is 40 m/131 ft; the wheel height is 7.3 m/24 ft.
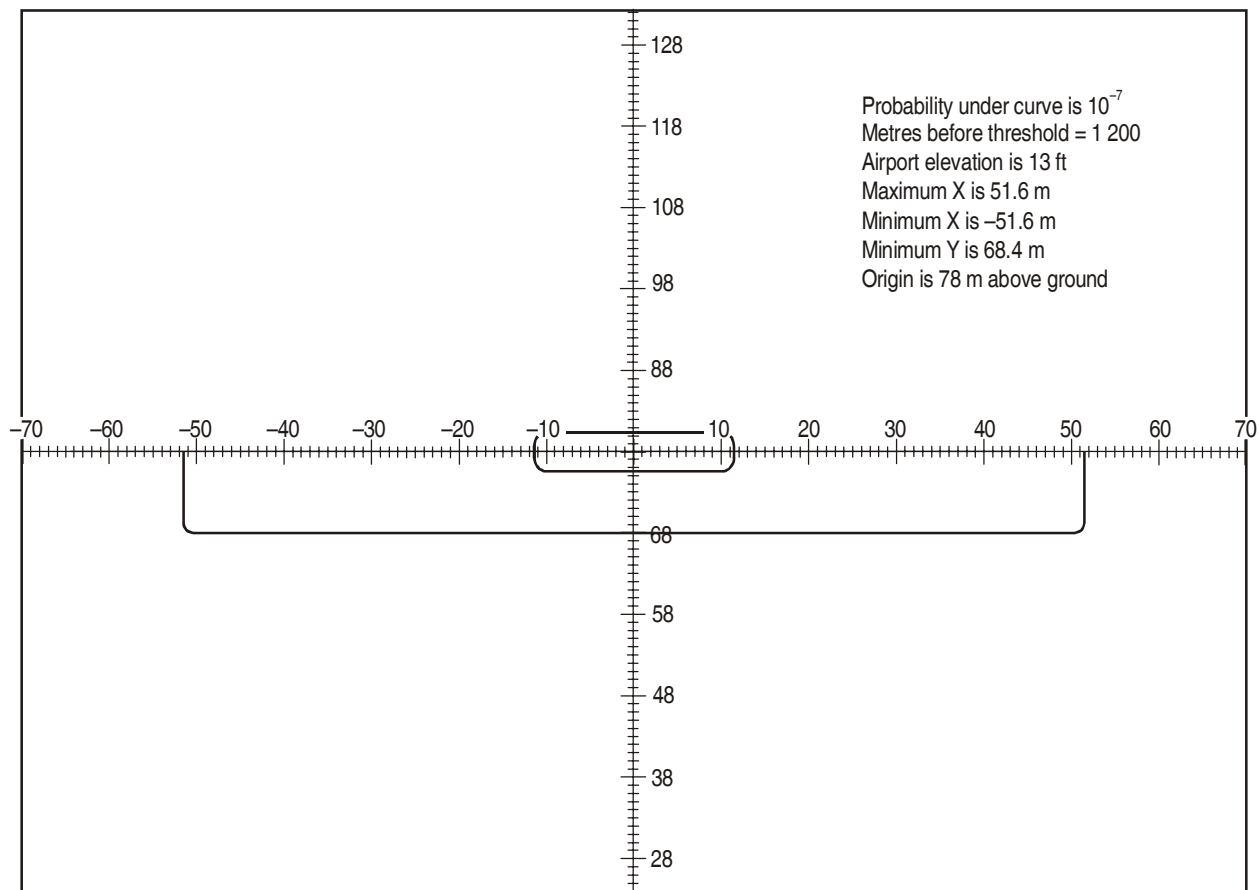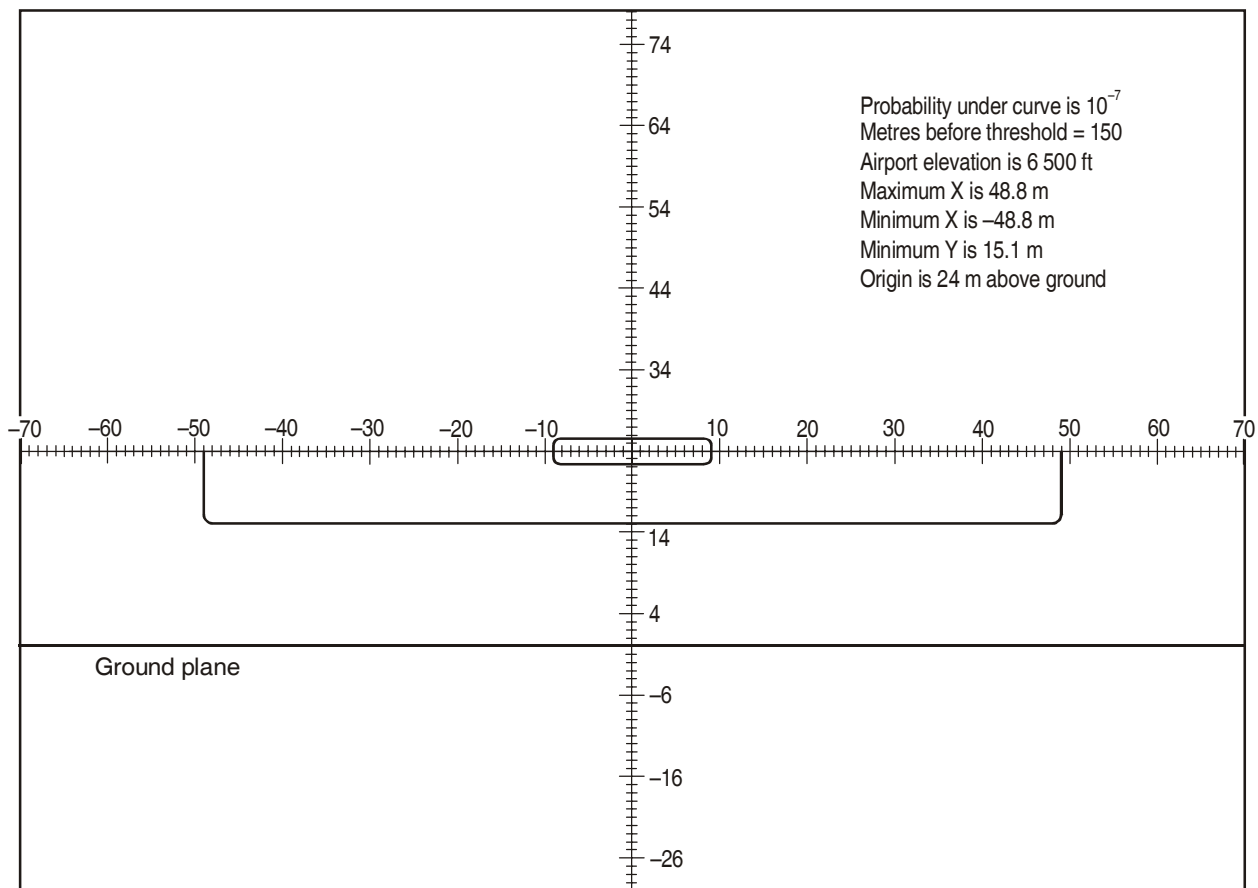
Figure 6-6H. 150 m before threshold at elevation of 6 500 ft

The oval-shaped curve is the curve that encloses the centre of gravity of the aircraft. The lower curve is the lower half of the oval curve corrected for semi-span and wheel height of the aircraft. The value of semi-span used is 40 m/131 ft; the wheel height is 7.3 m/24 ft.
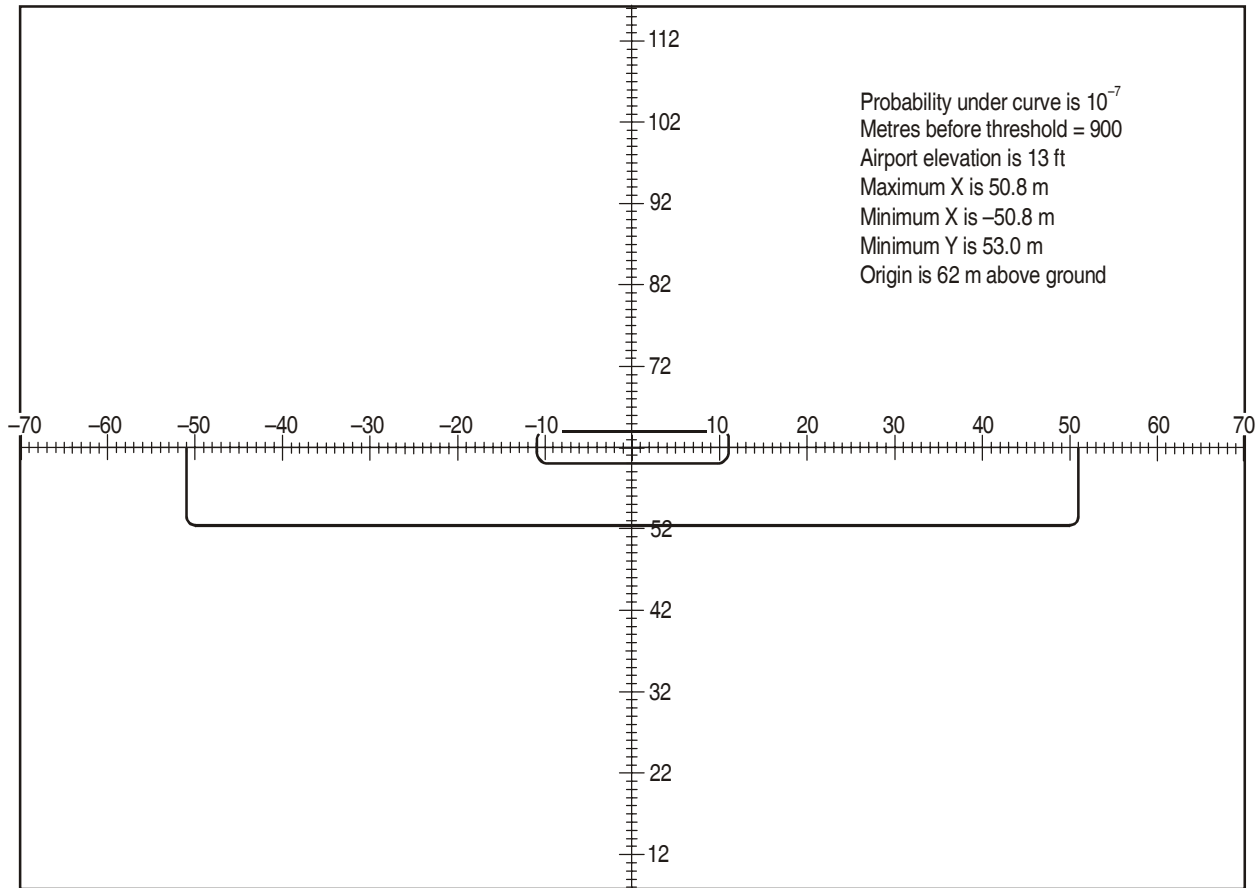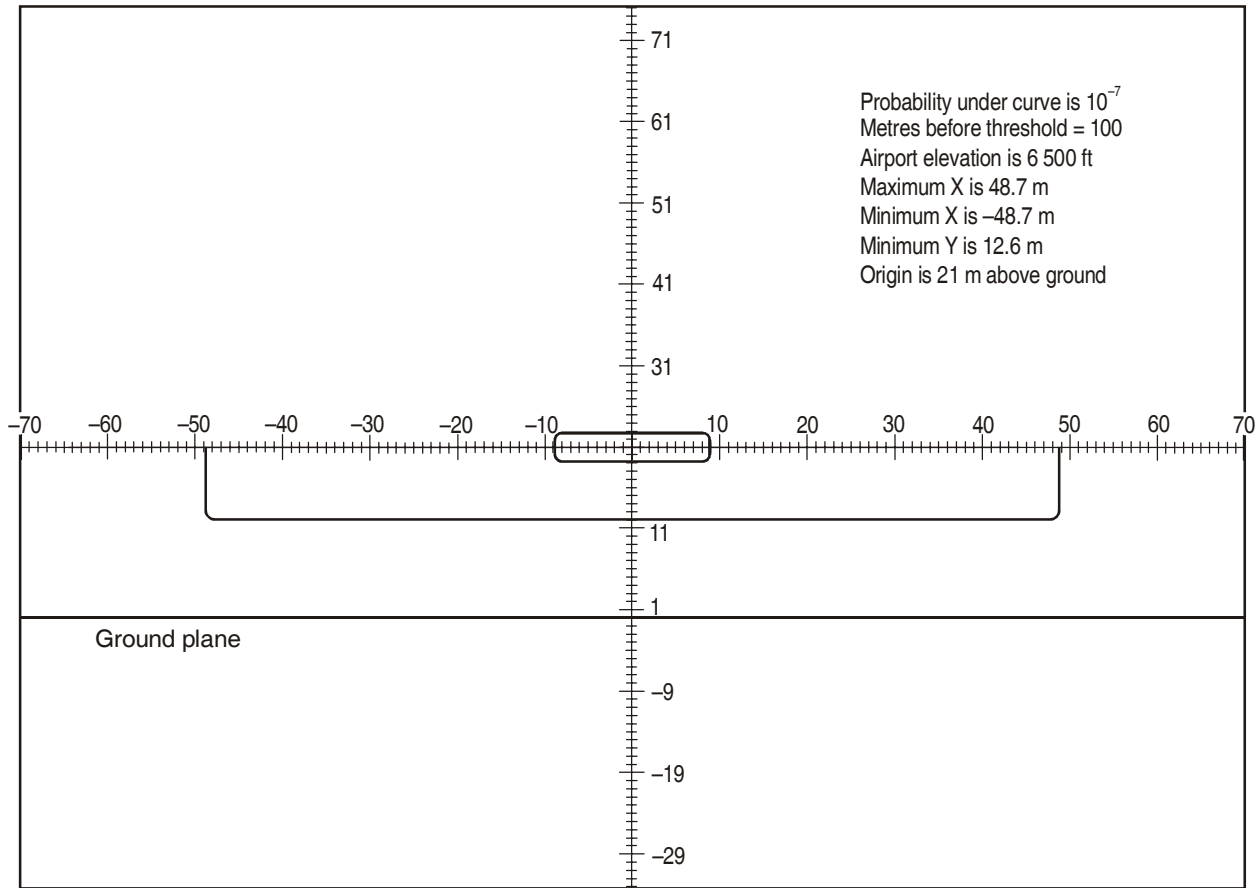
Figure 6-6I.   100 m before threshold at elevation of 6 500 ft

The oval-shaped curve is the curve that encloses the centre of gravity of the aircraft. The lower curve is the lower half of the oval curve corrected for semi-span and wheel height of the aircraft. The value of semi-span used is 40 m/131 ft; the wheel height is 7.3 m/24 ft.
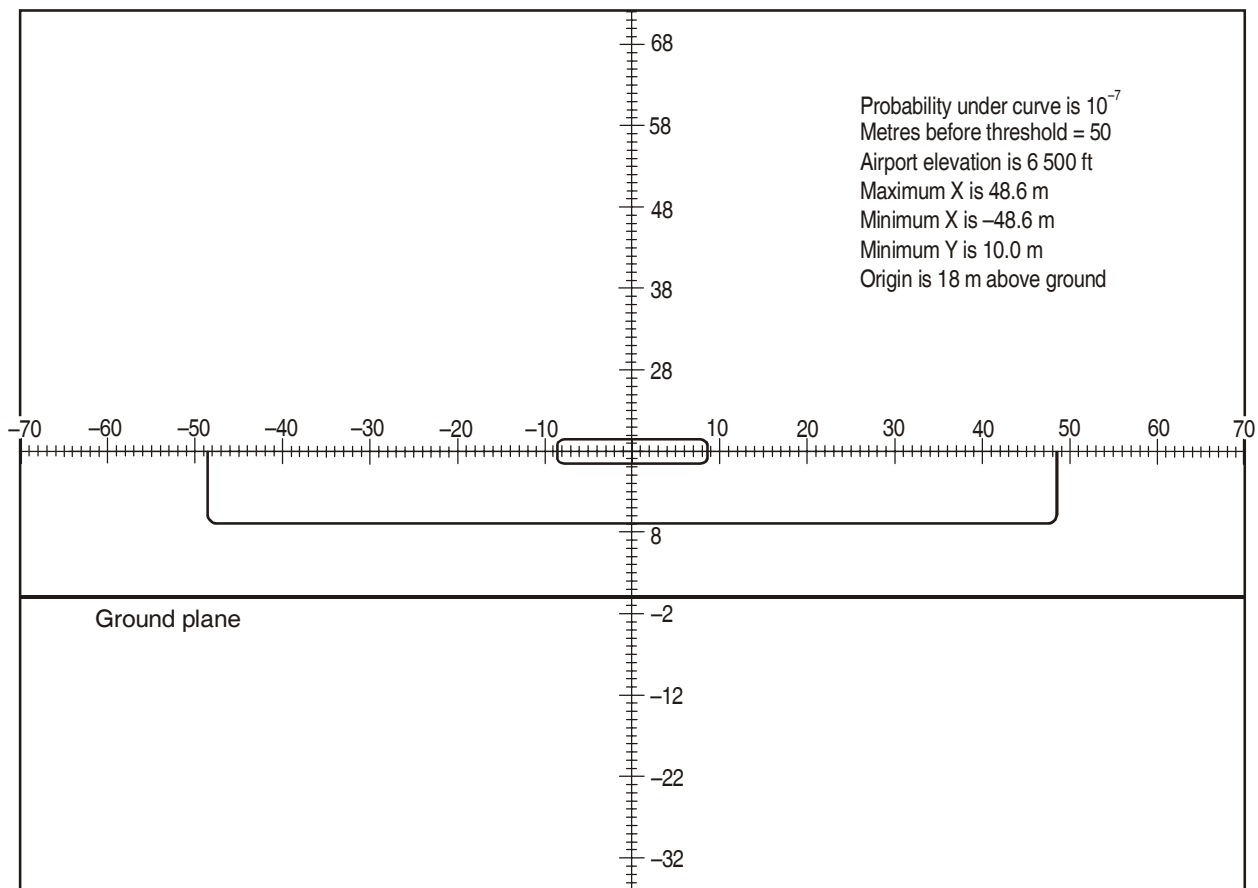
Figure 6-6J.   50 m before threshold at elevation of 6 500 ft

The oval-shaped curve is the curve that encloses the centre of gravity of the aircraft. The lower curve is the lower half of the oval curve corrected for semi-span and wheel height of the aircraft. The value of semi-span used is 40 m/131 ft; the wheel height is 7.3 m/24 ft.
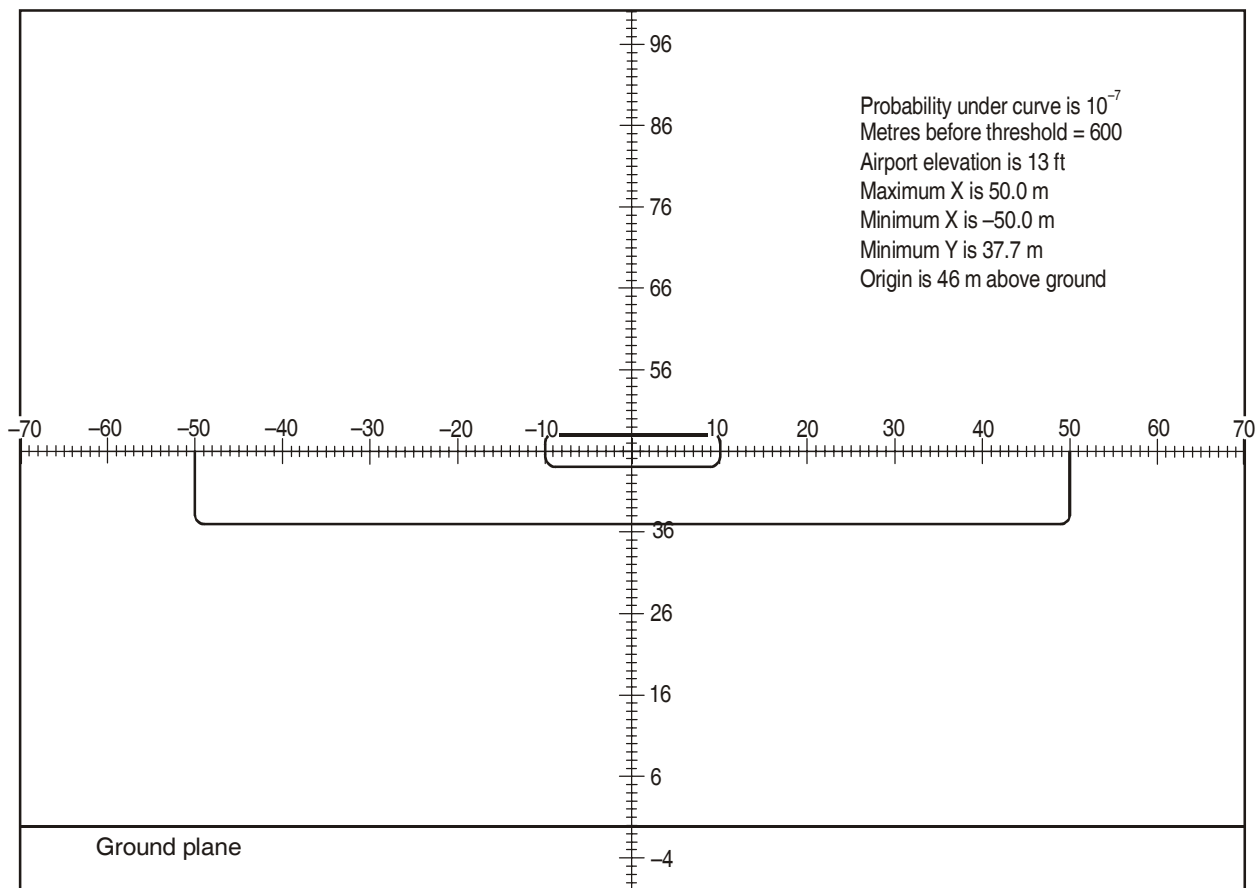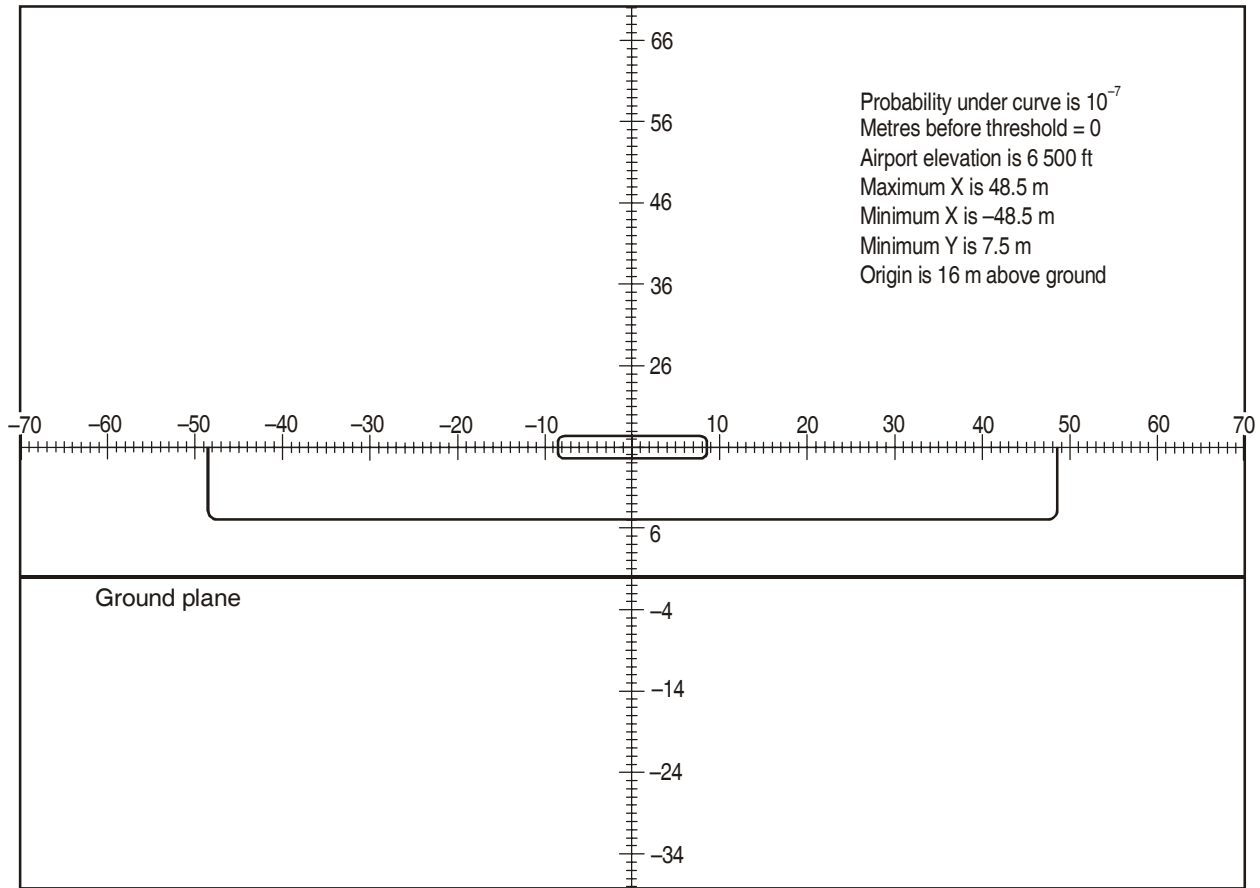
Figure 6-6K. 0 m before threshold at elevation of 6 500 ft

The oval-shaped curve is the curve that encloses the centre of gravity of the aircraft. The lower curve is the lower half of the oval curve corrected for semi-span and wheel height of the aircraft. The value of semi-span used is 40 m/131 ft; the wheel height is 7.3 m/24 ft.

Probability under curve is 10^{-7}
Metres after threshold = 50
Airport elevation is 6 500 ft
Maximum X is 48.4 m
Minimum X is –48.4 m
Minimum Y is 5.2 m
Origin is 13 m above ground

Ground plane
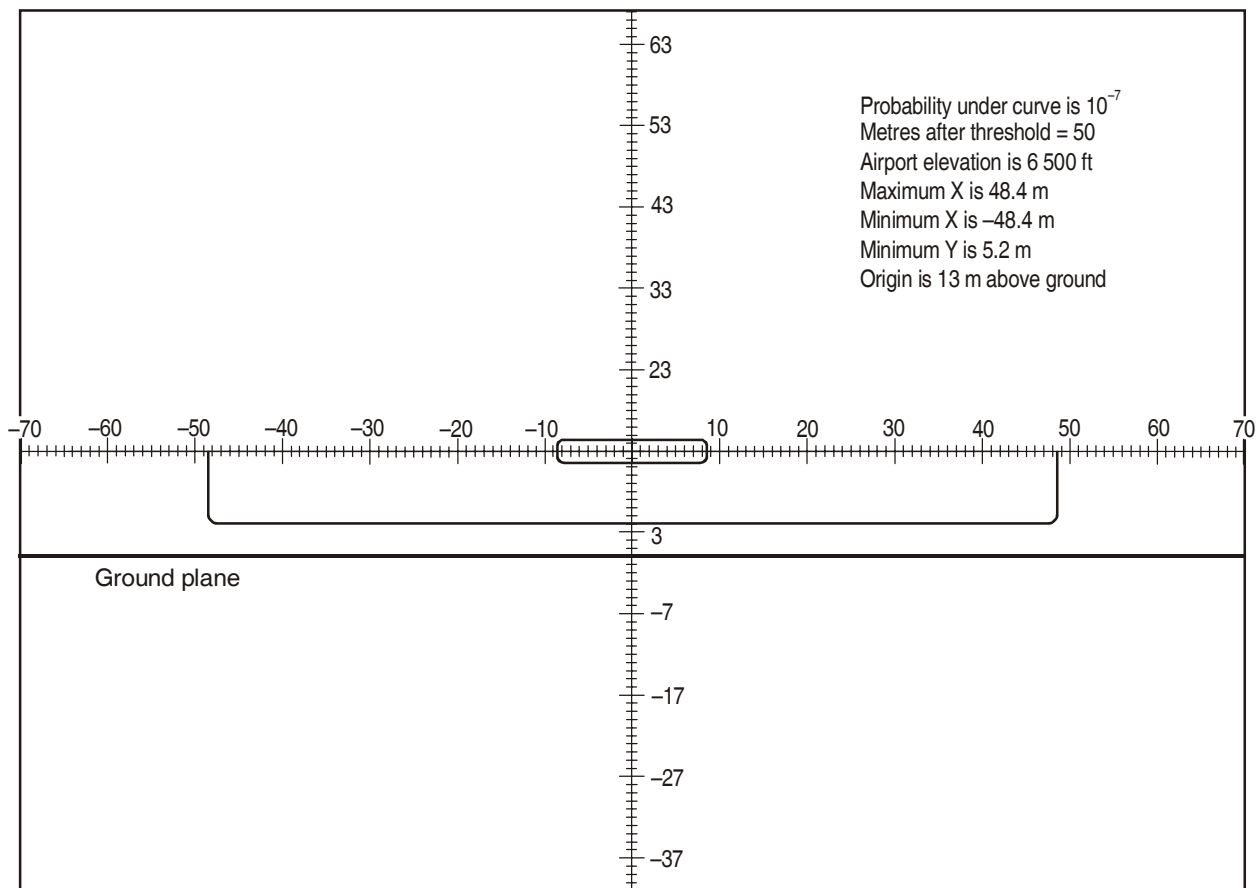
Figure 6-6L.   50 m after threshold at elevation of 6 500 ft

The oval-shaped curve is the curve that encloses the centre of gravity of the aircraft. The lower curve is the lower half of the oval curve corrected for semi-span and wheel height of the aircraft. The value of semi-span used is 40 m/131 ft; the wheel height is 7.3 m/24 ft.
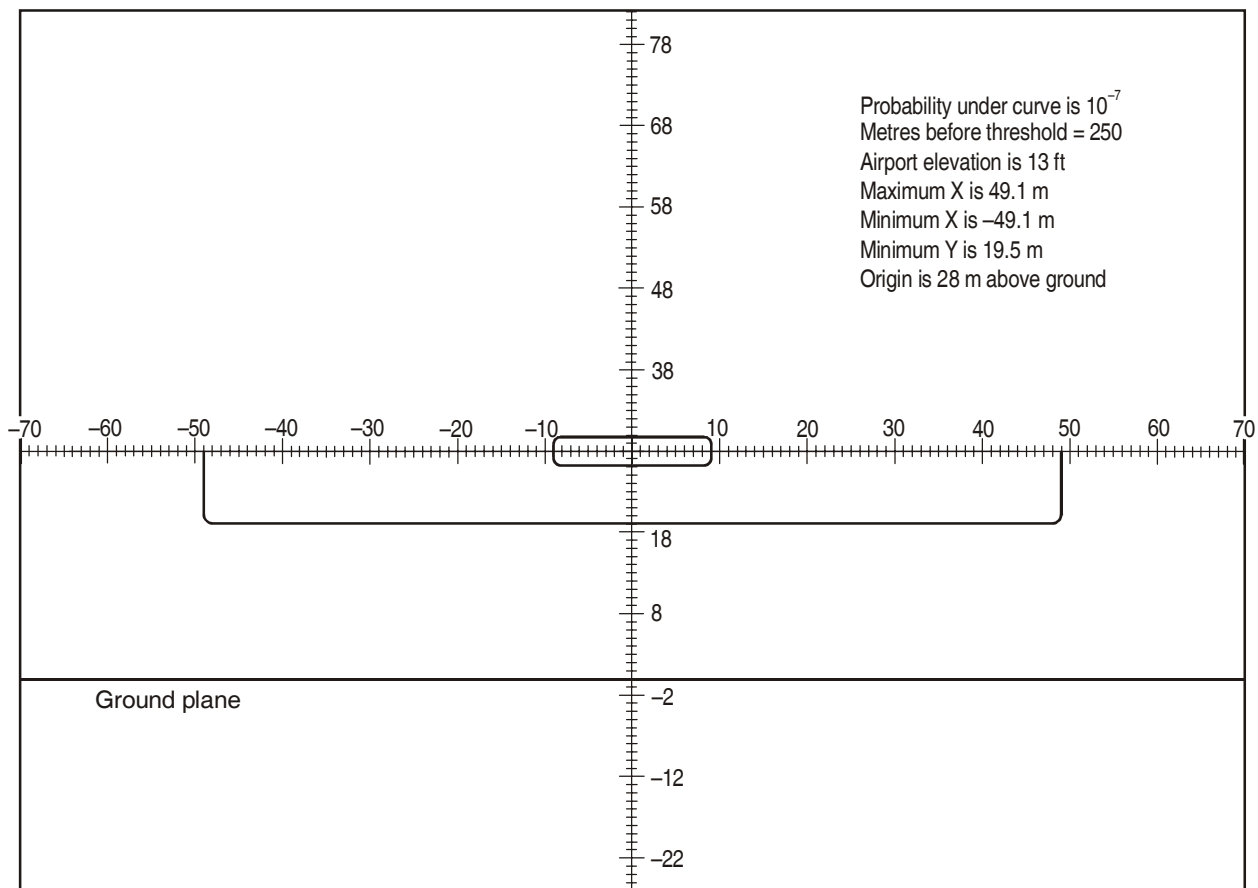
Probability under curve is 10^{-7}
Metres after threshold = 100
Airport elevation is 6 500 ft
Maximum X is 48.3 m
Minimum X is –48.3 m
Minimum Y is 3.2 m
Origin is 11 m above ground

Ground plane
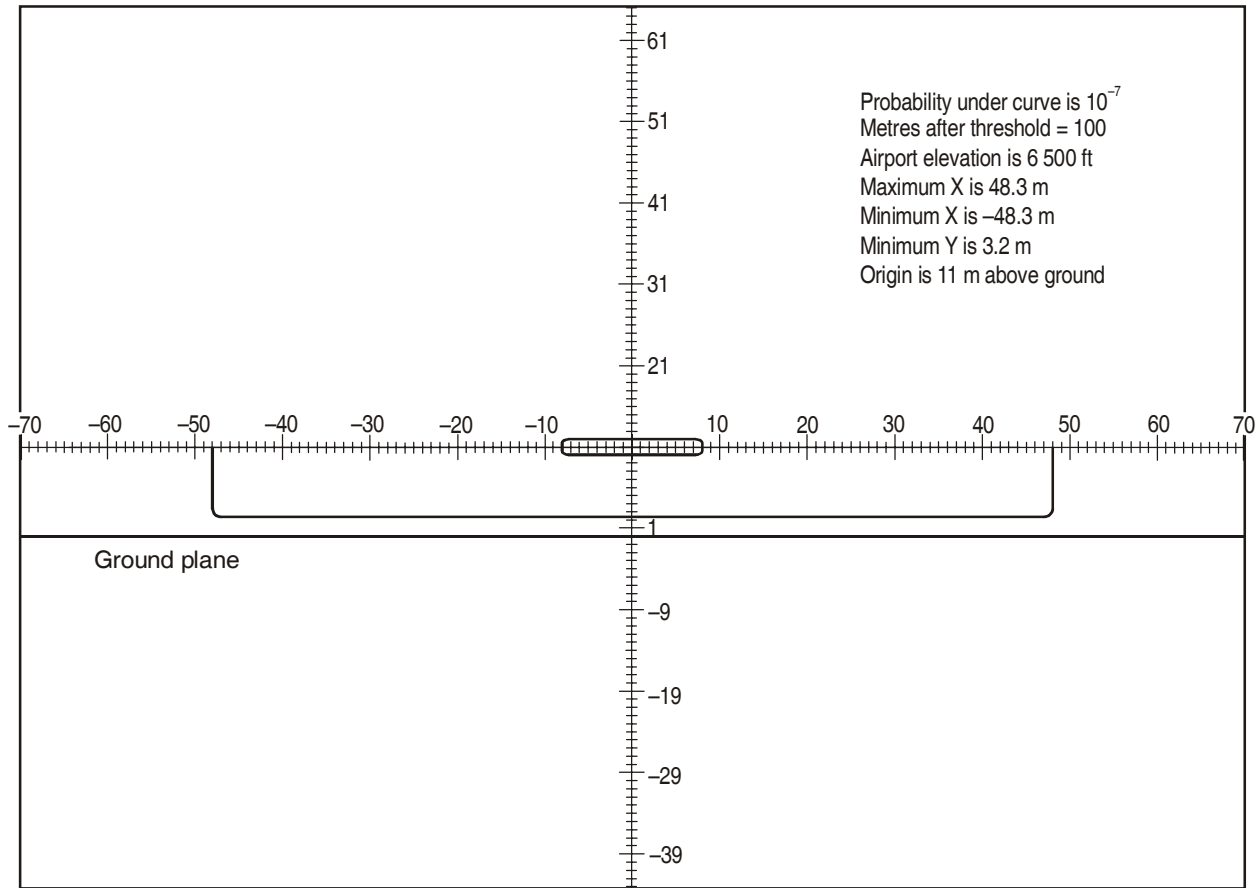
Figure 6-6M.   100 m after threshold at elevation of 6 500 ft

The oval-shaped curve is the curve that encloses the centre of gravity of the aircraft. The lower curve is the lower half of the oval curve corrected for semi-span and wheel height of the aircraft. The value of semi-span used is 40 m/131 ft; the wheel height is 7.3 m/24 ft.

Probability under curve is 10^{-7}
Metres after threshold = 150
Airport elevation is 6 500 ft
Maximum X is 48.2 m
Minimum X is –48.2 m
Minimum Y is 1.6 m
Origin is 9 m above ground

Ground plane
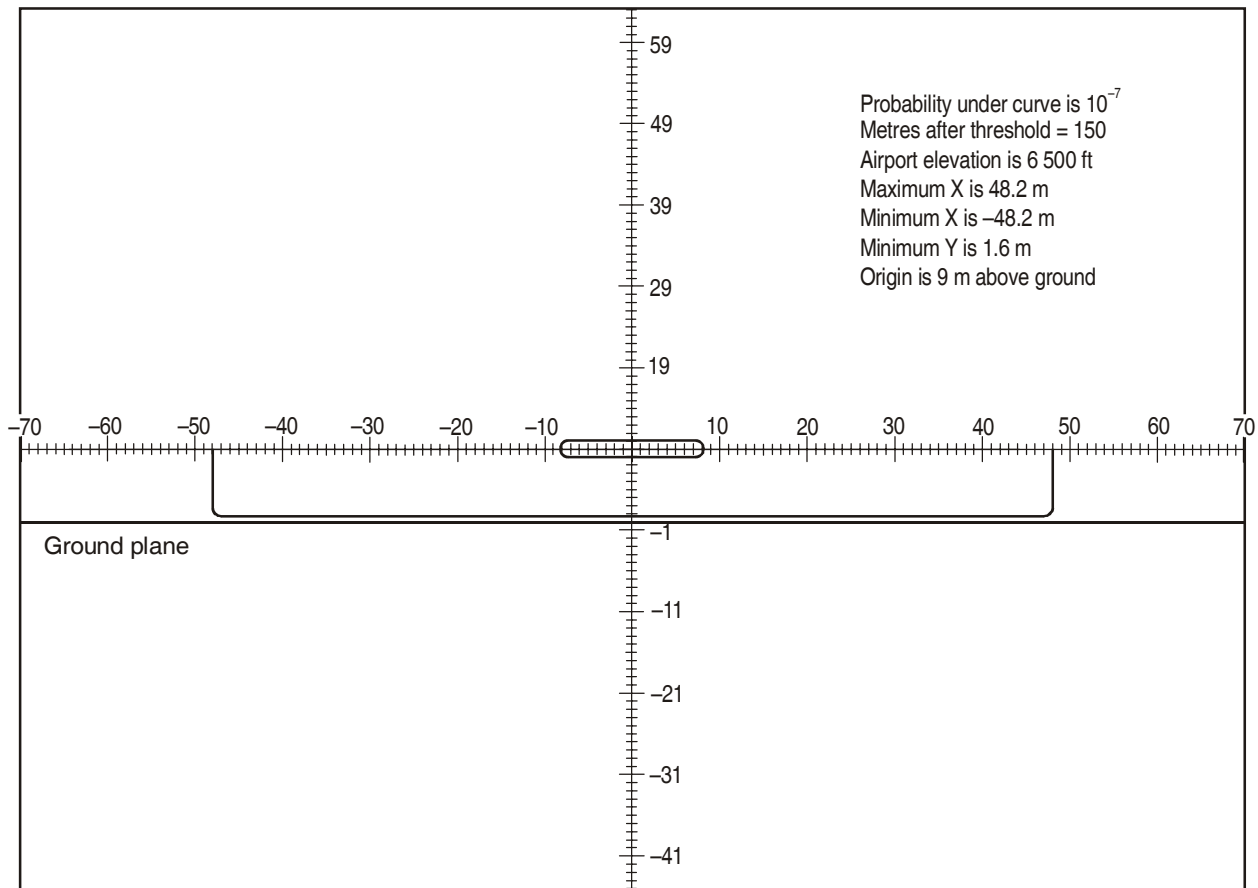
Figure 6-6N.   150 m after threshold at elevation of 6 500 ft

The oval-shaped curve is the curve that encloses the centre of gravity of the aircraft. The lower curve is the lower half of the oval curve corrected for semi-span and wheel height of the aircraft. The value of semi-span used is 40 m/131 ft; the wheel height is 7.3 m/24 ft.
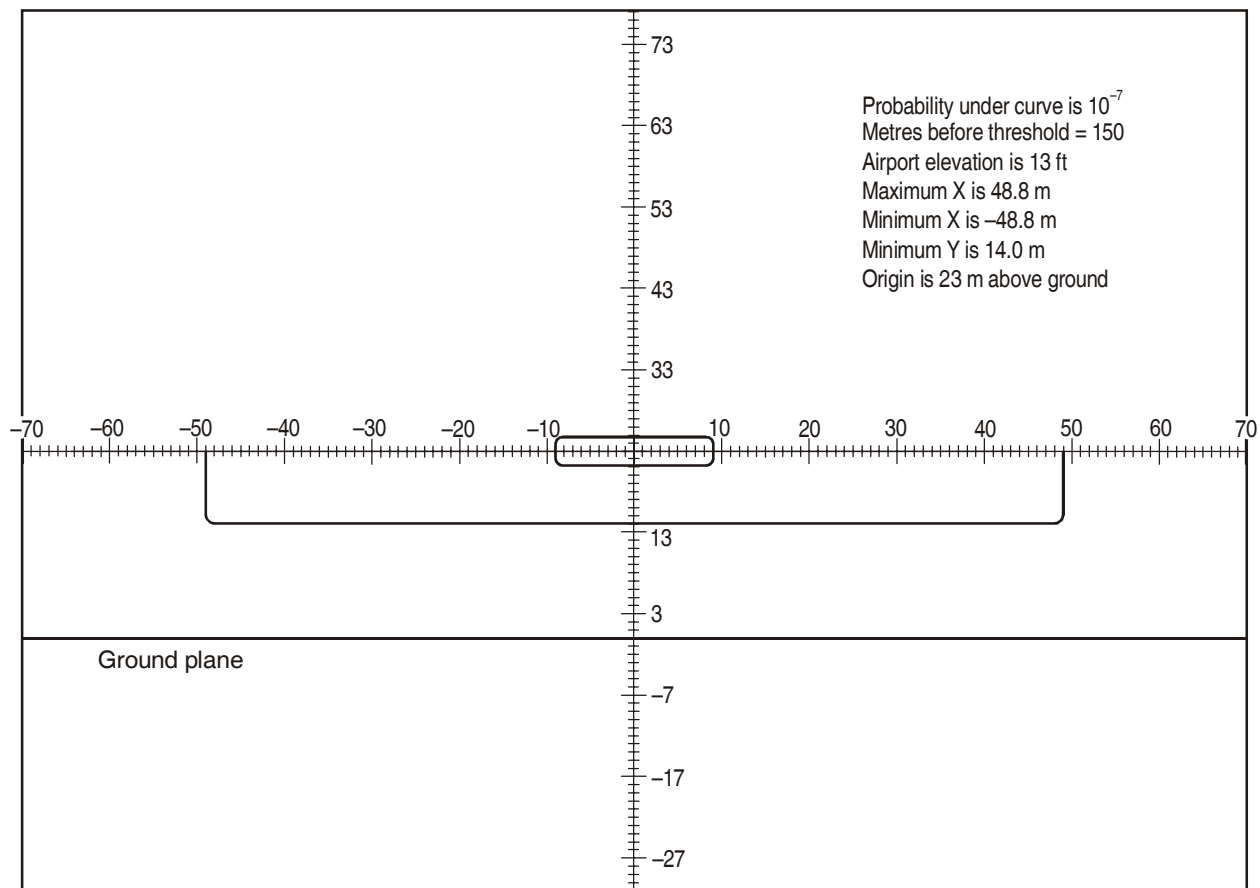
Figure 6-6O.   200 m after threshold at elevation of 6 500 ft

The oval-shaped curve is the curve that encloses the centre of gravity of the aircraft. The lower curve is the lower half of the oval curve corrected for semi-span and wheel height of the aircraft. The value of semi-span used is 40 m/131 ft; the wheel height is 7.3 m/24 ft.
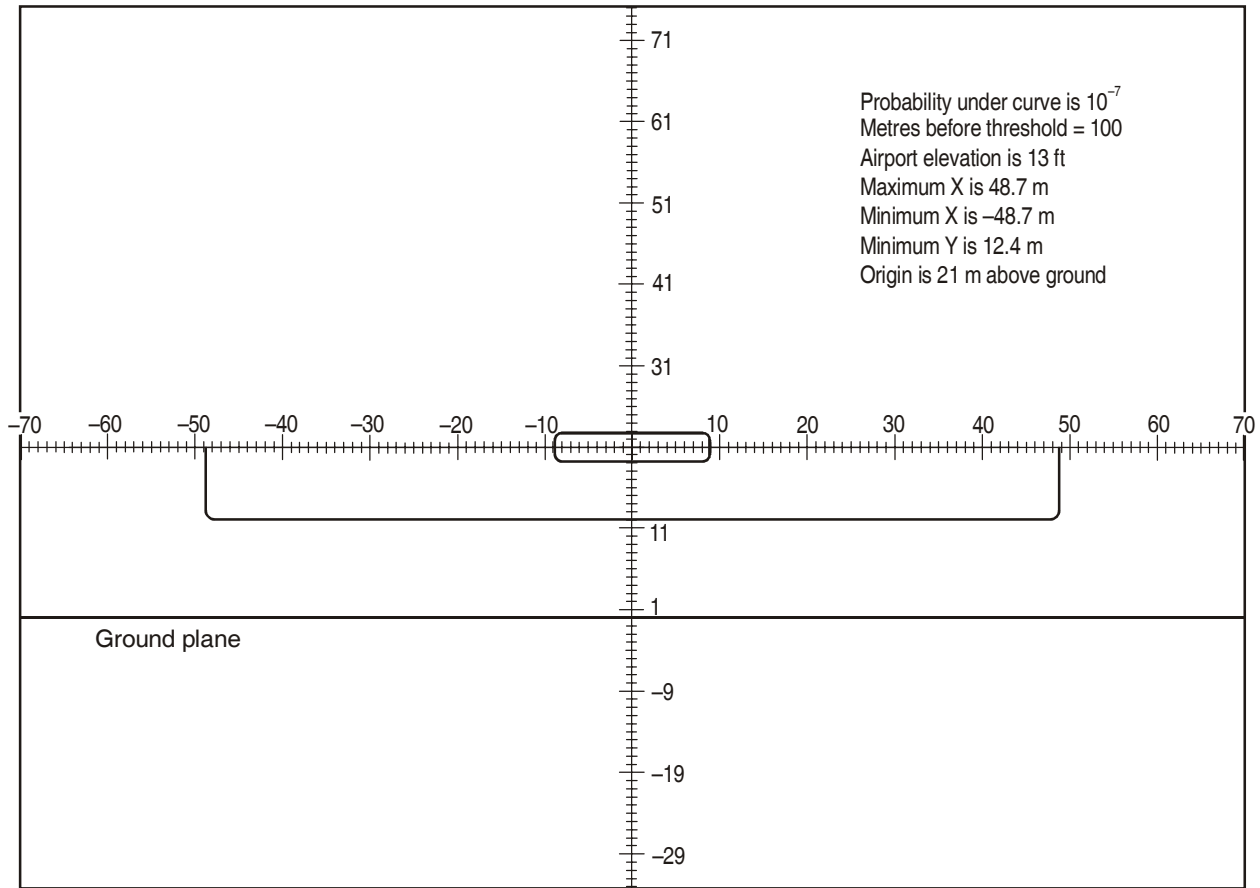
Probability under curve is 10^{-7}
Metres after threshold = 250
Airport elevation is 6 500 ft
Maximum X is 48.1 m
Minimum X is –48.1 m
Minimum Y is –1.6 m
Origin is 8 m above ground

Ground plane
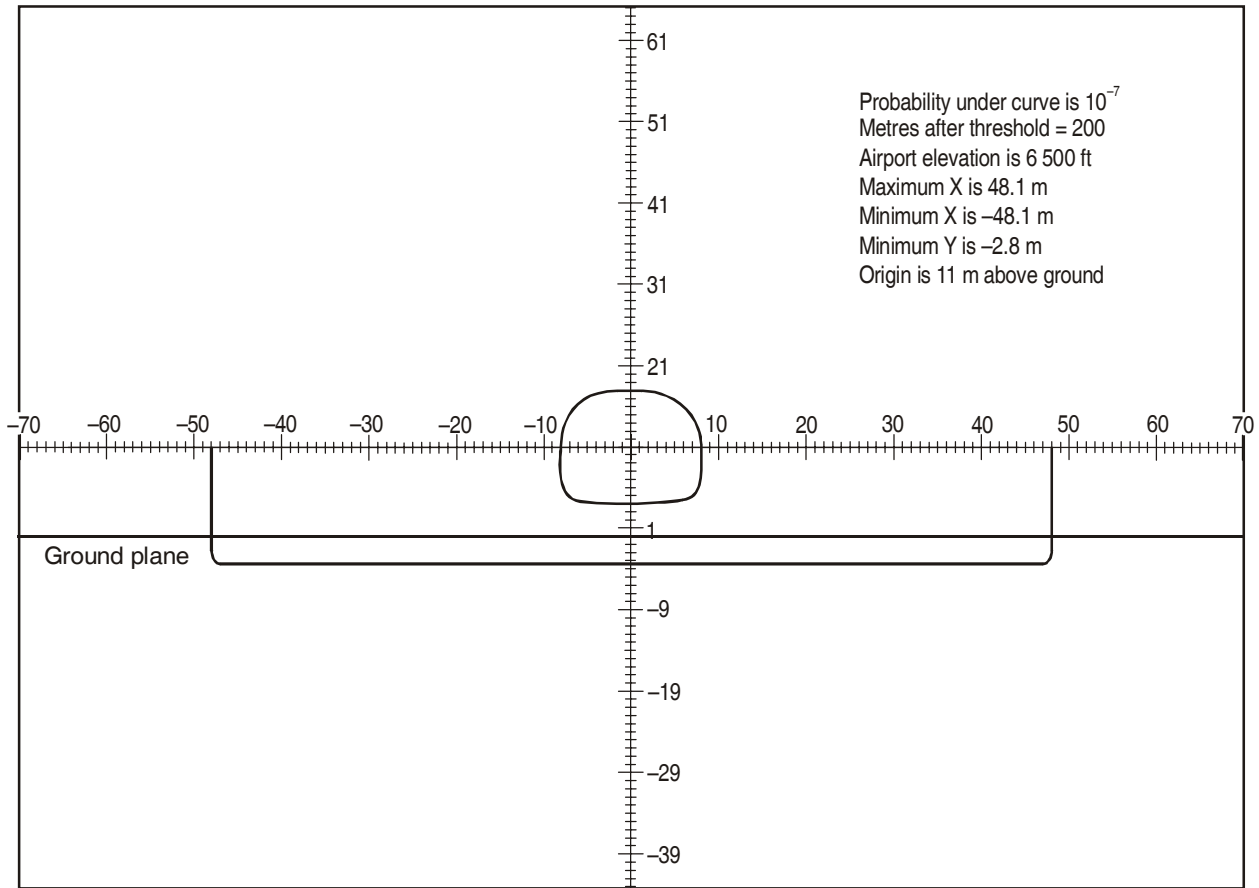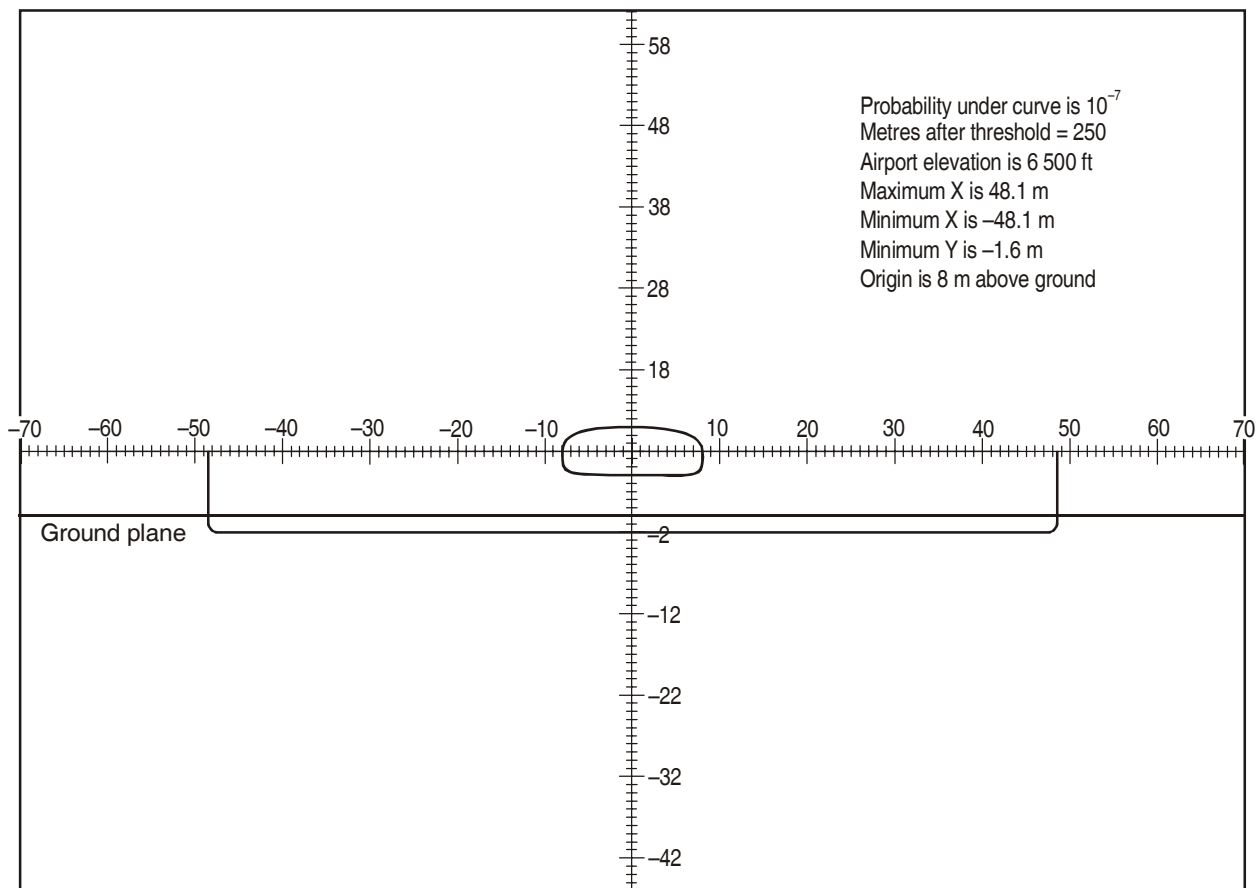
Figure 6-6P.   250 m after threshold at elevation of 6 500 ft

The oval-shaped curve is the curve that encloses the centre of gravity of the aircraft. The lower curve is the lower half of the oval curve corrected for semi-span and wheel height of the aircraft. The value of semi-span used is 40 m/131 ft; the wheel height is 7.3 m/24 ft.
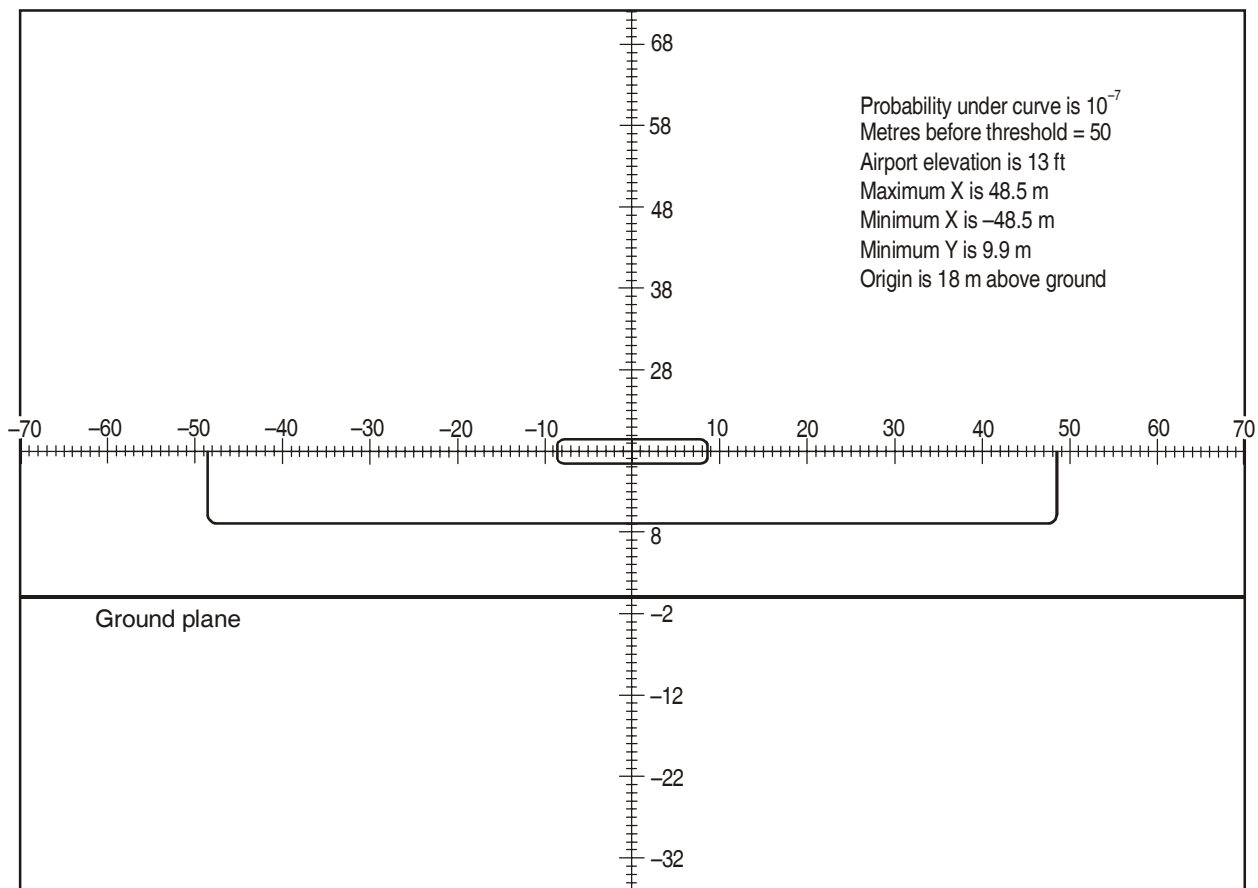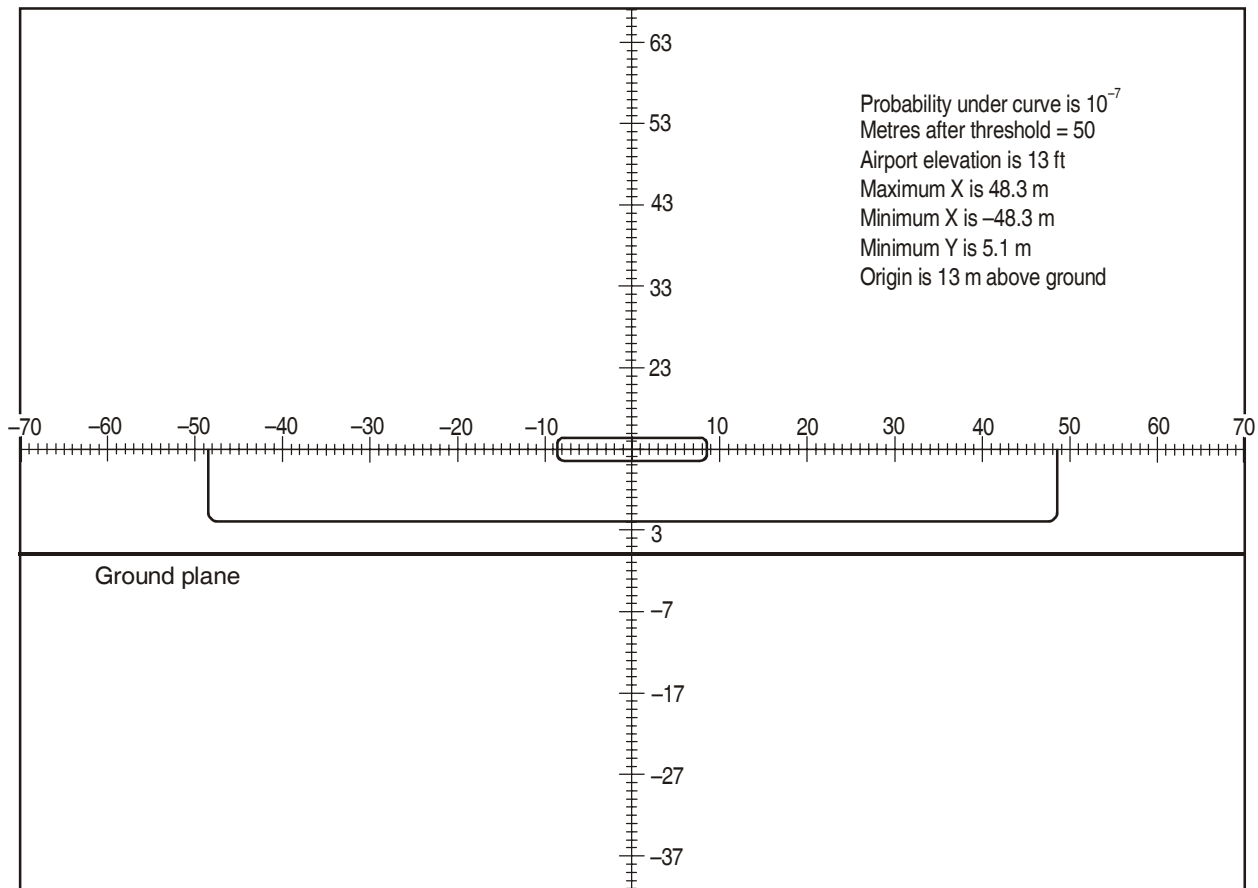
— — — — — — — —

Appendix to Chapter 6
A340-300/NLA VALIDATION OF
AUTOPILOT SIMULATIONS

INTRODUCTION

The NASA-AMES trials and the ASAT simulations that have been detailed in Part II, Chapter 6, found that the Code E OFZ surfaces would be suitable for a NLA conducting a balked landing with the autopilot engaged.

It was assumed that any future NLA with a modern autopilot would have similar or better performance to the 747-400 on which the initial autoland study was based. Therefore this finding could be read across to other NLAs that were not developed from the 747-400.

Despite this assumption, the OCP felt it was necessary to run some validation trials for the NLA in production to validate this finding. Consequently, a number of autocoupled balked landings were performed using A340-300 simulators, which were considered representative.

DESCRIPTION OF THE TESTS

A series of A340-300 simulator autoland trials took place during 2004 in Toulouse on 3 April and in Berlin from 24 August to 3 September. All scenarios involved low balked landings with limiting category II conditions of visibility and crosswind.

At Berlin, 127 autocoupled approaches were flown, out of which 87 resulted in the execution of a balked landing. Given the smaller size of the Toulouse sample, this appendix will focus only on the Berlin trials even though both trials had similar results.

Details of the Toulouse and Berlin sessions may be found in Part II, Chapter 3.

**Table 6-A-1.   Distribution of autocoupled and
flight director approaches at Berlin**

	Berlin trials
Autocoupled approaches	127
Flight director approaches	229
Total	356

RESULTS

In the analysis, the NLA was assumed to have a total span of 80 m as was used in the ASAT simulation study. Furthermore, consistent to the analysis of the flight director balked landing runs (Part II, Chapter 7), the lateral deviation data collected at the simulator was transformed to the non-dimensional variable s. The variable (s) was defined whose value was the percentage of lateral deviation of the wing tip from its position when the aircraft is on centre line to that when it touches the Code E inner transitional surface. The value of $s = 0$ occurred when the aeroplane was on the runway centre line, and that of $s = 100$, when the NLA wing tip touched the Code E OFZ (itself a function of wing-tip height). If the wing tip were exactly half way between nominal position and the surface, the value of s would be $s = 50$.

For each autoland run, the maximum s below 45 m height during the balked landings was calculated. The average and standard deviations are shown in Table 6-A-2.

In the trials, the aeroplane centre of gravity lateral deviations at the points that gave the largest value of s were all contained within ±12 ft (3.7 m) each side of the runway centre line.

Additionally, the equivalent NLA wing-tip position was plotted against the OFZ surfaces. Figures 6-A-1 through 6-A-3 are frontal views of representative balked landings with the autopilot engaged under high crosswind conditions. The wing-tip lateral position is plotted from 1 000 ft (CG height) in the approach until the aircraft reached 600 ft (CG height) in the climb-out. There are two slopes at each side; the inner one represents the Code E OFZ and the outer one the Code F OFZ.

Inspection of the plots showed that a considerable margin exists between the NLA wing tip and the Code E OFZ.

Earlier evaluations of the Airbus autopilot performance included examination of proprietary performance data by the FAA in 1999. The data provided supported the assumption that the Airbus autopilot performance was at least as good as the Boeing autopilot performance.

CONCLUSIONS

The above results support the assumption that for an NLA with an autopilot based on the A340-300 technology, the previous finding quoted in section 6.5 of Chapter 6 is applicable.

Compared to the balked landings under flight director, the autocoupled balked landings showed superior tracking accuracy.

**Table 6-A-2.   Maximum deviation of *s* below 150 ft
during the balked landings**

	Average (%)	*Std. Dev. (%)*	*Count*
Berlin autocoupled balked landings	4.01	0.81	87

— — — — — — — —
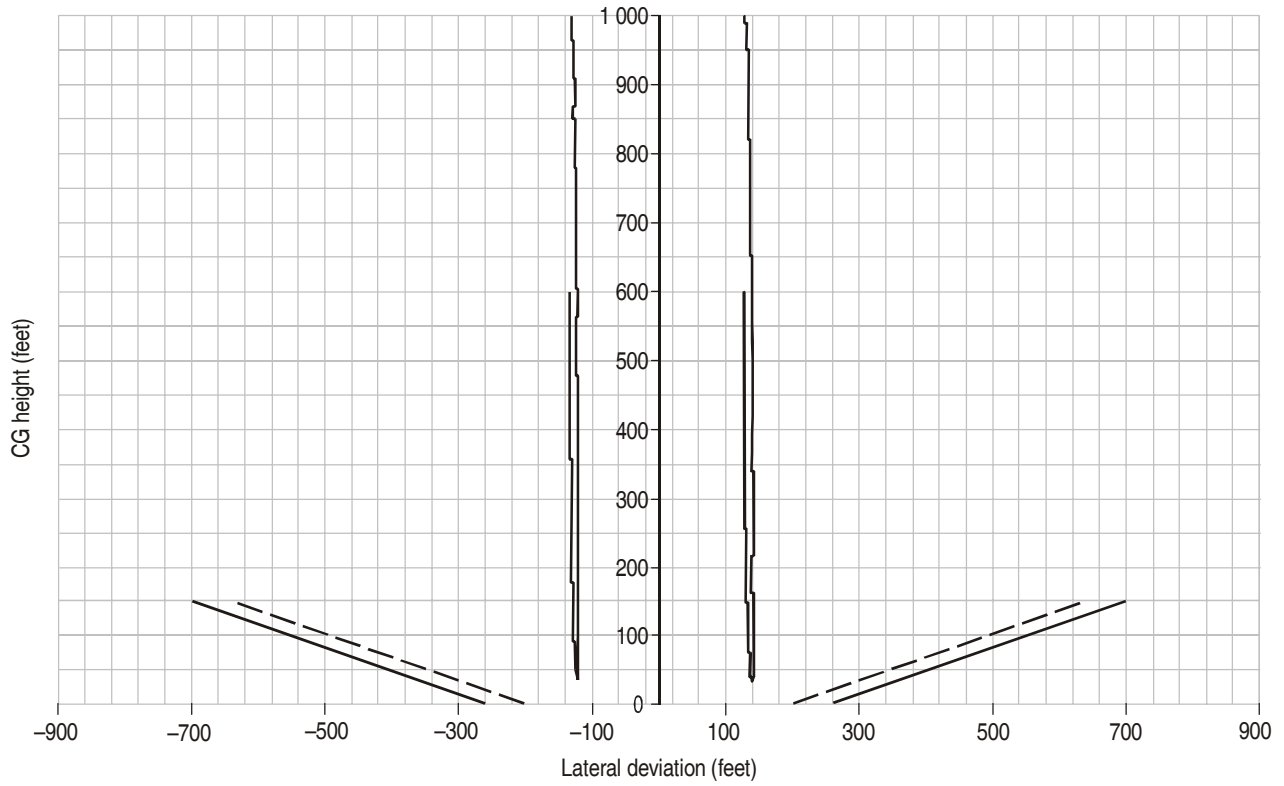
**Figure 6-A-1.   NLA wing-tip positions during an autocoupled balked landing
(Scenario #24, 27 August 2004)**
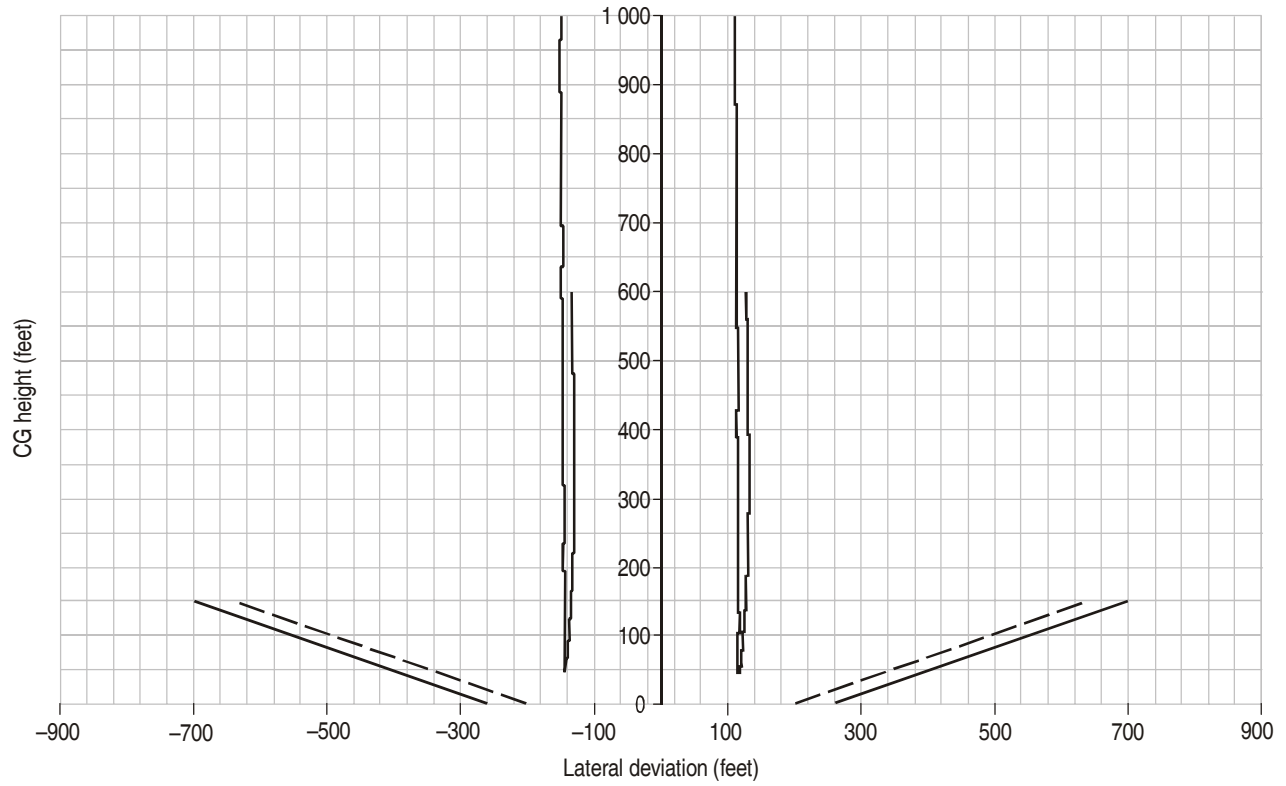
**Figure 6-A-2.   NLA wing-tip positions during an autocoupled balked landing
(Scenario #28, 30 August 2004)**
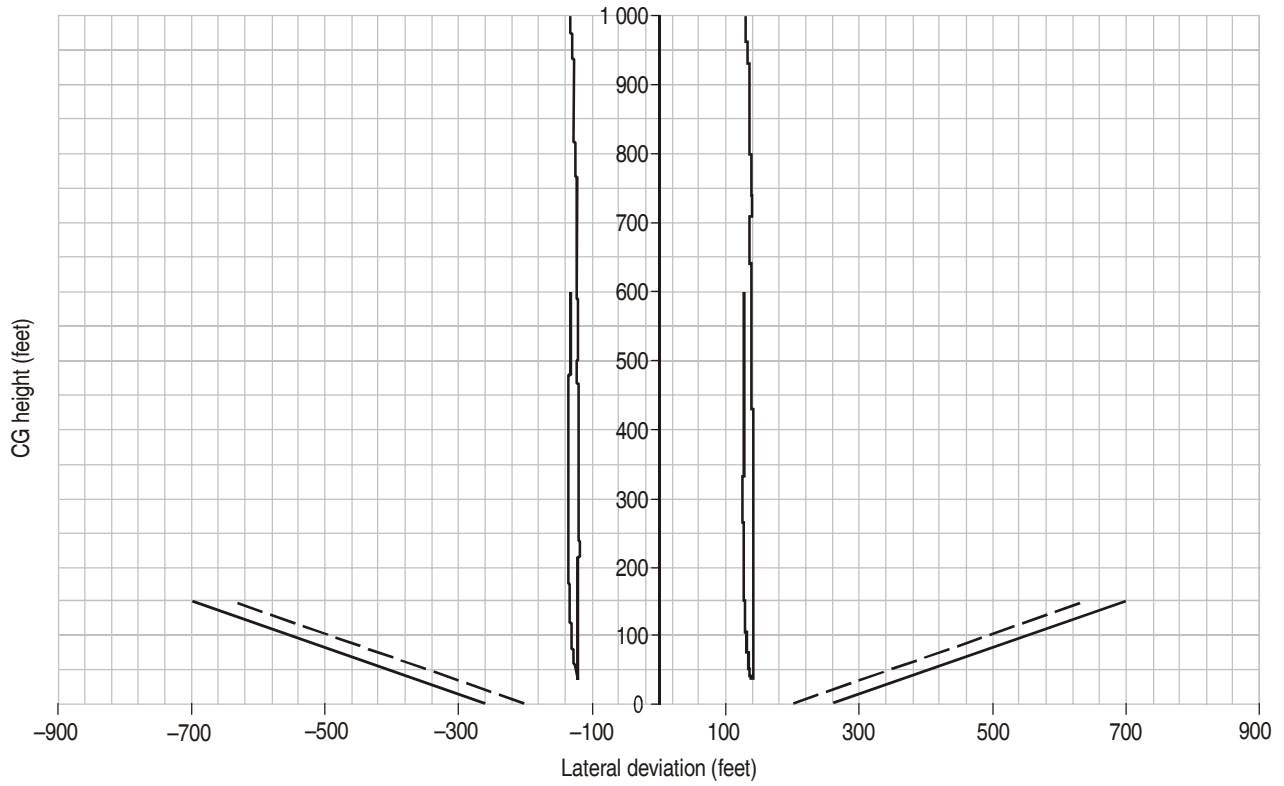
**Figure 6-A-3.   NLA wing-tip positions during an autocoupled balked landing
(Scenario #24, 31 August 2004)**

_____

Chapter 7
EXTREME VALUE ANALYSIS (EVA)
OF FLIGHT SIMULATOR DATA

7.1 INTRODUCTION

7.1.1　　　　For the flight director case, a model of the piloted flight director performance was not available for ASAT computer simulation and an alternative process was necessary. It consisted of statistical analysis using Extreme Value Analysis Techniques of flight simulator data to evaluate the risk of infringement on the Code E OFZ. Data collected from the flight simulator tests discussed in Chapter 3 were taken as representative of the expected NLA performance once appropriate scaling was applied to the wing span and wheel height.

7.1.2　　　　To ensure that severe conditions for balked landings were suitably investigated, the simulator tests were focused on high crosswind conditions and balked landings initiated at very low altitudes. As these were relatively low probability events, the resultant data were not optimal for conventional techniques and standard statistical analyses. Extreme Value Analysis (EVA) is particularly applicable in determining maximum value behaviour given appropriate sampling.

7.1.3　　　　The first step of the analysis was the identification of an appropriate metric. The obvious choice, distance from centre line, was not appropriate. The OFZ surface is sloped so that a deviation that would penetrate the OFZ at an altitude of 20 feet would not be significant at 120 feet. The larger deviations that occurred at higher altitudes, and were not a problem there, would "spread" the distribution and produce unacceptable risk figures at the lower altitudes. A dimensionless variable s was selected that represents the lateral margin between an NLA wing tip and the Code E OFZ boundary at the wing-tip height. The value of s was zero when the aeroplane was on the runway centre line, and was 100 when the NLA wing tip touched the Code E OFZ. The span selected was that of a Code F aeroplane (79.9 m).

7.1.4　　　　The flight simulator track data from each valid run was scanned and the largest s value identified. The resultant data were fitted to a Generalized Extreme Value (GEV) distribution and the relationship between the data and the GEV checked. Finally, the probability of an NLA wing tip infringing the OFZ boundary was estimated. The total probability per approach was determined by multiplying the above probability by the go-around rate and the probability allocated to the particular scenario. This process is discussed in considerably more detail in the rest of the chapter.

7.1.5　　　　The following two references in statistics, and their extensive bibliographies, may be consulted for technical details concerning the study of extreme value distributions: 1) *Statistics of Extremes* (2004) by Jan Beirlant, Yuri Goegebebeur, Johan Segers and Jozef Teugels; and 2) *An Introduction to Statistical Modeling of Extreme Values* (2001) by Stuart Coles.

7.2 EVA METHODOLOGY

7.2.1　　　　The central result of Extreme Value Theory is that under some general stabilizing conditions the distribution of sample maxima converges to one of three possible families of Extreme Value Distributions, regardless of the distribution of the underlying sampled population. These three families can

be combined into a single family of models called the generalized extreme value or GEV family. The three parameters characterizing each member of the GEV family are the location parameter μ, the scale parameter σ, and the shape parameter ξ. Depending on the value of the shape parameter, the GEV corresponds to one of the three extreme value distributions.

7.2.2   The form of the GEV distribution function is:

$$\text{GEV}(z) = \exp\left\{-\left[1+\xi\left(\frac{z-\mu}{\sigma}\right)\right]^{-1/\xi}\right\}$$

Defined on the set { z: 1+ ξ (z-μ)/σ >0}
where-∝<μ<∝, σ>0 and -∝<ξ<∝

The subcase ξ = 0 is interpreted as the limit of GEV(z) when ξ→0 leading to:

$$\text{GEV}(z) = \exp\left\{-\exp\left[-\left(\frac{z-\mu}{\sigma}\right)\right]\right\}, \quad \text{-∝<z<∝}$$

7.2.3   The following procedures were used to analyse the data:

a)   Since the Code E inner transitional surface is a sloping surface, the relationship between the NLA wing tip and the surface varies by height even if the wing tip does not deviate laterally. The ICAO Code E and Code F OFZs are depicted in Figure 7-1. For this reason, the measure of the distance from the wing tip to the OFZ surface is normalized.

b)   A variable (*s*) was defined whose value was the percentage of lateral deviation of the wing tip from its position when the aircraft is on centre line to that when it touches the Code E inner transitional surface. The value of *s* = 0 occurred when the aeroplane was on the runway centre line, and that of *s* = 100 when the NLA wing tip touched the Code E OFZ (itself a function of wing-tip height). If the wing tip were exactly halfway between nominal position and the surface, the value of *s* would be *s* = 50.

c)   The values for *s* for each data point were calculated along the aircraft's track ending when the aircraft's lower wing tip has exceeded the 45 metre height of the sloping inner transitional surface (where the surface becomes horizontal) on its balked landing ascent. The maximum *s* value for each of the balked landing runs was then determined and was again denoted by *s*.

d)   The transformed data points were next fitted to a GEV distribution. The three GEV distribution parameters (location μ, scale σ, and shape ξ) were estimated by means of maximum likelihood estimation involving numerical techniques. The quality of the GEV distribution fit was evaluated by displaying the relationship between the data and the fitted GEV by means of a probability plot and a histogram with an overlaid density plot. If the plots indicated that the distribution selected was a reasonable fit, the probability of *s* exceeding 100 (representing the NLA wing tip infringing the Code E OFZ) was calculated.

e)   Since the estimated probabilities determined were conditional based on the assumption that a balked landing had occurred, the risk analysis was completed by multiplying those probabilities by the probabilities of the balked landing occurring.
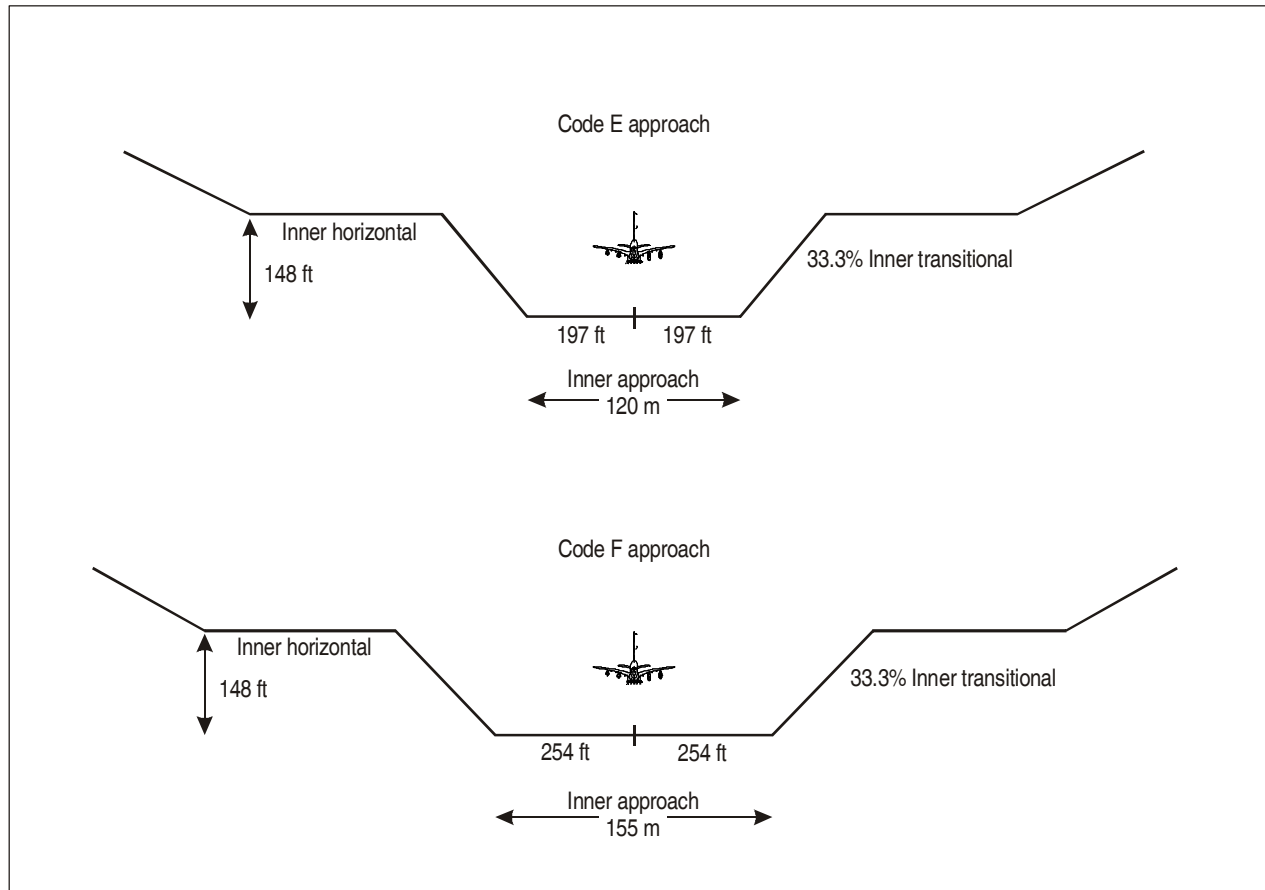
Figure 7-1.   ICAO Code E and Code F obstacle free zones

7.3   EVA FINDINGS

7.3.1   ZFB (Berlin) and Toulouse

7.3.1.1   In order to determine the probability of infringement with the Code E OFZ, a series of trials of the balked landing operation were performed using Airbus simulators in Toulouse and Berlin. These trials were designed to simulate the conditions of an A340/NLA balked landing operation as closely as possible. There were 156 operational runs in Toulouse and 356 runs in Berlin, all with qualified flight crews; the pilot flying was a line pilot. Of those 512 runs, 333 were hand-flown balked landing operations (the other 179 were either actual landings or autopilot operations). More details on the Berlin and Toulouse trials may be found in Part II, Chapter 3.

7.3.1.2   An EVA of the collected hand-flown data was performed following the methodology outlined in Section 7.2.

7.3.1.3   Reasons existed to believe that extreme crosswind conditions and very low balked landing initiation heights would increase the probability of OFZ infringement, so a disproportionate number of those cases were included in the test plan. This hypothesis was later confirmed by the results. The proportion of runs by crosswind speed and planned balked landing initiation height is indicated in Table 7-1.

**Table 7-1.   Proportion of simulator runs by crosswind
and balked landing initiation heights**

Initiation height (ft)	Crosswind (kt)						*Total*
	0	*10*	*18*	*21*	*23*	*25*	
10	4%	8%	13%	2%	0%	6%	34%
40	3%	9%	8%	2%	6%	6%	35%
70	3%	8%	11%	0%	6%	3%	31%
Total	10%	26%	32%	5%	12%	15%	100%

7.3.1.4   For analysis purposes, the variables of interest from the trials data for each run were: the maximum *s* value for the run (refer to 7.2.3 for details), the crosswind speed, and the planned height at which the balked landing was initiated. A table of these values for the 333 runs is included in Appendix 1 to this chapter.

7.3.1.5   Risk is the combination of:

      a)   the consequence (or severity) of a hazard event; and

      b)   the probability of its occurring within the case of interest.

7.3.1.6   The purpose of the present analysis was to determine the probability component of the risk of the hazard event: an A340/NLA wing tip infringing the ICAO Code E OFZ at least once during a case operation.

7.3.1.7   *Analysis Preliminaries.* Five *preliminary* hypotheses were evaluated before the analyses proper were undertaken:

      a)   It was confirmed that the Toulouse and Berlin data did not need to be analysed separately.

      b)   A conservative estimate for balked landings was established.

      c)   It was validated that higher crosswind speeds and lower balked landing initiation heights in fact affected the value of *s* as it had been supposed.

      d)   The crosswind speeds used in the trials were compared with typical representative crosswind speeds to establish that the crosswind speeds used in the trials were not representative.

      e)   The distribution of planned balked landing initiation heights used in the trials was compared with typical initiation heights to establish the fact that the trials initiation heights were not representative.

7.3.1.8   Hypotheses

Hypothesis 1: Toulouse and Berlin data should not be separated for analysis

Both a Kolmogorov-Smirnov test and a two-sample Chi-Square test were performed on the Toulouse and Berlin data to determine if they could be represented by the same distribution. The null hypothesis for each test was: the two sets of data represent the same distribution. The results of the two tests were consistent: each indicated that the null hypothesis should not be rejected; that is, there was no reason to separate the data for analysis since they appeared to represent a single distribution.

Hypothesis 2: The balked landing rate to use is less than the overall go-around rate of 1.9 per 1 000 landing attempts

Go-around rates available from five European airports and from Chicago O'Hare airport were compared (see Table 7-2). These rates are consistently around 1.9 go-arounds per 1 000 attempted landings. However, while every balked landing is a go-around, not all go-arounds are balked landings[1]. Since the data for actual balked landing rates were not available at the time the report was prepared, the go-around rate was used as an upper bound. Anecdotal information indicates that the balked landing rate may be on the order of one-tenth the go-around rate.

The upper bound go-around rate used in the analysis should be refined when more specific balked landing data become available from an airline flight operations quality assurance (FOQA) data collection process.

Table 7-2.   Go-around rates at European and U.S. airports

Airport	Year	Go-around rates		GA per approach	Approaches/GA
		Approaches	*GA*		
LFPG	2003	257 475	691	2.68E-03	373
LFPO	2003	103 248	150	1.45E-03	688
LEBL	2002	135 268	200	1.48E-03	676
LEBL	2003	140 275	237	1.69E-03	592
LEMD	2002	183 727	279	1.52E-03	659
LEMD	2003	189 173	369	1.95E-03	513
LEPA	2002	80 305	145	1.81E-03	554
LEPA	2003	84 387	139	1.65E-03	607
TOTAL		**1 173 858**	**2 210**	**1.88E-03**	**531**
ORD	**1998–2000**	**43 960**	**84**	**1.91E-03**	**523**

---

1. A balked landing is a missed approach initiated below the decision height. The overall go-around rate includes all go-arounds at heights as high as 2 000 ft.

Hypothesis 3: Crosswind and balked landing initiation height affect s

In developing the test plan, OCP suggested that crosswind speed would have a significant positive effect on lateral deviation from the nominal track (higher crosswind gives higher deviation) and that balked landing initiation height would have a significant negative effect (the lower the initiation height, the greater the lateral deviation) as measured by the variable *s*.

Figure 7-2 shows the graphical relationships among the three variables: *s*, crosswind speed, and planned initiation height. The coloured surface is a smoothed surface created from the *s*-means at each crosswind/height combination. The small circles represent actual *s* values at those crosswind/height coordinates.

The clear conclusion from this data is that the combination of both higher crosswind speed and lower planned initiation height leads to greater *s* values. (*s* values are plotted in the vertical axis in Figure 7-2.)
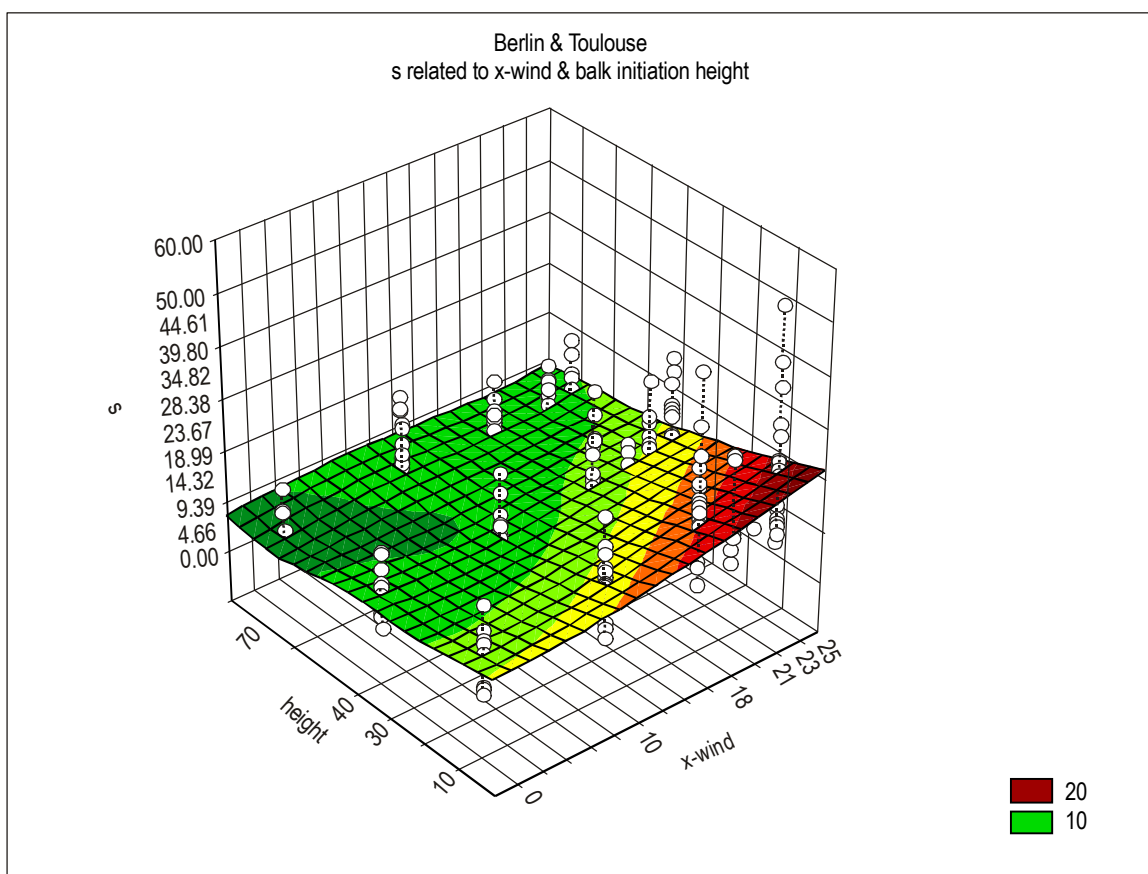
Figure 7-2.   *s* variable related to crosswind and balked landing initiation heights

Hypothesis 4: Crosswind speeds used in the trials were not representative

Since it was believed that higher crosswind speeds would affect lateral deviations *s*, many more high-wind speed runs were included in the trials than would be typical in an actual airport operational environment. The reason for this was to help in understanding the relationship between crosswind speed and balked landing lateral deviation.

The analysis should therefore compensate for this imbalance by using an actual crosswind speed distribution, comparing it to the test distribution. The distribution used as actual was from the table in Figure A4-3 of Appendix 4 to FAA Advisory Circular AC 120-28D. Table 7-3 lists the corresponding trials and actual distribution values.

Figure 7-3 displays the same information graphically. Note that the trials wind value of 10 knots represented 26% of the values and is divided between the 5–10 and 10–15 categories here giving 13% in each for a balanced comparison.

Table 7-3.   Crosswind speed distribution

Speed (kt)	Trials	Actual
0-5	10	55
5-10	13	30
10-15	13	10
15-20	32	4.5
20-25	32	0.5
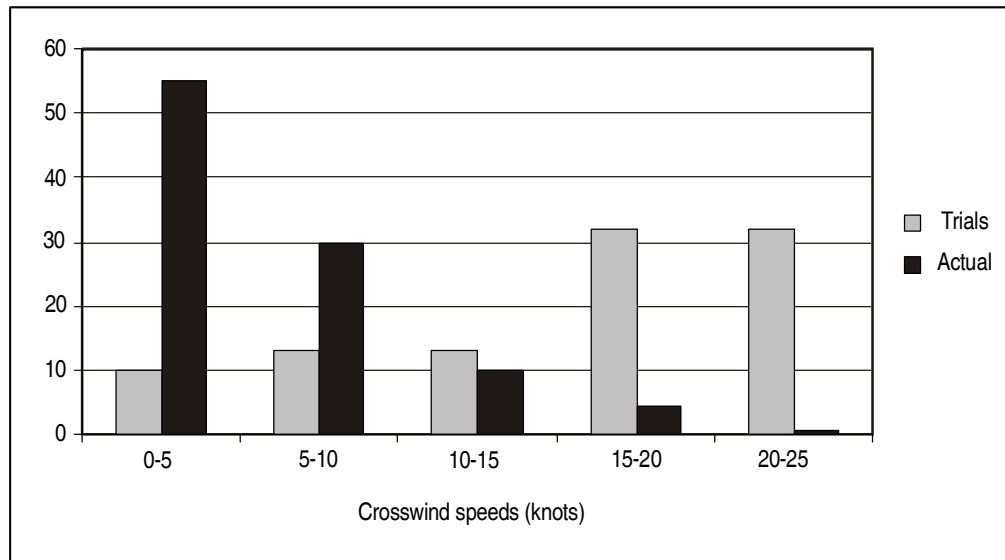
Figure 7-3.   Crosswind speed distributions

Hypothesis 5: Distribution of balked landings by planned initiation height is not representative

There is currently no reliable data available for this study that describe the distribution of balked landings by initiation height. The FAA AFS-420 Chicago O'Hare Land and Hold Short Study data indicate that almost all go-arounds are initiated above 70 feet (about 97%) and that certainly far less than 10% of them were initiated below 15 feet. However, the very small sample size of go-arounds at low altitudes in this data (combined with the fact that these are go-arounds and not specifically balked landings) prevents the determination of an accurate distribution of balked landing heights initiated below 70 feet.

The actual distribution of balked landings with heights should be applied if airline flight operations quality assurance (FOQA) data become available.

7.3.1.9   *Probability of OFZ confliction*

7.3.1.9.1   To calculate the probability that an A340/NLA wing tip infringes the Code E OFZ (inner transitional surface), a three-step methodology was used:

a)   The case of interest was established. This was the case to which the probability applied. It included attribute assumptions such as crosswind distribution, initiation height distribution, and type of landing.

b)   The data (See Appendix 1 to this chapter) were used to develop a distribution of maximum *s* values for case of Interest.

c)   This distribution was used to estimate the probability that *s* > 100%, that is, that a wing tip infringes the Code E OFZ surface under the case of interest.

7.3.1.10   *Case 1 (trials crosswinds, trials initiation heights)*

7.3.1.10.1   In this case, it was assumed that the actual crosswind and initiation height distributions are the same as those used in the 333 trials runs. It must be emphasized that this is a theoretical assumption based on the relationship between the actual crosswind speeds and those used in the trials (see Analysis Preliminaries, 7.3.1.7 d)) and the relationship between the (less well understood) apparent actual initiation height distribution and those planned for use in the trials (see Analysis Preliminaries, 7.3.1.7 e)).

7.3.1.10.2   Since (a) the proportion of both higher crosswind speeds and planned lower initiation heights in the trials was much higher than in actual conditions and (b) the relationship between those two variables and the variable *s* was such that higher crosswind speeds and lower initiation heights were directly related to higher values of *s* (see Analysis Preliminaries, 7.3.1.7 c)), then, this case would be expected to lead to a higher probability of OFZ infringement than one using actual conditions.

7.3.1.10.3   Assumptions:

• A hand-flown balked landing had occurred, as in the trials

• Crosswind speeds were those of the trials (not actual distributions)

• Balked landing initiation heights were those of the trials (not actual distributions)

7.3.1.11   *Develop a Distribution for Maximum s for Case 1*

7.3.1.11.1   Next, classical Extreme Value Theory was used to develop a distribution for the maximum *s* values. This theory provides, first, a family of distributions (called GEV, or Generalized Extreme Value distributions) that model block maximums such as those of the variable *s*. Second, it provides the vehicle for using a GEV distribution to extrapolate beyond the range of the maximum *s* values found in the trials data.

7.3.1.11.2   The family of GEV distributions is described by the distribution function:

$$GEV(x) = \exp \left\{ - \left[1 + \xi \left(\frac{x - \mu}{\sigma} \right) \right]^{-1/\xi} \right\}$$

where μ is the location parameter, σ is the scale parameter, and ξ is the shape parameter. Changing the value of any one of the parameters provides a different member of the family of GEV distributions.

7.3.1.11.3   We use the trials data and a standard extreme value technique (extreme value maximum likelihood estimation) to estimate the three parameter values and thus the specific distribution that fits our data.

7.3.1.11.4   For this case, the parameter values the estimation technique yields are:

μ = 6.336, σ = 3.677, and ξ = 0.075 with standard errors 0.227, 0.169, and 0.040, respectively.

7.3.1.11.5   The density function corresponding to GEV(z) with these parameters is plotted in Figure 7-4.
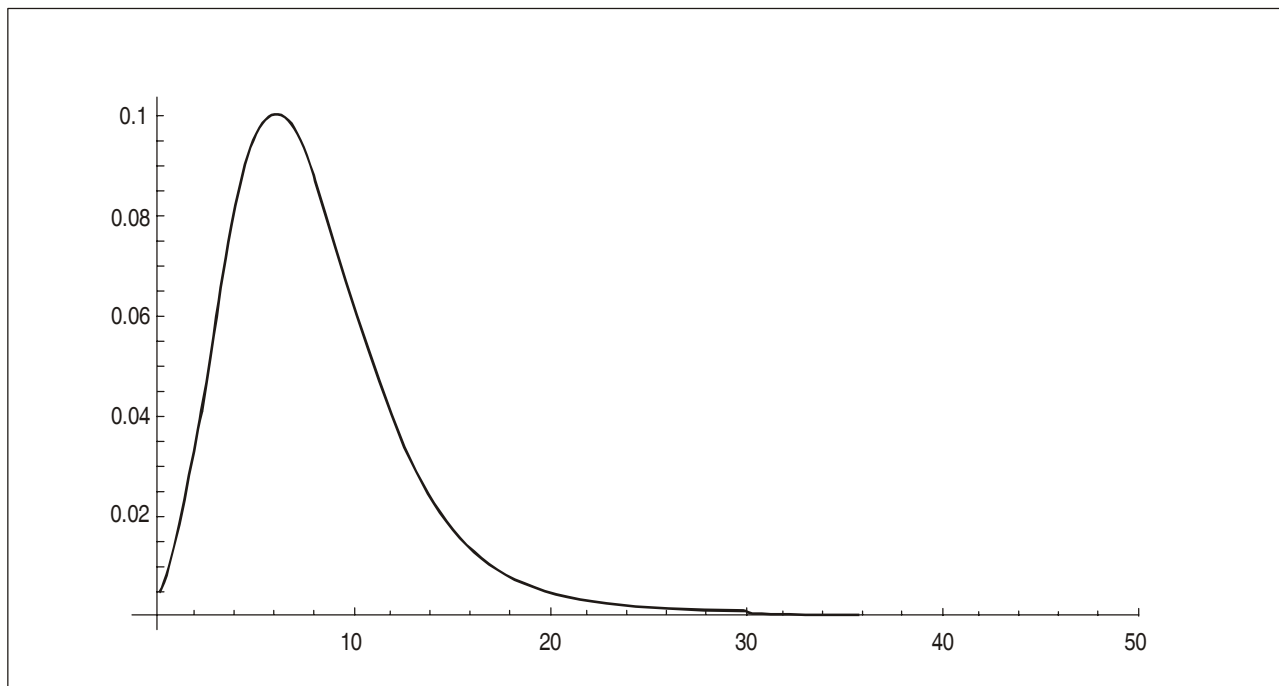
Figure 7-4.   Case 1 GEV density function

7.3.1.11.6   Estimate the probability that *s* > 100% for Case 1

7.3.1.11.7   We estimate the probability that *s* > 100%, given that a hand-flown balked landing has been attempted under this Case by calculating the area under the GEV density function to the right of 100 (See Figure 7-5). This area is 6.7 E-07 (meaning 6.7 multiplied by 10 to the negative seventh power) with a standard error of 1.9 E-06 (this standard error was calculated using the delta method which takes all three parameters into account), given this case: that a hand-flown balked landing has occurred and the trials crosswind and initiation height conditions are used. This estimate is likely high due to the use of the high trials crosswind distribution and the low trials initiation height distribution. However, it does provide an upper bound for the actual OFZ infringement probability. A 95% confidence interval estimate for this upper bound is 6.7E-07±3.8E-06.

7.3.1.12   *Establish Case 2*

7.3.1.12.1   In this case, the assumption was that the actual initiation height distribution was the same as that used in the 333 trials runs, but that the crosswind distribution was the actual distribution given in Analysis Preliminaries, 7.3.1.7 d). Again, it is emphasized that, while the crosswind situation represented actual conditions, the trials planned initiation height distribution used was a simulator trials assumption.

7.3.1.12.2   Since (a) the proportion of lower initiation heights in the trials is much greater than in actual conditions and (b) the relationship between this variable and the variable *s* is such that lower initiation heights are directly related to higher values of *s* (see Analysis Preliminaries, 7.3.1.7 c)), then, it is expected that this case (as with Case 1) will lead to a higher probability of OFZ infringement than one using actual conditions.

7.3.1.12.3   Assumptions:

* A hand-flown balked landing has occurred, as in the trials

* Crosswind speeds follow the actual distribution (not the trials distribution)

* Balked landing initiation heights are those of the trials (not actual)

7.3.1.13   *Develop a Distribution for Maximum s for Case 2*

7.3.1.13.1   Next, classical Extreme Value Theory was applied as in Case 1, except now the three distributions of the maximum *s* values were developed: one for each of three categories of crosswind speeds.

7.3.1.13.2   These three categories were based on the crosswind speed values 0–10, 10–20, and 20–25 knots. Where the first category includes the 0 and 10 crosswinds (it has 120 runs), the second category includes the 18 knot crosswinds (108 runs), and the last category includes the 21, 23, and 25 knot crosswinds (105 runs). These particular categories were chosen because the cutoff speeds are typical, the number of runs per category are similar, and the data within each category are homogeneous.

7.3.1.13.3   Next, the three GEV distributions were developed, one for each crosswind category.

7.3.1.13.4   The distribution for the first category, GEV1, has parameters $\mu = 5.307$, $\sigma = 3.372$, and $\xi = -0.024$ with standard errors 0.354, 0.260, and 0.078, respectively.

7.3.1.13.5   The distribution for the second category, GEV2, has parameters $\mu = 6.851$, $\sigma = 3.654$, and $\xi = 0.081$ with standard errors 0.399, 0.299, and 0.074, respectively.
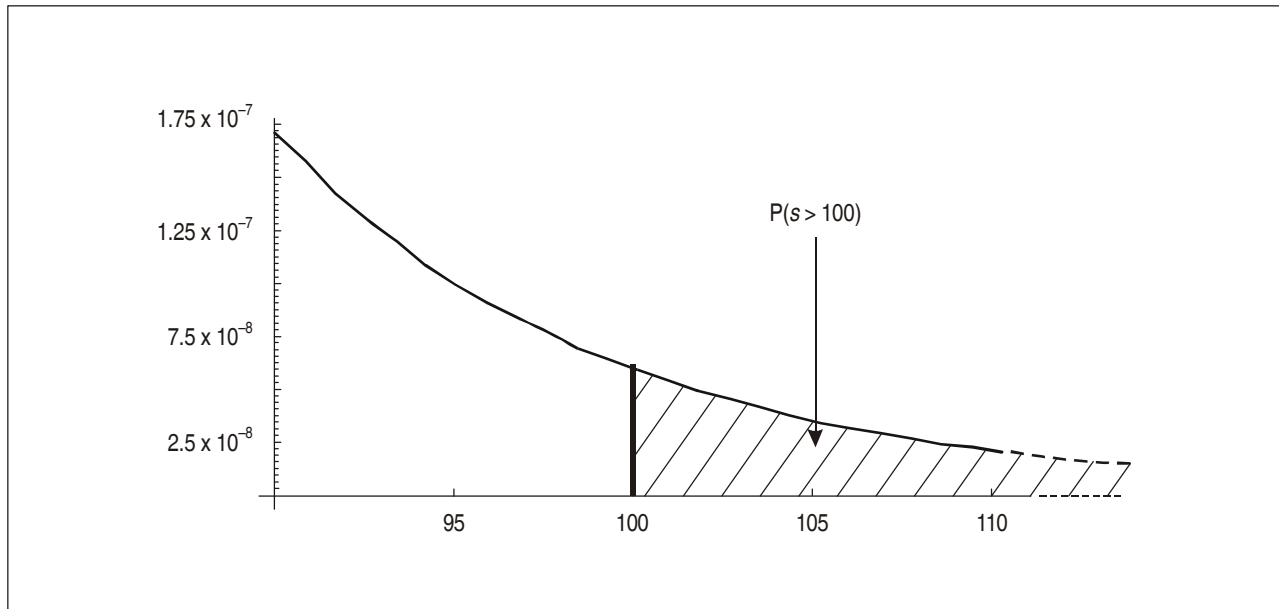
Figure 7-5.   Case 1 GEV density function detail

7.3.1.13.6   The distribution for the third category, GEV3, has parameters $\mu = 7.147$, $\sigma = 3.547$, and $\xi = 0.1923$ with standard errors 0.395, 0.314, and 0.083, respectively.

7.3.1.13.7   Figure 7-6 shows plots of these three distributions' density functions: GEV1 is the left-most, dotted curve, GEV2 is the next solid curve, and GEV3 is the dashed curve that begins below the GEV2 curve.

7.3.1.13.8   Estimate the probability that $s > 100\%$ for Case 2

7.3.1.13.9   For the hand-flown balked landing, the probability that $s > 100\%$ was estimated by calculating the area under each GEV density function (GEV1, GEV2, and GEV3) to the right of 100 and multiplying each of these areas by the likelihood of encountering a crosswind of that category.

7.3.1.13.10   This yields a mixed distribution, GEVALL, based on the three GEV distributions and the crosswind likelihood for each category (see Table 7-4):

$$GEVALL(z) = 0.85GEV1(z) + 0.145GEV2(z) + 0.005GEV3(z).$$

7.3.1.13.11   The calculations are summarized in Table 7-5.

7.3.1.13.12   Thus, P($s > 100\%$) = 5.76 E-07 with a standard error of 1.2E-06, given this case: that a hand-flown balked landing has occurred and the actual crosswind and trials initiation height conditions were used. A 95% confidence interval estimate for this upper bound is 5.76E-07±2.4E-06. Again, this estimate is clearly conservative due to the use of the low trials initiation height distribution. Note that even though actual crosswind distributions were used (as opposed to the high trials conditions used in Case 1), the estimate here in Case 2 is similar to that of Case 1, which tends to validate that the values are reasonably close.

7.3.1.13.13   Figure 7-7 shows the plot of the mixed GEVALL(z) density function.
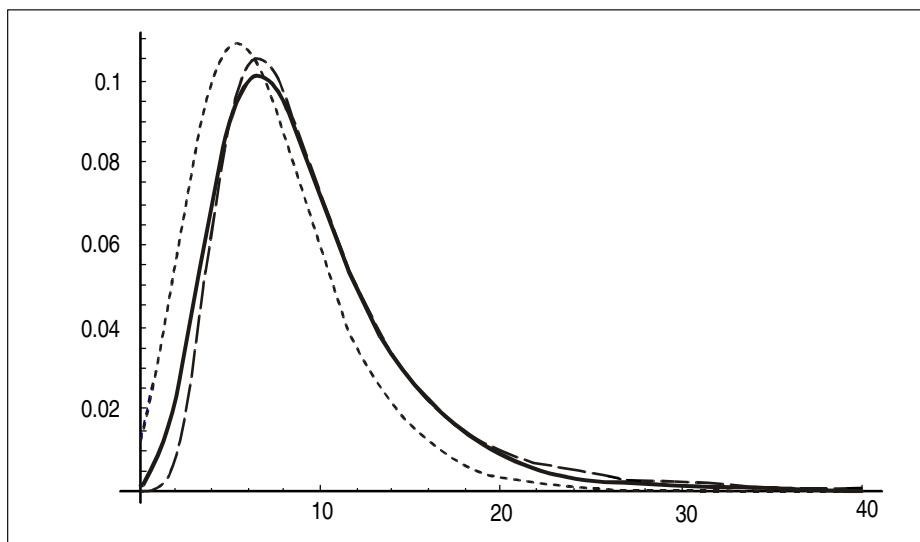
Figure 7-6.   Case 2 GEV density functions for each crosswind category

Table 7-4.   Crosswind speed distribution

Five speed categories	Actual %	Three speed categories	Actual %
0-5	55		
5-10	30	0-10	85
10-15	10		
15-20	4.5	10-20	14.5
20-25	0.5	20-25	0.5

Table 7-5.   Case 2 summary table

Wind category speed	Wind category actual %	GEV	P(s>100)	Actual % times P(s>100)
0-10	85	GEV1	0.0E-14	0.0
10-20	14.5	GEV2	9.7E-07	1.41E-07
20-25	0.5	GEV3	8.7E-05	4.35E-07
All	100	GEVALL		5.76E-07
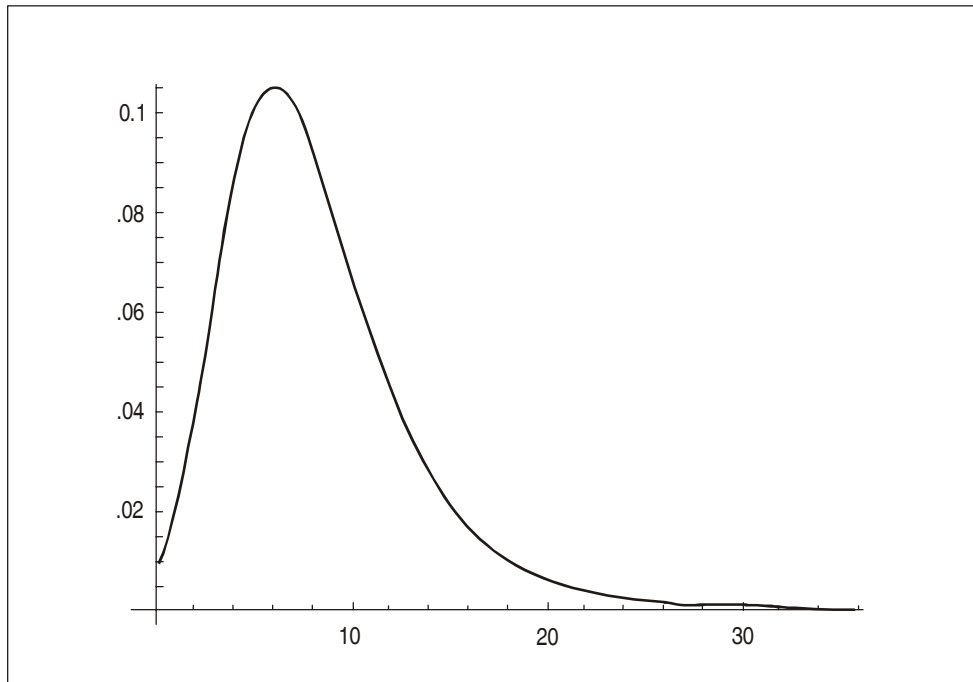
Figure 7-7.   Case 2 GEVALL density function

7.3.1.14   *Establish Case 3*

7.3.1.14.1   In this Case the crosswind distribution was assumed to be that of the simulator trials conditions and the assumption for the planned balked landing initiation height distribution given in Analysis Preliminaries, 7.3.1.7 e) was used. As indicated there, there is currently no accurate distribution of balked landings by initiation height, although one estimate was that the proportion of balked landings initiated below 15 feet is less than 10%.

7.3.1.14.2   Since (a) the proportion of high crosswinds in the trials was much greater than in actual conditions and (b) the relationship between this variable and the variable *s* is such that higher crosswind speeds are directly related to higher values of *s* (see Analysis Preliminaries, 7.3.1.7 c)), then, this case (as with Cases 1 and 2) would be expected to lead to a higher probability of OFZ infringement than one using actual conditions.

7.3.1.14.3   Assumptions:

- A hand-flown balked landing has occurred, as in the trials

- Crosswind speeds follow the trials distribution

- Balked landing initiation heights are closer to the actual distribution

7.3.1.15   *Develop a Distribution for Maximum s for Case 3*

7.3.1.15.1   Next, classical Extreme Value Theory was used as in Cases 1 and 2, except now two distributions were developed for the maximum *s* values: one for each of two categories of planned initiation heights (below 15 feet and above 15 feet). The first category includes the 10 foot initiation heights (it has 113 runs), the second category includes 40 and 70 foot initiation heights (220 runs).

7.3.1.15.2   Next, two GEV distributions were developed, one for each height category. The distribution for the first category, GEVA, has parameters $\mu = 8.299$, $\sigma = 4.511$, and $\xi = 0.032$ with standard errors 0.469, 0.337, and 0.058, respectively.

7.3.1.15.3   The distribution for the second category, GEVB, has parameters $\mu = 5.600$, $\sigma = 3.145$, and $\xi = 0.050$ with standard errors 0.238, 0.176, and 0.049, respectively.

7.3.1.15.4   Estimate the probability that *s* > 100% for Case 3.

7.3.1.15.5   For the hand-flown balked landing, the probability that *s* > 100% was estimated, for this case by calculating the area under each GEV density function (GEVA and GEVB) to the right of 100 and multiplying each of these areas by the likelihood of encountering a crosswind of that category.

7.3.1.15.6   This yields a mixed distribution, GEVBOTH, based on the two GEV distributions and the initiation height likelihoods for each category:

             GEVBOTH(z) = 0.10GEVA(z) + 0.90GEVB(z).

7.3.1.15.7   The calculations are summarized in Table 7-6.

7.3.1.15.8   Thus, P(*s* > 100%) = 2.6 E-08 with a standard error of 1.1E-07, given this case: that a hand-flown balked landing has occurred and the trials crosswind and estimated actual initiation height conditions are used. A 95% confidence interval estimate for the upper bound is 2.6E-08 ± 2.2E-07. Again, this estimate is likely high due to the use of the high crosswind distribution. It does, however, provide a check on the previous two estimates.

7.3.1.15.9   Although it would be possible to analyse a fourth case with assumptions for actual crosswind and initiation height distributions, the analysis was not attempted for three reasons. First, if the data was categorized by both crosswind and height, the number of runs in each category would be small. Second, assumptions about the relationship between the crosswind speed and height variables (such as independence) would be necessary that may be unwarranted. Third, an accurate distribution of balked landings by initiation height was unavailable at that time.

Table 7-6. Case 3 summary table

Height category	Height category actual %	GEV	P(s>100)	Actual % times P(s>100)
Below 15	10	GEVA	1.55E-07	1.6E-08
Above 15	90	GEVB	1.13E-08	1.0E-08
Both	100	GEVBOTH		2.6E-08

7.3.2   NASA Ames

7.3.2.1   In order to determine the probability of infringement on the Code E OFZ, a series of trials of the balked landing operation were performed using the Boeing 747-400 simulator in NASA Ames. These trials were designed to simulate the conditions of a 747/NLA balked landing operation in severe crosswind conditions as closely as possible. There were 110 flight director flown balked landings that were suitable for inclusion in the EVA. Other hand-flown balked landings were not considered as it was not possible to identify the initiation height. More details on the NASA Ames trials may be found in Part II, Chapter 3. Note that the NASA Ames scenarios included little variation in effective wind magnitude. All scenarios were performed in severe crosswind conditions.

7.3.2.2   An EVA of the collected data on hand-flown cases was performed following the methodology outlined in Section 7.2 and shown in detail for the Berlin/Toulouse data in Section 7.3.1.

7.3.2.3   *Establish Scenario*

7.3.2.3.1   In this scenario, we assume the actual crosswind and initiation height distributions are the same as those used in the 110 test runs. We must emphasize that this is an artificial assumption based on the relationship between the actual crosswind speeds and those used in the test and the relationship between the (less well understood) apparent actual initiation height distribution and those used in the test.

7.3.2.3.2   Since (a) the proportion of both higher crosswind speeds and lower initiation heights in the test is much higher than in actual conditions and (b) the relationship between those two variables and the variable *s* is such that the combination of higher crosswind speeds and lower initiation heights are directly related to higher values of *s*, then, we would expect this scenario to lead to a higher probability of OFZ infringement than one using actual conditions.

7.3.2.3.3   Assumptions:

- A hand-flown balked landing has occurred, as in the test

- Crosswind speeds are those of the test (not actual distributions)

- Balked landing initiation heights are those of the test (not actual distributions)

7.3.2.4   *Develop a Distribution for Maximum s for Scenario*

7.3.2.4.1   We use the test data and a standard extreme value technique (extreme value maximum likelihood estimation) to estimate the three GEV parameter values and thus the specific distribution that fits our data.

7.3.2.4.2   For this scenario, the parameter values the estimation technique yields are:

μ = 7.925, σ = 5.041, and ξ = -0.0876 with standard errors 0.536, 0.384, and 0.063, respectively.

7.3.2.4.3   Estimate the probability that s > 100% for Scenario 1

7.3.2.4.4   We estimate the probability that *s* > 100%, given that a hand-flown balked landing has been attempted under this scenario by calculating the area under the GEV density function to the right of 100 (see Figure 7-5). This area is 0.0 to the accuracy of the calculation with a standard error of 4.9 E-05 (this

standard error is computed using the delta method). Thus, P(s > 100%) = 0.0 ±4.9 E-05, given this scenario: that a hand-flown balked landing has occurred and the test crosswind and initiation height conditions are used. This estimate is likely high due to the use of the artificially high crosswind distribution and artificially low initiation height distribution. However, it does provide an upper bound for the actual OFZ penetration probability. A 95% confidence interval estimate for this upper bound is 0.0 ±9.8 E-05.

7.4   CONCLUSIONS

7.4.1   Berlin/Toulouse

7.4.1.1   Based on the three cases analysed, a reasonable upper bound on the probability of ICAO Code E OFZ infringement can be calculated. Table 7-7 summarizes the probability estimates from the three cases. It is important to note that these are conditional probabilities; that is, they are probabilities of OFZ infringement **given** that a hand-flown balked landing has occurred. The probability of a hand-flown balked landing occurring must be factored in to complete the calculation.

7.4.1.2   Each of these probabilities was developed using assumptions that would tend to produce higher rather than lower values. They differ primarily because of the variations in the sets of runs used to fit the various distributions. Note that Case 1 is a theoretical case not representative of an actual case.

7.4.1.3   To calculate a reliable upper bound on the OFZ infringement probability, the following further assumptions were made:

- Use the greatest of the three cases (6.7E-07).

- Use the balked landing rate in Analysis Preliminaries, 7.3.1.7 b), which is actually an upper bound of 1.9 balked landings per 1 000 landing attempts.

- Focus only on OFZ infringements due to balked landings, assuming that a normal landing produces effectively no infringement.

7.4.1.4   The probability of hand-flown A340/NLA ICAO OFZ infringement during a balked landing (OFZP) is given by:

P(OFZP) = P(Balk) • P(OFZP | Balk) **+** P(no Balk) • P(OFZP | no Balk).

which reduces to:

P(OFZP) = P(Balk) • P(OFZP | Balk),

since P(OFZP | no Balk) is effectively zero;.that is, "no Balk", or normal landings, produce effectively zero infringement by Assumption 3 above.

7.4.1.5   Since P(OFZP | Balk) < 6.7E-07, by Assumption 1 above and P(Balk) < 1.9 E-03, by Assumption 2 above, then P(OFZP) < 1.3 E-09; that is, an estimate of an upper bound for the probability of an A340/NLA ICAO Code E OFZ infringement during a hand-flown balked landing is determined to be 1.3E-09.

7.4.1.6   An even more conservative assumption would be to use the upper end of the 95% confidence interval for the infringement probability so that instead of using an infringement probability of 6.7E-07, we use 4.5E-06. This would lead to an upper bound for the probability of an A340/NLA ICAO Code E OFZ infringement during a hand-flown balked landing of 8.6E-09.

**Table 7-7.   Probabilities of infringement given a
hand-flown balked landing has occurred**

Case	Probability of Infringement
1	6.7E-07
2	5.76E-07
3	2.6E-08

7.4.2   NASA Ames

7.4.2.1   Based on the scenario analysed, we can calculate a reasonable upper bound on the probability of ICAO Code E OFZ infringement. To calculate a reliable upper bound on the OFZ penetration probability, we make these further assumptions:

- Use the scenario probability (0.0).

- Use the balked landing rate upper bound of 1.9 balked landings per 1 000 landing attempts.

- Focus only on OFZ infringements due to balked landings, assuming that a normal landing produces effectively no infringement.

7.4.2.2   The probability of hand-flown B747 ICAO OFZ infringement during a balked landing (OFZP) is given by:

P(OFZP) = P(Balk) • P(OFZP | Balk) **+** P(no Balk) • P(OFZP | no Balk).

which reduces to:

P(OFZP) = P(Balk) • P(OFZP | Balk),

since P(OFZP | no Balk) is effectively zero; that is, no Balk (i.e. normal landings) produce effectively zero penetrations by Assumption 3 above.

7.4.2.3   Since P(OFZP | Balk) = 0.0, by Assumption 1 above, and P(Balk) < 1.9 E-03, by Assumption 2 above, then, P(OFZP) = 0.0; that is, an estimate of an upper bound for the probability of a 747/NLA ICAO Code E OFZ infringement during a hand-flown balked landing is determined to be 0.0. Incorporating the standard error estimate, a 95% confidence interval for the penetration probability is determined to be 0.0 ± (9.8 E-05)(1.9 E-03) or 0.0 ± 1.9 E-07.

7.4.2.4   The results above for infringement probability have been validated by a slightly different approach to probability estimation. Instead of estimating the probability of the variable s exceeding 100%, we examine the relationship between the value of s and the height (h) of the critical wing tip at go-around. Using this perspective, we generate iso-probability curves for various values of probabilities.

7.4.2.5   In Figure 7-8, we use probabilities of p = 0.99999 and p = 0.999999. The corresponding curves are where the probability of s exceeding the curve boundaries are 1.0 E-05 and 1.0 E-06 respectively. Multiplying these probabilities by the probability of a balked landing (P(BALK) = 1.9 E-03) yields probabilities for infringement above the curves between 1.9 E-08 and 1.9 E-09.

7.4.3   OFZ adequacy

7.4.3.1   Note that we developed these estimates using several assumptions, each of which would tend to produce a higher value rather than a lower one. We may therefore conclude that these estimates are a reliable upper bound on the actual probability.

7.4.3.2   Given that several series of flight simulator tests on two different aircraft configured to have performance equivalent to that expected from the new large aeroplane produced results via extreme value analysis supporting the conclusion that the aeroplanes could safely perform a balked landing and stay within Code E OFZ boundaries to a high degree of probability, the conclusion of this analysis is that such operations can be authorized with an acceptable level of risk.
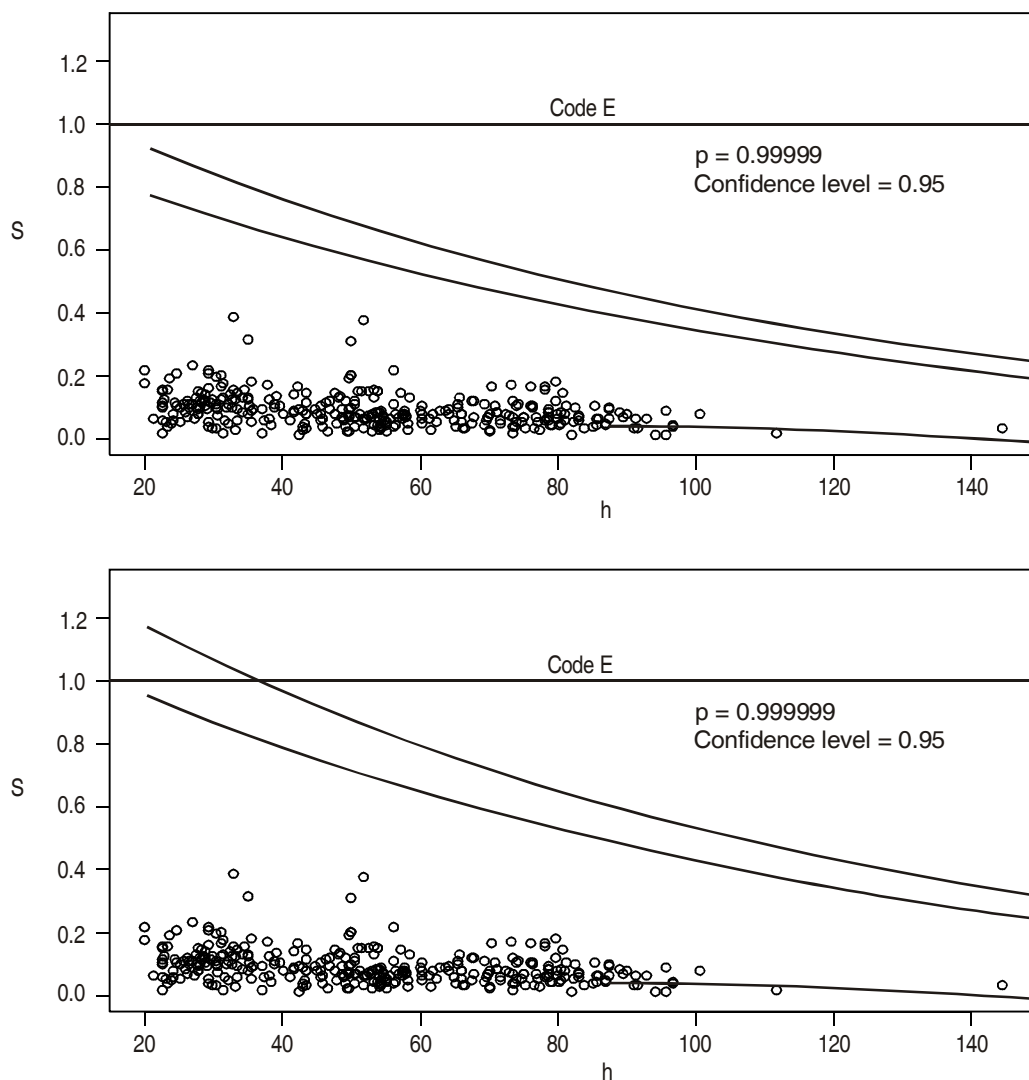
**Figure 7-8.   Iso-probability curves for *s* as a function of wing-tip height in feet (h),
with probabilities p = 0.99999 and p = 0.999999**

— — — — — — — — —

Appendix 1 to Chapter 7

Trials data summary for 333 Toulouse/Berlin runs

Location	Date	Scenario	Height (ft)	Crosswind (kt)	s Max (%)
Berlin	23-Aug-04	2	10	10	11.63
Berlin	23-Aug-04	3	10	18	9.65
Berlin	23-Aug-04	4	10	25	31.26
Berlin	23-Aug-04	5	40	0	8.00
Berlin	23-Aug-04	6	40	10	6.16
Berlin	23-Aug-04	7	40	25	19.63
Berlin	23-Aug-04	8	70	10	5.58
Berlin	23-Aug-04	9	70	18	3.99
Berlin	23-Aug-04	10	70	25	14.36
Berlin	23-Aug-04	17	10	0	10.94
Berlin	23-Aug-04	19	10	10	10.90
Berlin	23-Aug-04	20	10	18	9.94
Berlin	23-Aug-04	21	10	25	3.26
Berlin	23-Aug-04	22	40	10	6.20
Berlin	23-Aug-04	23	40	18	14.84
Berlin	23-Aug-04	25	40	25	3.62
Berlin	23-Aug-04	26	70	0	2.52
Berlin	23-Aug-04	27	70	10	6.24
Berlin	23-Aug-04	29	70	18	11.54
Berlin	24-Aug-04	2	10	10	9.50
Berlin	24-Aug-04	3	10	18	12.18
Berlin	24-Aug-04	4	10	25	16.11
Berlin	24-Aug-04	5	40	0	3.22
Berlin	24-Aug-04	6	40	10	5.66
Berlin	24-Aug-04	6.2	40	10	6.54
Berlin	24-Aug-04	7	40	25	14.51
Berlin	24-Aug-04	8	70	10	5.19
Berlin	24-Aug-04	9	70	18	6.13
Berlin	24-Aug-04	10	70	25	7.58
Berlin	24-Aug-04	17	10	0	11.96
Berlin	24-Aug-04	19	10	10	11.66
Berlin	24-Aug-04	20	10	18	10.73

Location	Date	Scenario	Height (ft)	Crosswind (kt)	s Max (%)
Berlin	24-Aug-04	21	10	25	9.29
Berlin	24-Aug-04	22	40	10	3.90
Berlin	24-Aug-04	23	40	18	15.03
Berlin	24-Aug-04	25	40	25	6.41
Berlin	24-Aug-04	26	70	0	2.25
Berlin	24-Aug-04	27	70	10	7.79
Berlin	24-Aug-04	29	70	18	6.46
Berlin	25-Aug-04	2	10	10	10.90
Berlin	25-Aug-04	3	10	18	14.14
Berlin	25-Aug-04	4	10	25	11.97
Berlin	25-Aug-04	5	40	0	14.47
Berlin	25-Aug-04	6	40	10	4.12
Berlin	25-Aug-04	7	40	25	10.62
Berlin	25-Aug-04	8	70	10	5.93
Berlin	25-Aug-04	9	70	18	7.77
Berlin	25-Aug-04	10	70	25	6.37
Berlin	25-Aug-04	17	10	0	10.39
Berlin	25-Aug-04	17.2	10	0	15.36
Berlin	25-Aug-04	19	10	10	12.62
Berlin	25-Aug-04	20	10	18	11.27
Berlin	25-Aug-04	21	10	25	20.87
Berlin	25-Aug-04	22	40	10	1.90
Berlin	25-Aug-04	23	40	18	12.41
Berlin	25-Aug-04	25	40	25	2.54
Berlin	25-Aug-04	26	70	0	5.56
Berlin	25-Aug-04	27	70	10	7.81
Berlin	25-Aug-04	29	70	18	1.78
Berlin	26-Aug-04	2	10	10	3.58
Berlin	26-Aug-04	3	10	18	20.17
Berlin	26-Aug-04	4	10	25	23.02
Berlin	26-Aug-04	5	40	0	6.97
Berlin	26-Aug-04	6	40	10	2.74
Berlin	26-Aug-04	6.2	40	10	14.86
Berlin	26-Aug-04	7	40	25	18.57
Berlin	26-Aug-04	8	70	10	17.76

Location	Date	Scenario	Height (ft)	Crosswind (kt)	s Max (%)
Berlin	26-Aug-04	9	70	18	9.31
Berlin	26-Aug-04	10	70	25	9.82
Berlin	26-Aug-04	17	10	0	2.71
Berlin	26-Aug-04	19	10	10	9.55
Berlin	26-Aug-04	20	10	18	18.93
Berlin	26-Aug-04	21	10	25	37.29
Berlin	26-Aug-04	22	40	10	6.20
Berlin	26-Aug-04	23	40	18	19.62
Berlin	26-Aug-04	25	40	25	7.26
Berlin	26-Aug-04	26	70	0	8.94
Berlin	26-Aug-04	27	70	10	12.45
Berlin	26-Aug-04	29	70	18	4.79
Berlin	27-Aug-04	2	10	10	9.01
Berlin	27-Aug-04	3	10	18	9.75
Berlin	27-Aug-04	4	10	25	14.90
Berlin	27-Aug-04	5	40	0	12.79
Berlin	27-Aug-04	6	40	10	5.36
Berlin	27-Aug-04	7	40	25	6.47
Berlin	27-Aug-04	8	70	10	16.32
Berlin	27-Aug-04	9	70	18	6.43
Berlin	27-Aug-04	10	70	25	16.13
Berlin	27-Aug-04	17	10	0	5.41
Berlin	27-Aug-04	17.2	10	0	7.67
Berlin	27-Aug-04	19	10	10	10.75
Berlin	27-Aug-04	20	10	18	10.47
Berlin	27-Aug-04	21	10	25	13.01
Berlin	27-Aug-04	22	40	10	1.63
Berlin	27-Aug-04	23	40	18	5.99
Berlin	27-Aug-04	25	40	25	5.70
Berlin	27-Aug-04	26	70	0	7.56
Berlin	27-Aug-04	27	70	10	11.53
Berlin	27-Aug-04	29	70	18	4.38
Berlin	30-Aug-04	2	10	10	7.27
Berlin	30-Aug-04	3	10	18	6.06
Berlin	30-Aug-04	4	10	25	13.62

Location	Date	Scenario	Height (ft)	Crosswind (kt)	s Max (%)
Berlin	30-Aug-04	5	40	0	7.27
Berlin	30-Aug-04	6	40	10	13.92
Berlin	30-Aug-04	7	40	25	13.29
Berlin	30-Aug-04	8	70	10	4.37
Berlin	30-Aug-04	9	70	18	7.45
Berlin	30-Aug-04	10	70	25	5.06
Berlin	30-Aug-04	17	10	0	9.79
Berlin	30-Aug-04	17.2	10	0	8.24
Berlin	30-Aug-04	19	10	10	9.22
Berlin	30-Aug-04	20	10	18	7.41
Berlin	30-Aug-04	21	10	25	14.70
Berlin	30-Aug-04	22	40	10	5.50
Berlin	30-Aug-04	23	40	18	4.22
Berlin	30-Aug-04	25	40	25	7.56
Berlin	30-Aug-04	26	70	0	6.18
Berlin	30-Aug-04	27	70	10	5.60
Berlin	30-Aug-04	29	70	18	7.88
Berlin	31-Aug-04	2	10	10	20.48
Berlin	31-Aug-04	3	10	18	12.60
Berlin	31-Aug-04	4	10	25	6.19
Berlin	31-Aug-04	5	40	0	11.35
Berlin	31-Aug-04	6	40	10	2.91
Berlin	31-Aug-04	7	40	25	5.37
Berlin	31-Aug-04	8	70	10	3.84
Berlin	31-Aug-04	9	70	18	3.91
Berlin	31-Aug-04	10	70	25	5.87
Berlin	31-Aug-04	17	10	0	5.54
Berlin	31-Aug-04	17.2	10	0	1.24
Berlin	31-Aug-04	19	10	10	10.21
Berlin	31-Aug-04	20	10	18	21.58
Berlin	31-Aug-04	21	10	25	15.62
Berlin	31-Aug-04	22	40	10	2.35
Berlin	31-Aug-04	23	40	18	10.45
Berlin	31-Aug-04	25	40	25	9.19
Berlin	31-Aug-04	26	70	0	3.54

Location	Date	Scenario	Height (ft)	Crosswind (kt)	s Max (%)
Berlin	31-Aug-04	27	70	10	4.34
Berlin	31-Aug-04	29	70	18	2.54
Berlin	1-Sep-04	2	10	10	5.42
Berlin	1-Sep-04	3	10	18	38.18
Berlin	1-Sep-04	4	10	25	4.89
Berlin	1-Sep-04	5	40	0	6.23
Berlin	1-Sep-04	6	40	10	3.72
Berlin	1-Sep-04	6.2	40	10	6.69
Berlin	1-Sep-04	7	40	25	14.04
Berlin	1-Sep-04	8	70	10	4.80
Berlin	1-Sep-04	9	70	18	10.24
Berlin	1-Sep-04	10	70	25	7.43
Berlin	1-Sep-04	17	10	0	9.90
Berlin	1-Sep-04	19	10	10	4.63
Berlin	1-Sep-04	20	10	18	11.89
Berlin	1-Sep-04	21	10	25	19.08
Berlin	1-Sep-04	22	40	10	3.25
Berlin	1-Sep-04	23	40	18	6.12
Berlin	1-Sep-04	25	40	25	7.75
Berlin	1-Sep-04	26	70	0	10.70
Berlin	1-Sep-04	27	70	10	5.64
Berlin	1-Sep-04	29	70	18	6.48
Berlin	2-Sep-04	2	10	10	10.45
Berlin	2-Sep-04	3	10	18	8.79
Berlin	2-Sep-04	4	10	25	17.19
Berlin	2-Sep-04	5	40	0	0.77
Berlin	2-Sep-04	6	40	10	7.46
Berlin	2-Sep-04	6.2	40	10	4.41
Berlin	2-Sep-04	7	40	25	12.30
Berlin	2-Sep-04	8	70	10	7.63
Berlin	2-Sep-04	9	70	18	7.16
Berlin	2-Sep-04	10	70	25	10.44
Berlin	2-Sep-04	17	10	0	2.68
Berlin	2-Sep-04	19	10	10	7.25
Berlin	2-Sep-04	20	10	18	5.28

Location	Date	Scenario	Height (ft)	Crosswind (kt)	s Max (%)
Berlin	2-Sep-04	21	10	25	10.02
Berlin	2-Sep-04	22	40	10	9.03
Berlin	2-Sep-04	23	40	18	11.59
Berlin	2-Sep-04	25	40	25	30.36
Berlin	2-Sep-04	26	70	0	1.80
Berlin	2-Sep-04	27	70	10	3.54
Berlin	2-Sep-04	29	70	18	6.10
Berlin	3-Sep-04	2	10	10	1.15
Berlin	3-Sep-04	3	10	18	8.13
Berlin	3-Sep-04	4	10	25	7.18
Berlin	3-Sep-04	5	40	0	3.11
Berlin	3-Sep-04	6	40	10	0.20
Berlin	3-Sep-04	6.2	40	10	6.21
Berlin	3-Sep-04	7	40	25	4.09
Berlin	3-Sep-04	8	70	10	5.79
Berlin	3-Sep-04	9	70	18	4.65
Berlin	3-Sep-04	10	70	25	5.63
Berlin	3-Sep-04	17	10	0	1.53
Berlin	3-Sep-04	19	10	10	4.90
Berlin	3-Sep-04	20	10	18	11.22
Berlin	3-Sep-04	21	10	25	7.62
Berlin	3-Sep-04	22	40	10	7.11
Berlin	3-Sep-04	23	40	18	4.39
Berlin	3-Sep-04	25	40	25	7.13
Berlin	3-Sep-04	26	70	0	2.71
Berlin	3-Sep-04	27	70	10	1.26
Berlin	3-Sep-04	29	70	18	6.47
Toulouse	21-May-04	2.1	40	18	13.28
Toulouse	21-May-04	3.1	70	23	2.62
Toulouse	21-May-04	3.2	70	23	9.77
Toulouse	21-May-04	4.1	10	10	5.85
Toulouse	21-May-04	6.1	40	23	14.16
Toulouse	21-May-04	7.1	10	18	2.93
Toulouse	21-May-04	8.1	70	18	5.92
Toulouse	21-May-04	9.1	70	10	0.89

Location	Date	Scenario	Height (ft)	Crosswind (kt)	s Max (%)
Toulouse	21-May-04	12.1	40	23	8.88
Toulouse	21-May-04	13.1	10	18	7.43
Toulouse	21-May-04	14.1	70	23	4.02
Toulouse	21-May-04	17.1	10	23	7.10
Toulouse	4-Jun-04	2	40	18	19.25
Toulouse	4-Jun-04	3	70	23	12.74
Toulouse	4-Jun-04	4	10	18	8.12
Toulouse	4-Jun-04	5	10	21	3.33
Toulouse	4-Jun-04	8	70	18	10.05
Toulouse	4-Jun-04	9	40	21	7.35
Toulouse	4-Jun-04	11	40	23	11.78
Toulouse	4-Jun-04	12	10	18	11.07
Toulouse	4-Jun-04	15	70	18	1.93
Toulouse	4-Jun-04	16	40	18	3.83
Toulouse	7-Jun-04	2	40	18	8.47
Toulouse	7-Jun-04	3	70	23	8.74
Toulouse	7-Jun-04	4	10	18	11.14
Toulouse	7-Jun-04	7	40	23	9.32
Toulouse	7-Jun-04	8	70	18	6.01
Toulouse	7-Jun-04	11	40	23	9.88
Toulouse	7-Jun-04	12	10	18	9.88
Toulouse	7-Jun-04	13	70	23	7.42
Toulouse	7-Jun-04	15	40	18	8.38
Toulouse	7-Jun-04	17	10	10	12.35
Toulouse	7-Jun-04	18	40	10	6.07
Toulouse	7-Jun-04	19	70	10	7.80
Toulouse	18-Jun-04	2	40	18	7.05
Toulouse	18-Jun-04	3	70	23	2.91
Toulouse	18-Jun-04	4	10	18	14.71
Toulouse	18-Jun-04	5	10	21	9.71
Toulouse	18-Jun-04	7	40	23	6.14
Toulouse	18-Jun-04	9	40	21	7.97
Toulouse	18-Jun-04	11	40	23	7.20
Toulouse	18-Jun-04	12	10	18	6.27
Toulouse	18-Jun-04	13	70	23	4.37

Location	Date	Scenario	Height (ft)	Crosswind (kt)	s Max (%)
Toulouse	18-Jun-04	15	70	18	3.97
Toulouse	18-Jun-04	16	40	18	4.00
Toulouse	18-Jun-04	17	10	10	6.24
Toulouse	1-Jul-04	2	70	23	8.97
Toulouse	1-Jul-04	3	40	18	9.90
Toulouse	1-Jul-04	4	10	18	5.23
Toulouse	1-Jul-04	6	10	21	4.67
Toulouse	1-Jul-04	7	40	23	5.19
Toulouse	1-Jul-04	8	70	18	10.23
Toulouse	1-Jul-04	11	40	23	14.48
Toulouse	1-Jul-04	12	10	18	11.74
Toulouse	1-Jul-04	13	70	23	4.91
Toulouse	1-Jul-04	15	70	18	3.57
Toulouse	1-Jul-04	16	40	18	2.08
Toulouse	6-Jul-04	2	70	23	10.19
Toulouse	6-Jul-04	3	40	18	8.77
Toulouse	6-Jul-04	4.1	10	18	13.22
Toulouse	6-Jul-04	4.2	10	18	22.46
Toulouse	6-Jul-04	6	10	21	9.97
Toulouse	6-Jul-04	7	40	23	6.43
Toulouse	6-Jul-04	8	70	18	6.64
Toulouse	6-Jul-04	9	40	21	10.22
Toulouse	6-Jul-04	11	40	23	5.84
Toulouse	6-Jul-04	12	10	18	18.10
Toulouse	6-Jul-04	13	70	23	7.95
Toulouse	6-Jul-04	15	70	18	3.36
Toulouse	6-Jul-04	16	40	18	2.83
Toulouse	6-Jul-04	17	10	10	15.41
Toulouse	6-Jul-04	18	40	10	1.84
Toulouse	6-Jul-04	19	70	10	5.23
Toulouse	16-Jul-04	2	70	23	6.73
Toulouse	16-Jul-04	3	40	18	8.29
Toulouse	16-Jul-04	4	10	18	16.83
Toulouse	16-Jul-04	6	10	21	7.80
Toulouse	16-Jul-04	7	40	23	7.93

Location	Date	Scenario	Height (ft)	Crosswind (kt)	s Max (%)
Toulouse	16-Jul-04	8	70	18	4.27
Toulouse	16-Jul-04	9	40	21	14.02
Toulouse	16-Jul-04	11	40	23	10.67
Toulouse	16-Jul-04	12	10	18	12.14
Toulouse	16-Jul-04	13	70	23	3.88
Toulouse	16-Jul-04	15	40	18	11.81
Toulouse	16-Jul-04	16	70	18	15.74
Toulouse	16-Jul-04	17	10	10	7.44
Toulouse	16-Jul-04	18	40	10	7.97
Toulouse	16-Jul-04	19	70	10	10.52
Toulouse	20-Jul-04	2	70	23	7.26
Toulouse	20-Jul-04	3	40	18	3.09
Toulouse	20-Jul-04	4	10	18	7.35
Toulouse	20-Jul-04	6	10	21	7.01
Toulouse	20-Jul-04	7	40	23	4.00
Toulouse	20-Jul-04	8	70	18	6.69
Toulouse	20-Jul-04	9	40	21	6.69
Toulouse	20-Jul-04	11	40	23	8.35
Toulouse	20-Jul-04	12	10	18	12.55
Toulouse	20-Jul-04	13	70	23	2.97
Toulouse	20-Jul-04	15	40	18	9.65
Toulouse	20-Jul-04	16	70	18	3.79
Toulouse	20-Jul-04	17	10	10	14.03
Toulouse	20-Jul-04	18	40	10	3.88
Toulouse	20-Jul-04	19	70	10	3.24
Toulouse	22-Jul-04	2	70	23	8.23
Toulouse	22-Jul-04	3	40	18	8.70
Toulouse	22-Jul-04	4	10	18	9.53
Toulouse	22-Jul-04	6	10	21	15.91
Toulouse	22-Jul-04	7	40	23	8.93
Toulouse	22-Jul-04	8	70	18	7.95
Toulouse	22-Jul-04	9	40	21	11.71
Toulouse	22-Jul-04	11	40	23	21.76
Toulouse	22-Jul-04	12	10	18	14.48
Toulouse	22-Jul-04	13	70	23	6.10

Location	Date	Scenario	Height (ft)	Crosswind (kt)	s Max (%)
Toulouse	22-Jul-04	15	40	18	8.88
Toulouse	22-Jul-04	16	70	18	8.88
Toulouse	22-Jul-04	17	10	10	4.61
Toulouse	22-Jul-04	18	40	10	8.49
Toulouse	22-Jul-04	19	70	10	16.63
Toulouse	26-Jul-04	2	70	23	6.26
Toulouse	26-Jul-04	3	40	18	10.57
Toulouse	26-Jul-04	4	10	18	10.32
Toulouse	26-Jul-04	6	10	21	15.30
Toulouse	26-Jul-04	7	40	23	6.34
Toulouse	26-Jul-04	8	70	18	5.02
Toulouse	26-Jul-04	9	40	21	9.25
Toulouse	26-Jul-04	11	40	23	5.58
Toulouse	26-Jul-04	12	10	18	14.28
Toulouse	26-Jul-04	12.1	10	18	10.11
Toulouse	26-Jul-04	13	70	23	10.16
Toulouse	26-Jul-04	15	40	18	6.63
Toulouse	26-Jul-04	16	70	18	3.27
Toulouse	26-Jul-04	17	10	10	9.57
Toulouse	26-Jul-04	18	40	10	6.48
Toulouse	26-Jul-04	19	70	10	16.96

— — — — — — — —

Appendix 2 to Chapter 7

Trials data summary for 110 NASA Ames runs

Location	Scenario	Run	Height (ft)	Crosswind (kt)	s Max (%)
NASA Ames	1	1106	95*	25	17.58
NASA Ames	1	1113	79*	25	4.68
NASA Ames	1	1114	89*	25	5.89
NASA Ames	1	1118	90*	25	6.36
NASA Ames	1	1119	117*	25	8.98
NASA Ames	1	1120	111*	25	7.24
NASA Ames	1	128	116*	25	12.03
NASA Ames	1	129	114*	25	5.02
NASA Ames	1	130	83*	25	3.53
NASA Ames	1	202	116*	25	0.69
NASA Ames	1	203	123*	25	4.63
NASA Ames	1	204	70*	25	4.26
NASA Ames	1	205	121*	25	1.39
NASA Ames	1	206	79*	25	4.66
NASA Ames	1	209	77*	25	6.57
NASA Ames	1	210	96*	25	3.57
NASA Ames	1	211	85*	25	4.97
NASA Ames	11	1106	10	25	14.42
NASA Ames	11	1114	10	25	7.78
NASA Ames	11	1118	10	25	8.94
NASA Ames	11	1119	10	25	19.22
NASA Ames	11	1120	10	25	12.18
NASA Ames	14	1106	69*	25	8.31
NASA Ames	14	1113	28*	25	10.32
NASA Ames	14	1118	78*	25	1.44
NASA Ames	14	1119	81*	25	11.66
NASA Ames	14	1120	113*	25	10.86
NASA Ames	2	128	88*	25	11.49
NASA Ames	2	130	64*	25	2.97
NASA Ames	2	202	120*	25	0.08
NASA Ames	2	204	111*	25	3.91
NASA Ames	2	205	104*	25	8.21

Location	Scenario	Run	Height (ft)	Crosswind (kt)	s Max (%)
NASA Ames	2	206	83*	25	3.94
NASA Ames	2	210	82*	25	7.15
NASA Ames	2	211	66*	25	2.63
NASA Ames	3	1106	10	25	16.83
NASA Ames	3	1114	10	25	11.20
NASA Ames	3	1118	10	25	15.86
NASA Ames	3	1119	10	25	13.74
NASA Ames	3	1120	10	25	13.41
NASA Ames	3	128	10	25	15.90
NASA Ames	3	129	10	25	12.09
NASA Ames	3	130	10	25	16.20
NASA Ames	3	202	10	25	7.48
NASA Ames	3	203	10	25	11.55
NASA Ames	3	204	10	25	9.37
NASA Ames	3	205	10	25	14.22
NASA Ames	3	206	10	25	1.26
NASA Ames	3	209	10	25	9.53
NASA Ames	3	210	10	25	12.55
NASA Ames	3	211	10	25	6.83
NASA Ames	4	128	10	25	7.21
NASA Ames	4	129	10	25	13.73
NASA Ames	4	130	10	25	7.74
NASA Ames	4	202	10	25	15.77
NASA Ames	4	204	10	25	22.57
NASA Ames	4	205	10	25	18.15
NASA Ames	4	206	10	25	16.24
NASA Ames	4	209	10	25	17.77
NASA Ames	4	210	10	25	13.22
NASA Ames	4	211	10	25	12.12
NASA Ames	4	203	10	25	13.91
NASA Ames	5	1106	20	25	16.24
NASA Ames	5	1113	20	25	9.75
NASA Ames	5	1114	20	25	4.17
NASA Ames	5	1118	20	25	26.82
NASA Ames	5	1119	20	25	8.91

Location	Scenario	Run	Height (ft)	Crosswind (kt)	s Max (%)
NASA Ames	5	1120	20	25	15.78
NASA Ames	5	129	10	25	5.38
NASA Ames	5	130	10	25	18.42
NASA Ames	5	202	10	25	15.76
NASA Ames	5	203	10	25	15.44
NASA Ames	5	204	10	25	8.74
NASA Ames	5	205	10	25	17.68
NASA Ames	5	206	10	25	16.39
NASA Ames	5	209	10	25	13.34
NASA Ames	5	210	10	25	8.54
NASA Ames	5	211	10	25	32.83
NASA Ames	5	502	10	20	6.63
NASA Ames	5	505	10	20	20.20
NASA Ames	5	506	10	20	17.30
NASA Ames	5	507	10	20	18.33
NASA Ames	5	508	10	20	16.16
NASA Ames	5	509	10	20	10.15
NASA Ames	5	512	10	20	7.62
NASA Ames	5	513	10	20	9.21
NASA Ames	6	1114	-2*	25	2.03
NASA Ames	7	1106	30*	25	10.04
NASA Ames	7	1114	44*	25	4.99
NASA Ames	7	1118	63*	25	4.31
NASA Ames	7	1119	37*	25	8.60
NASA Ames	7	1120	47*	25	4.69
NASA Ames	7	1113	71*	25	9.69
NASA Ames	8	1114	117*	25	3.46
NASA Ames	8	129	50*	25	6.12
NASA Ames	8	130	112*	25	1.29
NASA Ames	8	202	90*	25	10.07
NASA Ames	8	203	46*	25	14.94
NASA Ames	8	204	12*	25	11.13
NASA Ames	8	205	49*	25	7.59
NASA Ames	8	206	41*	25	12.87
NASA Ames	8	209	43*	25	3.35

Location	Scenario	Run	Height (ft)	Crosswind (kt)	s Max (%)
NASA Ames	8	210	37*	25	5.18
NASA Ames	8	211	23*	25	12.24
NASA Ames	9	1106	35	25	14.12
NASA Ames	9	1113	35	25	7.87
NASA Ames	9	1114	35	25	14.43
NASA Ames	9	1118	35	25	18.17
NASA Ames	9	1119	35	25	13.77
NASA Ames	9	1120	35	25	12.78

* Scenario involved runway incursion. Altitude shown is where TO/GA button was pressed.

   Note.— Identical scenario numbers over different test periods may not necessarily correspond to the same test condition.

_____

Appendix A
REFERENCE TABLES FOR ICAO/FAA DESIGN STANDARDS AND AEROPLANE DIMENSIONS

1. Appendix A includes tables and figures, which are frequently referenced in this circular, as follows:

    a)   Table A-1 — contains the dimensions and slopes for the surfaces found in Figures A-1 and A-2;

    b)   Table A-2 — defines the ICAO aerodrome reference codes, namely, the code numbers and letters;

    c)   Table A-3 — contains the taxiway minimum separation distances by aerodrome reference code; and

    d)   Figures A-1 and A-2 — describe the obstacle limitation surfaces and the balked landing surfaces.

2. Other tables included in this appendix are:

    a)   Tables A-4.1, A-4.2, A-4.3, A-4.4 and A-4.5 — provide comparisons between aeroplane dimensions for some existing large aeroplanes;

    b)   Table A-5 — provides a cross-reference between the ICAO and FAA aerodrome classification schemes; and

    c)   Table A-6 — provides a cross-reference between ICAO and FAA design standards for aerodromes.

Table A-1.[1] Dimensions and slopes of obstacle limitation surfaces — approach runways

	RUNWAY CLASSIFICATION									
	Non-instrument Code number				Non-precision approach Code number			Precision approach category I Code number		II or III Code number
Surface and dimensions[a] (1)	1 (2)	2 (3)	3 (4)	4 (5)	1,2 (6)	3 (7)	4 (8)	1,2 (9)	3,4 (10)	3,4 (11)
CONICAL										
Slope	5%	5%	5%	5%	5%	5%	5%	5%	5%	5%
Height	35 m	55 m	75 m	100 m	60 m	75 m	100 m	60 m	100 m	100 m
INNER HORIZONTAL										
Height	45 m	45 m	45 m	45 m	45 m	45 m	45 m	45 m	45 m	45 m
Radius	2 000 m	2 500 m	4 000 m	4 000 m	3 500 m	4 000 m	4 000 m	3 500 m	4 000 m	4 000 m
INNER APPROACH										
Width	—	—	—	—	—	—	—	90 m	120 m[e]	120 m[e]
Distance from threshold	—	—	—	—	—	—	—	60 m	60 m	60 m
Length	—	—	—	—	—	—	—	900 m	900 m	900 m
Slope								2.5%	2%	2%
APPROACH										
Length of inner edge	60 m	80 m	150 m	150 m	150 m	300 m	300 m	150 m	300 m	300 m
Distance from threshold	30 m	60 m	60 m	60 m	60 m	60 m	60 m	60 m	60 m	60 m
Divergence (each side)	10%	10%	10%	10%	15%	15%	15%	15%	15%	15%
First section										
Length	1 600 m	2 500 m	3 000 m	3 000 m	2 500 m	3 000 m	3 000 m	3 000 m	3 000 m	3 000 m
Slope	5%	4%	3.33%	2.5%	3.33%	2%	2%	2.5%	2%	2%
Second section										
Length	—	—	—	—	—	3 600 m[b]	3 600 m[b]	12 000 m	3 600 m[b]	3 600 m[b]
Slope	—	—	—	—	—	2.5%	2.5%	3%	2.5%	2.5%
Horizontal section										
Length	—	—	—	—	—	8 400 m[b]	8 400 m[b]		8 400 m[b]	8 400 m[b]
Total length	—	—	—	—	—	15 000 m	15 000 m	15 000 m	15 000 m	15 000 m
TRANSITIONAL										
Slope	20%	20%	14.3%	14.3%	20%	14.3%	14.3%	14.3%	14.3%	14.3%
INNER TRANSITIONAL										
Slope	—	—	—	—	—	—	—	40%	33.3%	33.3%
BALKED LANDING SURFACE										
Length of inner edge	—	—	—	—	—	—	—	90 m	120 m[e]	120 m[e]
Distance from threshold	—	—	—	—	—	—	—	[c]	1 800 m[d]	1 800 m[d]
Divergence (each side)	—	—	—	—	—	—	—	10%	10%	10%
Slope	—	—	—	—	—	—	—	4%	3.33%	3.33%

a.   All dimensions are measured horizontally unless specified otherwise.
b.   Variable.
c.   Distance to the end of strip.
d.   Or end of runway whichever is less.
e.   Where the code letter is F, the width is increased to 155 m.

---

1.   Table 4-1 in Annex 14, Volume I.

Table A-2.[2]   Aerodrome reference code

Code element 1		Code element 2		
Code number (1)	Aeroplane reference field length (2)	Code letter (3)	Wing span (4)	Outer main gear wheel span[a] (5)
1	Less than 800 m	A	Up to but not including 15 m	Up to but not including 4.5 m
2	800 m up to but not including 1 200 m	B	15 m up to but not including 24 m	4.5 m up to but not including 6 m
3	1 200 m up to but not including 1 800 m	C	24 m up to but not including 36 m	6 m up to but not including 9 m
4	1 800 m and over	D	36 m up to but not including 52 m	9 m up to but not including 14 m
		E	52 m up to but not including 65 m	9 m up to but not including 14 m
		F	65 m up to but not including 80 m	14 m up to but not including 16 m

a.   Distance between the outside edges of the main gear wheels.

Note.— Guidance on planning for aeroplanes with wing spans greater than 80 m is given in Doc 9157 — Aerodrome Design Manual, *Parts 1 and 2.*

---

2.   Table 1-1 in Annex 14, Volume I.

Table A-3.[3]   Taxiway minimum separation distances

Code letter	Distance between taxiway centre line and runway centre line (metres)								Taxiway centre line to taxiway centre line (metres)	Taxiway, other than aircraft stand taxilane, centre line to object (metres)	Aircraft stand taxilane centre line to object (metres)
	Instrument runways Code number				Non-instrument runways Code number						
	1	2	3	4	1	2	3	4			
(1)	(2)	(3)	(4)	(5)	(6)	(7)	(8)	(9)	(10)	(11)	(12)
A	82.5	82.5	—	—	37.5	47.5	—	—	23.75	16.25	12
B	87	87	—	—	42	52	—	—	33.5	21.5	16.5
C	—	—	168	—	—	—	93	—	44	26	24.5
D	—	—	176	176	—	—	101	101	66.5	40.5	36
E	—	—	—	182.5	—	—	—	107.5	80	47.5	42.5
F	—	—	—	190	—	—	—	115	97.5	57.5	50.5

Note 1.— The separation distances shown in columns (2) to (9) represent ordinary combinations of runways and taxiways. The basis for development of these distances is given in Doc 9157 — Aerodrome Design Manual, *Part 2.*

Note 2.— The distances in columns (2) to (9) do not guarantee sufficient clearance behind a holding aeroplane to permit the passing of another aeroplane on a parallel taxiway. See Doc 9157 — Aerodrome Design Manual, *Part 2.*

---

3. Table 3-1 in Annex 14, Volume I.

Table A-4.1.   Aeroplane dimensions

Aeroplane dimensions	Code F				Code E		
	A380-800	B747-Advanced*	C5	An 124	A340-600	B747-400ER	B777-300ER
Wing span	79.8 m	68.7 m	67.9 m	73.3 m	63.4 m	64.9 m	64.8 m
Outer main gear wheel span	14.3 m	12.7 m	11.4 m	8.0 m	12.6 m	12.6 m	12.9 m
Fuselage length	70.4 m	72.2 m 73.7 m**	70.3 m	69.9 m	73.5 m	68.6 m	73.1 m
Overall length	72.7 m	74.2 m 75.7 m**	75.5 m	69.9 m	75.3 m	70.7 m	73.9 m
Fuselage width	7.1 m	6.5 m	7.1 m	7.3 m	5.6 m	6.5 m	6.2 m
Fuselage height at operating empty weight (OEW)	10.9 m	10.2 m	9.3 m	10.2 m	8.5 m	10.2 m	8.7 m
Main deck sill height***	5.4 m	5.4 m	2.7 m	2.8 m	5.7 m	5.4 m	5.5 m
Upper deck sill height***	8.1 m	7.9 m	7.1 m	7.5 m	—	7.9 m	—
Tail height at OEW	24.1 m	20.1 m	19.9 m	21.0 m	17.4 m	19.6 m	18.7 m
Wingspan	79.8 m	68.7 m	67.9 m	73.3 m	63.4 m	64.9 m	64.8 m
Wingspan (full fuel)#	—	—	—	—	63.6 m	64.9 m	—
Wingspan (jig) ##	79.8 m	68.7 m	67.9 m	73.3 m	63.4 m	64.4 m	64.8 m
Wing-tip vertical clearance at maximum take-off weight (MTOW)	5.3 m	~5.1 m	3.2 m	3.7 m	6.0 m	5.1 m	7.2 m
Wing-tip vertical clearance at OEW	6.1 m	~5.7 m	4.0 m	Unknown	6.2 m	5.7 m	7.5 m
Maximum wing-tip height at MTOW	7.5 m	~5.1 m	3.2 m	3.7 m	7.6 m	6.7 m	7.2 m
Maximum wing-tip height at OEW	8.3 m	~5.7 m	4.0 m	Unknown	7.8 m	7.3 m	7.5 m
Cockpit view at OEW: - Cockpit height - Cockpit cut-off angle - Obscured segment	7.2 m 20° Max.19.8 m	8.7 m 18.4° 25.8 m	8.2 m Unknown Unknown	8.3 m Unknown Unknown	5.7 m 20° 15.7 m	8.7 m 18.4° 25.8 m	5.9 m 21° 14.6 m
Taxi camera	Yes	No	No	No	Yes	No	Yes
Pilot distance from nose landing gear	2.1 m	2.3 m	5.0 m	2.4 m	4.3 m	2.3 m	3.6 m
Pilot distance from main landing gear	31.8 m	28.4 m 29.9 m**	27.2 m	25.3 m	37.4 m	26.4 m	34.2 m

~   Symbol indicates "approximately".
*   B747 Advanced is a proposed aircraft and, therefore, the specifications are subject to change.
**   Freighter version values provided where appropriate.
*** Highest door at OEW.
#   For aircraft with large winglets (significant wing and winglet deflection with full fuel).
For aircraft without winglets, reference is frequently made to 'jig' span, i.e. the span as measured in the manufacturing jig (straight wing without 1G droop).

Table A-4.2.   Weights and landing gear geometry

| | Code F | | | | Code E | | |
	A380-800	B747-Advanced*	C5	An 124	A340-600	B747-400ER	B777-300ER
Weight							
Maximum ramp weight (MRW)	562 t 602 t**	423 t 437 t**	381 t	405 t	369 t	414 t	341 t
Maximum take-off weight (MTOW)	560 t 600 t**	422 t 435 t**	379.6 t	398 t	368 t	413 t	340 t
Maximum landing weight (MLW)	386 t 427 t**	296 t 333 t**	288.4 t	330 t	256 t	296 t 302 t**	251 t
Landing gear dimensions							
Wheel track	12.5 m	11.0 m	7.9 m	6.3 m	10.7 m	11.0 m	11.0 m
Outer main gear wheel span	14.3 m	12.7 m	11.4 m	8.0 m	12.6 m	12.6 m	12.9 m
Wheel base	29.7 m	26.1 m 27.6 m**	22.2 m	22.9 m	33.1 m	24.1 m	30.6 m

*   B747 Advanced is a proposed aircraft and, therefore, the specifications are subject to change.
** Freighter version values are provided where appropriate.

Table A-4.3.   Engine data

| Engine data | Code F | | | | Code E | | |
	A380-800	B747-Advanced*	C5	An 124	A340-600	B747-400ER	B777-300ER
Number of engines	4	4	4	4	4	4	2
Bypass ratio	8.7	~9	8.0	~5.7	7.5	~5	~7
Engine thrust	70 klb 77 klb**	65-67 klb	41 klb	52 klb	56 klb	56-63 klb	115 klb
Engine span (CL to CL)	51.4 m	41.7 m	37.7 m	37.9 m	38.5 m	41.7 m	19.2 m
Engine vertical clearance at MTOW	1.1 m (inner) 1.9 m (outer)	0.7 m 1.4 m	2.5 m 1.7 m	3.5 m 3.1 m	0.5 m 1.6 m	0.7 m 1.4 m	0.9 m
Reverse system	Only inboard thrust reversers	Yes	Yes	Yes	Yes	Yes	Yes

~   Symbol indicates "approximately".
*   B747 Advanced is a proposed aircraft, and therefore the specifications are subject to change.
** Freighter version values are provided where appropriate.

Note.— Jet blast velocity contours are available in Section 6 of the "Airplane Characteristics for Airport Planning" document on the website of the respective manufacturer.

Table A-4.4.   Maximum passenger capacity

| | Code F | | | | Code E | | |
Layout and capacities	A380-800	B747- Advanced*	C5	An 124	A340-600	B747-400ER	B777-300ER
Three-class reference layout	555	450	—	—	380	416	365
Maximum passenger carrying capacity	~800	~650	—	—	~475	~620	550

~   Symbol indicates "approximately".
*   B747 Advanced is a proposed aircraft and, therefore, the specifications are subject to change.

**Table A-4.5.   Landing incidence/attitude and final approach speed
at MLW and forward centre of gravity**

| | Code F | | | | | Code E | |
Attitude approach data	A380-800	B747-Advanced*	C5	An 124	A340-600	B747-400ER	B777-300ER
Approach attitude at 3° glide slope	1°	~3°	Unknown	Unknown	3.5°	3.0°	~3°
Approach speed	~145 kt	~157 kt	~135 kt	~124 kt	154 kt	157 kt	~150 kt
Start of visual segment	290 ft				338 ft		

~   Symbol indicates "approximately".
*   B747 Advanced is a proposed aircraft and, therefore, the specifications are subject to change.

Note.— B747-Advanced, B777-300ER and A380-800 data are estimated values.

Table A-5.   ICAO aerodrome code letters and FAA design groups

ICAO	Span limit	Track width	FAA	Span limit
Code letter C	<36 m (118.1 ft)		Group III	<118 ft (36 m)
Code letter D	<52 m (170.6 ft)	<9 m (29.5 ft)	Group IV	<171 ft (52 m)
Code letter E	<65 m (213.2 ft)	<14 m (45.9 ft)	Group V	<214 ft (65 m)
Code letter F	<80 m (262.4 ft)	<16 m (52.5 ft)	Group VI	<262 ft (80 m)

Table A-6. Comparison of aerodrome design standards

Design element	FAA group V		FAA group VI		ICAO group E		ICAO group F	
	feet	metres	feet	metres	feet	metres	feet	metres
Width								
Runway	150	45	200	60	150	45	200	60
Runway shoulder	35	10.5	40	12	50	15	50	15
Runway strip (graded portion)*	500	150	500	150	492	150	492	150
Taxiway	75	23	100	30	75	23	82	25
Separation								
					599	182.5**	623	190**
Runway to taxiway	400	120	600	180	351	107.5***	377	115***
Taxiway to taxiway	267	81	324	99	262	80	320	97.5
Taxiway to object	160	48.5	193	59	156	47.5	189	57.5
Taxilane to object	138	42	167	51	139	42.5	166	50.5
Wing-tip clearance								
Taxiway	53	16	62	19	50	15	57	17.5

* FAA runway safety area
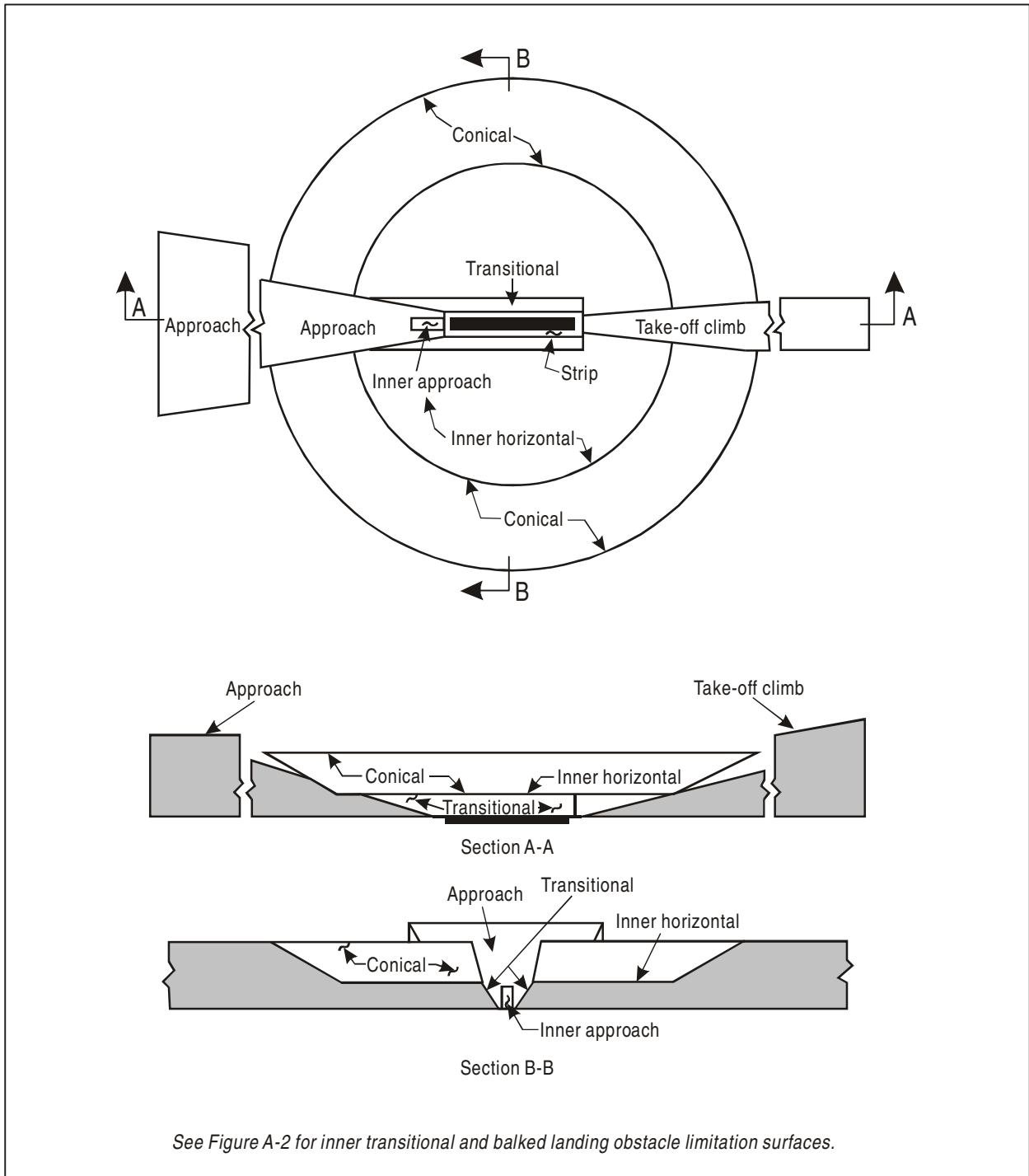** Instrument runway
*** Non-instrument runway

— — — — — — — —

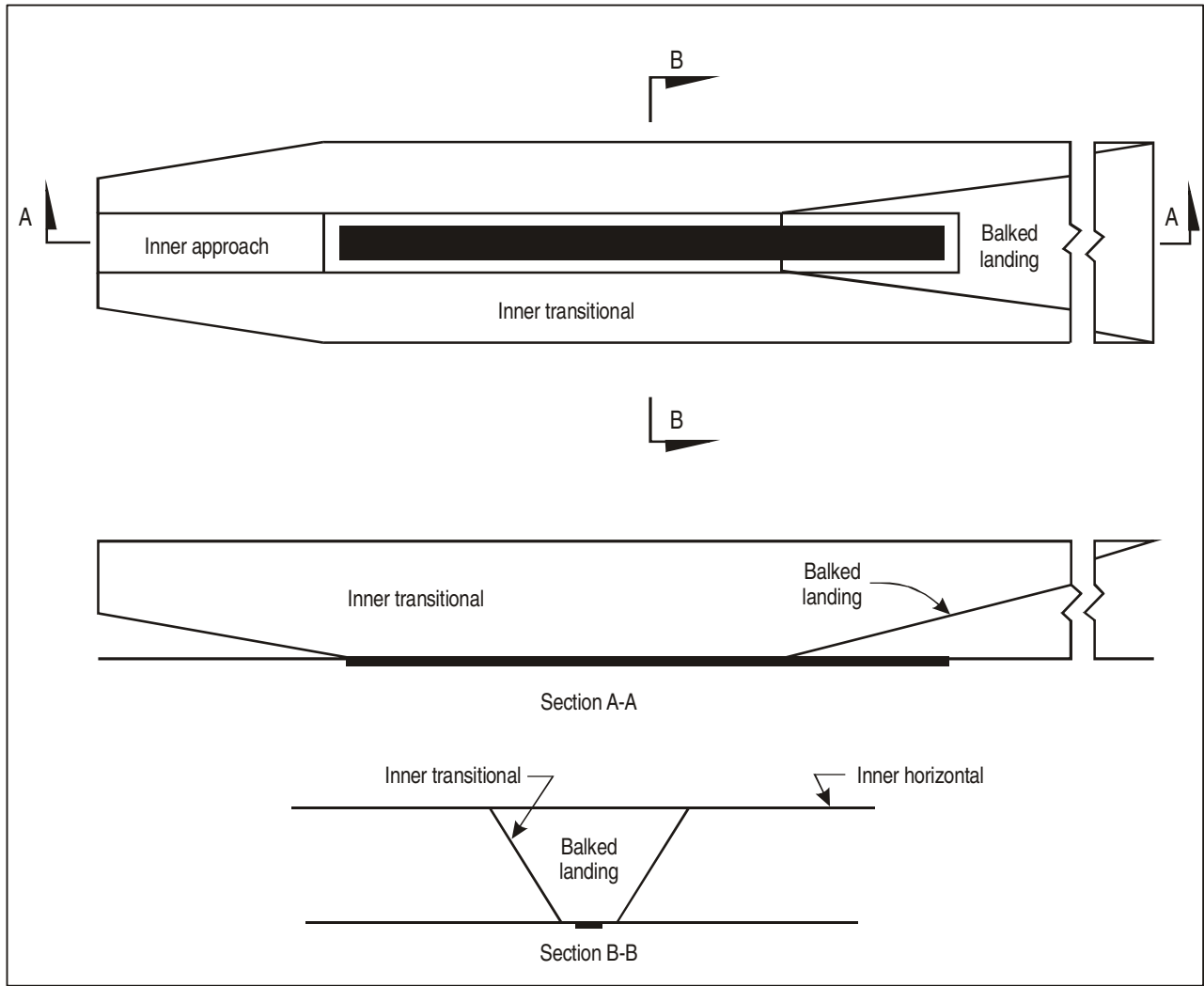**Figure A-1.   Obstacle limitation surfaces**

Figure A-2.   Inner approach, inner transitional and balked landing obstacle limitation surfaces

————————————

Appendix B
FAA/JAA WIND MODEL FOR APPROACH
AND LANDING SIMULATION

Reprinted with permission. Minor editorial changes introduced by ICAO.

Note.— The following text and figures were taken from FAA Advisory Circular FAA AC 120-28D. The figures were renumbered for this appendix. This revision of the AC has included harmonization with the wind models found in the JAR All Weather Operations document Chapter 131.

In carrying out the performance analysis, one of the following models of wind, turbulence and windshear may be used:

WIND MODEL A

Mean wind

The mean wind is the steady state wind measured at landing. This mean wind is composed of a downwind component (headwind and tailwind) and a crosswind component. The cumulative probability distributions for these components are provided in Figure B-1 (downwind) and Figure B-2 (crosswind). Alternatively, the mean wind can be defined with magnitude and direction. The cumulative probability for the mean wind magnitude is provided in Figure B-3, and the histogram of the mean wind direction is provided in Figure B-4. The mean wind is measured at a reference altitude of 20 ft AGL. The models of the wind shear and turbulence given in following sections assume this reference altitude of 20 ft AGL is used.

Wind shear

The wind shear component is that portion which affects the air mass moving along the ground (i.e., ground friction). The magnitude of the shear is defined by the following expression:

$$V_{wref} = 0.20407 \ \bar{V}_{20} \ \ln\left(\frac{h+0.15}{0.15}\right)$$

Where V_{wref} is the mean wind speed measured at h ft and $\bar{V}_{20}$ is the mean wind speed at 20 ft AGL.

Turbulence

The turbulence spectra are of the Von Karman form.

Vertical component of turbulence

The vertical component of turbulence has a spectrum of the form defined by the following equation:

$$\Phi_W(\Omega) = \frac{L_W \sigma_W^2 \left(1 + 2.67\left(1.339 L_W \Omega\right)^2\right)}{2\pi\left(1 + \left(1.339 L_W \Omega\right)^2\right)^{11/6}}$$

Where:

Φ_w = Spectral density in $(ft/s)^2$
σ_w = root mean square (rms) turbulence magnitude = $0.1061\ \bar{V}_{20}(kt)$
L_w = scale length = h (for h < 1 000 ft)
Ω = Spatial frequency in radians/ft = ω/V_T
ω = Temporal frequency in radians/s, and
V_T = aeroplane speed in ft/s.

Horizontal component of turbulence

The horizontal component of turbulence consists of a longitudinal component (in the direction of the mean wind) and lateral component. The longitudinal and lateral components have spectra of the form defined by the following equations:

Longitudinal component:

$$\Phi_u(\Omega) = \frac{L_u \sigma_u^2}{\pi\left(1 + \left(1.399\Omega L_u\right)^2\right)^{5/6}}$$

Lateral component:

$$\Phi_V(\Omega) = \frac{L_V \sigma_V^2 \left(1 + 2.67\left(1.339 L_V \Omega\right)^2\right)}{2\pi\left(1 + \left(1.339 L_V \Omega\right)^2\right)^{11/6}}$$

Where the rms turbulence scales are defined as below

$$\sigma_w = 0.1061\ \bar{V}_{20}(kt)$$

a. When $h \geq 1\ 000\ ft$ $\sigma_u = \sigma_v = \sigma_w$

b. When $h < 1\ 000\ ft$

$$\sigma_u = \sigma_v = \sigma_w \left[\frac{1}{0.177 + 0.000823h}\right]^{0.4}$$

c. When $h \leq 0\ ft$

$$\sigma_u = \sigma_v = \sigma_w \left[\frac{1}{0.177}\right]^{0.4}$$

and where the turbulence scales are defined as below

    a. When $h \geq 1\,000$ *ft* $L_u = L_v = L_w = 1000$

    b. When $h < 1\,000$ *ft* $L_w = h$

$$L_u = L_v = h \left[\frac{1}{(0.177 + 0.000823h)} \right]^{1.2}$$

    c. When $h \leq 0$ *ft* $L_u = L_v = L_w = 0$

WIND MODEL B

Mean wind

It may be assumed that the cumulative probability of reported mean wind speed at landing, and the crosswind component of that wind are as shown in Figure B-7. Normally, the mean wind, which is reported to the pilot, is measured at a height, which may be between 6 m (20 ft) and 10 m (33 ft) above the runway. The models of wind shear and turbulence given in the following paragraphs assume this reference height is used.

Wind Shear

Normal wind shear

Wind shear should be included in each simulated approach and landing, unless its effect can be accounted for separately. The magnitude of the shear should be defined by the expression:

        $u = 0.43\ U \log_{10}(z) + 0.57\ U$, for $z \geq 0.05$ m   (1)
        $u \equiv 0$, for $z < 0.05$ m

where   z is the height in metres

           u is the mean wind speed at height z metres,

           U is the mean wind speed at 10 m (33 ft)

Abnormal wind shear

The effect of wind shears exceeding those described above should be investigated using known severe wind shear data.

Turbulence

Horizontal component of turbulence

It may be assumed that the longitudinal component (in the direction of mean wind) and lateral component of turbulence may each be represented by a Gaussian process having a spectrum of the form:

$$\Phi(\Omega) = \frac{2\sigma^2}{\pi} \cdot \frac{L}{1+\Omega^2 L^2} \tag{2}$$

where $\Phi(\Omega)$ = a spectral density in (metres/second)^2 per (radian/meter).

σ = root mean square (rms) turbulence intensity = 0.15 U

L = scale length = 183 m (600 ft)

Ω = frequency in radians/metre.

Vertical component of turbulence

It may be assumed that the vertical component of turbulence has a spectrum of the form defined by equation (2) above. The following values have been in use:

σ = 1.5 knots with L = 9.2 m (30 ft)

or alternatively

σ = 0.09 U with L = 4.6 m (15 ft) when z < 9.2 m (30 ft)

and

L = 0.5 z when 9.2 < z < 305 m (30 < z < 1 000 ft)
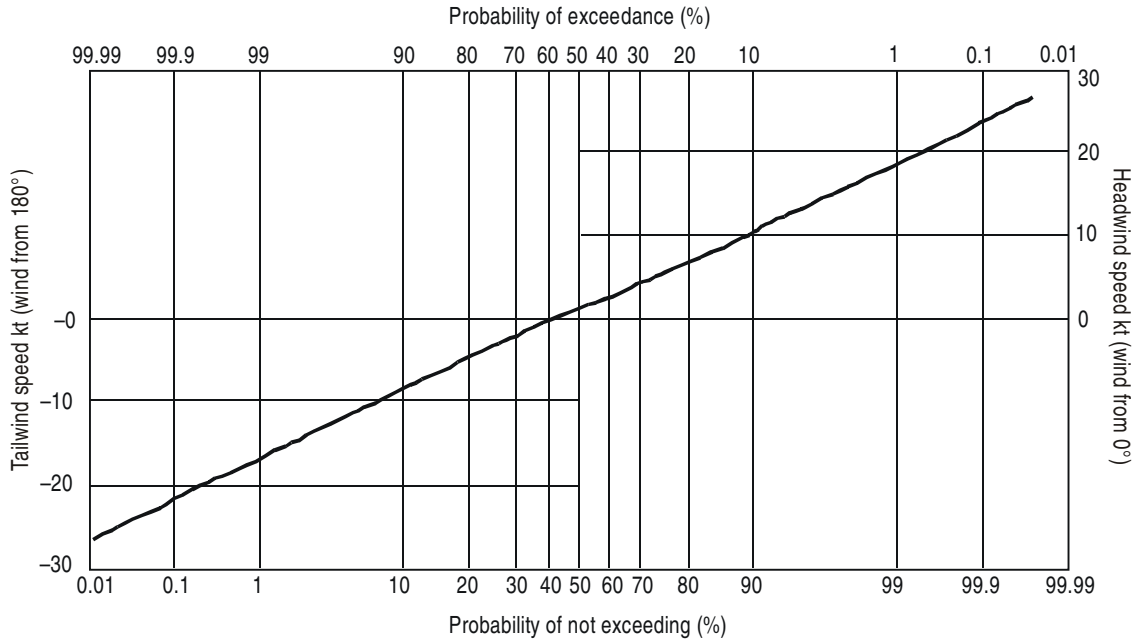
— — — — — — — —

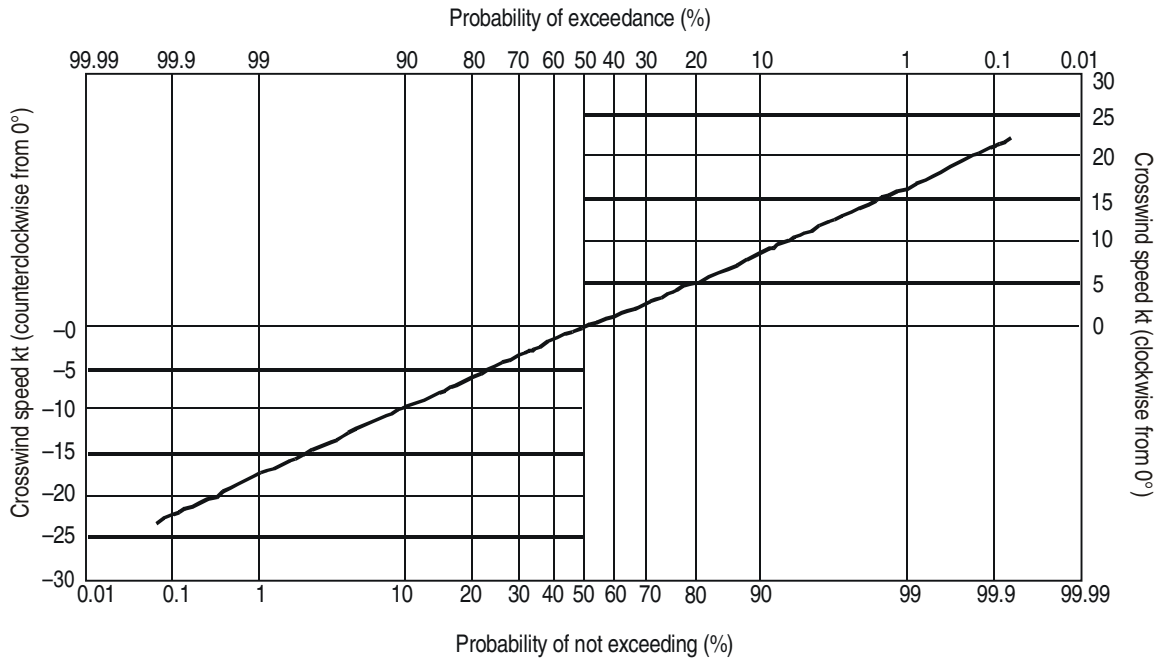**Figure B-1.   Headwind-tailwind description**

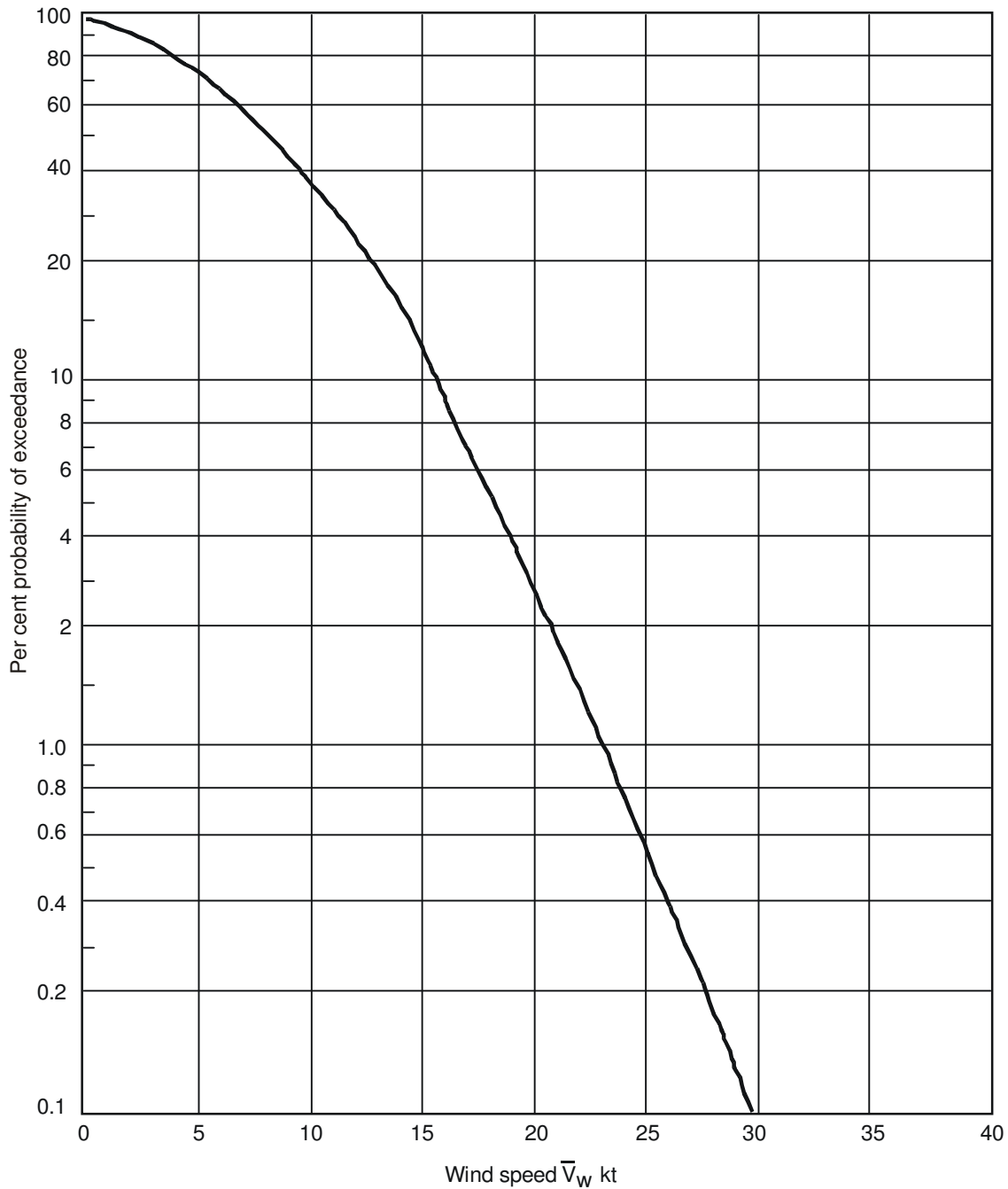**Figure B-2.   Crosswind description**

**Figure B-3.   Annual per cent probability of mean wind speed
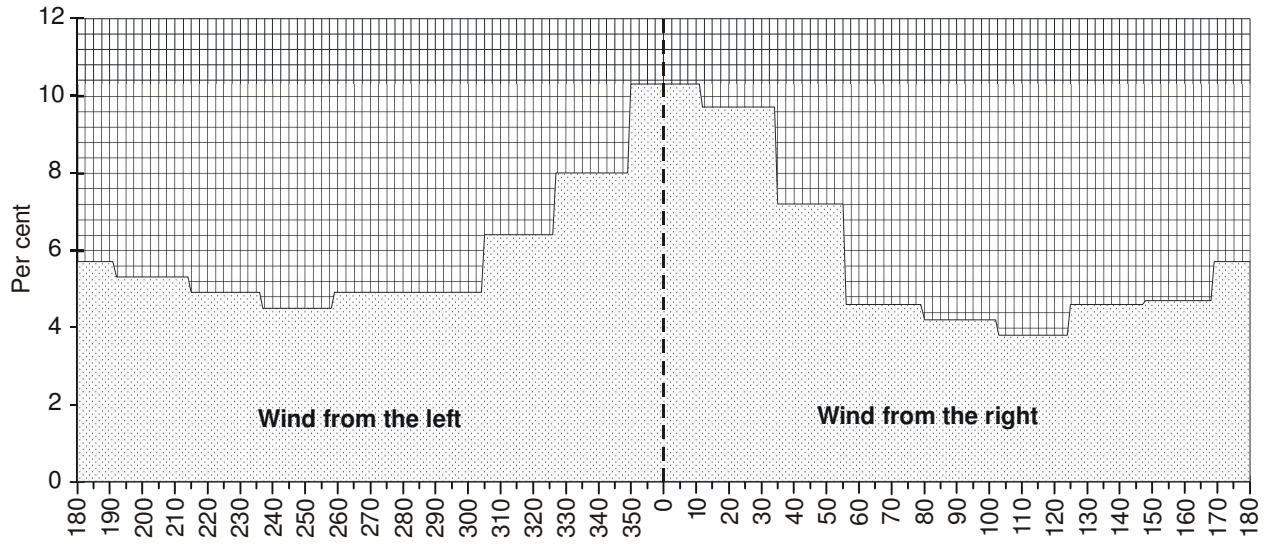equalling or exceeding given values**

Figure B-4.   Wind direction relative to runway heading

$$\frac{\sigma_u}{\sigma_w} = \frac{\sigma_v}{\sigma_w} = \begin{cases} [\dfrac{1}{0.177 + 0.823\, h/h_i}]^{.4} & h < h_i \\ 1.0 & h \geq h_i \end{cases}$$

**Figure B-5.   Selected description for variances
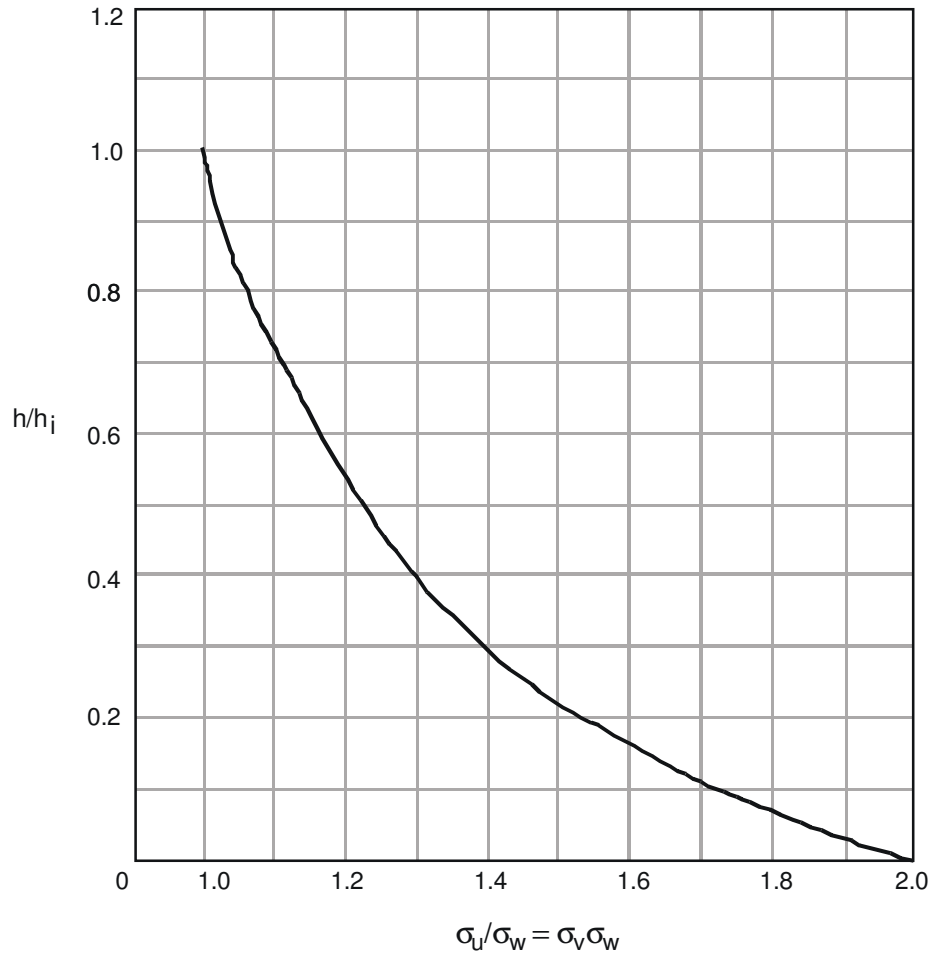of horizontal turbulence components**

$$L_w = \begin{cases} h, h < h_i \\ d, h = h_i \end{cases}$$

$$L_u = \begin{cases} L_w \left(\dfrac{\sigma_u}{\sigma_w} \right)^3 = \dfrac{h}{[0.177 + 0.823 \, h/h_i]^{1.2}} & h < h_i \\ \\ d & h > h_i \end{cases}$$

$$L_v = L_u$$

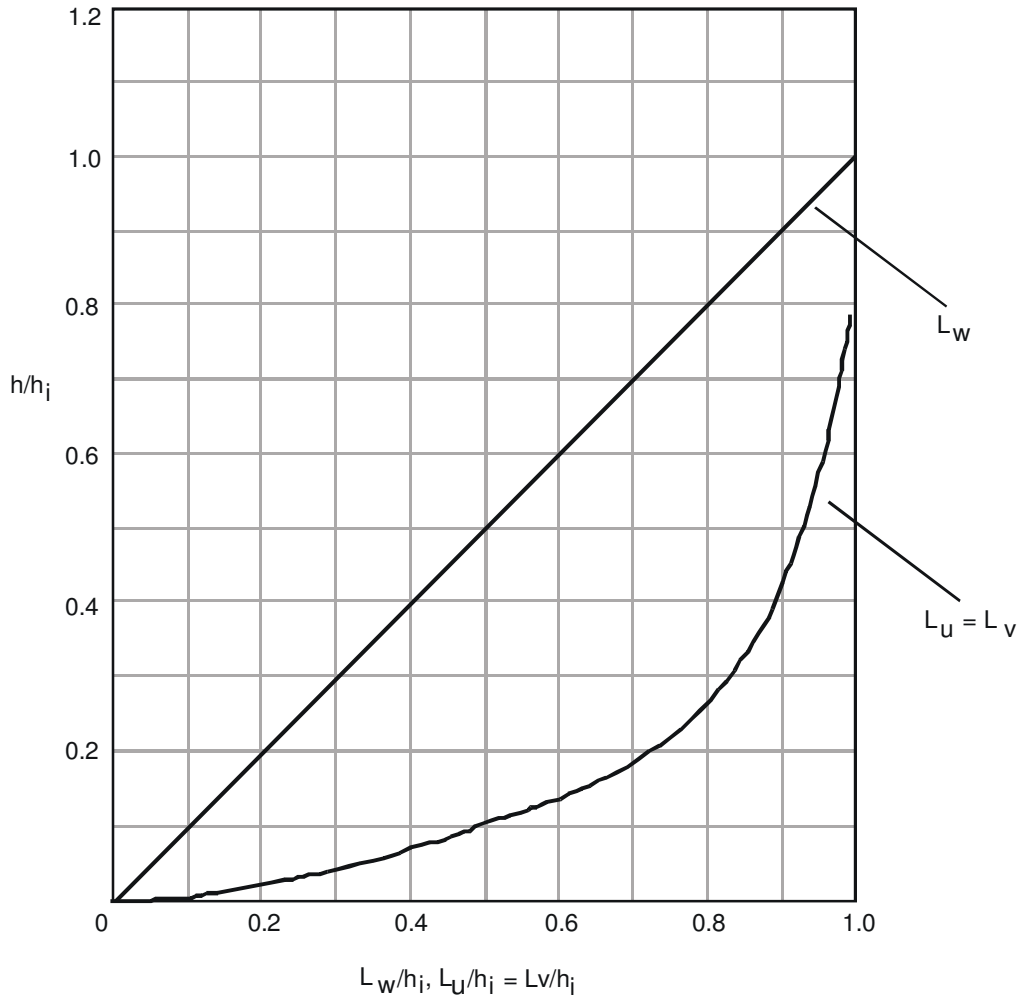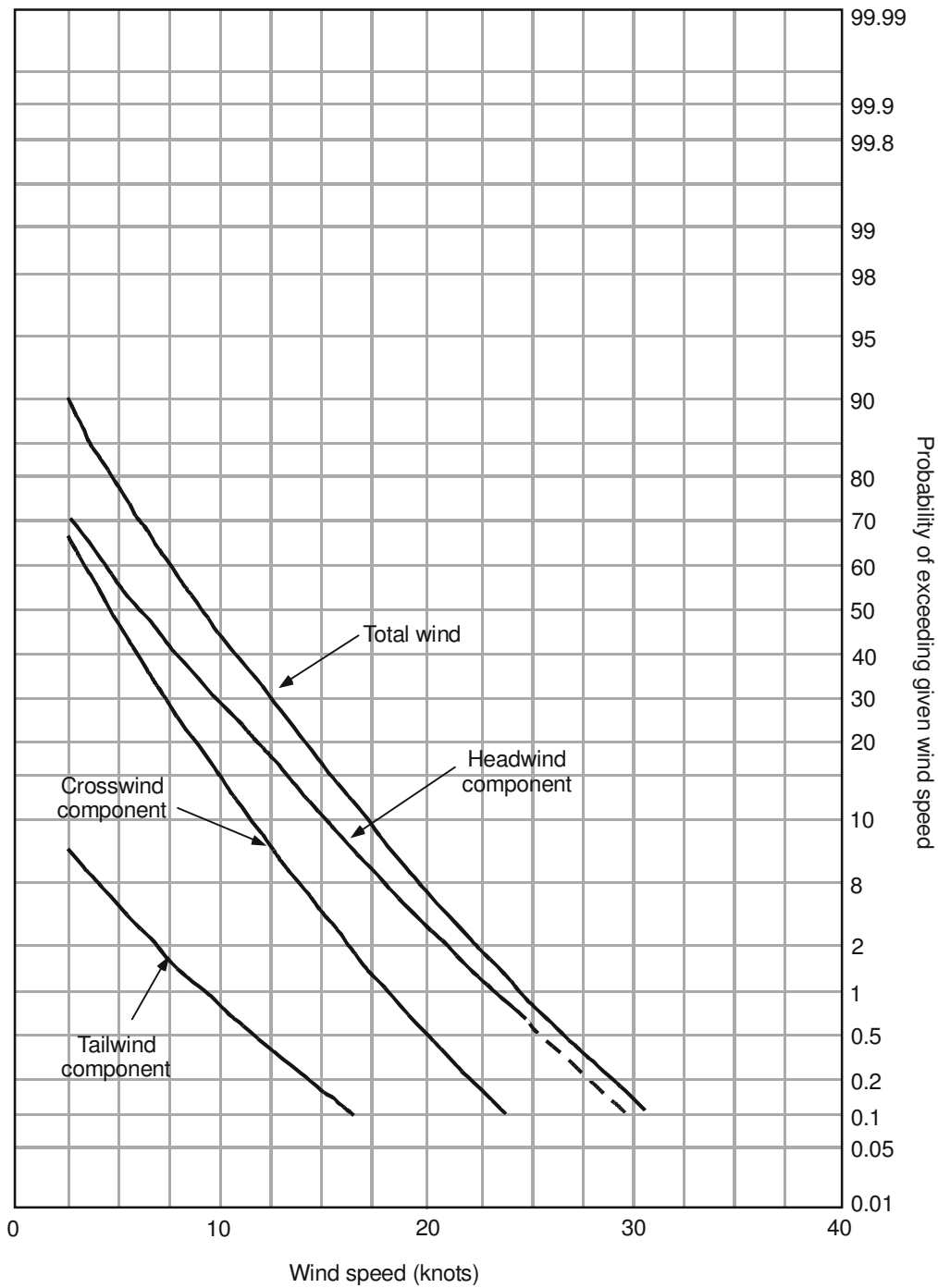h_i = Altitude above which turbulence is isotropic

Figure B-6.   Selected integral scale description

Note.— This data is based on worldwide in-service operations of U.K. airlines (sample size about 2 000)

**Figure B-7.   Cumulative probability of reported mean wind and headwind,
tailwind and crosswind components, when landing**

_____

Appendix C
ASAT DESCRIPTION

Printed with permission. Minor editorial changes introduced by ICAO.

The criteria for development of Terminal Instrument Procedures (TERPS), within the Federal Aviation Administration (FAA), are the responsibility of the FAA Flight Procedure Standards Branch, AFS-420 (and its predecessors). Much of the analytical work of the branch is performed by the Flight Operations Simulation and Analysis Branch, AFS-440. Both branches are part of the FAA Flight Standards Service.

The Airspace Simulation and Analysis Tools (ASAT) was developed by AFS-440 and AFS-420 to perform complex multiple aircraft simulations. Obstacle clearance requirements for new airspace standards – such as multiple parallel approaches, GNSS operations, and new larger aeroplanes are being studied. ASAT is also being used for reevaluation of existing standards, such as holding patterns, in light of modern system capabilities and operational considerations.

The ASAT system is a collection of models and simulations that can be used to analyze safety and risk factors for a large range of aviation scenarios.

- At the heart of the system are the extremely high fidelity engineering flight dynamics models of three Boeing aircraft (737, 767 and 747) against which the lesser models normally used in the high speed simulations are frequently checked. (ASAT is in the process of bringing three manufacturer-provided helicopter models on line in 2005 to do IFR helicopter studies. We are also in the discussion phase with Airbus to acquire some of their models.) Model performance can also be driven by empirical data collected in flight simulators and flight tests.

- Avionics are modeled based on requirements of the particular scenario. ASAT has access to most of the logic used in the operational flight programmes of Smith and Honeywell FMSs and has developed pilot models based on empirical data to provide steering commands to the airframe models.

- Environmental factors are also defined on a scenario basis. The aero models respond to the atmosphere around them, so temperature and density are handled almost automatically and wind profiles, including vertical components, are programmed as required for the scenario.

- Our models of the navigation infrastructure are based on many years of GPS data collection, with and without augmentation. We have models of ILS and MLS based on flight inspection and flight test data. This office developed the current DME/DME screening model used by the FAA.

- The "world" in which we run our scenarios is defined by official FAA databases providing precise geographic locations of airports, runways, navaids, and obstacles and terrain features as well as air routes and fixes. Information from external databases can easily be added to the system for analysis of foreign airfields, etc.

- Air traffic impacts on scenarios are based on computer models of radar systems built from manufacturer- and government-provided specifications and studies done to measure ATC response times, system latencies, and tolerances.

- ASAT models can also include other components such as ADS-B or TCAS. The system also can generate and track wake vortices and identify encounters between wakes and aircraft in the scenario.

Setting up a typical scenario will involve evaluation of the flight maneuvers involved. For straight-in approaches, path following accuracy is determined. This is generally the flight technical error and the navigation system error. For the pilot models, this drives various filters, weights and delays. For maneuvers that involve turns, various additional parameters will be evaluated such as nominal bank, roll rate, lead distance calculations, pilot delays in beginning the turn, etc. If altitude changes are involved there will be other additional parameters on climb/descent rates, target altitude over/undershoots, rate of change of climb/descent rate… Indicated airspeed is usually placed at a nominal value for the aircraft category, altitude, and operation, and random normal "noise" added. If Air Traffic is involved, there will be yet more parameters on surveillance delays, surveillance accuracy, controller response time, and pilot response delays to air traffic commands. All of these values are normally fitted to distributions that may be Gaussian, uniform, or Johnson (a four parameter family of curves that map to Gaussian but may describe bounded, skewed or kurtotic data). Variations in wind velocities, directions and temperature may also be represented by distributions.

Once the scenario is defined and set up, the simulation process can begin. The aircraft is (are) initialized, which normally means a trimmed condition at a particular airspeed, positioned (another scenario dependent variable – for approaches, lateral and vertical deviations from glideslope are usually based on the ICAO Collision Risk Model distributions, other scenarios may be based on provided radar track data), and released to fly the scenario.

Since we are continually updating the state vector(s) for the aircraft, basically any desired parameter can be extracted to an output file. Normally, we are most interested in the geographic position of the aircraft to establish its position relative to the ground, the runway, obstacles, terrain, other aircraft, or obstacle protection surfaces. We routinely monitor aircraft attitude to ensure that unusual flight attitudes are not required to accomplish the scenario. If some combination of winds and speeds require a 60-degree bank to accomplish a maneuver, then the maneuver needs more work.

As the aircraft fly the scenario, parameters are selected as needed from the defined distributions and applied to the scenario. For instance, when a go-around is initiated, delays will be generated for pilot recognition of decision height, activation of TOGA, setting of flaps and gear, etc. A rate of climb, a rate of rate of climb, thrust changes, etc., will be generated and the model commanded accordingly. Within the constraints of the pilot commands, the aircraft model will try to navigate to the defined approach path and missed approach track.

When the run is completed (or some success/failure condition has been met), the run counter is incremented, the appropriate pass/fail counter incremented, any parameters of interest, such as closest point of approach, are recorded and the procedure is repeated with a new set of input parameters drawn from the various distributions.

With the latest generation of desktop computers, large numbers of runs can be accomplished in quite reasonable amounts of time. It is not unusual to do 100 000 runs per scenario. 10 000 is probably the least we would consider doing for an analysis that involved a lot of scenarios. The number of scenarios is very problem-dependent and can range from 2 or 3 to 50 or 60. One study we are doing, examining the Converging Runway Display Aid order, will involve over 100 cases of runway convergence angles and

threshold-to-intersection distances. Generally we choose a small set of worst-case wind conditions (usually defined by the group requesting the analysis) and include some more nominal conditions for environment settings.

Given the versatile output format and the programming skills available, programme output can be tailored to meet almost any need. We generally produce a set of numeric results for each run and these are segmented or "binned" in some way and distributions developed as needed. We are normally interested in 10^{-7} or 10^{-8} type numbers and so extrapolation is usually necessary even when we can do a million runs.

ASAT Features

A. Functions
    1. Monte Carlo simulation of aviation related scenarios
    2. Visual playback of recorded or "live" flight tracks
    3. Statistical analysis of track data and operational parameters
    4. Playback of almost any recorded flight track
    5. Recording of ongoing flight simulator sessions
    6. Capacity studies
    7. Integrated Noise Model analysis
    8. Flight simulator data analysis
    9. Wake turbulence analysis/visualization
    10. Validation/Documentation of models

B. Track generation

    1. Flight modes
        a. Hand flown
        b. Flight director
        c. Autopilot

    2. ATC response
        a. ASR-9/FMA
        b. ASR-9/FDADS
        c. E-scan

    3. Navigation
        a. ICAO ILS distributions
        b. U.S. flight inspection distributions
        c. LDA
        d. MLS
        e. GPS
            i.   Raw/SA
            ii.   WAAS
            iii. LAAS
        f. VOR/DME
        g. NDB
        h. RNP
        i. FMS
            i.   Smiths
            ii. Honeywell

4.   Flight dynamics
    a.   Kinematic models
        i.   B-727
        ii.   B-737
        iii. B-747
        iv. MD-80/90
        v.   ATR-42
        vi. ATR-72
    b.   Six degrees of freedom
        i.   B-727
        ii.   B-737
        iii. B-747
        iv. B-767
        v.   NLA
        vi. MD-11
        vii. MD-90
        viii. Seneca
        ix. Commander
        x.   Helicopter
    c.   Boeing engineering models
        i.   B-737
        ii.   B-747
        iii. B-767

5.   Radar error models
    a.   ASR-9 (principal U.S. terminal area radar)
    b.   PRM/E-scan (high update radars)
    c.   Various other long range radar systems (ARSR-4)

6.   Environmental factors (generally a standard atmosphere model is used with appropriate temperatures and pressures. Various wind models are available but any wind profile can be programmed into the simulations.)
    a.   ALPA wind model
    b.   ICAO wind model
    c.   Landing and approach wind models for simulator certification
    d.   Microbursts/Wind shear
    e.   Wake vortex

7.   Geodetic Coordinates (in WGS-84) are available for almost any element related to aviation in the U.S. NAS
    a.   Obstacles
    b.   Terrain
    c.   Airport/Runway
    d.   Navigation aids
    e.   Routes
    f.   SIDS/STARS
    g.   Approach procedures

8.   Pilot/Air traffic controller response times (primarily for blunder scenarios where one aircraft in a multiple parallel approach scenario deviates toward the other aeroplane(s).)

C. Scenarios
1. Precision approach using ILS, MLS, WAAS (SBAS), LAAS (GBAS)
2. Dual/Triple/Quadruple simultaneous parallel approach operations
3. Converging approach operations
4. Holding operations based on
   a. Airman's Information Manual directions
   b. DME based navigation
   c. RNP based navigation
5. Departures
6. Multiple airport interaction of traffic flows
7. LDA/Offset LDA approach operations
8. En-route separation requirements
9. Evaluation of wake encounter risks for parallel and converging operations

_____

Appendix D
747-400 INTEGRATED AIRCRAFT CONFIGURATION (IAC) DESCRIPTION

Printed with permission. Minor editorial changes introduced by ICAO.

Text and figures provided by The Boeing Company.

The name "747-400 Integrated Aircraft Configuration (IAC)" refers to the integration of airplane/avionics computer models into an executable simulation of the 747-400 aeroplane. The 747-400 IAC was used in the autoland balked landing simulation study for the investigation of the obstacle free zone. The 747-400 IAC is a product of The Boeing Company and was provided to two branches of the Federal Aviation Administration (FAA) Flight Standards Organization, AFS-420 and AFS-440, to support this study and the development of flight procedures in the terminal area.

Figure D-1 illustrates the components of the 747-400 IAC simulation. These include simulation models of the following airplane/avionics systems:

- Autopilot
- Flight management computer
- Thrust management computer
- Engines
- Flight controls
- Sensors
- Electrical
- Hydraulic
- Landing gear

The software is under periodic review and configuration management which involves extensive inspection and software quality assurance.

Figure D-2 illustrates the inputs and outputs of the IAC in the form of products and services. Some of these inputs involve the specifications and designs for avionics, flight controls, propulsion and aerodynamic performance. The IAC serves as a tool for the following purposes:

- Research and development of new aircraft systems
- Customer service support
- Producing simulator and checkout data documents
- Pilot, airline, and government demonstrations
- Flight crew training
- Aircraft certification
- Accident/Incident investigations

Figure D-3 illustrates the steps from development to validation of the IAC and its relation to the so-called *"Simulator Data Package"* (which includes the simulator data, checkout data and Proof of Match Documents). The first step starts with initial versions of the various aeroplane systems being combined into an integrated model. The integrated model is compared against flight test data for a variety of maneuvers such as takeoffs, landings, go-arounds, etc. The model is adjusted to match the data. An iterative process of comparisons will

continue until certain criteria and tolerances are satisfied resulting in a validated simulation model, which becomes the IAC.

The IAC forms the basis for producing a Simulator Data Document. The Simulator Data is checked for compliance against the test standards and methods described in the ICAO *Manual of Criteria for the Qualification of Flight Simulators* (Doc 9625).

The validity of the IAC is documented in the proprietary *"Proof of Match"* document, which is provided to the simulator manufacturers and their customers. A version of the IAC is supplied to the FAA to support the balked landing study and the development of flight procedures.

Figure D-4 illustrates the performance of the simulation against actual flight test data for go-arounds between the ground level and 100 feet above ground. The flight test data corresponds to the use of the autopilot in either single- or multi-channel mode. The simulation data are the result of a Monte Carlo type study. The Monte Carlo study varied a number of parameters, such as wind speed and direction, airfield dimension, sensor performance, etc. The flight test data are within one or two sigma of the average (mean) of the simulation results. Numerical details have been omitted for proprietary reasons.
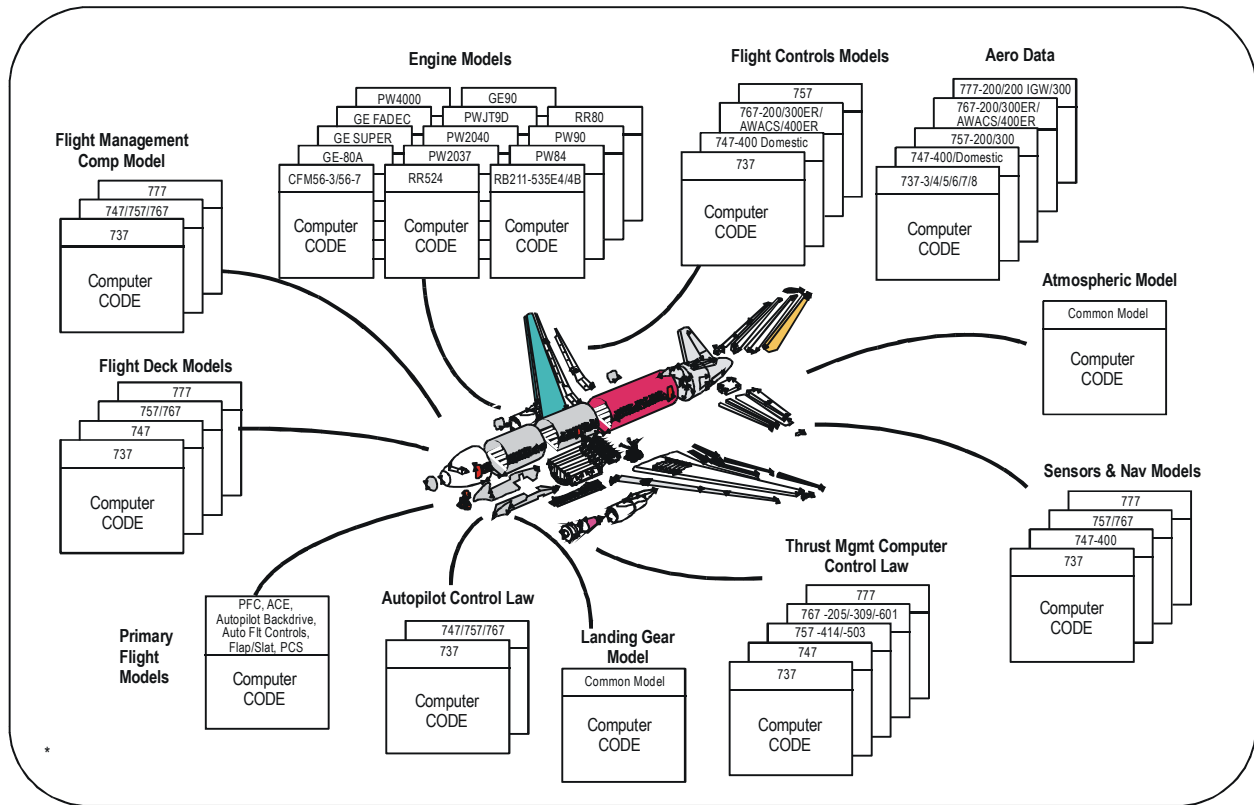
— — — — — — — —

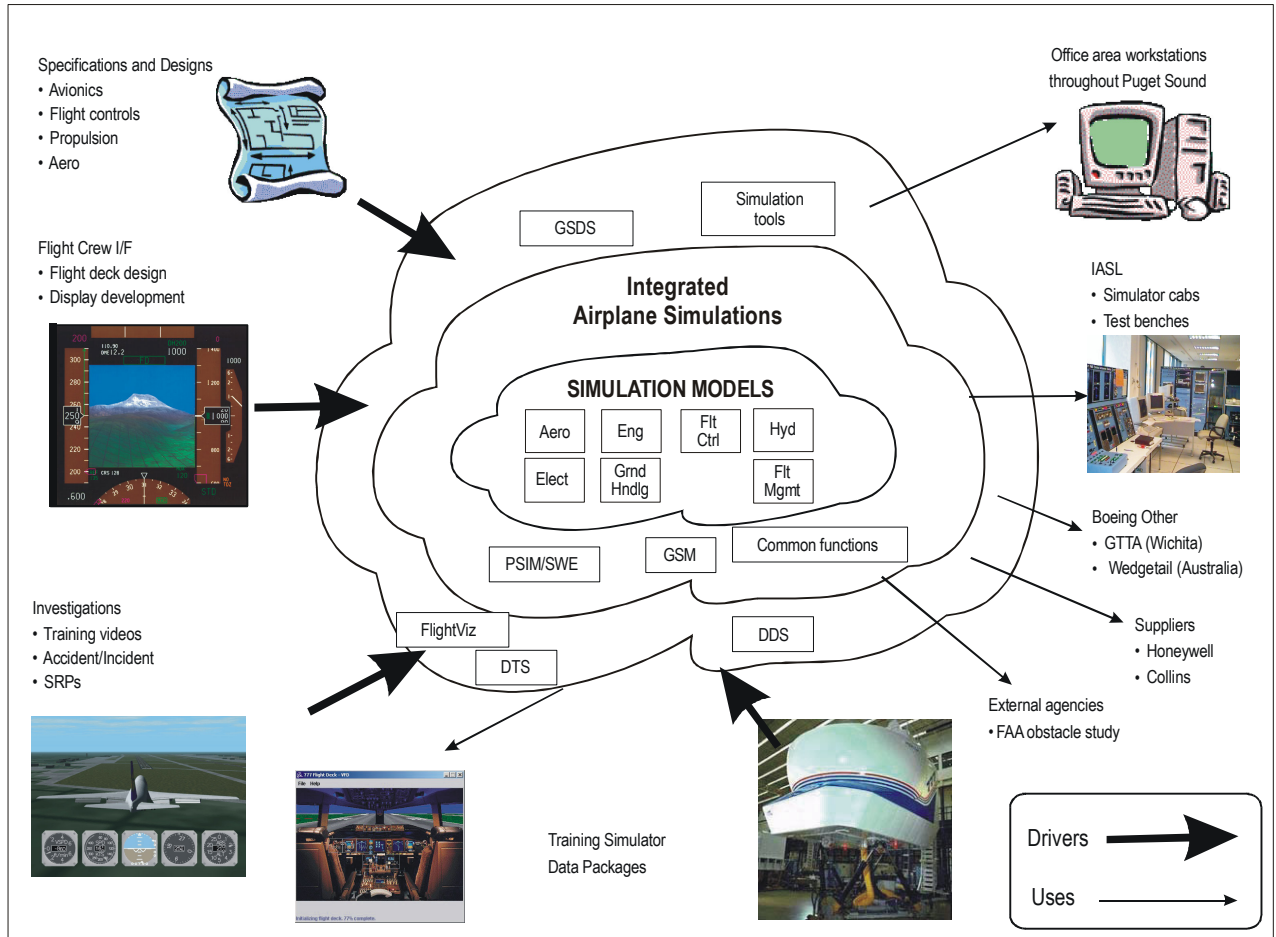**Figure D-1.   Boeing software simulation models**

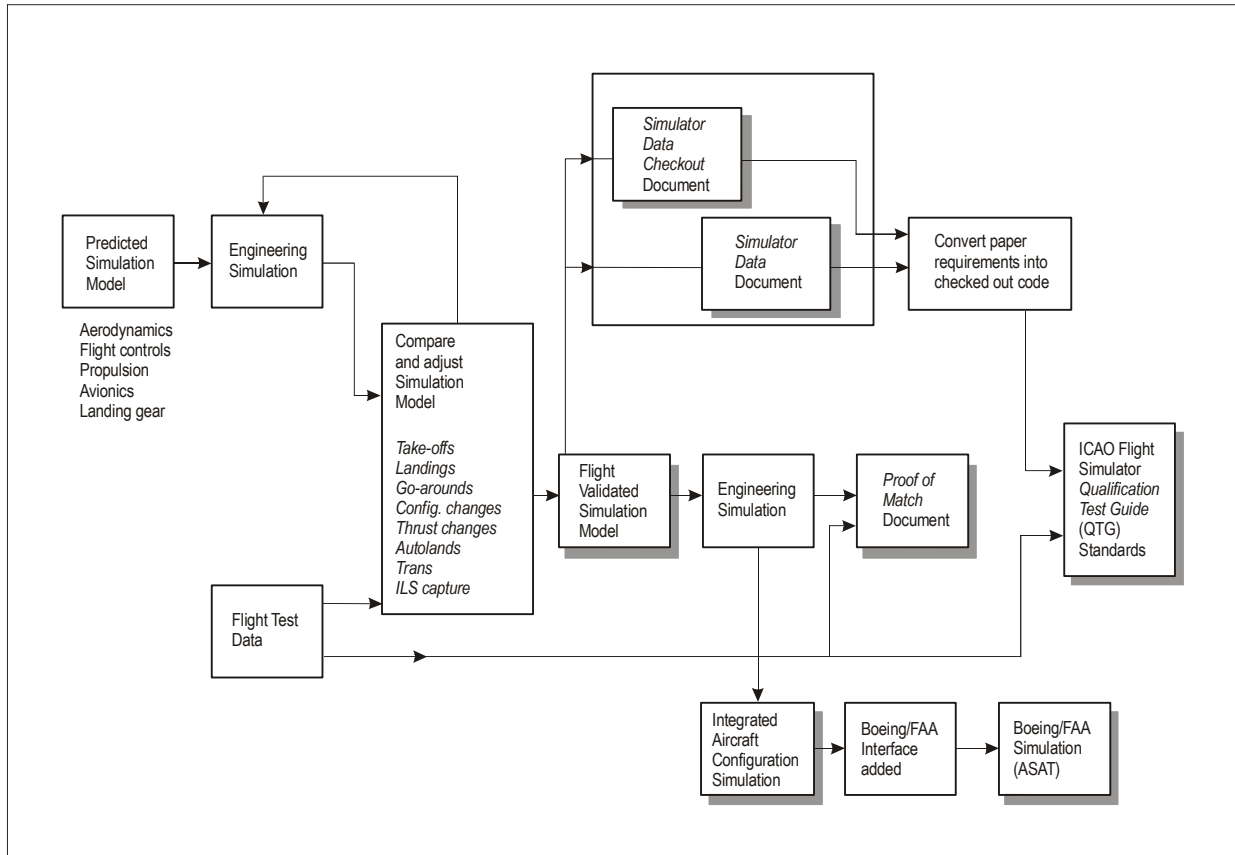**Figure D-2.   Boeing Simulation Engineering — products and services**

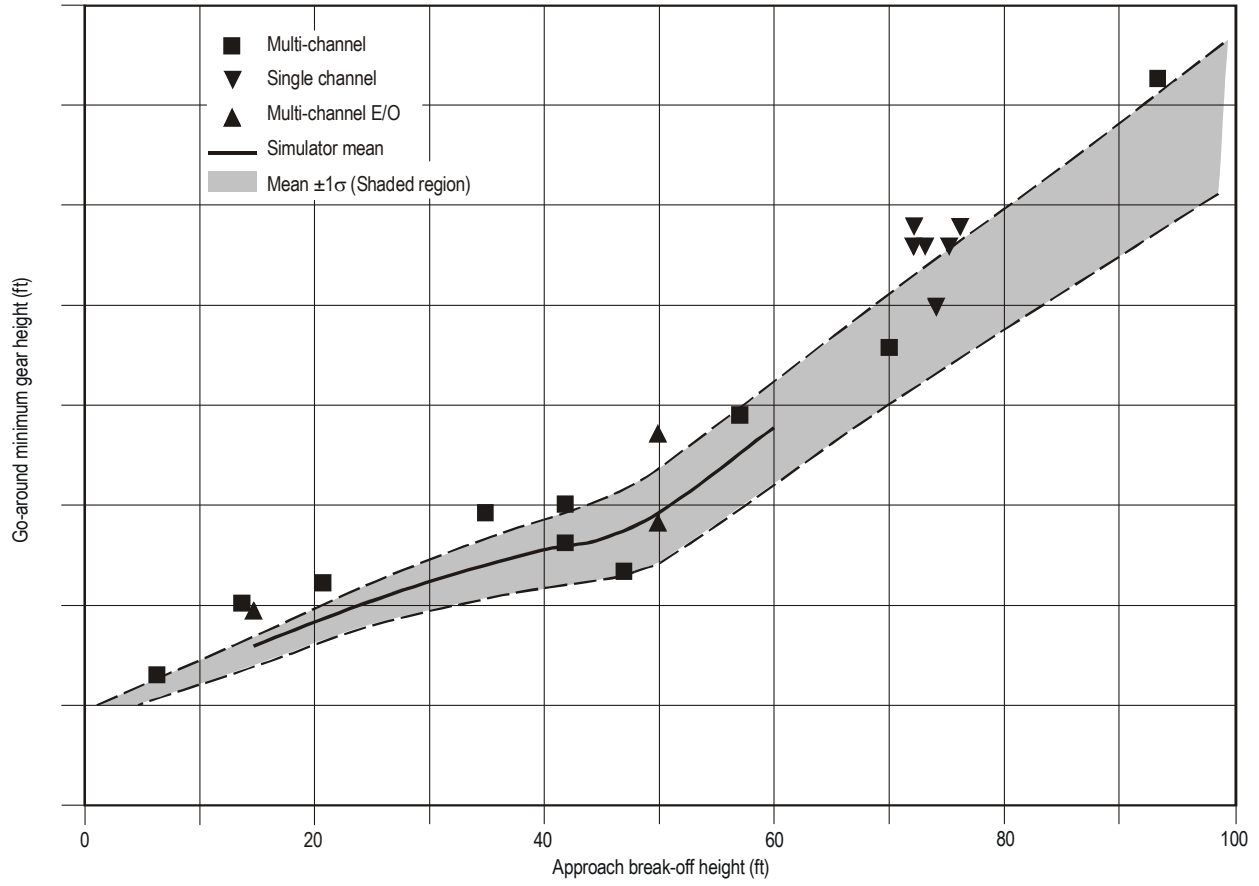**Figure D-3.   Boeing aircraft simulation model validation**

Figure D-4.   Minimum gear height during go-around flight test to simulator correlation

———————————

Appendix E
CREW-VEHICLE SYSTEMS RESEARCH FACILITY
(NASA AMES INFORMATION BULLETINS)

Reprinted with permission. Minor editorial changes introduced by ICAO.

This appendix provides a copy of the Information Bulletin received from NASA Ames describing their simulator facility as employed in the Balked Landing Study.

INFORMATION BULLETIN
National Aeronautics and
Space Administration

Ames Research Center
Moffett Field, California 94035-1000
(650) 604-9000

CREW-VEHICLE SYSTEMS RESEARCH FACILITY

The Crew-Vehicle Systems Research Facility (CVSRF), a unique national research resource, was designed for the study of human factors in aviation safety. The facility is used to analyze performance characteristics of flight crews; formulate principles and design criteria for future aviation environments; evaluate new and contemporary air traffic control procedures; and develop new training and simulation techniques required by the continued technical evolution of flight systems. The Crew-Vehicle Systems Research Facility allows scientists to study the effects of automation, procedural changes, advanced instrumentation and other factors, such as fatigue, on human performance in aircraft.

The facility includes two flight simulators—a Boeing 747-400 and an Advanced Concepts Flight Simulator (ACFS)—and a simulated Air Traffic Control (ATC) System that provides radar scope style information to controllers. The CVSRF also employs data interchange technology that allows full participation with other simulation facilities including Future Flight Central airport control tower simulator.

Both flight simulators in the CVSRF are capable of full-mission simulation. Each has a dedicated experimenter's control lab, capable of monitoring and controlling its simulator. Visual systems provide out-the-window cues in both cockpits. The Air Traffic Control System simulator provides a realistic air traffic control environment, including communication with the cockpits allowing study of air-to-ground communications systems as they impact crew performance.
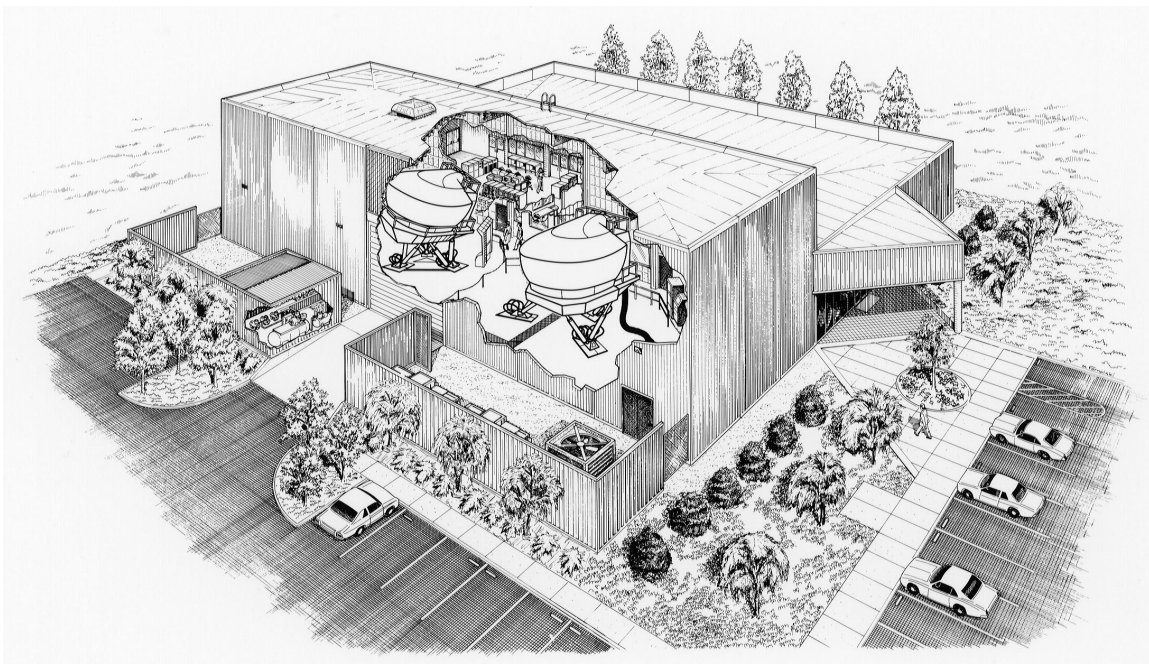
Cut-away view of Crew-Vehicle Systems Research Facility

Simulators

Human Factors research requirements demand a facility capable of producing realistic simulation of both current and future aviation operations. The Boeing 747-400 simulator represents a current technology state-of-the-art glass cockpit aircraft. Rigorous control and high fidelity ensures that aircrew behavior in simulated flights is representative of actual flight operations.

In contrast, the Advanced Concepts Flight Simulator, configured with multiple electronic displays, advanced crew-aircraft interfaces and flight control devices, is designed to permit virtually unlimited flexibility in information presentation, and command and control by the aircrew. Such flexibility permits the simulation of operations that may be possible with advanced aircraft and air traffic control concepts and equipment of the future.

Both aircraft simulators can operate in conjunction with Air Traffic Control (ATC) Simulators. The facility's ATC simulator can be configured to represent either today's aviation system or various possible systems of the future. Connection of any or all of the CVSRF simulators with other Flight Simulation facilities is supported through High Level Architecture (HLA). HLA is an architecture, developed by the DoD, to support interoperability of simulations. Using this technology, multiple facility simulations have become increasingly important, allowing the study of high density airspace ATC coordination in a realtime environment.

The research being performed in the CVSRF demands highly realistic external visual scene presentations in the aircraft cockpits. Both simulators are equipped with state of the art Flight Safety International VITAL VIIIi image generator computers and 180-degree field of view projection systems that provide an extremely realistic out-the-window representation. These systems use highly detailed databases identifying the visual features of numerous airports and routes throughout the world.

Boeing 747-400 Simulator

A key component of the facility is a Boeing 747-400 flight simulator. This simulator represents a cockpit of one of the more sophisticated airplanes flying today. The simulator is equipped with programmable flight displays that can be easily modified to create displays aimed at enhancing flight crew situational awareness and thus improving system safety. The simulator also has a fully digital control loading system, a six degree-of-freedom motion system, a digital sound and aural cues system and a fully integrated autoflight system that provides aircraft guidance and control. It is also equipped with a weather radar system simulation and a Flight Safety International VITAL VIIIi visual system. The visual system can depict out-the-window scenes in either day, dusk, night or twilight modes. The visual, weather radar, and motion systems are tightly coupled simulating weather effects with a high degree of realism. The host computer driving the simulator is part of the IBM 6000 series of computers utilizing IBM's reduced instruction set computer (RISC) technology. This computer also supports the collection and storing of simulated flight data requested by experimenters to achieve their experiment documentation goals.

The 747-400 simulator provides all modes of airplane operation from cockpit preflight to parking and shutdown at destination. The simulator flight crew compartment is a fully detailed replica of a current airline cockpit. All instruments, controls and switches operate as they do in the aircraft. All functional systems of the aircraft are simulated in accordance with aircraft data. To ensure simulator fidelity the 747-400 simulator is constantly maintained to the highest possible level of certification for airplane simulators as established by inspectors of the Federal Aviation Administration (FAA). This ensures credibility to the results of research programs conducted in the simulator.

Advanced Concepts Flight Simulator

Another key element of the facility is the Advanced Concepts Flight Simulator (ACFS). Like the B747-400 simulator, the ACFS is also equipped with a six degree-of-freedom motion system, programmable flight displays, digital sound and aural cueing system, and a Flight Safety International VITAL VIIIi visual system with a 180-degree field of view. The simulator systems provide an extremely realistic full mission environment. The ACFS is configured as a generic commercial transport aircraft employing many advanced flight systems as well as features existing in the newest aircraft being built today. Among its advanced flight systems, the ACFS includes touch sensitive electronic checklists, advanced graphical flight displays such as airport moving maps and graphical aircraft systems schematics, a flight management system linked to ATC, and a Head Up Display (HUD) guidance system. In addition, the ACFS utilizes sidestick controllers for aircraft control in the pitch and roll axes.

The ACFS generic aircraft was formulated and sized on the basis of projected user needs well into the twenty-first century. The generic aircraft used was also the basis to design the cockpit and provide details of the flight deck:

    Maximum gross weight 225 000 pounds
    200 passenger capacity
    Twin engine; 41 000 pounds thrust each engine
    Speed: .78 Mach; range 2 500 miles
    Two-person flight crew
    All-electric airplane (no hydraulics)
    Fly-by-wire; active flight controls
    Relaxed static margin; load alleviation
    T-tail, low wing, supercritical airfoil
    Composites for primary and secondary structures
    High-density fuel

Air Traffic Control Simulator

The Air Traffic Control (ATC) environment is a significant contributor to pilot workload and, therefore, to the performance of crews in flight. Full-mission simulation is greatly affected by the realism with which the ATC environment is modeled.

From the crew's standpoint, this environment consists of dynamically changing verbal or data-link messages, some addressed to or generated by the crew, others addressed to or generated by other aircraft flying in the immediate vicinity.

The ATC simulator is capable of operating in three modes: stand-alone, without participation by the rest of the facility; single-cab mode, with either the ACFS or the 747-400 participating in the study; and dual-cab mode, with both cabs participating.

Experimenter Facilities

Two experimenter stations are provided, one for each of the flight simulators. Each experimenter station contains a suite of computer graphic displays, keyboards and terminals for interacting with the simulation computers, status lights and emergency controls, communication systems and other equipment useful for controlling flight simulators and conducting simulation experiments.

Each experimenter's laboratory also contains an audio station so that experimenters may communicate with the simulator crews during an experiment or with observers located "on-board." In addition to the main experimenter consoles, an experimenter (or observer) station is located aboard each of the flight simulators. Communicating with the Air Traffic Control simulator is possible from each of the experimenter stations.

Typical Experiments

The CVSRF supports NASA, FAA, and industry research programs, including the NASA Airspace Capacity Improvement Programs and the Aviation Safety Initiative. Recent research experiments conducted at the CVSRF include:

- Advanced Air Transportation Technology Free Flight utilizing advanced air-to-air data-link and communications to provide enhanced air traffic separation and decrease time enroute.

- Converging Approaches and Multiple Parallel Approaches studies by the FAA to improve capacity at airports with difficult airport approach conditions, especially in poor weather or reduced visibility conditions.

- Propulsion Controlled Aircraft studies to provide an aircraft crew with the capability to land safely with all hydraulic systems failed or malfunctioning.

- Taxi Navigation And Situation Awareness (T-NASA) utilizing a Head-Up Display and electronic airport Moving Map system to improve traffic flow on the airport surface in bad weather for greater safety and efficiency.

The facility is managed by personnel in the Aerospace Simulation Operations Branch within the Aviation Systems Division, part of the Aerospace Directorate at Ames Research Center.

Points of Contact:

Barry T. Sullivan
Chief, Aerospace Simulation Operations Branch
(650) 604-6756

Thomas S. Alderete
Chief, Simulation Planning Office
(650) 604-3271

Terrence K. Rager
Manager, CVSRF
(650) 604-3127

_____

Appendix F
ZENTRUM FÜR FLUGSIMULATION BERLIN GMBH (ZFB)[*]
(Information Bulletin)

Reprinted with permission. Minor editorial changes introduced by ICAO.

This appendix provides a copy of the Information Bulletin received from ZFB describing their simulator facility as employed in the Balked Landing Study.

1 Zentrum für Flugsimulation Berlin GmbH

The ZFB Zentrum für Flugsimulation Berlin GmbH simulator, manufactured by the Canadian company CAE Electronics Ltd. and located at the Institute of Aeronautics & Astronautics of the Technische Universität Berlin, began operation in 1993. The use of a full flight simulator for research as well as airline pilot training was already conceived in 1980.

Support came from Deutsche Lufthansa AG, CAE Electronics Ltd., Airbus Deutschland GmbH, German Aerospace Centre (DLR), the Federal Government and the Senate of Berlin *(Senat von Berlin)*.

The A330/A340 full flight simulator in Berlin is the first in the world to have a dedicated scientific research facility.

The site is managed and maintained in close cooperation between ZFB and Lufthansa Flight Training Berlin (located near Airport Berlin-Schönefeld (EDDB)).

The ZFB simulator is certified for the following aircraft types (for details, see Appendices I and II):

- Airbus A330-322 (D-AERF),

- Airbus A330-301 (EI-CRK),

- Airbus A340-311 (D-AIGA).

Generally, cockpit interface, avionics and system architecture are nearly the same for the Airbus A330 and A340. The major differences are, of course, type and number of engines. To provide both aircraft types (A340 and A330), a partial conversion of the flight crew compartment is necessary. During this conversion, the overhead-panel and the thrust-lever are exchanged. Also all type-specific original avionics are switched accordingly. Finally, the corresponding simulation software is loaded. A complete conversion takes approximately 30 minutes.

The photo below shows the direct view into the A330 configured cockpit. Visible are the original instruments

---

[*] ZFB Zentrum für Flugsimulation Berlin GmbH, Marchstrasse 12, D-10587 Berlin, Germany. www.zfb-berlin.de

and the realistic outdoor view, which is based on a 3D-computer animation. This animation is able to simulate day, night, dawn and various types of meteorological effects.

A330 FFS Cockpit at ZFB

The simulator operates twenty-four hours a day, seven days a week. Normally, simulator scheduling and confirmation take place at least one month in advance; however, to ensure booking in preferred time slots it is recommended that customers book at least 3 months in advance. The A330/A340 simulator is used for recurrent, transition and type-rating training.

Normally, customers book the simulator for FFS (Full Flight Simulator) or FBS (Fixed Based Training) on a dry lease basis. Wet lease training can be arranged if required.

2 Description of the A330/340 Full Flight Simulator

2.1 Scientific Research Facility

The Airbus A330/340 Full Flight Simulator (qualified according to JAR-STD-1A) and the associated Scientific Research Facility (SRF, usually but not exclusively available for the A330) consists of several IBM RISC/6000 workstations providing all necessary functions to develop and apply user-appropriate simulation software. The research host computer, as the main part of the SRF, is identical to and independent from the training host computer, but is equipped with additional scientific research features such as:

   •   direct simulator source code access,

   •   display development,

   •   testing of experimental avionic units, and

   •   audio, video and data recording,

and will be used for software development and validation. One main advantage to this approach is the separation of the training environment from the research environment.

To guarantee the highest quality of flight simulation, original avionic components and computers are used. Also, for the complete cockpit environment, e.g. displays, flight controls, switches etc., only original components are used. The host computer simulates other components such as the flight mechanical model, the aircraft's sensor technology, atmospheric model, engines, hydraulic and any other sub-system available in the real aircraft. For exact calibration of the simulator's behaviour and performance, flight test data from the reference aircraft are used.

One of the outstanding characteristics of such a simulation is the perfect connection, communication and interaction of original aircraft avionics with simulated components. Requirements for this are an all-embracing network and the consequent management of all simulation parameters on the simulation host computer inside a so-called Common Data Base (CDB). The CDB consists of approximately 90 000 parameters, which can be monitored, recorded and modified online.

The simulation host computer does not comprise other important simulation systems such as the visual system, the motion system and the control loading system. Those systems are connected via the simulation network. For details, see Appendix I.

2.2 Visual System

The former Visual System Rediffusion SP-X 550AT was replaced in October 2004 by the brand new Evans & Sutherland EP1000-CT, equipped with a wide-angle infinity display. Three video projectors generate 150-degree horizontal and a 40-degree vertical view for both pilots with more than 4.5 million pixels. In addition, up to 15 000 calligraphic luminous spots such as strobe lights can be displayed simultaneously. The display is created as a so-called back beam projection on a spherical mirror with a dimension of 9 m by 2.4 m.

2.3 Motion System

Comprising all components of the flight crew compartment, the associated avionics and sub-systems, a mass of approximately 12 000 kg has to be held and moved by the motion system. The motion system provides six degrees of freedom to ensure the correct behaviour of the simulated aircraft to the pilots. During operation the following performance can be attained:

- Maximum vertical excursion: 1.70 m ($\pm$ 1 g)
- Maximum lateral excursion: 2.44 m ($\pm$ 0.8 g)
- Maximum longitudinal excursion: 2.84 m ($\pm$ 0.8 g)
- Maximum pitch excursion: +33.5°, -37.5°
- Maximum roll excursion: ±28°
- Maximum yaw excursion: ±37.5°

2.4 Control Loading System

The control loading (C/L) system is designed to generate the simulated load feel at the flight controls, while the motion system imparts realistic acceleration to the flight compartment. Since all Airbus aircraft from the A320/A330/A340 series use a side-stick, only the rudder pedals, the wheel of the horizontal trimmable stabilizer and the nose-wheel steering are connected to the C/L system. The motion system as well as the control loading system is controlled by a high-pressure hydraulic system with 3 000 PSI.

2.5 Instructor Operator Station

The Instructor Operator Station (IOS) is a graphical user interface to give the instructor control, during experiments and training, of several simulation parameters such as weather settings, repositioning, creation of malfunctions, etc. The IOS consists of two 19'' touch-screens located in the flight compartment behind the Captain's seat.

2.6 Central Time Reference

In order to provide synchronized video, audio and data recording, an IRIG-B (Inter-Range Instrumentation Group) time generator/inserter is used. The time code generator (TCG) provides a standard IRIG-B serial time code for two parallel channels. One channel output is sent to the so-called K1 cabinet for time stamping of recorded hard data of the simulation process. The second channel is sent to the IRIG-B video inserter. The IRIG-B video inserter (PAL format) inserts the same time stamp into the cameras' video signals, which are recorded by three Super VHS recorders.

2.7 Video Recording

Video recording is done by closed-circuit TV cameras. Two monochrome low-light cameras (back view) equipped with exchangeable lenses can be installed in the cockpit to record the pilot's and co-pilot's actions as well as to provide a centre view. For various projects, an additional wide-view microcamera was integrated into the front area of the flight compartment to record and observe the pilot's interactions from the front. A video scan converter is used to convert the RGB signal of one IOS to a video signal. Three Super VHS video recorders are installed outside and can be controlled from the instructor station. The video recording has a time reference feature. Three table-mounted monitors are installed in the SRF control room.

2.8 Audio Recording

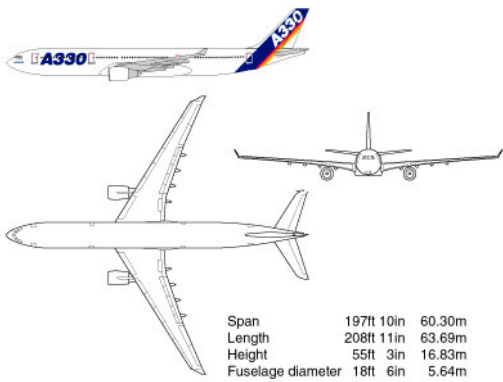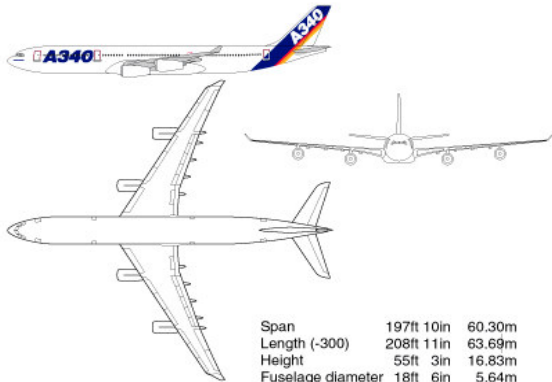The audio recording capability is provided for:

- Captain headset,
- Captain microphone,
- First Officer headset,
- First Officer microphone,
- Observer headset,
- Instructor microphone,
- Cockpit voice recorder microphone.

The recording uses the stereo-HiFi audio band of the VCRs. A software mixer is provided through the instructor station to relate the sources to the six possible outputs.

2.9 Data recording from the simulation process

The Data Gathering Utility (DGU) is a tool to create log files of the simulation state as stored in the CDB. All desired simulation parameters for recording have to be written in a profile. The DGU scans this profile at regular intervals (up to 60 Hz) and writes all values specified by the profile to be logged into a file.

APPENDIX I

SRF Block Diagram

Appendix II

Simulator	Airbus A330-300		Airbus A340-300
Simulator manufacturer	CAE Electronics Ltd.		
In-service date	1997		1993
Master aircraft	A330-322 D-AERF S/N 082 (PW 4168)	A330-301 EI-CRK S/N 183 (GE CF6-80E1A2)	A340-311 D-AIGA S/N 020 (CFM56-5C2)
Aircraft layout (© Airbus)	Span 197ft 10in 60.30m Length 208ft 11in 63.69m Height 55ft 3in 16.83m Fuselage diameter 18ft 6in 5.64m		Span 197ft 10in 60.30m Length (-300) 208ft 11in 63.69m Height 55ft 3in 16.83m Fuselage diameter 18ft 6in 5.64m
Simulator host computer	IBM RISC System/6000 Model 7013 – 580		
Motion system	CAE Series 500, 6 DOF, digital		
Control loading	Digital		

Aircraft systems	Airbus A330-300		Airbus A340-300
Basic engine data	**2x PW 4168**	**2x GE CF6-80E1A2**	**4x GE CFM56-5C-2**
FMGEC	2x SEXTANT (A330-300 PW)	2x SEXTANT (A330-300 GE)	2x SEXTANT (A340-300)
TCAS II	1x BENDIX		
ACARS	1x Allied Signal (a/c AMU)		
Visual system	**Airbus A330-300**		**Airbus A340-300**
Visual system manufacturer	Evans & Sutherland		
Type of image generator	EP-1000 CT		
Type of display	3x Suprawide, 150° × 40° FOV		
Illumination levels	Day (60 Hz) / Dusk/Night (40 Hz)		
Number of airport scenes	World database (more than 100 airport definitions)		

Instructor station	Airbus A330-300	Airbus A340-300
Computer	2x IBM RISC System/6000 Model 320	
Displays	2x CRTs with capacitive touch screen	
Plotter	1x PRINTRONIX and 1x HP LaserJet 4000	

Instructor station	Airbus A330-300	Airbus A340-300
Number of malfunctions	More than 400	
Automated training lessons	Available for Base Check, TCAS, Transition, LOFT, Refresher, Route Qualification	
ATIS	4 channels	
Audio and video recording	3x SVHS System (2x Cameras)	
Options	**Airbus A330-300**	**Airbus A340-300**
Scientific research	Simulator is equipped with a scientific research facility and located at the Technical University Berlin	
Approvals	**Airbus A330-300**	**Airbus A340-300**
LBA (Germany)	Code No 95FZ01D annually, Zero Flight Time	Code No 95FZ02D annually, Zero Flight Time
JAA (Europe)	JAA STD 1A (D-1A-017)	JAA STD 1A (D-1A-016)
CAA (GB)	Now JAA	Now JAA
DGAC (France)	Now JAA	Now JAA

— END —